Isomerization behavior of photochromic molecules in direct contact with noble metal surfaces

Im Fachbereich Physik
der Freien Universität Berlin
eingereichte Dissertation

Sebastian Hagen

Mai 2009

This work was done between September 2005 and April 2009 in the group of Professor Martin Wolf at the Physics Department of the Freie Universität Berlin.

Berlin, April 2009

Erstgutachter: Prof. Dr. Martin Wolf

Zweitgutachter: Prof. Dr. Jose Ignacio Pascual

Datum der Disputation: 24.06.2009

Abstract

This work investigates the isomerization behavior of photochromic molecules upon adsorption onto a noble metal surface. 2-photon photoemission (2PPE) has been employed to study the corresponding electronic structure and the charge charier dynamics. In the case of tetra-*tert*-butyl-Azobenzol (TBA) adsorbed on Au(111) the isomerization processes has been demonstrated based on the light and temperature induced changes in the electronic structure. Here, 2PPE proved to be an ideal tool for the analysis of the underlying excitation mechanism, the reaction kinetics as well as the efficiency of the photoinduced switching.

The initial excitation leading to the photoisomerization of TBA/Au(111), in contrast to the free molecule, does not occur via a direct optical transition between the highest occupied (HOMO) and the lowest unoccupied molecular orbital (LUMO). Instead a thermally assisted, substrate mediated process has been identified. Therefore a hole is created in the gold d-bands upon photoexcitation of an electron. Subsequently the hole is transferred to the HOMO of the TBA initiating a conformational change.

As for the free TBA a second thermally driven isomerization channel is available which converts the meta stable cis-isomer into the trans configuration. Due to the influence of the substrate-adsorbate interaction the range of molecular motions is strongly limited. Moreover the energy barrier separating the two isomers in the ground state is lowered by a factor of four.

To elucidate the influence of the substrate on the photoisomerization TBA is adsorbed onto an Ag(111) surface. Although the absorption behavior is almost identical to the results obtained from the Au(111) substrate, no switching has been observed. Here, the absence of a substrate mediated photoisomerization can be correlated to the differences in the band structures and in particular the energetic position of the respective d-bands. For silver these are located in an energy region where they cannot overlap with the with the HOMO of the TBA which is involved in the substrate mediated isomerization process.

In further experiments the influence of different functional groups on the isomerization behavior has been investigated. Therefore TBA is replaced by the isoelectronic, likewise tetra-*tert*-butyl substituted molecules imine (TBI) and stilbene (TDS). These enable the analysis of the switching process with respect to the properties of the free molecule which differ significantly for the three used species, viz. the available isomerization pathways, like e.g. rotation or inversion, and the height of the ground state barrier. In the corresponding 2PPE spectra of TBI and TBS adsorbed on Au(111) no light induced changes have been observed and thus no photoisomerization could be identified.

The results presented in this work show that the adsorption of the studied molecular switches leads to a significant change of their isomerization behavior. Two important aspect arise from the substrate-adsorbate interaction: The first is the influence of the electronic coupling between molecular orbitals and the metal band structure. On one hand it can reduce the lifetime of the excited molecular state which is a possible reason for the suppressed isomerization upon intramolecular excitation. On the other hand it creates additional excitation pathways via a substrate mediated charge transfer. The second aspect is the geometric confinement of the molecules. It can suppress molecular motions required for an isomerization and thus presents another possible explanation for the observed quenching of switching process initiated by intramolecular excitations.

Kurzfassung

Diese Arbeit untersucht das Isomerisierungsverhalten von photochromen Molekülen adsorbiert auf Edelmetalloberflächen. Dazu wurden die elektronische Struktur und die Ladungsträgerdynamik der entsprechenden Proben unter Verwendung von 2-Photonen Photoemissions Spektroskopie (2PPE) bestimmt. Für tetra-*tert*-butyl-Azobenzol (TBA) adsorbiert auf einer Au(111)-Oberfläche konnte anhand der licht- und temperatur-induzierten Änderungen in der elektronischen Struktur ein erfolgreiches Schalten demonstriert werden. Hierbei erweist sich 2PPE als ein ideales Werkzeug zur Analyse des zugrundeliegende Anregungsmechanismus, der Reaktionskinetik, sowie der Wirkungsquerschnitte im Falle des photoinduzierten Schaltens.

Im Gegensatz zum freien Molekül erfolgt für TBA/Au(111) die initiale elektronische Anregung nicht mittels eines optisch angeregten, resonanten Übergangs zwischen dem höchsten besetzten (HOMO) und dem niedrigsten unbesetzten Molekülorbital (LUMO), sondern durch einen thermisch assistierten, substratvermittelten Prozess. Hierbei wird zunächst ein Loch im Au(111) d-Band mittels Photoanregung eines Elektrons erzeugt. Anschließend tunnelt das Loch in das HOMO woraufhin eine Konformationsänderung ausgelöst wird.

Ähnlich dem freien Molekül zeigt auch das adsorbierte TBA einen thermisch aktivierten Isomerisierungskanal welcher die meta-stabilen cis-Isomere zurück in die stabile trans Konfiguration schaltet. Aufgrund der Wechselwirkung mit dem Substrat ist der Bewegungsfreiraum der einzelnen Molekülgruppen stark eingeschränkt. Zudem wird die Energiebarriere, welche im Grundzustand die Isomere voneinander trennt, durch die Adsorption auf ein Viertel ihrer ursprünglichen Höhe reduziert.

Um den Einfluss des Substrates auf die Photoisomerisierung zu klären wurden das Schaltermolekül TBA auf einer Ag(111)-Oberfläche untersucht. Obwohl das Adsorptionsverhalten annähernd identisch ist, konnte kein photoinduziertes Schalten beobachtet werden. In diesem Fall kann das Fehlen eines substrat-vermittelten Prozesses mit der elektronischen Struktur des Silbers erklärt werden. Im Gegensatz zum Gold befinden sich hier die d-Bänder nicht in unmittelbarer energetischer Nachbarschaft zu dem am Schalten beteiligten HOMO.

In weiteren Experimenten wurde der Einfluss der Schalteinheit auf das Isomerisierungsverhalten untersucht. Dazu werden die mit Azobenzol isoelktronischen Schaltermoleküle Imin und Stilben, bzw. deren tetra-*tert*-butyl substituierte Derivate, TBI und TBS, benutzt. Dies ermöglicht eine Analyse des Schaltens unter Einbeziehung der ursprünglichen Eigenschaften welche sich für die drei verwendeten Moleküle signifikant unterscheiden. Insbesondere treten Differenzen bei den vorhandenen Isomerisationspfaden, z.B. Rotation und/oder Inversion und der Höhe der Grundzustandsenergiebarriere auf. Dies führt dazu, dass im Gegensatz zu TBA/Au(111) bei den Systemen TBI/Au(111) und TBS/Au(111) keine photoinduzierte Isomerisierung beobachtet werden kann.

Die Ergebnisse dieser Arbeit demonstrieren, dass die Adsorption der hier verwendeten molekularen Schalter zu einer grundlegenden Änderung ihres Schaltverhaltens führt. Diese resultiert aus der Adsobat-Substrat Wechselwirkung welche in zwei Hauptkomponenten, die elektronische Kopplung und sterische Effekte, unterteilt werden kann. Die elektronische Kopplung ermöglicht einerseits einen schnelleren Zerfall des angeregten Molekülzustands und führt so mitunter zu einer Abschwächung oder Unterdrückung des photoinduzierten Schaltens. Zum anderen eröffnet diese Kopplung neue Anregungskanäle über substratvermittelte Prozesse. Die sterischen Effekte hingegen schränken die molekularen Freiheitsgrade ein. Dies kann in einer Unterdrückung bestimmter, für die Isomerisierung notwendiger, Reaktionspfade resultieren, so dass ein Schalten unmöglich wird.

Contents

List of Figures

List of Tables

1 Introduction

Motivation

Why investigate molecular switches on surfaces

In the second half of the past century the development of semiconductor based transistors allowed to significantly reduce the size and the manufacturing costs of electric circuits. This initiated a technical revolution which introduced an increasing number of electronic devices into every day life. Their performance is mainly determined by the density of circuits fit onto a single chip. Thus it has been a major goal to further miniaturize those components. In 1965 Gordon E. Moore predicted that due to technological advances the average number of transistors per unit area would double every two years. This prophecy, well known as Moore's law, soon became a guideline for developers and has proven to be right well into the current millennium. Continuing at this speed the size of the smallest electronic components will have to reach an atomic scale within the next 10 - 20 years. However the availability of affordable devices is limited since the development of new production techniques required for building such small functional units is very costly. Moreover the miniaturization will advance into regimes where no longer the bulk properties but surface and quantum size effects dominate the behavior of these components [Bar05].

A second, related field suffering from a similar problem in downsizing is the data storage. The common methods use ferromagnetic materials that record the binary information in domains of opposing magnetization. They are limited to an estimated minimum size of 10^5 atoms in order to maintain a sufficient thermal threshold which prevents a spontaneous change in the direction of the magnetization [Bar05].

Currently there is an intensive search for alternative methods to satisfy the increasing needs for both, data processing and data storage capabilities. A very promising approach which in recent years has moved into the center of attention is the field of molecular electronics. The fundamental idea of using organic molecules as rectifiers in electric circuits has already been proposed in the early 1970s by Aviram and Ratner [Avi74]. However it took another 20 years to overcome the experimental challenges and to finally obtain evidence by measuring the conductance of a single molecule [Ree97]. Sparked by the technical evolution of preparation and probing techniques the access to physical phenomena at the molecular level has rapidly increased in the past decade [Cun05]. The ultimate vision in this respect would be to develop a computer in which computing and memory operations are performed entirely by molecules. Its main advantage is evidentally the small size. Moreover by creating devices that employ photo-driven operations the heat load produced could be vastly reduced thus increasing their efficiency. In addition such processes mostly occur on a subpicosecond timescale which in return allows for equally fast processing speeds [Fer01].

Although there are no fully functional molecular devices yet, there have been successful demonstrations of wiring [Tan97] and moreover of data storage [Has90] and switching [Wil98]. The latter clearly require molecules which exhibit at least two distinguishable states. Examples for such a behavior can be found in many biological systems where they are, amongst others, of crucial importance for eye sight or allosteric regulation. Here the molecules commonly undergo a conformational change, e.g. an isomerization, induced by optical excitations with a high quantum yield. Hence they are ideal candidates to establish new light driven computing, memory and even sensor applications. In order to implement molecular switches into the respective complex functional devices they have to be separately and directly addressable. Consequently one has to confine them to a solid state surface. The interaction with the substrate however will influence the basic properties of the switch in many different ways: additional channels for charge transfer and energy dissipation are created, the degrees of freedom for nuclear motion are reduced, the electronic structure of the molecule couples to the substrate, the intermolecular forces are imprinted by the arrangement (ordering) on the surface. Thus the symbiosis of molecule and substrate can be expected to yield a new unique functional system. For the development of future applications it is of tremendous importance to gain a detailed understanding of the fundamental interactions involved. Eventually this knowledge will allow to design and manipulate the functionality of molecule based switching systems in almost any desired direction which goes far beyond the capabilities of the presently used semiconductor devices.

The investigated systems

In the framework of this thesis derivatives of the photochromic molecules azobenzene, imine and stilbene have been studied upon evaporation onto a noble metal surface. Photochromism refers to molecular systems exploiting two states having a different optical absorption behavior [Iri00]. Consequently the reversible conversion between these states is induced by light of different wavelength and is commonly accompanied by significant changes in the electronic and geometric structure. Therefore photochromic molecules are highly interesting systems for combining optics with molecular electronics and also with nanoscale mechanics [Fer01].

Figure 1.1 sketches the basic switching concept of such molecules. The first step is an optically induced direct transition from the ground state to an excited potential energy surface. In the ground state the two molecular configurations are separated by an energy barrier while the excited state is usually barrier free with an energy minimum at an intermediate configuration. Therefore the molecule starts to relax by engaging in a nuclear motion occurring on a femto- to picosecond timescale. The subsequent electronic decay leaves the system on top of the ground state energy barrier. From there it can continue to relax into its switched state. Accordingly the excitation process and the lifetime of the excited state are crucial for a successful photoinduced switching.

Contacting the molecule to a (metal) surface however will create new decay chan-

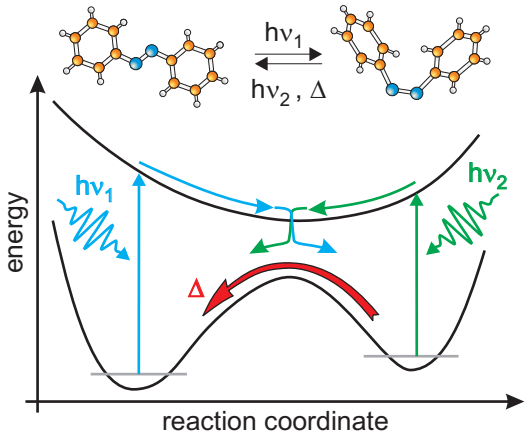

Figure 1.1: Photochromism scheme based on a simplified potential energy diagram of the the azobenzene cis-trans isomerization. The optical excitations of the trans and the cis isomer occur at different photon energies ($h\nu_1$ and $h\nu_2$). On the excited potential energy surface the relaxation to the intermediate conformation takes place on a femto to picosecond timescale. A thermally activated channel is available for the conversion from the metastable cis-isomer to the stable trans-isomer.

nels. Here the fundamental question is how the lifetime of the excited state and thus the photoinduced switching behavior is affected by the electronic coupling between adsorbate and substrate. On the other hand the surface confinement can lead to new excitation pathways via a substrate mediated charge transfer. A main goal of this thesis will be the identification of such channels as they will have a significant impact on the switching behavior. In this respect it is important to investigate the electronic structure of the adsorbed molecules because it yields valuable information on: (i) A possible change in the energetic separation of the molecular orbitals which is decisive for the intramolecular excitation energies. (ii) The overlap of electronic states from the substrate and the molecule required for the analysis of possible charge transfer reactions.

In addition to the previously discussed excitation scheme many of the photochromic molecules also exploit an unidirectional, thermally activated switching channel (see figure 1.1) [Fer01]. Its reaction kinetics is mainly determined by the accessible range of nuclear motion and the height of the energy barrier separating the different molecular configurations. Again the confinement to a surface is expected to influence these properties. To understand the respective substrate induced steric effects and the intermolecular interactions arising from a possible ordering at the surface is essential for a future functionalization.

The most challenging, but also the crucial part, in the investigation of adsorbed photochromic molecules is to find a system that is capable of switching. According to the above given considerations the choice of an appropriate adsorbate-substrate combination is influenced by two aspects: the electronic coupling and the binding to the surface. The latter can be controlled via the substrate properties. Here, a weak interaction is preferred to preserve the electronic structure of the molecule and to minimize steric hinderance. In this respect using noble metal substrates like Au(111) and Ag(111) is highly favorable. Simultaneously they exhibit a high density of electronic states required for a possible charge transfer reaction. The electronic coupling on the other hand will be controlled via the properties of the molecular switch.

For our initial experiments azobenzene has been chosen since it is a prototypical photochromic molecule [Fer01]. Its cis-trans isomerization is accompanied by large changes in the geometric and electronic structure as well as its dipole moment making it an ideal system for the investigation with spectroscopic methods. A main advantage of this molecule is the possibility to attach different molecular substituent groups without significantly altering its isomerization behavior. This enables a modification of the electronic coupling to the substrate e.g. by using bulky endgroups to increase the distance between the functional unit and the metal substrate. A corresponding approach has been used within this thesis since a strong coupling is believed to suppress the switching due to an enhancement if the relaxation channel. Therefore azobenzene is symmetrically substituted with four *tert*-butyl groups acting as spacer legs.

With imine and stilbene two isoelectronic molecules are available which likewise exhibit a photoisomerization but show differences in their respective excitation energies and the accessible range of molecular motion. They as well are substituted with four *tert*-butyl ligands and can be thus be used to study the influence of the functional group on the adsorption, the electronic structure and the isomerization behavior.

Why use 2-photon photoemission

The key to understanding photoinduced molecular switching (isomerization) reactions is the investigation of the underlying excitation mechanism and thus of the electronic structure. For the free molecule optical transitions are limited to direct (intramolecular) transitions between the occupied and unoccupied orbitals. Based on the corresponding absorption behavior it is generally possible to identify the involved electronic states. For surface confined molecules on the other hand this approach is not applicable as most of the light will interact with the substrate rather than the adsorbate. Moreover the number of available excitation channels is increased due to the additional possibility of charge transfer reactions. An ideal tool to investigate the respective electronic structure and gain access to the involved electronic transitions is the 2-photon photoemission (2PPE). It is the only method capable of simultaneously addressing the occupied and the unoccupied states of the adsorbate-substrate system.

It can well be assumed that most molecules exhibit deviations in the electronic structure of their switched and non-switched configurations. Therefore the application range of the 2PPE can be vastly extended. Here investigating the time and temperature dependent changes of the electronic structure allows to analyze the reaction dynamics with respect to the maximum isomerization yield under equilibrium conditions and the quantum yield of the different reaction channels but also with respect to thermodynamical properties like the energy barrier separating the isomers or the range of nuclear motion.

The photon energies required for 2PPE experiments are well in the range of the optical excitations commonly leading to the switching. Hence it should in princi-

ple be possible to use the probing method as stimuli and vice versa which is very beneficial for the accuracy of the measurements. Moreover 2PPE requires high laser intensities due to the non-linear nature of the underlying processes. Consequently this method is ideally suited for systems with low quantum yields.

A critical point of switching surface confined molecules is their interaction with the substrate and in particular the electronic coupling. Since the photoisomerization is based on the excitation of the molecule a fast decay will lead to a quenching of this process. In return the lifetime of a molecular state can yields valuable information to elucidate its contribution to the switching reaction. Here again the 2-photon photoemission proves to be an excellent method as it has the potential to investigate electronic decay processes on a femtosecond timescale.

How this thesis is organized

An overview over the general concepts of molecular switches will be given in chapter 1. Here we will present useful considerations regarding the specific molecules but also regarding the noble metal substrates used in the framework of this thesis. Background knowledge is supplied for the electronic structure and the elementary electron dynamics at metal-molecule interfaces. The final part of this chapter introduces the concepts of the 2-photon photoemission as our main spectroscopic method used for the analysis of the electronic structure and thus the photoisomerization processes.

In chapter 2 we will present the experimental setup of the laser system and the ultra high vacuum chamber. Particular attention is given to the principle of the time-of-flight spectrometer used for the 2PPE measurements. A further topic will be preparation of the sample including the adsorption of the molecules via chemical vapor deposition.

The discussion of the molecules is started in chapter 3 with the azobenzene derivative on the Au(111) substrate. At first we will give a detailed overview over the electronic structure followed by the analysis of the photoinduced switching mechanism. As will be shown, the excitation mechanism via intramolecular transitions is quenched and a new substrate mediated process dominates the photoisomerization. A second major part is the investigation of the thermal behavior in terms of an unidirectional back switching channel and a thermally assisted photo induced reaction.

To elucidate the influence of the substrate we switched from a Au(111) to a Ag(111) substrate. The corresponding results for the azobenzene derivative are presented in chapter 4. They show that indeed the role of the substrate and especially the role of its electronic structure is very critical to the success of the substrate mediated photoisomerization.

Finally, in chapter 5 we return to the gold substrate and investigated the switching behavior of the isoelectronic derivatives of imine and stilbene to analyze the influence of different functional groups. Again we start with discussing the adsorption behavior and the electronic structure of the individual systems. It is followed by a comparison of the three molecule-metal systems and a thorough analysis why only the azobenzene derivative is capable of preforming a photoisomerization.

2 Theoretical Background

This chapter introduces the fundamental theoretical concepts for the present work on the isomerization behavior of adsorbed molecular switches.

At first the basic properties of the photochromic molecules studied in this thesis are discussed. After a general introduction we will focus in particular on the isomerization mechanism and the underlying excitation schemes as derived from experiments in the gas phase and in solution. Furthermore we will address the range of possible interactions resulting from the deposition of the molecules onto a metal surface, e.g. electronic coupling, binding and the adsorbate induced work function shift.

Secondly the electronic properties of the noble metal substrates Au(111) and Ag(111) are discussed. They are of great interest for possible charge transfer scenarios. Moreover a detailed knowledge of the electronic structure is beneficial for the analysis of the 2-photon photoemission spectra. Of special interest in this respect are also states arising from the potential at the various interfaces, viz. at the metal-vacuum and the metal-molecule interface.

Finally the basic principle of the 2-photon photoemission and the thermal desorption spectroscopy are presented. The techniques are our main tools for the investigation of the absorption behavior and the electronic structure.

2.1 Molecular switches

The term molecular switch commonly refers to a system of at least two stable or meta-stable states which differ in their physical properties [Fer01]. It requires a reversible and moreover a controllable interconversion initiated by an external stimulus such as e.g. optical excitations, magnetic or electric fields or pressure. In most cases the switching evokes a change in the molecular conformation which is accompanied by a modification of the electronic structure. This will lead to differences in the quantum yield, the absorption and emission behavior and the dielectric properties of the molecules. Furthermore the distinct molecular arrangements can exploit differences in their dipole moment influencing their magnetic properties and also the intermolecular dipole interactions.

Of high interest for possible applications are photochromic molecular switches. These are systems which take advantage of the different absorption spectra of the two configurations [Dür03]. Consequently the direction of the conversion can selected via the wavelength of the electromagnetic radiation (see figure 2.1). Well known examples in this respect are the isomeric molecules azobenzene, imine and stilbene which have been studied within the framework of this thesis. Their individual properties are of interest for the comparison between free and surface bound molecules and will be presented in the following.

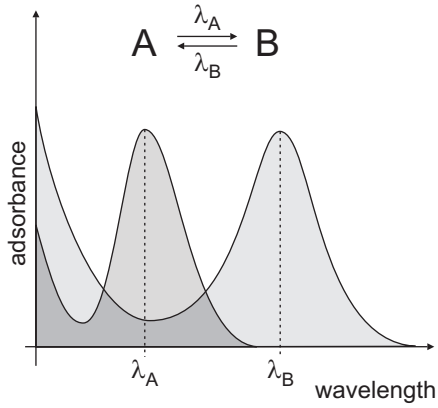

Figure 2.1: Photochromism. Adapted from ref. [Fer01]

2.1.1 Azobenzene

One of the most prominent examples of a photochromic switch is azobenzene which is composed of two phenyl rings which are connected via a double bonded nitrogen bridge, the so-called azo-group. It has been extensively studied in solution [Arm95] [Näg97] [Sat03], in the gas-phase [Fan90] and discussed in numerous theoretical publications [Cat99] [Che03] [Fuc06] [Mon82]. Azobenezene is a stereo-isomeric molecule. In its trans form both phenyl rings are located at different sides of the molecular axis along the azo-group (see figure 2.2). This configuration is planar and due to its high symmetry exhibits a vanishing dipole moment. The cis form on the other hand is three-dimensional due to steric effects between the phenyl rings. Consequently their planes are rotated by 60° with respect to each other. Moreover the interaction of the phenyl rings prevents a complete electronic relaxation leading to a cis ground state energy which is 600meV above the energy of the trans-isomer.

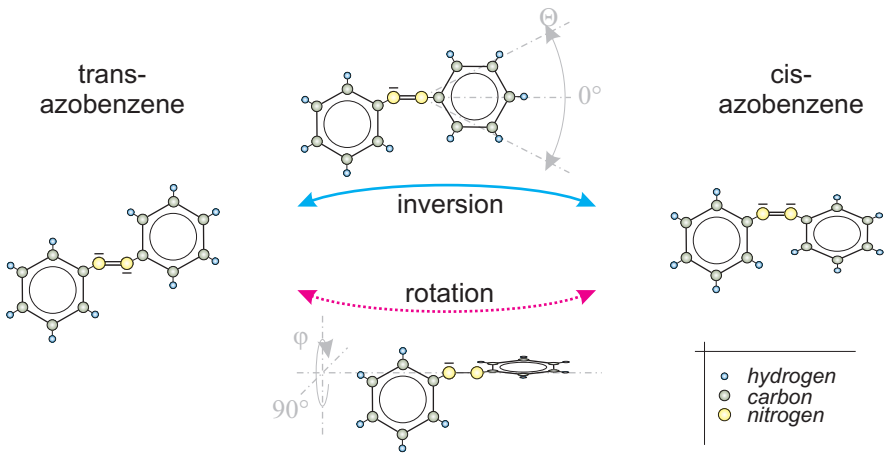

Figure 2.2: Geometric configuration of the two azobenzene isomers and the corresponding transition pathways. The double bonded azo group creates a rigid connection between the two phenyl rings. It has to be broken, e.g. by a photo excitation, to enable a rotational motion. Hybridization of the nitrogen valence orbitals creates a second channel for the isomerization. Here the bond to the phenyl ring loses its directionality enabling an inversion.

The cis-azobenzene has a dipole moment of ≈3 Debye perpendicular to the molecular axis resulting from the two lone electron pairs located at the same side of the nitrogen double bond [Fuc06] [Ber41].

Two of the cis-trans isomerization pathways for azobenzene are depicted in figure 2.2. The first is an inversion of the phenyl ring induced by the excitation of an electron from the nitrogen lone pair which leads to a sp^3-hybridization of the the valence shell. The second pathway is a rotation around the azo-group axis. Here the double bond between the nitrogen is broken by the optical excitation of an electron into the lowest unoccupied molecular orbital (LUMO) enabling the respective conformational change. In solution the transformation occurs on a timescale of ≈170fs and is thus one of the fastest isomerization reactions known [Näg97]. A third optically induced pathway, viz. a concerted inversion, has been proposed by Wei-Guang Diau taking into account a combination of several molecular motions [WGD04]. Note, that there is an ongoing discussion which of these possible channels is actually involved in the isomerization of azobenzene.

Despite this controversy it is a well known fact that the two above mentioned excitations are involved in the switching. In principle the corresponding transitions between (i) the lone pair orbital and the LUMO and (ii) the nitrogen double bond orbital and the LUMO can be observed for either of the azobenzene isomers. However they exhibit significant differences in their respective photon absorption efficiencies [Näg97]. At wavelength around 320nm, inducing transition (ii), the excitation of the trans isomer is strongly favored. The situation is vice-versa at wavelength around 430nm (transition (i))where the absorption and thus the excitation efficiency is higher for the cis isomer. Consequently the isomerization of azobenzene is wavelength selective, hence it can be driven in different directions using distinct photon energies.

A simple potential energy diagram depicting the photoisomerization process is sketched in figure 2.3. It also shows the energy barrier between the ground state potential wells of the trans and the cis isomer which can not only be overcome by optical excitations but also by thermal activation. Since the ground state energy of the cis azobenzene is increased with respect to the trans isomer this process is unidirectional. Experiments in solution [Hag08a] and quantum-chemical calculations [Dok09b] yield a corresponding barrier height of 1eV.

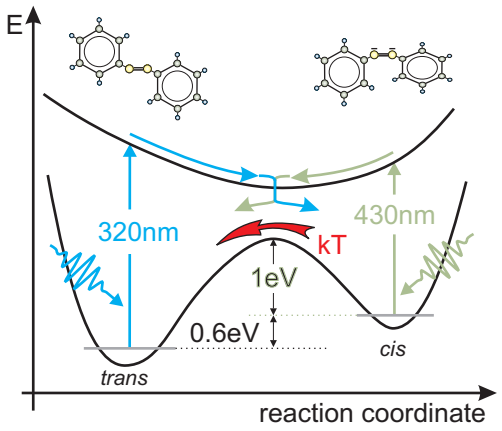

Figure 2.3: Azobenzene isomerization.

2.1.2 Imine

A second stereo-isomeric molecule used within the framework of this thesis is imine. Its functional group, N=C-H, is isoelectronic to the N=N azo-group of the previously introduced azobenzene. The nitrogen lone pair of the imine forms a conjugated system with the adjacent phenyl ring resulting in a twisted geometry [Koz93][Fig90]. A sketch of the molecule is given in figure 2.4. It shows the main angles needed to describe its geometry. The corresponding values for the cis and the trans isomer are obtained from ab initio DFT calculations [Gae07]. Due to the asymmetry of the imine both its isomers show a dipole moment which differs only slightly from the cis (2.1 Debye) to the trans configuration (1.82 Debye) [Wei71].

The cis-to-trans photoisomerization of imine at a wavelength of 313nm occurs predominantly as an inversion of the phenyl ring around the nitrogen [Lew82] [Wei71]. A rotational pathway induced by a breaking of the double bond is reported as well but appears far less efficient [Gae07]. The transformation of the cis isomer to the thermodynamically more stable trans isomer can either be induced by illumination at larger wavelength or by heating of the molecule. Here the ground state energy barrier has a height of ≈750meV [And65] [Wei71].

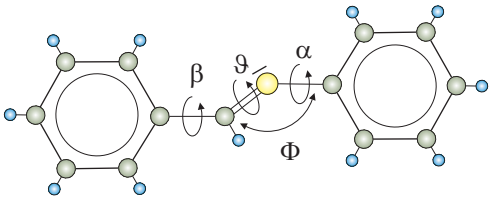

Imine

angle in °	ϑ	Φ	α	β
trans	177	120	39	0
cis	4	234	76	13

Figure 2.4: Geometric structure of imine. The three dihedral and the bending angle have been obtained from reference [Gae07].

2.1.3 Stilbene

Stilbene completes the group of isoelectronic molecular switches investigated. Correspondingly its functional unit consist a H-C=C-H group. Like azobenzene the thermodynamically more stable trans configuration of stilbene is almost planar with a vanishing dipole moment whereas the cis isomer is twisted [Han02] [Wal91]. The angle between the planes of the phenyl rings is 43° and can again be assigned to steric effects.

The switching mechanism of stilbene is quite interesting since it displays a meta stable, excited trans state. Here the corresponding excited potential energy surface has a small dip in the Franck-Condon region of the optically induced transition as can be seen in figure 2.5. The required activation energy is provided by the vibrational modes of the molecule. Subsequently the molecule rotates around the axis of the functional group until it reaches the global minimum. In the final step it is electronically relaxed onto the top of the ground state barrier from where the reaction branches into a cis and a trans pathway. A detailed review on this topic is given in [Wal91]. For the trans isomer the photon absorption spectra has a maximum at 313nm. The corresponding spectra for the cis-stilbene is shifted to shorter wavelength and exhibits a lower efficiency. In contrast to azobenzene and imine there is no thermally activated isomerization possible as the ground state barrier has a height of >3.5eV. It can however be catalytically lowered.

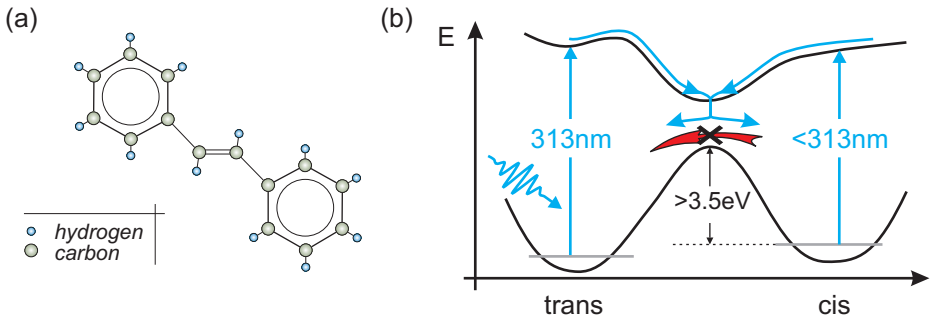

Figure 2.5: (a): Geometric structure of Stilbene. **(b):** Schematic depiction of the isomerization potential energy landscape after [Wal91]. The thermally induced cis-to-trans isomerization is suppressed due to height of the barrier.

2.1.4 Adsorbed molecular switches

Bringing molecules close to a metal substrates leads to a complex interaction which will influence the basic properties of both components. In general the binding to the surface can be classified either as physisorption or as chemisorption. The latter is present when the molecule and the substrate create a chemical bond through hybridization of the respective orbitals and bands. This is commonly the case in the limit of strong interactions [Lin06]. Physisorption on the other hand refers to systems which interact only weakly though van-der-Waals or dispersive forces [Zan88]. Here

a polarization of the molecule is caused by (i) the classical image potential created by the valence electrons in front of the metal surface [Lin06] and (ii) a quantum mechanical exchange-correlation force [Bag08]. In combination with the repulsive forces, due to equally charged particles, a shallow potential well is formed a few angstroms in front of the surface.

The control of the binding to the surface is of eminent importance for the switching behavior of adsorbed molecules. Especially in cases where the conformational changes involve extended nuclear motions e.g. for adsorbates exhibiting a cis-trans isomerization like azobenzene. If a chemical bond is created between orbitals located at its phenyl rings and the (metal) substrate it can well be expected to fix the molecule to the surface and suppress the switching. Therefore it is necessary to avoid a strong binding of atomic groups which require a rearrangement in the switching process. Nevertheless it can generally be assumed that the confinement to the surface, even in the limit of weak interaction, will reduce the molecular degrees of freedom based on steric effects. These are not only induced by the presence of the substrate but also by the intermolecular interactions.

The adsorption of molecular switches has several consequences for the electronic properties of the (metal) substrate and the adsorbate. A first well known phenomena is the change in the metal work function caused be the above discussed dipole induced within the molecules [Cri02] [Bag08] [Wit05] [Yam07]. However the magnitude of this effect is only secondary to the net dipole moment of the adsorbed species [DR05]. As previously mentioned, the conformational change of isomeric molecular switches is commonly accompanied by a change of their intrinsic dipole moment. Hence a successful switching of surface bound molecules is expected to influence the work function of the system.

A second important aspect of the adsorption is the energy level alignment which is decisive for chemical reactions. Again the example of azobenzene can be employed. Its photoisomerization requires a resonant electronic transition. If the adsorption alters the electronic structure of the molecule this will consequently lead to a modification of its absorption behavior. Although there have been promising attempts to describe the energy level alignment in dependence of the substrate and molecular electronic properties the mechanism is still not very well understood [Kaw08] [Váz07] [Vaz07b]. Nonetheless, it can be expected that in case of a weak electronic coupling the molecular states experience only slight deviations with respect to the free molecule.

One of the main questions addressed in this thesis is the influence of the substrate on the isomerization behavior of the adsorbed molecules. Two aspects have been already mentioned above, viz. steric hinderance and a shift of the intramolecular excitation energies required. In addition the (metal) substrate is known to open up new pathways for chemical reactions based on a charge transfer [Guo99] [Dai95] [Zhu94] [Tho06] [Osg06]. Principally it should be possible to employ these for the switching of the molecules as well. On the other hand it has to be considered that the electronic coupling also creates new decay channels which can lead to a faster relaxation of excited molecular states. This in return may reduce the probability of

the switching since the respective molecular motion requires timescales in the range of a few hundred femtoseconds up to several picoseconds .

Evidence for a charge transfer induced switching reaction has been given by STM measurements on the azobenzene derivative Disperse Orange 3 adsorbed on Au(111) [Hen06]. Although the injection of the electrons occurred through the tip of the STM and has been enhanced by applying a bias voltage it demonstrated the general possibility of an excited isomerization process that has not been induced by an optical transition. A second non-optical mechanism which has recently been discovered is the electric field induced isomerization [Ale06]. Here again an azobenzene derivative has been adsorbed on Au(111) substrate. The corresponding electric field has been created with the tip of an STM and is believed to deform the potential energy landscape along the isomerization pathway [Gri08].

Given the complex interaction between the molecule and the substrate it is very challenging to predict which systems support a switching of the adsorbed species, especially if one wants to take advantage of the alternative excitation pathways offered. Based on the above discussed properties a preferable approach is to choose a weak coupling because: (i) In this regime the steric hinderance is expected to have less impact, since no molecule-substrate bond breaking is required for a conformational change. (ii) The charge transfer times are expected to be reduced. This creates the opportunity for molecular excitations with lifetimes sufficient to perform a switching. A tuning of the adsorbate-metal interaction can be achieved either by the choice of the substrate or by variation of the molecular properties via substituting different atomic groups.

2.1.5 Tuning of the isomerization properties

As pointed out before, a great advantage of molecular switches is the ability to tune their properties by attaching complementary molecules or substituting a part of the initial building blocks. Here the aim of the modification determines the choice of molecules. A very common approach is the use of charge donating substituents. They of course will interfere with the local charge distribution in the switch and initiate a redistribution. Such a case has been studied by Blevins et al. for azobenzene symmetrically substituted with different amino compounds [Ble04]. The results

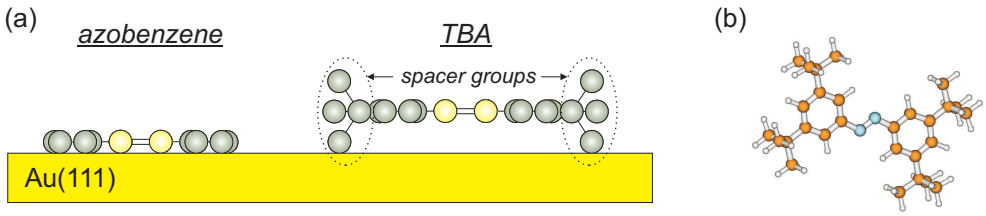

Figure 2.6: Concept of molecular spacer groups. **(a):** Schematic comparison of flat adsorbed azobenzene and its derivative tetra-*tert*-butyl-azobenzene (TBA). Lifting the functional unit is expected to decrease the electronic coupling. Also a weaker bonding of the phenyl rings to the surface is desired. **(b):** Geometric structure of TBA.

show an obvious variation in the ground state barrier height and the branching ratios of the optical isomerization channel, hence, the isomerization yield is altered. Similar results have been obtained for the asymmetric case of push-pull substituents [Sch04].

A second prominent option is the use of rather neutral groups to conserve the initial properties. Usually the main goal in those cases is to reduce the interaction with the environment [Sch08a]. A similar approach is used in this thesis where we use *tert*-butyl substituted derivatives of the above introduced molecules azobenzene, imine and stilbene. Due to the bulky nature of those groups they are very well suited as spacer legs increasing the distance of the inclosed molecule to e.g. the substrate (see figure 2.6) [Mor01][Jun97]. Moreover they interact only weakly with the electronic states of the functional group and thus the initial switching properties are conserved. From this substitution we expect (i) a weaker bonding of the phenyl rings to the surface and (ii) a reduced electronic coupling between the functional group and the substrate.

2.2 Electronic structure of the metal substrates

A key factor to many properties of the molecule/metal system is the electronic structure of the substrate surface. It is e.g. decisive for the binding, the charge transfer from and to the adsorbate and also for the respective electron dynamics. These properties on the other hand are of crucial importance for a successful switching process. Thus the proper choice of suitable substrates benefits from a detailed knowledge of the corresponding electronic structure. Furthermore it is a inevitable requirement for analyzing and understanding the behavior of the adsorbed molecules.

A main reason for choosing Au(111) and Ag(111) in this thesis has been their noble metal character. The inertness of the respective surfaces implies a weak interaction with the adsorbed molecules. This is very desirable as one aims to alter their electronic structure as little as possible. In the following we will give an introduction on the basic properties of both substrates. A complete overview of the electronic states is found in table 2.1.

2.2.1 Au(111)

Gold, unlike any other noble metal shows a distinct surface reconstruction of its Au(111) surface. In the $[1\bar{1}0]$ direction of the top layer 23 atoms are fit onto 22 latice sites. The resulting stress, based on this mismatch, is compensated by the creation of altering fcc and hcp sub-domains as shown in figure 2.7. The corresponding $(22\times\sqrt{3})$ unit cell creates 3 domains which differ by an angle of 120°. Two of these combine to form a zig zag pattern commonly known as the herringbone structure [Bar90]. It is believed to further lower the surface energy [Nar92]. The reconstruction of the Au(111) directly influences the electronic structure creating band gaps in the surface Brillouin zone [Rei04]. However the corresponding effects are rather small and require a high experimental resolution for detection.

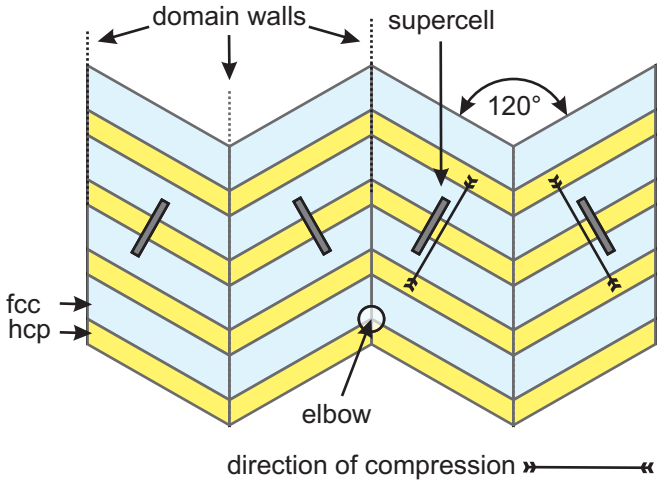

Figure 2.7: Schematic depiction of the herringbone reconstruction as found on a Au(111) surface. The supercell structures are composed of altering domains exploiting hcp and fcp stacking. Due to the compression along these cells a superstructure is created creating herringbone like domains tilted by 120° [Nar92].

A second interesting feature of the lattice mismatch is found at the crossing of the unit cell domains with the domain walls of the fcc-hcp stacking. At every other of these so-called elbows a pair of atoms is found having 5 and 7 bonds respectively instead of the usual 6. This creates favorable adsorption sites for molecules and atoms.

The work function of the Au(111) surface is reported between 5.3 and 5.55eV [Han78][Pan95][Reu96]. A theoretical band structure of the gold by Eckhard et al. [Eck84] is presented in figure 2.8. The low reactivity of the gold surface is mainly attributed to its filled d-shell [Ham95]. We find the corresponding bands in the region 2-9eV below the Fermi level as indicated in the band structure diagram. The d-band overlaps with a hybridized band of s and p-orbitals. It extends from 4eV below the Fermi level to ac couple eV above the vacuum level. For the (111) surface of the gold it exploits a projected band gap in the region of -0.6 $< E_B <$ 3.6eV as depicted in the graph [Woo86]

Within this gap a new state evolves which is confined to the surface and decays into the bulk as well as into the vacuum. This surface state(SS) has a reported binding energy in the range of $-0.45 < E_B < -0.38eV$ and an effective mass of $m^* = 0.255m$ [Cou86][Nic01]. The latter value has been obtained from angle resolved photoemission experiments. Besides the delocalization in the surface plane a splitting of the SS is observed, resulting from spin orbit interactions of the sp-state at the vacuum interface [Rei04]. A second surface induced state has been found by Woodruff et al.[Woo86]. It is, in agreement with electron tunneling spectroscopy [Jak75], assigned to an image potential state (n=1) at $E_B = 3.6eV$ coinciding with the upper edge of the band gap. Higher lying states of the corresponding Rydberg series have been identified in [Reu96].

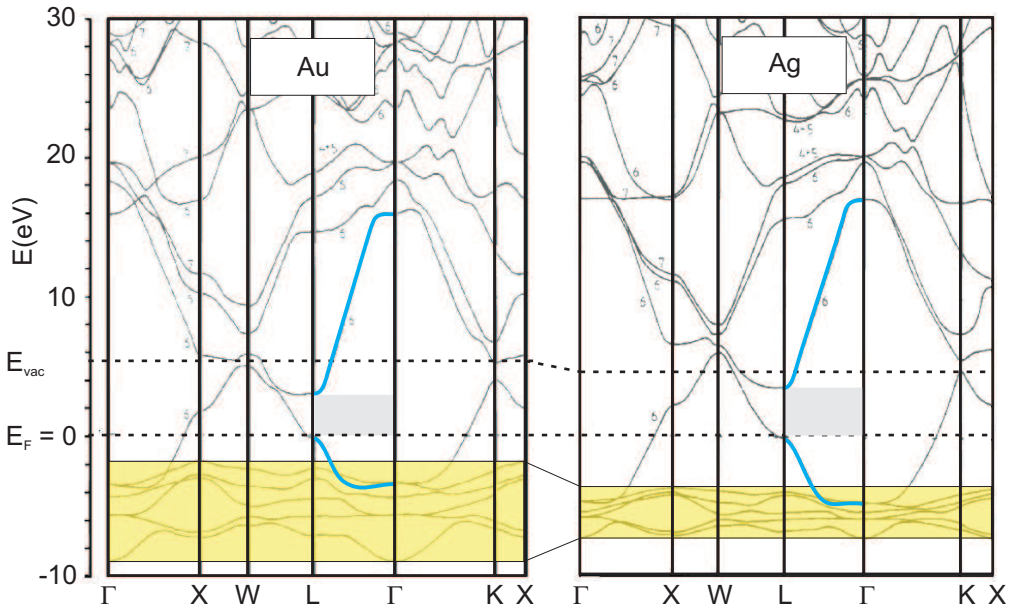

Figure 2.8: Theoretical band structures of gold and silver taken from [Eck84].The d-band region which plays a key role in charge transfers discussed in this thesis are highlighted in yellow. Further attention is given to the band gap (gray) and the sp-bands (blue) along the ΓL-line. The here drawn vacuum level indicates the work function of the respective (111) surfaces.

A number of studies also showed a temperature dependence of the electronic structure of gold which is mainly attributed to heat induced lattice expansion [Pan95]. This structural change reduces the band gap with a rate of $6.5 \cdot 10^{-4} eVK^{-1}$ [Win76]. It also affects the binding energy of the surface state as has been measured by Paniago et al. yielding a shift of $\Delta E_B = 2.6 \cdot 10^{-4} eVK^{-1}$. This effect is crucial to this thesis as some important aspects of the trans-cis isomerization have to be investigated in respect to their thermal behavior.

2.2.2 Ag(111)

Contrary to gold no reconstruction is observed for the Ag(111) surface. Cutting the bulk crystal in the respective plane exposes a simple fcc type ordering. Having a valence configuration of $4d^{10}5s^1$ its low reactivity can again be explained by the filled d-bands. Indeed the overall electronic structure is quite similar to the gold as can be seen in figure 2.8. This leads to a number of equal properties. A main difference however can be found in the structure of the d-bands. In silver those are dispersed over a smaller range extending only from 3.8 - 7.5eV below the Fermi level. Due to the large density of states associated with the d-bands they are highly interesting for the interaction with adsorbate states. Thus the difference in positioning and width between gold and silver gives us an excellent opportunity to tune this property.
The s and p states of the silver are hybridized to form the strongly dispersing sp-band

as highlighted in the graph. It is separated by a projected band gap in the region of $-0.3 > E_{gap} > -3.9eV$. The magnitude of the gap is temperature dependent having a slope of $4.9 \cdot 10^{-4} eVK^{-1}$ [Win76].

Woodruff et al. report a work function of 4.56eV for the Ag(111) surface [Woo86]. In this orientation one also finds a surface state with a binding energy of -64meV [Rei01]. It displays a similar temperature dependence as its Au(111) counterpart [Pan95]. Also a series of image potential states is detected at the clean surface with the lowest one being 770meV below the vacuum level [Gie85].

At this point we shall point out a special peculiarity of photoemission experiments performed on the Ag(111) and Au(111) metal substrates. Due to the strong dispersion of the corresponding sp-bands the intraband excitation from the occupied to the unoccupied part is highly momentum selective [Mil96]. Hence in dependence on the photon energy the transition will favorably take place at some point along the ΓL-line where a direct transition is possible. In this case the energetic position of the sp-band in respect to the Fermi level appears to be shifting with the excitation energy. This behavior can be found in the 2-photon photoemission as well as has been shown for Ag(111) [Pon05].

	Au(111)	Ag(111)
work function	5.3 - 5.55	4.56
d-bands	-2.0 to -9	-3.8 to -7.5
projected band gap	-0.6 to 3.6	-0.3 to 3.9
surface state	-0.45	-0.06 - -0.12
image state (n = 1)	4.75	3.72

Table 2.1: Binding energies in eV with respect to the Fermi level for key electronic features of the Ag(111) and Au(111) noble metals. Values taken from [Eck84] [Woo86] [Win76] [Cou86] [Reu96] and references therein.

2.3 Electronic properties of metal interfaces

The physical properties of organic-metal interfaces are one of the most discussed issues in recent surface physics and chemistry. Although a large number of systems have been experimentally investigated and numerous theoretical work delivered promising approaches there has not yet been a model capable of giving a general description. The problems become quite obvious when looking at the different contribution like orientation of the molecule, binding energies, charge transfer, charge redistribution, substrate-adsorbate wave function overlap, to name only a few. Giving a complete introduction to this topic would go beyond the scope of the thesis. Nevertheless understanding the switching mechanism of adsorbed molecules will be closely connected to understanding their electronic structure. In this context a short introduction to the basic concepts of the interface induced states, the charge transfer

from and to the adsorbate and the main decay channels in solids will be given in this section. For more detailed information the reader is referred to the reviews given in [Bru07]and [Lin06].

2.3.1 Image potential and interface states

The surface of a metal gives rise to new electronic states located in the interface region to the vacuum. A specific kind of those viz. the image potential states (IPS) have attracted a lot of interest in recent years [Hot07]. Their origin is motivated by the interaction of an electron placed in front of a sample and the surface. Due to a polarization in the top most metal layers it sees an attractive coulomb potential of the form[1]:

$$V_{IP}(z) = \frac{-e^2}{4z} \tag{2.1}$$

where z is the distance from the charge to the surface. In the classical picture this is described by an image charge having an opposite charge and sitting at the mirrored position (-z) inside the metal (see figure 2.9). If the substrate exploits a projected band gap close to the vacuum level the electron is trapped within the image potential. The possible energetic levels form a Rydberg like series of

$$E_n = \frac{-0.8504}{(a+n)^2} \text{ with } n = 1, 2, 3... \tag{2.2}$$

given in eV with respect to the vacuum energy (see figure 2.10). Here n denotes the main quantum number of the system and a is the so called quantum defect. It is related to the electronic structure of the substrate [Smi85]. The electron is confined perpendicular to the surface but is enabled to move freely in the lateral directions. Correspondingly the IPS exhibit a dispersion with an effective mass close to mass m_e of the free electron.

The wave function of an image state decays rapidly into the bulk if its energetic position is within the band gap of the substrate [Ech89]. On the other hand states above or at the the upper band gap edge show a wave function mixing with the bulk bands. For both cases the maximum probability density is in front of the surface. It is shifted further away from the crystal as the quantum number n increases. Simultaneously the bulk penetration depth of the IPS is reduced [Har97].

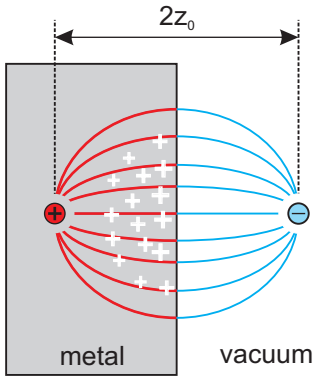

Figure 2.9: Image charge of an electron in front of a metal surface.

The differences in mixing with the bulk states create a high interest in image potential states as they present an excellent opportunity to study the relaxation behavior of excited electrons. Here it has

[1] in atomic units

been shown that states within the band gap have an extend lifetime due to a weak electronic coupling with the crystal [Wei02]. In contrast IPS coupling to bulk states have access to an increased phase space for particle interactions like the electron-electron scattering which leads to a much faster decay. In addition to the energetic position the localization of the wave function has to be considered when discussing the dynamics of excited electrons. As mentioned above the probability density shifts away from the surface as one moves up the Rydberg series. Consequently the electronic coupling and thus the lifetime is reduced, scaling in good approximation with n^3 [Ech00].

Adsorbate covered surfaces The properties of an image potential state, viz. its binding energy and lifetime, change upon adsorption of molecules. This can be attributed mainly to two reasons: One is the commonly observed change of the substrates work function which is accompanied by a change in the binding energy of the image state. A well known example is the xenon covered Cu(111) surface [Wol96]. Here the work function upon adsorption of a monolayer is lowered from 4.9 to 4.4eV. Simultaneously the n=1 IPS binding energy with respect to the Fermi energy is shifted from 4.08 to 3.69eV. Thus it is energetically separated from the lower conduction band edge at 4.1ev which leads to a lifetime increases by a factor of 4 [Wol96]. The second effect is the formation of a dielectric barrier by the molecular layers. This pushes the wave function of the IPS further away from the surface hence decreasing the overlap and increasing the lifetime [Lin96]. A discussion of different models describing the adsorbate induced changes on the image potential is given in [Hot07].

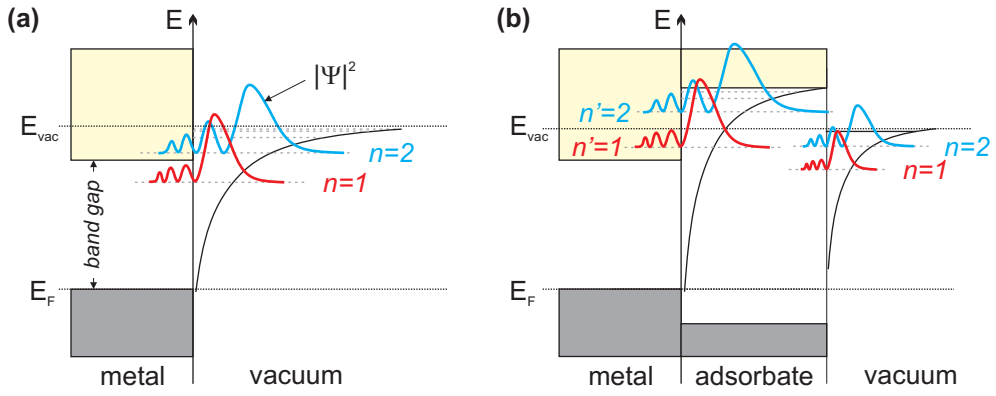

Figure 2.10: Schematic potential energy diagram for a clean (a) and an adsorbate covered metal surface (b), adapted from ref. [Güd05]. **(a):** The image potential at the metal-vacuum interface gives rise to a Rydberg-series of states (n=1,2,..). Their maximum probability density moves further away from the surface with increasing energy. **(b):** Adsorbate layers can give rise to a second potential and thus to another series of states (n'=1,2,..). The properties of these interface states are similar to the ones of the image potential states. For details see text.

In return the IPS can be used to analyze the morphology of the adsorbate due to its sensitivity to corrugations in the surface potential and the adsorbate thickness. A well suited example in this respect in the adsorption of cyclooctatetraene multilayer on Ru(001) [Teg05]. Here, two observations can be directly related to the characteristics of the IPS: the existence of an initially unordered coverage and the formation of 3D islands upon annealing. The former is associated to a significant broadening of the IPS resulting in a suppression of its photoemission signal. The latter is explained based on the invariance of the multilayer image state binding energies in respect to a stable bi-layer system.

Interface states Besides the local and energetic displacement of the image states the adsorbate layer can create new type of states. The basic idea is sketched in figure 2.10. Here the initial image potential as seen in scheme (a) is shielded by the dielectric adsorbate and pushed away from the surface (scheme (b)). A new potential,$V_{IF}(z)$, is created which is a superposition of an image potential due to a charge in front of the metal surface and the atomic potential of the adsorbate, V_{ads} [Güd05]:

$$V_{IF}(z) = V_{ads}(z) - \frac{-e^2}{4z} \tag{2.3}$$

Note that V_{ads} depends on the distance to the interface as well. This is easily understood as the electronic structure and thus the atomic potentials are subject to change by interaction with the metal substrate. Moreover the adsorbate exhibits a second interface viz. to the vacuum. Hence, in the limit of thin films, $V_{IF}(z)$ is also dependent on the layer thickness.

Similar to the image potential at the clean surface the new potential will give rise to bound states localized at the metal/ardsorbate interface. First evidence for the existence of such states has been given by the group of Höfer investigating thick argon films on a Cu(111) crystal [Roh05]. The results show a state confined in the plane parallel to the metal surface. In contrast to an IPS it is not pinned to the vacuum level of the sample but to the conduction band minimum (E_{CBM}) of the adsorbate crystal forming at high coverages. The corresponding energetic position (in eV) yield yet another Rydberg series given by:

$$E_{n'} = E_{CBM} - \frac{0.8504}{(a+n')^2}\frac{m_{eff}}{\epsilon^2} \text{ with } n' = 1, 2, 3... \tag{2.4}$$

Here a again denotes the quantum defect of the wave function matching at the interface whereas m_{eff} and ϵ are parameters describing the dispersion of the conduction band and the dielectric constant of the argon.

Brief outlook The above introduced interface states are very promising in respect to the investigation of charge transfer processes. This approach is especially interesting for the fields where one is rather interested in the dynamics at the buried

interface than in the interface to the vacuum. However thus far information is limited as most spectroscopic methods have no access to these states. Also in recent years the focus has been set rather on the investigation of the IPS.

Elucidating the electronic structure of different adsorbed molecular switches we were able to identify such interface states. Most interestingly they appear already at very low coverages below the monolayer. Moreover they appear very sensitive to the molecular orientation and configuration. Due to a different main subject of this work only a limited number of experiments have been performed on those states. Nevertheless, the above mentioned preliminary results strongly suggest to continue the investigation of those systems.

2.3.2 Substrate-adsorbate charge transfer

A crucial part of driving reactions involving surface adsorbed molecules is the excitation of their electronic states. In a free molecule the required wavelength for optically induced transitions lie in the visible and UV range. At these energies however optical excitations within the substrate will be favored over excitations within the adsorbate. The reason can be found in the discrete nature of the molecular transitions. Their energy window for resonant excitations is very narrow, slightly broadened only by the vibrational structure. In contrast a metal offers a large number of possible transitions induced by its band structure. Hence most of the light will be adsorbed by the substrate.

On the other hand the presence of the substrates opens up new channels for the excitation through an electron transfer from the crystal to the molecule [Zhu02][Gah04]. This leads to the deposition of an additional charge at the creating a so called negative ion resonance (NIR). Their excitation has to be distinguished based on two scenarios: In the first scenario the wave function of the molecule is spatially localized in front of the surface which is commonly the case for states within the projected band gap of the substrate. As depicted in figure 2.11 two excitation channels are available: (i) Resonant transitions from states which are likewise localized at the interface e.g. surface states. (ii) Indirect transitions via scattering of excited bulk electrons e.g. hot electrons. In the scenario the molecular wave functions mix with electronic states from the crystal. Here a resonant transition within the crystal creates an excited electron which propagates into the molecular resonance. The decay of the molecular states usually occurs via inelas-

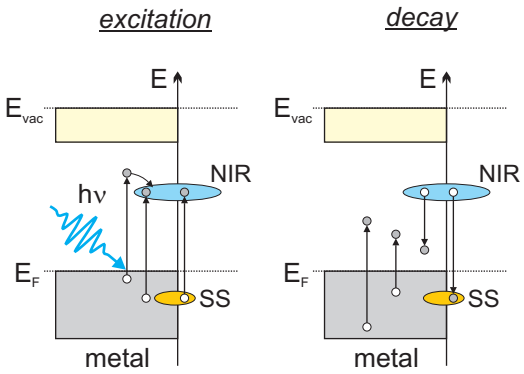

Figure 2.11: Charge transfer scenarios between the metal substrate and a molecular orbital: Excitation and decay of a negative ion resonance (NIR). Adapted from [Gah04].

tic scattering with electrons from the substrate (see figure 2.11) under simultaneous creation of an electron hole pair [Gah04].

2.3.3 Scattering processes in solids

In the following we will briefly describe the quasi particle interactions involved in the decay of excited states and thus in the charge transfer to and from adsorbate states. Those are classified as elastic and inelastic electrons-electrons (e-e)scattering and as scattering of electrons with phonons (e-ph) and defects [Ech00][Ech04][Chu06][Hai95].

Elastic electron electron scattering: An elastic scattering event between two electrons changes their momentum but conserves their energy. Hence a depopulation of a state can only be achieved by interband scattering. In any case the elastic scattering contributes to the destruction of the quasi particle phase relation viz. the dephasing.

Inelastic electron electron scattering: Inelastic scattering is the main decay channel for an excited state in solids. Due to the equal masses of the involved electrons the energy transfer is rather large. Usually the excited electron interacts with an electron of the Fermi sea which is excited and leaves behind an additional hole. Thus the scattering leads to a population decrease of energetic states far above the Fermi level whereas an increasing amount of so-called secondary electrons is created in the region close to the Fermi level.

Electron-phonon scattering: Since the energy of a phonon in the meV range is rather low the main impact of the electron phonon scattering is a change in the momentum of the electron. Due to the thermal occupation of the phonons this channel and thus the respective contribution to the decay is temperature dependent. In return e-ph scattering is the main relaxation pathway for low excitation energies like the secondary electron distribution created by the inelastic e-e scattering.

Electron-defect scattering: Lattice distortions, imperfections or even adsorbates lead to corrugations of the otherwise homogenous potentials at surfaces and in the bulk. The interaction of the electrons with those defects leads mainly to a change in their momentum while the energy remains constant in a first approximation.

2.4 Photoemission spectroscopy

Photoemission spectroscopy (PES) is a common method to investigate the electronic structure of solids. It is based on the photoelectric effect where the illumination of a sample leads to emission of electrons which can be detected and analyzed in the energy domain [Hüf95]. Using monochromatic light the PES can be used to map the distribution of occupied states. Here, in a simple picture the electron having a

binding energy of E_B adsorbs a photon with $E = h\nu$. If the energy transfer is large enough to overcome the potential barrier at the surface, viz. the work function Φ, it is ejected from the sample with a kinetic energy of:

$$E_{kin} = h\nu + E_B - \Phi \tag{2.5}$$

Note that for E_B different reference points are used throughout the literature. Within this thesis a consistent assignment to the Fermi level E_F is used. Hence for occupied states E_B is always negative. This choice is especially suitable for the energetic description and comparison of samples having different work functions.

Contrary to the simple one electron picture many body effects have to be considered for the real solid. Especially the screening which takes place after the initial N particle state is converted to a N-1 particle state upon photoemission. However, a justification of the above approach is given by the sudden approximation. It assumes that the systems response, viz. the rearrangement of the charges, is much slower than the actual process of the photoemission [Kor06].

A second quantity accessible in PES experiments is the dispersion of bands and states. For photon energies $h\nu << m_e c^2$ the momentum of the emitted electron is parallel to the surface, $k_{||}$, is conserved. In the perpendicular direction on the other hand it experiences a momentum change due to the potential barrier at the interface. Hence $k_{||}$ is recorded as a function of detection angle and the kinetic energy of the electrons (see fig. 2.13):

$$k_{||}(\alpha, E_{kin}) = sin\alpha\sqrt{\frac{2m_e E_{kin}}{\hbar^2}} \tag{2.6}$$

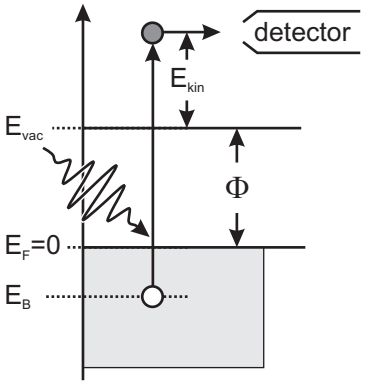

Figure 2.12: Direct photoemission scheme. The electron absorbs the energy of a photon and is excited above the vacuum level. A detector records the excess energy in terms of E_{kin}.

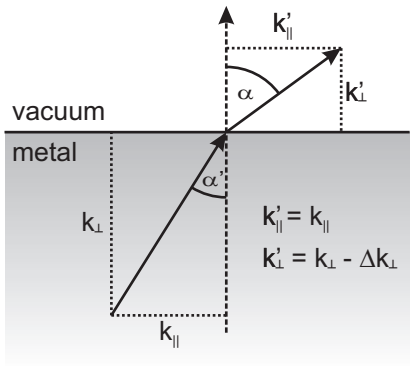

Figure 2.13: Electron emission in off-normal direction. The momentum parallel to the surface is conserved. Its perpendicular component is altered by the sample work function.

2.4.1 One and three-step model of photoemission

A detailed analytical description of the photoemission process yields a complicated many body problem. To simplify this problem two models have been proposed using different approaches [Hüf95].

Three-step model: The three step model separates the emission of the electron in three distinct parts.

1. In the first step the electron is locally excited by the photon within the band structure of the solid. Due to the negligible momentum of the photon the transition is vertical, not changing the momentum of the electron.

2. The second step describes the transport of the electron to the surface. It is a result of the scattering with defects and other electrons. These collisions have two important implementations. (i) They are the limiting factor of the escape depth. In dependence of the energy and the material values between 5 and 100Åcan be observed [Sea79]. (ii) Electrons experiencing energetic losses by the scattering create a background to the photoemission signal

3. The electron leaves the sample conserving parallel momentum and altering its momentum perpendicular to the surface due to the work function (surface potential).

In this picture the current of photoemitted electrons, I_{PES}, is dependent on the distribution function F, the density-of-states (DOS) for the initial (i) and the final (f) state, the transmission function T, the transition matrix elements M_{if} and an exponential weighing of the escape depth [Sch03]:

$$I_{PES}(E_{kin}) = T(E_{kin})D(E_B)D(E_B + h\nu)M_{if}\int_0^\infty F(E_B)e^{-z/\lambda_{PES}}dz \tag{2.7}$$

One-step model: In this approach the ejection of an electron into the crystal is described in the inversed time-domain. In the vacuum the electron can be represented by a plane wave whereas in the solid sample its wave function decays exponentially due to scattering events. The corresponding penetration depth is equal to the inverse escape depth of the optical excitation. The electron wave function is now overlapped with the Bloch wave of an unoccupied final state. This step is motivated by the quantum dynamical description of low energy electron diffraction (LEED), hence these final states are commonly referred to as inverse-LEED-states (Ψ_{LEED}) [Feu78][Mah70a][Mah70b].

As a result of this depiction the photoemission can be described as a one step transition from an initial state into this coupled final state. Here the photocurrent I is proportional to:

$$I(E_{kin}, k_{||}) \propto \sum |\langle \Psi_{LEED}(E_f)|W|\Psi_i\rangle|^2 A(k_{||}, E_B) \tag{2.8}$$

The interaction of the laser vector potential $\vec{A}$ with the electrons is expressed as the operator $W = \vec{A} \cdot \vec{p} + \vec{p} \cdot \vec{A}$. Using the dipole approximation and first order perturbation theory it is transformed to

$$W = A_0(E_f - E_B)\vec{e}\vec{r} \tag{2.9}$$

with A_0 the amplitude of the light wave, $\vec{e}$ its polarization vector and E_f and E_B the energies of the final and initial states respectively.

2.4.2 2-photon-photoemission

A main shortcoming of the direct photoemission, or one-photon photoemission, is its inability to resolve the unoccupied region of the electronic structure. This however is a crucial part in the investigation of surface adsorbed molecular switches. An alternative is the inverse photoemission. It is based on the injection of monochromatic electrons into the unoccupied states. In a subsequent step they relax under the emission of a photon yielding an energy spectrum. This method, on the other hand, suffers from a lack of sufficient count rates and energy resolution [Smi88]. Moreover it requires additional (spectroscopic) methods if one is interested in the occupied states as well. Finally it fails to resolve the electron dynamics which supply valuable information about charge transfer, relaxation and surface chemistry processes [Ech04] [Har97] [Rei00].

With the 2-photon photoemission a powerful method has been available and continuously developed for more than two decades which combines the advantages of direct and inverse photoemission, probing occupied and unoccupied states simultaneously. In addition it implements the use of short laser pulses, allowing to conveniently measure in a time resolved fashion by employing a pump-probe scheme. The fundamental idea of 2PPE is a two step process where the electron is excited into an unoccupied state by a first photon and subsequently emitted from there by a second photon. This obviously restricts the maximum photon energies ($h\nu$) suitable to values below the work function of the sample, $h\nu < \Phi$.

In contrast to direct photoemission 2PPE is a 2nd order process requiring a high spacial and temporal density of photons which motivates the use of pulsed lasers mentioned above. The corresponding spectra exhibit overlapping contributions from the occupied and unoccupied regions of the electronic structure. To identify the peaks within a spectra and correlate them to a specific state it is necessary to investigate their photon energy dependence. A listing of the different available electronic state observable in 2PPE and their corresponding excitation schemes are depicted in figure 2.14 and will be introduced in the following.

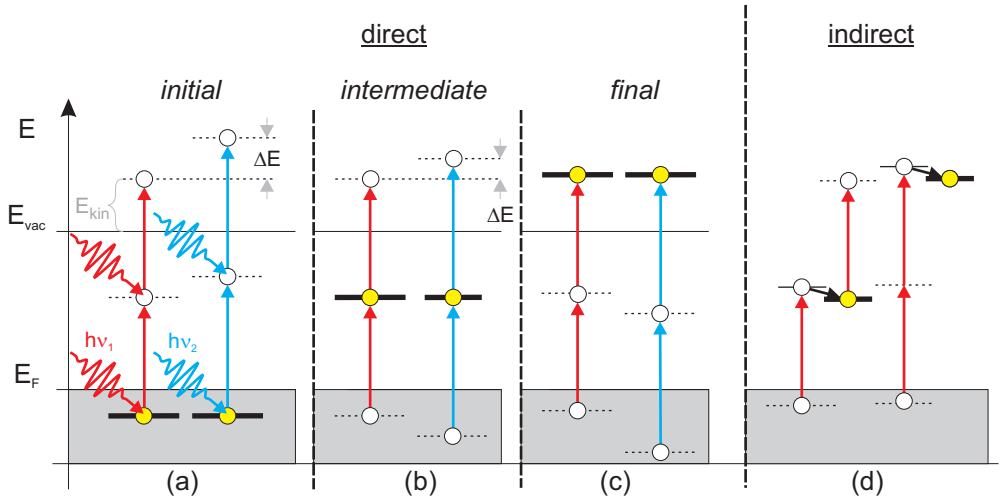

Figure 2.14: Excitation schemes in 2-photon photoemission with yellow circles marking the corresponding probed states. Their distinct photon energy dependencies can be used to analyze the experimentally obtained spectra. Therefore the sample is probed with at least two different photon energies ($h\nu_1$ and $h\nu_2$). According to the kinetic energy shift (ΔE) of the peaks observed in the spectra those can be assigned to either initial, intermediate or final states. For details see text.

Excitation schemes

- **Occupied initial states** These states belong to the occupied region of the electronic structure. Here, in a simple picture, the energy of two photons is transferred to the corresponding bound electron giving it sufficient energy to overcome the work function. For a proper theoretical description virtual (intermediate) states have to be introduced. They represent a quasi excited state with an infinitesimally short lifetime. Having a fixed initial state energy the kinetic energy of the photoelectron has to scale with twice the photon energy: $\Delta E_{kin} = 2\Delta h\nu$) as can be seen in graph 2.14(a) of the excitation scheme.

- **Unoccupied intermediate states** Real intermediate states are intrinsic features of the samples electronic structure located in the energy region between the Fermi and the vacuum level. Their population can either occur through a direct or an indirect transition. In the latter case a neighboring state with higher energy is directly excited and decays through scattering events into the intermediate state as depicted in figure 2.14(d). A special situation evolves for photon energies which enable a direct transitions between an initial into an intermediate state. These resonant excitations usually lead to a strong increase in the obtained signal [Ste95]. In both of the above cases the photon energy of the initial excitation step is not relevant for the kinetic energy of the emitted electron. Hence the signal shifts with $\Delta E_{kin} = \Delta h\nu$.

- **Unoccupied final states** Final states are located energetically above the vacuum level. This can e.g. be the case for electronic states of adsorbed molecules. Final states can be directly and indirectly excited as well. Here, the electron is subsequently emitted in an auto-detachment process. Since electrons in the final state do not experience another excitation their kinetic energy is independent of the initial photon energy. Thus the corresponding spectral feature remains at a constant value: $\Delta E_{kin} = 0\Delta h\nu_2 = const.$ (see figure 2.14(c)).

In the above example photons of a single energy (one-color) have been used for pumping and probing respectively. A better access to unoccupied states is usually given using a two-color (2C) setup. It allows to choose a resonant excitation scheme which enhances the photoemission yield of these states. The two photon energies used commonly exhibit a 1:2 or a 1:3 ratio due to either experimental restrictions or for convenience. Note, that an a priori assignment as pump and probe beam is not possible as it depends on the energetic position of the investigated state. In regions close to the Fermi level the low energy beam, usually in the visible range, will be responsible for the pumping as its photon energy is usually to small to emit electrons from such states. In regions close to the vacuum energy the situation is vice versa. Here respective photons of the ultraviolet range are required for the pumping of states which cannot be occupied using visible light (see also pump-probe scheme in figure 2.16).

Energy scaling Most of the investigated crystals and especially the adsorbate covered samples studied in this thesis have a rich energetic structure showing at least one initial and one intermediate state. For a proper depiction of the data it can be

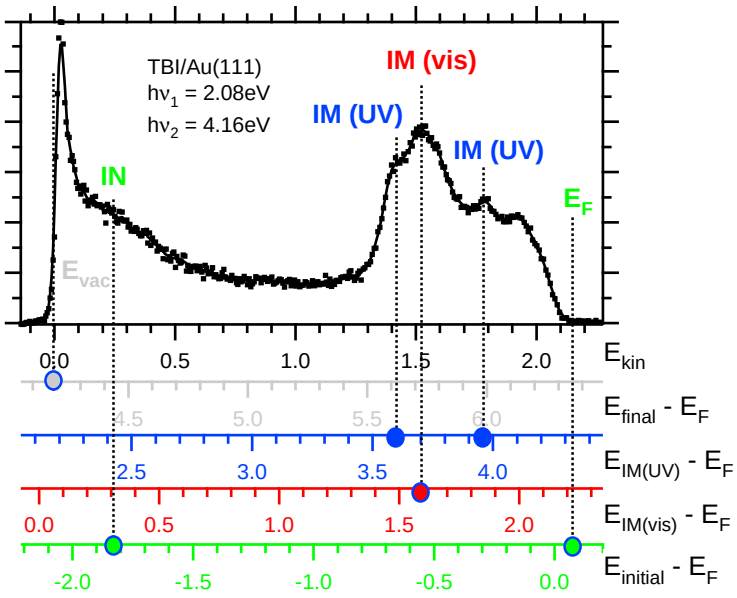

Figure 2.15: Different energy scales for a 2-color 2PPE spectra. The states in the spectra are color coded and labeled according to their origin: initial states = IM (green), intermediate states vis-pumped = IM(vis) (red), intermediate states UV-pumped = IM(UV) (blue). In the final state scale the work function can be directly obtained from the position of the vacuum cutoff edge.

very convenient to use different energy scales depending on the key message of the presented data. A useful example is given in figure 2.15. Here a 2PPE spectra from a TBI covered gold crystal having a variety of initial and intermediate states is shown. The uppermost energy scale corresponds to the raw data representing the kinetic energy of the emitted electrons. Below the final state energy gives the peak position with respect to the Fermi level of the metal substrate. It can be used to directly obtain the work function which, in this scaling, coincides with the vacuum cutoff edge as marked in the graph. This depiction is also suitable to visualize the binding energy of final states (not observed in this spectra). The two intermediate state (IM) energy scales are consequently used for a better depiction of the intermediate state binding energies. Here it has to be distinguished between states pumped with either visible or UV light. Final the initial state scale is most applicable for occupied states below the Fermi level. Here the Fermi cutoff edge, as a reference point, is found at an energy of 0eV.

2.4.3 Time resolved two-photon photoemission (TR-2PPE)

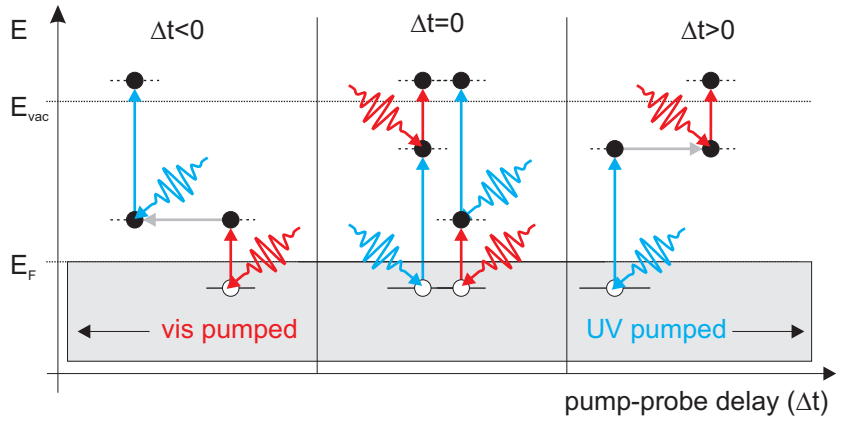

Figure 2.16: Time resolve pump-probe scheme for different delays. At $\Delta t = 0$ both beams, visible and UV, arrive simultaneously. For positive delays the visible pulse trails the UV one. Consequently it can only probe states that have been previously pumped by the UV light and have not yet decayed. Varying the delay will yield the time dependent population of the state and thus its lifetime. For negative delays the order of the pulses is reversed. Here the visible pulses are used for pumping and the UV for probing. As a result the energetic position of the states (visible or UV pumped) can be distinguished based on the asymmetry in the decay signal (see also figure 2.17).

Another major advantage of the 2-photon photoemission is its ability to resolve the temporal evolution of excited states. This is realized by splitting the laser beam into two pulse trains of either the same or preferably two different photon energies. Between the two pulses a temporal delay can is imposed by varying one of the respective optical path length. The experiment is conducted in a pump-probe scheme as depicted in figure 2.16. Depending on the direction of the delay

(positive or negative) it can be used to investigate either UV or visible light pumped intermediate states. Therefore an electron is excited by a first photon and probed after a delay time Δt by the second photon. Varying Δt will yield the time dependent population and thus the lifetime of the intermediate state.

In an one-color experiment, the temporal evolution of the signal intensity is a folding of the laser pulse length and the population decay of the probed states. As previously mentioned the spectroscopy of initial states occurs via excitation of virtual intermediate states. Their lifetime can be expressed in terms of a delta function hence the corresponding signal is reduced to the folding of the laser pulse with its duplicate. This is an enormously convenient way to determine the pulse length which is usually referred to as an autocorrelation. The draw back of the one-color setup becomes obvious when investigating the lifetime of real intermediate states. Due to the equal characteristics of the laser pulses an a priori classification as pump and probe pulse is impossible. Thus the folding with the decay of the intermediate state will lead to a symmetric broadening of the autocorrelation function. To retrieve the respective lifetime an accurate knowledge of the laser pulse length is required.

A more elaborate way is the use of pulses having different photon energies. Figure 2.16 depicts data from such a TR-2PPE experiment taken on an adsorbate covered gold surface. The horizontal time axis expresses the temporal delay of the two pulses. At $t = 0$ both arrive simultaneously at the sample. At positive delays the UV pulse of $h\nu_2 = 4.16eV$ is responsible for the pumping and the visible light of $h\nu_1 = 2.08eV$ is used for the subsequent probing. At negative delays the assignment is vice versa as is depicted in the sketch on top of the graph. In the right side graph a series of 1D-spectra from the energy domain at different delay times is presented. In similar fashion a series of horizontal cuts reveals the temporal evolution of the photoemission signal. Several of those cross-correlation[2] curves for the marked energies are shown in the bottom graph. States having a distinct lifetime will show an asymmetry in their traces which is the result of having two distinguishable pump-probe schemes (see also figure 2.16). In general this information can also be used to extract the energetic position of a state, complementary to the previously introduced method of taking a photon energy dependence.

Analytical description of the decay rates The modeling of the decay is usually done by employing the optical Bloch equations [Lou00]. They give a full quantum mechanical description of a 3-level system system with an initial, an intermediate and a final state. Bloch equations are suitable to analyze the decay of populated states as well as the phase correlations in between participating states [Her96][Hof97][Wol99]. Their use is limited as additional information, viz. the dephasing rates of the system, is required. However in case of strictly non-resonant excitations one can simplify them to a set of classical rate equations. Those yield a time dependent description

[2] correlation based on two different laser pulses, in contrast to autocorrelation

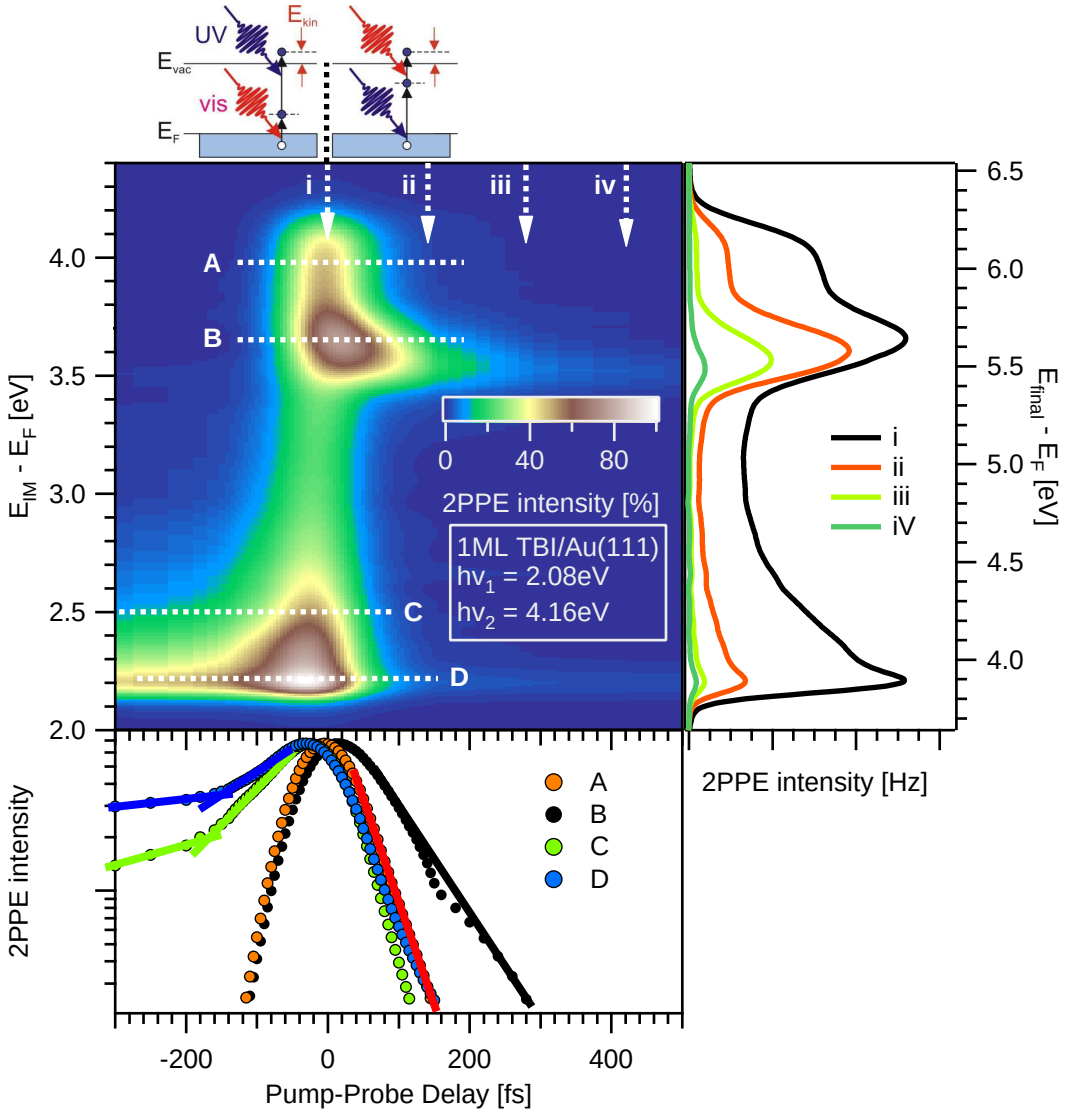

Figure 2.17: Time-resolved 2PPE data from 1ML TBI/Au(111). The center graph presents a 2-dimensional depiction of 2PPE spectra taken at different pump-probe delays. For negative delays electronic states are pumped by the visible light and probed by the UV beam as is sketched in the picture on top. For positive delays the assignment is vice versa. Single spectra for different delays (i - iv) are depicted in the right side graph. They show two obvious peaks labeled as A and B in the center plot. In addition an exponentially decaying background from the hot electron distribution is visible. Cutting the spectra along an axis of constant energy yields the time dependent 2PPE intensity as shown in the bottom graph for the marked spectral features (A-D). The cross correlation trace of A is symmetric indicating a very short lifetime. B on the other hand exhibits a lifetime towards positive delays, hence it is the signal of an UV pumped state. Due to its lifetime it can be resolved in the 1D 2PPE spectra iii and iv whereas all other contributions are almost eliminated. The hot electrons on the other hand are clearly pumped by the visible light and thus display a slowly decaying population towards negative delays (represented by the cuts along C and D).

of the 2PPE intensity:

$$I(\Delta t) \propto \int_{-\infty}^{+\infty} dt' \int_{-\infty}^{\infty} dt'' |E_1(t')|^2 |E_2(t''-\Delta t)|^2 \Theta(t''-t') e^{-\Gamma(t''-t')} \tag{2.10}$$

As mentioned before the signal is the folding of the two laser pulses with their respective electric fields of E_1 and E_2 and an exponentially decaying state. This model will be used for the analysis of our time resolved 2PPE measurements in chapter 4.3, 6.1.2 and 6.2.2.

2.5 Thermal desorption spectroscopy

Thermal desorption spectroscopy (TDS), also known as temperature programmed desorption (TPD), is a common tool to investigate the adsorbate coverage of a surface[Pis74] [Red62] [Ehr61] [Kin75] [Bru07]. Moreover it gives insight into the dynamics of the desorption process yielding valuable information on thermal barriers. To obtain a spectra the sample temperature is linearly increased at a rate β while simultaneously recording the pressure. Typical heating rates are usually in the range of 1 to $10Ks^{-1}$. For an element specific analysis the use of a mass spectrometer is preferred as it is able to record the changes of partial pressure induced by the desorption of the adsorbate. An analytical description of this process is given by the Polanyi-Wigner equation:

$$\frac{d\Theta}{dt} = \Theta^n k_0 exp(-\frac{E_i}{k_B T}) \tag{2.11}$$

Here Θ represents the number of adsorbed molecules or atoms and n the order of the reaction. The Arrhenius term at the end expresses the rate of this thermally activated reaction. It is a function of the desorption energy E_i, the temperature T, the Boltzmann constant k_B and the frequency factor k_0.

For an implementation of the Polanyi-Wigner equation in the experiment it has to be modified to accommodate the temperature ramp:

$$\frac{d\Theta}{dt} = \frac{dT}{dt}\frac{d\Theta}{dT} \tag{2.12}$$

which yields

$$\frac{d\Theta}{dT} = \frac{dt}{dT}\Theta^n k_0 exp(-\frac{E_i}{k_B T}) \tag{2.13}$$

This equation allows for a qualitative analysis of the obtained experimental spectra. They are mainly influenced by the reaction order as described in the following. A graphical depiction of the corresponding spectral shapes is shown in figure 2.18.

zero order desorption The desorption rate is independent of the Θ. Thus for different initial coverages Θ_0 the slope of the spectra is equal but the peak maximum shifts to higher temperatures T_{max} for larger Θ_0. After reaching

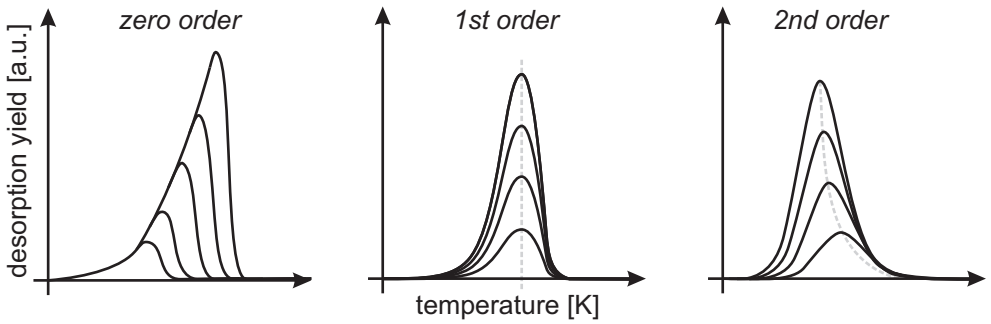

Figure 2.18: Sample TDS specta of different desorption order. Adapted from [Lüt93].

T_{max} the desorption ends almost instantaneously leading to a sharp drop in the spectra. This behavior is usually associated with the evaporation of a multilayer.

1st order desorption In this case the desorption rate scales linearly with Θ but here T_{max} is constant for all coverages. A second feature of this reaction order is the asymmetric shape of the spectra. It is used to describe the desorption of single molecules or atoms directly from their binding sites independent of interactions with their environment.

2nd order desorption A symmetric shape of the spectra can be observed with a peak maximum shifting to higher temperatures for smaller initial coverages. The second order indicates a two step process like in the case of associative molecular desorption. A similar behavior is also expected for strong intermolecular interactions which increase at high coverages leading to a lowering of the binding energy.

As can be seen from the above the reaction order is crucially determined by the interacting of the desorbing molecule with its surrounding. Hence for more complex systems a description requires the use of non-integer values of n. Besides the qualitative results TDS experiments can also be analyzed to yield the desorption energy barrier, as seen in the Polanyi-Wigner equation, or the initial coverage prior to the desorption. The latter will be an important tool in the frame work of this thesis in order to characterize the molecule-metal systems.

3 Experimental Details

In the following we will introduce the main parts of the experimental setup used for the measurements conducted within the framework of this thesis, viz. a femtosecond laser system and an ultra high vacuum chamber Furthermore we will describe useful considerations regarding the employed data acquisition and processing schemes as well as the preparation and characterization of the samples.

The central building block of the femtosecond laser system consist of a commercially available combination of an oscillator and a regenerative amplifier providing 5mJ pulses at a repetition rate of 300KHz. It enables a simultaneous pumping of two parametric amplifiers supplying laser beams which can be separately tuned to almost every wavelength in the range from 200 to 1600nm.

The ultra high vacuum chamber supports a contamination free preparation and characterization of the molecule-metal samples. It is equipped with a sample transfer system enabling a fast in situ exchange of the metal substrate. The investigated molecules are stored in a separately pumped compartment and thus can be replaced without breaking the vacuum of the main chamber. They are adsorbed onto the metal surface via chemical vapor deposition. This process is controlled by means of thermal desorption spectroscopy.

The kinetic energy of the photoemitted electrons is recorded using a time-of-flight spectrometer. To elucidate the electronic structure of the investigated samples the corresponding 2PPE spectra are accumulated and analyzed with the help of computer based routines.

3.1 Laser system

The heart of the one and 2-photon photoemission experiments is our femtosecond laser system. It is fitted on two laser tables providing space for a large number of optics needed to manipulate and combine the different pulses in the visible and UV wavelength range. Their generation and amplification involves a number of subsequent nonlinear processes which crucially depend on a temporal and spacial overlap of highly focused beams. As the beam pathes extend over several meters distance it is of eminent importance to assure the mechanical and thermal stability of the components and the environment.

Protection of the system against shock waves is realized by a series of air pressurized damping posts. High frequency oscillations on the other hand are sufficiently suppressed due to the heavy mass of the tables. A tent surrounding the laser system reduces the dust load exposed onto the optics while air conditioning provides a constant temperature and keeps the humidity at a low level.

3.1.1 Generation and amplification of fs-pulses

An overview sketching the basic components used to provide the necessary photon energies for our experiments is given in figure 3.1. In the following we will briefly describe the main parts. A more detailed introduction on the generation, amplification and control of short laser pulses can be found in the literature [Boy92] [Dem03] [Rul98] [Tre02], the laser system manuals [Gro07] [Gro93] [Gro94] and previous thesis works [Kir09] [Stä07] [Lis05] [Gah04].

Except for the custom build nonlinear optical parametric amplifier (NOPA) all components for the generation and amplification of the light are supplied by the COHERENT company. A MIRA(900 B) seed oscillator delivers short laser pulses at a repetition rate of 80MHz. Its center wavelength is tunable in the range of 770-830nm having a temporal width of <40fs and an energy of 2-3nJ per pulse. For further use the pulses have to be amplified in a regenerative amplifier (RegA 9050) to pulse energies of 6-7μJ at a repetition rate of 300kHz. Both units, MIRA and RegA are pumped with continuous wave laser (Verdi V18) delivering a 16W at a wavelength of 533nm . Its output is split using a waveplate and a thin-film polarizer sending 4.5W to the oscillator and 11.5W to the amplifier.

The amplification process of fs-laser pulses leads to very high peak powers p_{max} which exceed the damage threshold of the optics. In order to reduce p_{max} the pulses are stretched in time before entering the RegA and compressed afterwards. This is accomplished by a grating based stretcher-compressor unit. After this final stage of the generation and amplification process pulses of 800nm having apulse length of 50fs and a power of 5mJ are available for further manipulation based on the aim of the experiment. Here two optical parametric amplifiers (OPAs), a NOPA and several frequency doubling crystals allow to access a variety of different photon energies in the range from 1.5 to 6eV with the following specifications.

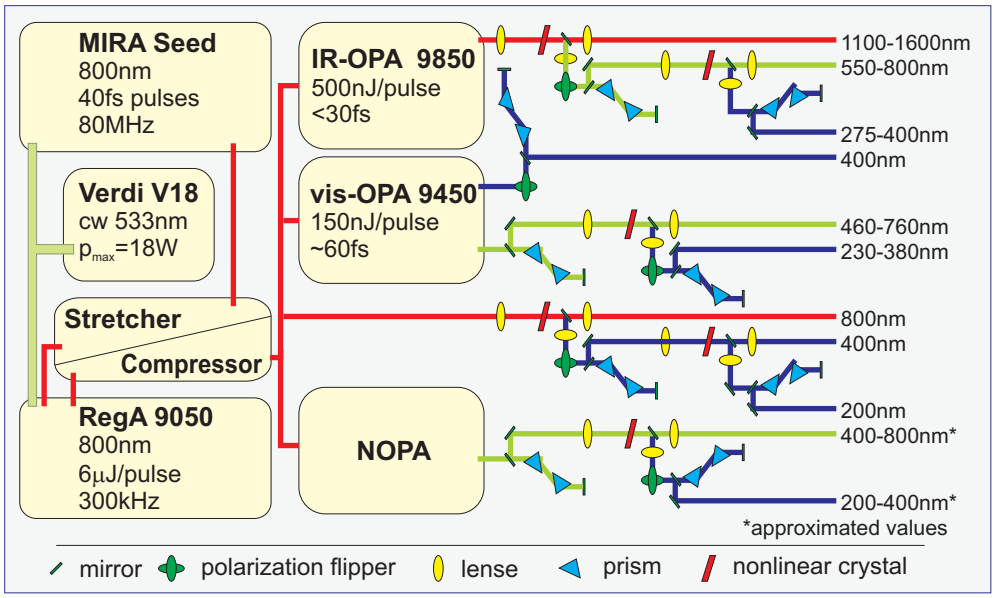

Figure 3.1: Sketch of the lasersystem used in the framework of this thesis. A 18W Verdi cw-laser pumps a fs-oscillator (MIRA) and a regenerative amplifier (RegA). Three optical parametrical allow to access nearly every photon energy in the range of 200-1600nm.

The Coherent OPA-9450 has an output in the visible range (vis-OPA) of 460-760nm at a minimum pulse duration of ≈55fs and up to 150nJ/pulse. It can be frequency doubled using a β-barium-borate (BBO) crystal to access the $230-380nm$ UV region. The second OPA (OPA-9850) is used to cover the IR range(1100nm-1600nm) having shorter (≈30fs) and more intense (up to 500μJ) pulses. Its output can be frequency doubled twice extending its range to the visible (1st doubling) and ultraviolet (2nd doubling). A third, nonlinear, parametric amplifier is currently set up and developed. It has been partially tested in the work of this thesis. The NOPA operates in the visible range as well and will yield pulses of less than 20fs duration. In the presented experiments however it was mainly used as a second option of supplying tunable photon energies for two-color 2PPE measurements.

For the conduction of direct photoemission experiments a part of the amplified seed is frequency doubled twice to generate 6eV photons. This energy is sufficient to overcome the work function of most metals. The same setup can be used to obtain a 3eV beam by omitting the second doubling stage. Due to its strong intensity it is perfectly suited for fluence dependence measurements which require a power tuning over several orders of magnitude.

Due to the Heisenberg uncertainty principle, $\Delta E \Delta t = \frac{\hbar}{2}$, fs-laser pulses require a large bandwidth (>30nm). Passing through optical components its temporal width is increased as the different wavelength exploit different propagation velocities. This dephasing in the time-domain, the so called chirp, has to be compensated by using folded prism compressor stages which are implemented into each beam path.

The current setup allows to operate at least two of the above mentioned laser tuning devices simultaneously. Thus, in principle, all available wavelength can and have been paired up for two-color 2PPE measurements. This gives us the great opportunity to individually select the wavelength for pump and probe pulses without being confined to the commonly used 1:2 ratio of fundamental and frequency doubled photons. The huge advantage of this setup has recently been shown in measurements using a combination of 1.5 and 6eV beams for time and angle resolved photoelectron spectroscopy [Sch08b].

3.1.2 Pulse incoupling

For a stable positioning of the beams on the sample the ultra high vacuum chamber (see section 3.2.1) is directly attached to the laser table. The inevitable high frequency oscillations e.g. from its turbomelecular pumps are sufficiently damped by the heavy mass of the setup. To employ the pump-probe technique the beams have to be temporally and spatially overlapped on the sample. A schematic drawing of the incoupling setup used is given in figure 3.2(a). The components outside the UHV chamber are mounted on a removable bread-board. Here each of the collimated beams ($h\nu_1$ and $h\nu_2$) first passes through an adjustable focusing lens (f=500mm) which is used to modify the spot size on the sample (see figure 3.2(b)). They are

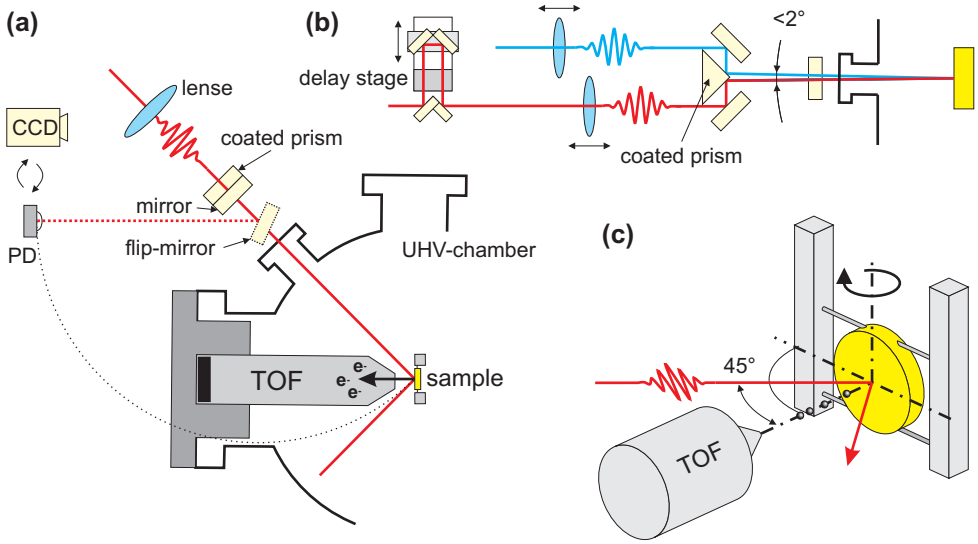

Figure 3.2: Schematic drawing of the laser pulse incoupling. **(a):** Top view showing the bread-board with the components necessary for the beam adjustment (lenses, mirrors, photodiode (PD) and CCD camera). **(b):** Side view of the laser pathways. The beams can be separately focused and guided by the respective lenses and mirrors. They reach the sample almost collinearly (<2° deviation). A motor driven stage is used to manipulate the temporal delay. **(c):** Sample-detector geometry. The angle between the laser beam and the TOF is fixed at 45° while the sample can be rotated for angle-resolved measurements. Its distance to the tip of the flight tube is ≈ 3mm.

then reflected onto a metal coated prism (Al on the uppers side for the UV beam and Ag on the lower side for the vis beam). From there the beams are guided in a quasi-collinear geometry (deviation angle <2°) through an UV transmitting MgF_2 window and spatially overlap on the sample. For the beam adjustment a flip-mirror has been installed in front of the vacuum chamber. It is used to reflect the beams to a CCD camera (ImagingSource DMK 21AF04) mirroring the sample position. The camera is also used to record the intensity profile of the laser which is needed for the analysis of the TBA/Au(111) isomerization process (see appendix D).

To find the temporal overlap the CCD camera can be replaced with an ultrafast photodiode (PD). The delay of the pulses is measured in respect to a reference signal of a second PD placed at the exit of the amplifier system using a broadband oscilloscope. A rough adjustment is accomplished by properly matching the pathlength of the two beams on the lasertable (see previous section). To tune the overlap on a femtosecond timescale a motorized delay stage(Physics Instruments M-505) is implemented in the vis beam path. It is used to slowly vary the traveling distance while the temporal overlap is monitored via the cross correlation signal of the sample.

As depicted in figure 3.2(c) the sample is hit by the laser beam under an angle of 45° with respect to the spectrometer axis. Rotating the sample for angle-resolved (AR) measurements does not change this geometry but only the incidence angle onto the sample. Consequently the electric field component of the light impinging on the sample is altered depending on the rotation angle. Here, for the commonly used p-polarization, the component perpendicular to the surface is increased or decreased depending on the direction of the rotation. This will in return influence the 2PPE intensity of states exploiting a distinct polarization dependence of their photoemission yield [Gah04]. Due to the proximity of the sample and the TOF (see sec 3.3) we are limited to a maximum rotation angle of $\alpha_{max} = \pm 28°$. Turning the sample to negative angles however will reflect the laser pulses off the sample directly into the analyzer creating a large background photoemission signal. Thus the effective sampling regions is further reduced to $28° > \alpha > -4°$.

3.1.3 Beam analysis

The analysis of the 2PPE data requires detailed information about the employed laser pulses. For this purpose a variety of equipment is available. The spectrum of the visible and near UV pulses is recode with a fiber optic grating spectrometer (B&M) recording the data in a custom build LabView environment. Figure 3.3(a) shows an exemplary data set taken in this work. It is fitted with a Gaussian function yielding the central wavelength and the bandwidth. Together with two additional spectrometer for IR-(APE Wavescan) and UV-wavelength(LOT-Oriel Andor) it covers the full range of photon energies available in the here presented setup.

The alignment CCD-camera used for spatially overlapping the beams is also used to record the laser spot profiles as seen in figure 3.3(b). This information, in combination with the pulse energy, is very important for the determination of the switching efficiency and will be discussed in detail in appendix D. Because the

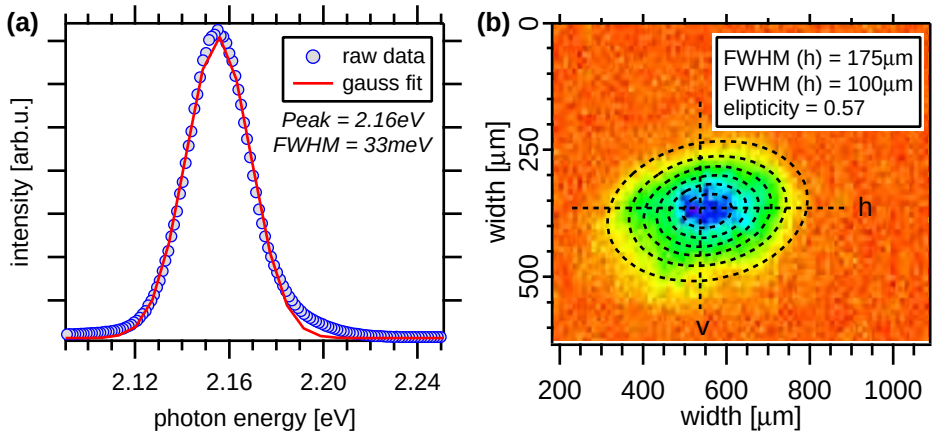

Figure 3.3: Analysis of the laser beam. **(a):** Energy spectrum of a visible laser pulse as commonly used in the experiments. The central photon energy and the bandwidth (FWHM) are obtained from a Gaussian fit. **(b):** False color image of the corresponding laser intensity profile. Here a 2D Gaussian fit (black dotted circles) is employed to retrieve the dimensions. A more detailed analysis as required for the investigation of the photoisomerization kinetics is presented in appendix D.

camera can only record relative not absolute intensities the assignment of the spatial intensity profile is done in two steps. First the total power of the beam is measured using a Melles Griot 13PEM001 powermeter and then correlated to the camera image. To maximize the resolution and take full advantage of the 8-Bit data range a series of optical filters is used to adjust the laser intensity just below the saturation threshold. The camera is oriented perpendicular to the laser beam as opposed to the sample which is hit under a 45° angle. This difference is accounted for by distorting the camera image by a factor of $\sqrt{2}$ in the horizontal direction. The small angle deviation in the vertical direction resulting from the almost collinear incoupling of the beams can be neglected without significantly increasing the error. Under the usual experimental conditions it is reasonable to fit the image with a 2-dimensional Gaussian profile. From the obtained fit parameters the average fluence of the laser pulse can be deduced.

To determine the pulse duration the cross correlation signal of a non-resonantly probed occupied state has to be recorded. In this case the 2PPE process occurs via the excitation of a virtual intermediate state having an infinitesimal short lifetime. Correspondingly the temporal width of the measured 2PPE signal ($I_{XC}(t)$) results from the convolution of the transient laser beam intensities $I_1(t)$ and $I_2(t)$:

$$I_{XC}(t) = \int_{\infty}^{\infty} d\tau I_1(t) I_2(t-\tau) \tag{3.14}$$

It can be retrieved in good approximation by fitting the cross correlation trace using either a Gaussian or the more favorable sech^2-function and assuming an equal pulse length for both beams [Rul98].

3.2 Ultra high vacuum system

Basic research on the electronic structure of well ordered molecular films requires a contamination free environment. A common approach is the conduction of experiments under ultra high vacuum conditions. In the following an introduction to the system used in this work will be given.

3.2.1 Vacuum chamber

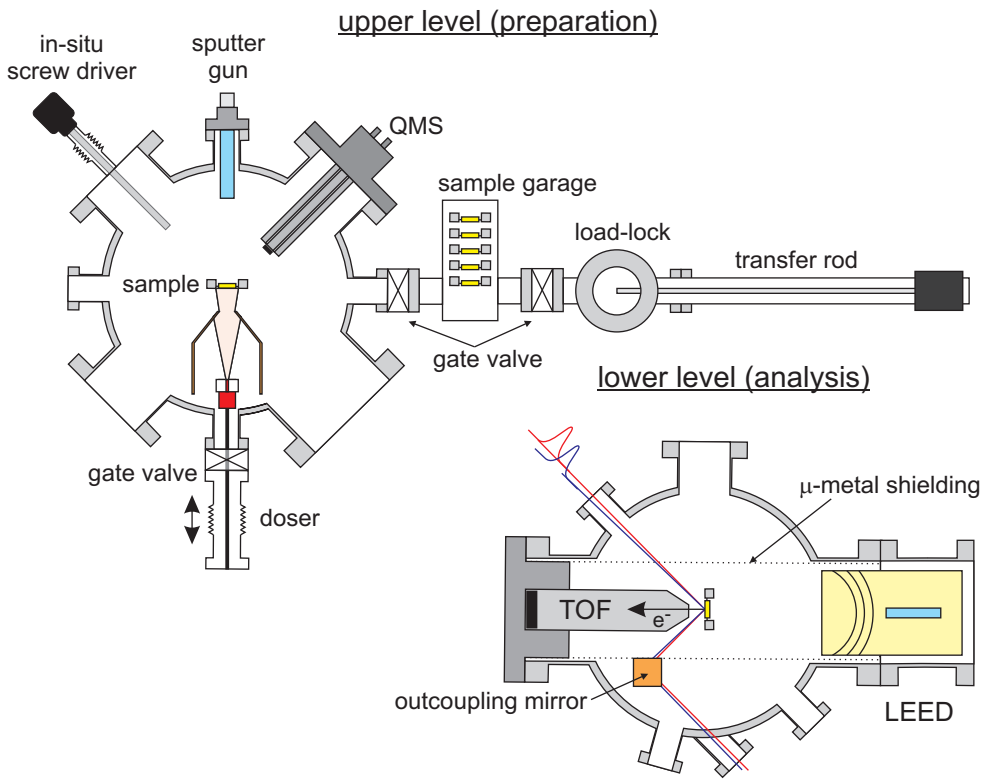

Figure 3.4: Sketch of the preparation and analysis level of the UHV chamber used in the framework of this thesis. The upper (preparation) level is connected to a sample transfer system enabling an in situ exchange of the investigated substrates.

For achieving ultra high vacuum (UHV) conditions a two level custom build chamber is used. A schematic depiction of the setup is given in figure 3.4. The upper half accommodates the equipment for the preparation and transfer of the sample, the lower half consists of a time of flight spectrometer and and low energy electron diffraction (LEED) device for analysis. A 360° rotatable manipulator allows for the movement of the sample in between the levels, as well as in the lateral directions. To establish vacuum a three unit pumping stage, including two turbo molecular pumps, has been used. The first one with a pumping speed of 520L/s (Balzers TPU 520), is located at the bottom of the chamber. It is backed up by a Pfeiffer TMU 071P

which is also used to differentially pump the rotational stage of the manipulator. Pre-vacuum conditions are generated by a Pfeiffer MD4 membrane pump. Additional pumping is supplied by a custom build titan sublimation pump and an ion getter pump (Varian VacIon Plus 75). To determine the quality of the vacuum the composition of the residual gas is monitored with a Balzers quadrupol mass spectrometer (QMG 112) while the pressure is measured with a Varian ion gauge. After a two day bakeout procedure, heating all components at 150°C, the system reaches a base pressure of $\approx 5^{-11}$mbar. Daily operation, including multiple cycles of molecular deposition, leads to a continuous contamination especially through adsorption at the chamber walls. To maintain UHV conditions an infrared (IR) lamp (Heraeus Noblelight GmbH) is used to heat the setup in between measurements limiting the maximum experimental pressure to $< 2.0^{-10}$mbar.

3.2.2 Sample holder

To mount the substrates investigated within this thesis we used the self made, exchangeable sample holder system schematically depicted in figure 3.5). It consists of two parts suitable for an in situ sample transfer. The upper part establishes the connection between the cryostat and the exchangeable lower part (boat). It is made

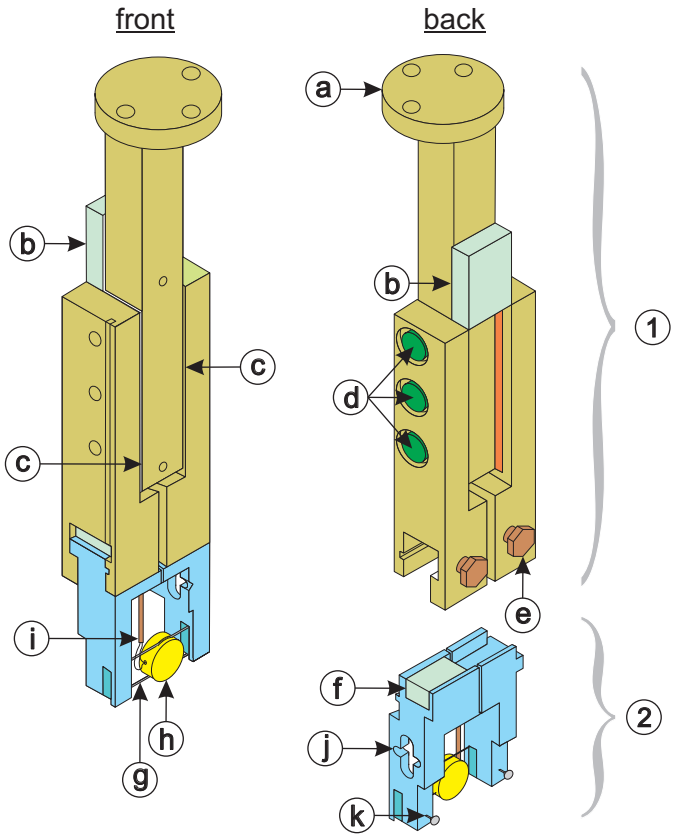

Figure 3.5: Schematic drawing of the sample holder. The upper part made of UHV suitable copper is coated with gold to prevent oxidation. The lower part (boat) is made of copper or molybdenum depending on the experimental requirements.

1-upper sample holder
2-lower sample holder (boat)

connection to cryostat (a)
mount for heating (b)
sapphire plates (c)
marcor isolated screws (d)
screws to fix boat (e)
marcor isolated TC pins (f)
tantalum heating wires (g)
metal substrate (h)
thermocouple (i)
port for transfer (j)
screws to fix sample (k)

of UHV compatible copper with a very low carbon concentration. To prevent an oxidation of the sample holder its surface has been passivated by coating it with gold. The boat used to fix various kinds of solid samples is available as a copper and a molybdenum version which can be be exchanged depending on the experimental requirements. In this work a gold (Au(111), MaTtecK GmbH) and a silver single crystal (Ag(111), MaTecK GmbH) have been used. Both were mounted using a pair of 0.3mm tantalum wires. These were guided through special notches on the crystals edge and fixed to the legs of the sample holder (see figure 3.5). The Ta-wires were also used for resistive heating of the sample.

To accomplish an electric circuit the sample holder and boat are divided in a left and a right part each contacted to an electrical feedthrough. Proper isolation with sufficient thermal coupling is realized by separating the different parts with 0.5mm sapphire plates (CrysTec GmbH). The whole setup is also isolated from the cryostat enabling an individual adjustment of the sample potential with respect to the ground. To connect both parts the boat can be slipped into the sample holder and fixed with two molybdenum screws on its backside. Those can be tightened using an in-situ vacuum screw driver located in the preparation level.

To monitor the sample temperature a type K thermocouple is inserted into a small hole at the edge of the crystals. Its loose ends are guided to the top of the boat where a pair of marcor isolated pins establishes the connection to the upper sample holder part. From there the TC wire continues to a feedthrough and then to a temperature controller. The current design offers space for the attachment of additional heating and thermocouples (see fig. 3.5) which however have not been used within this thesis. Cooling is realized by a flow through cryostat(VAb GmbH) operated with either liquid helium or liquid nitrogen. It allows for minimum temperatures of 35K and 88K, respectively. A build in resistive heater can be used to heat the entire sample holder to above 500K. This is very convenient to change the sample temperature during a measurement without affecting its potential. A drawback however is the slow rate at which this is done and the increase of pressure due to the desorption of the cold-trapped residual gas.

The sample holder design is optimized for the usage with low energy electron spectroscopy methods. Its front-side is flat to avoid inhomogeneous electric fields in the vicinity of the sample. To improve the position error for angle resolved measurements the rotational axis coincides with the center axis of the sample surface.

3.2.3 Doser

Although the molecules used in this thesis have a low gas pressure suitable for in situ UHV use they are kept in a separate dosing unit. This is beneficial for three reasons: (i) Exchanging the molecules can be done without breaking the main chamber vacuum. (ii) Contaminants are pumped directly by the dosers own turbo molecular pump (Pfeiffer TMU 071P). (iii) To adsorb the molecules onto the surface the chemical vapor deposition method is employed which requires the heating of the molecules. Shutting the gate valve will thus solve the problem of post dosing contamination.

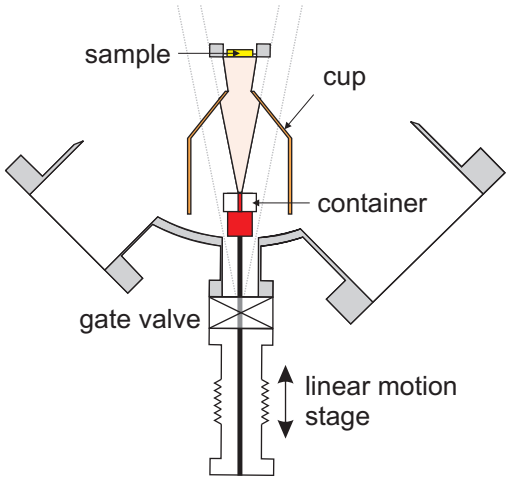

Figure 3.6: Sketch of the heatable dosing unit. The molecule container is fixed onto a linear motion stage to reduce the distance to the sample. This decreases the background contamination of the chamber as indicated by the gray lines representing the molecular beam at different positions. A further improvement of the experimental conditions is achieved by installing a cup inside the UHV-chamber.

The molecules are stored in a small molybdenum container wrapped in polyimide coated heating wire. It can be heated up to 400K which is monitored by a type K thermocouple. Heating will increase the pressure inside the container by evaporating and accelerating the molecules. A 1mm hole at the front side enables them to leave the container and creates a conical molecular beam as seen in figure 3.6. This beam can be blocked by a molybdenum shutter operated by a rotational feedthrough at the end of the doser. It blocks the direct exposition onto the sample, enhancing control over the amount of deposited material.

Having a conical beam the amount of molecules passing by the sample and thus contaminating the sample is proportional to the square of the sample-doser distance. To reduce this distance and the contamination the doser is put onto a linear motion stage. Further improvement is achieved by installing a cup inside the main chamber. It consists of a conical copper tube with a sample size hole at its front side. Excess molecules are trapped inside this tube and can be heated off in between measurements.

3.2.4 Transfer system

The transfer system (see figure 3.4) has been designed to connect two different UHV chambers enabling an investigation of the same sample with different experimental methods, viz. 2PPE and high resolution electron energy loss spectroscopy (HREELS). In the absence of the second chamber the load lock and sample garage have been directly attached to our setup. The load lock has a separate turbo molecular pump and can achieve a vacuum of $p < 1 \cdot 10^{-7} mbar$ in less than an hour. For the transport of the sample a transfer rod is used. It is equipped with a spring coupling which is inserted into a hole on the side of the sample holder boat (see figure 3.5). A gate valve separates the load lock from the garage. Here up to 8 samples can be stored under high vacuum conditions ($p < 5 \cdot 10^{-9} mbar$). The main chamber can be reached through a second gate valve on the opposite side of the garage. Due to the

successively arranged components and the corresponding differential pumping there is almost no contamination of the main vacuum. In addition, unused crystals can be stored under clean conditions which reduces the time of their initial preparation (see section 3.5).

3.3 Time-of-flight spectrometer

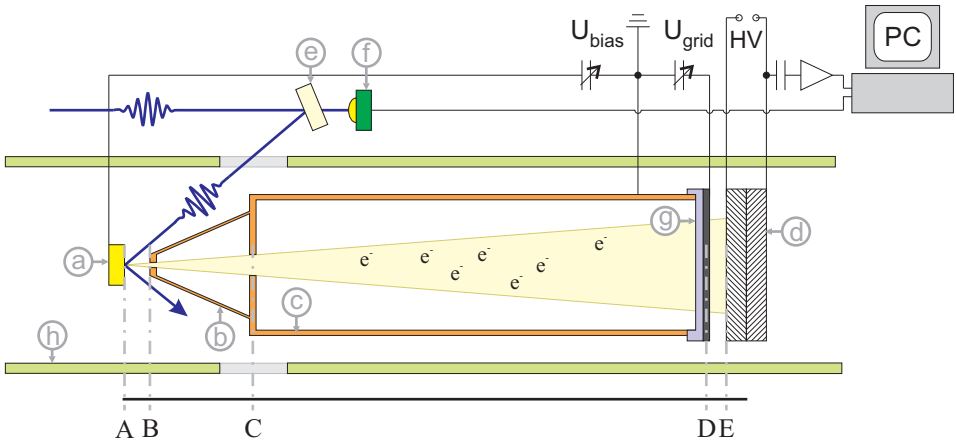

Figure 3.7: Schematic drawing of the time-of-flight spectrometer. The laser beam is guided onto the sample (a) using a mirror (e) in front of the UHV-chamber. After a short distance $\overline{AB}$ the photoemitted electrons enter a 210mm field free flight tube (c) through a small hole (1mm) in its conical tip (b). A mesh (g) with and adjustable potential prevents the penetration of the high voltage field from the MCPs (d) which are used to create a detectable voltage pulse. This pulse, together with the signal from a reference photodiode (f), is used in a computer based flight-time measurement. In combination with the traveling distance ($\overline{AE}$) it yields the kinetic energy of the detected electron. To shield the low energy electrons from magnetic fields the analyzer is placed inside a *mu*-metal casket (h).

The centerpiece of the vacuum system is the time-of-flight spectrometer (TOF) as schematically depicted in figure 3.7. Here the photoemitted electrons are propagated to a detector and their velocity is determined by the respective traveling distance $d = \overline{AE}$ and time t. This yields their kinetic energy (E_{kin}) based on the fundamental relationship:

$$E_{kin} = \frac{1}{2} m_e \left(\frac{d}{t}\right)^2 \tag{3.15}$$

Dealing with charged particles it is necessary to ensure a field free space to avoid retardation, acceleration and deviations from the initial trajectory to obtain accurate results. In the present case this is realized using a flight tube, (b) and (c), made of UHV compatible copper. Its inside is completely coated with graphite giving it a smooth surface with a homogeneous work function of 4.3eV. In addition the hole spectrometer is shielded from magnetic fields via a μ-metal housing (h) from s.a.m.Products. The cone like tip of this flight tube (b) enables the illumination of

the sample under an incident angle of 45° while keeping the distance to the field free part ($\overline{AB}$) at a minimum. Simulations of the electric field between sample and tip have been made (using the SimIon software) to optimize the geometry and the size of the cone. The flight tube ends approximately 4mm in front of a chevron micro-channel plate (MCP) stack. To avoid the penetration of electric fields it is capped by a fine meshed grid with an adjustable potential (U_{grid}). Across the MCP stack a high voltage of 2.7kV is applied which accelerates a photoemitted electron onto the channel walls thereby creating a charge cloud of several thousand electrons. The corresponding voltage drop can be detected using a capacitor which is directly connected to a pre-amplifier (Ortec). The pulse continues through a constant-fraction-discriminator before serving as a stop pulse for the computer based flight-time measurement (for details see section 3.4). For the respective start pulse the signal of a photodiode placed at the output of the lasers regenerative amplifier has been used. In the present setup the sample is separated approximately 3mm from the flight tube and can be rotated ±28° giving us the opportunity to conduct angle-resolved measurements.

3.3.1 2PPE data analysis

Despite the simple fundamental relationship between the electron velocity and its kinetic energy (equation 3.15) the analysis of the data is not straight forward. While the traveling distance can well be determined the flight time, measured as the difference of a start and a stop pulse, is masked by two effects. (i) The start signal is obtained from a reference photodiode and thus does not reflect the time of the photoemission event. (ii) Transmission and processing of start and stop signal are not instantaneous and therefore cause a temporal delay. Both contributions add a constant offset to the actual flight time which has to be considered in the data analyis.

The transformation from the time to the energy domain also has some important consequences. (i) The signal intensity has to be re-scaled according to:

$$\frac{dN}{dE} = \frac{dN}{dt}\frac{dt}{dE} = \frac{dN}{dt}\frac{t^3}{m_e L^2} \tag{3.16}$$

(ii) The resolution of the spectrometer decreases with increasing kinetic energy due to its quadratic dependence on the flight time (see equation 3.15. Here, main sources of error are inaccuracies in determining the field free flight path and the timing. In addition the acceleration field between the TOF and the MCP stack as well as the potential between TOF and sample have not yet been accounted for. (iii) From equation 3.15 it can also be seen that the data density increases towards lower kinetic energies. This causes a worse signal to noise ratio in the corresponding regions of the energy domain.

To estimate the actual resolution of the TOF-spectrometer we shall shortly discuss the error sources mentioned in (ii). The acceleration field in front of the MCP's

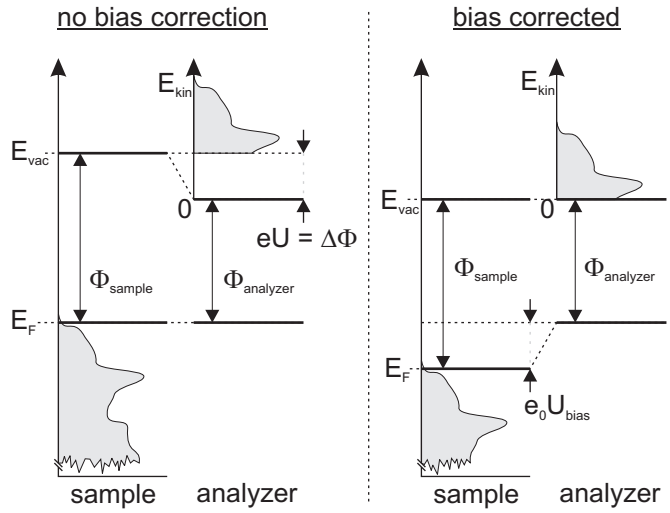

Figure 3.8: Energy diagram for a biased and an unbiased sample. Without the correction an electric field, induced by the work function difference ($\Delta\Phi$) between sample and analyzer, accelerates the emitted electrons. Putting the sample on a voltage of $e_0 U_{bias} = \Delta\Phi$ levels the vacuum energies and annihilates the electric field. For details see text.

is significantly shorter than the flight tube thus it can be neglected in good approximation as shown by Hotzel [Hot99]. Also the distance between the sample and the TOF is rather short. Here however the electrons can experience an acceleration or retardation prior to entering the field free flight tube and thus the altered velocity is maintained over almost the entire flight distance. The magnitude of the error depends on the electric field which results from the work function difference $\Delta\Phi$ between sample and analyzer. In addition the photo emitted electrons are mapped with respect to analyzer work function. This leads to a shift of the spectra for $\Delta\Phi \neq 0$ as depicted in figure 3.8. To compensate this shift and to annihilate the electric field the sample is put on a constant voltage (U_{bias}) with respect to the ground potential. U_{bias} is chosen to level the work function difference. An intrinsic calibration is given by the vacuum cutoff edge representing the slowest emitted electrons of almost vanishing kinetic energy. For a more convenient data analysis it is favorable to fully resolve this vacuum edge and thus the bias voltage has to be slightly adjusted. The thereby induced small field can be neglected.

According to equation 3.16 the resolution increases with the length of the flight tube. Estimations from Hotzel for a similar setup yield values in the range of 10 to 20meV which do not account for the energetic width of the laser pulses [Hot99]. Depending on the experimental conditions we estimate the actual value to be in the range from 30 to 60meV. A good measure for the resolution is the width of the vacuum cutoff edge observed on a homogenous clean surface. Unfortunately those conditions are not present for most of the here studied adsorbate systems. However the width is usually well below 60meV proving the above estimate reasonable.

Another quantity of interest is the angular resolution of the spectrometer. From the basic design (see figure 3.7) it is obvious that acceptance angle for detected electrons is determined by the length of the flight tube and the diameter of the MCP stack. In our case it is limited to a value of 6°.

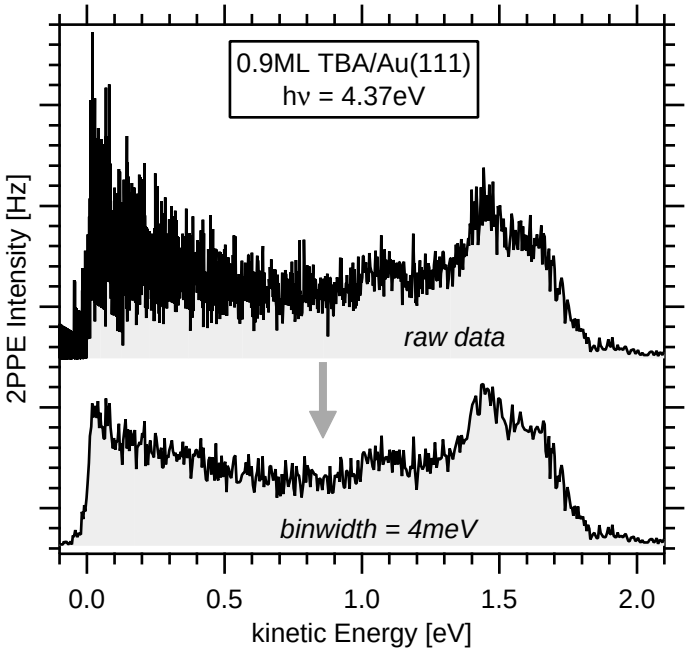

Figure 3.9: Energy binning of 2PPE spectra. The data density of the raw spectra increases quadratically towards lower energies due to the time-of-flight method. This leads to an unfavorable signal-to-noise ratio (SNR) in short term measurements. Binning averages the values within a given energy window (binwidth) improving the SNR.

Finally we want to return to the problem of the signal to noise ratio at low kinetic energies (iii). This effect is usually compensated through accumulation over a large number of events. However for some of the here presented experiments we are limited to low statistics. On the other hand valuable information is hidden in the low energy region. To resolve this problem we manipulate the data with a so-called binning routine. It averages values within a given (binning) energy window ΔE. Depending on the particular statistics we use binwidth of $\Delta E = 1 - 6meV$ which is well below the above given resolution. A sample spectra exposed to such a procedure can be seen in figure 3.9.

3.4 Data acquisition

For the data acquisition we used a Pentium4, 3.3GHz personal computer having 1GB of memory. Communication with the different experimental instruments is realized through a self programmed LabView 6.x environment. It addresses several hardware components as depicted in the connection scheme in figure 3.10.

The electron flight-time required for the 2PPE experiments is measured with a 4 GHz multiple-event time digitizer from FAST ComTec (P7887). It sweeps the time domain triggered by a start pulse and sorts the following multiple stop events into an 8192 bin matrix having a binwidth of 0.25ns. The data can be directly read out with LabView where it is accumulated and saved. To trigger a sweep the signal of the reference photodiode set up at the output of the amplifier system is used. The respective stop events are obtained from the voltage pulse created by the electron cascades in the MCPs of the TOF analyzer (see section 3.3). Before reaching the

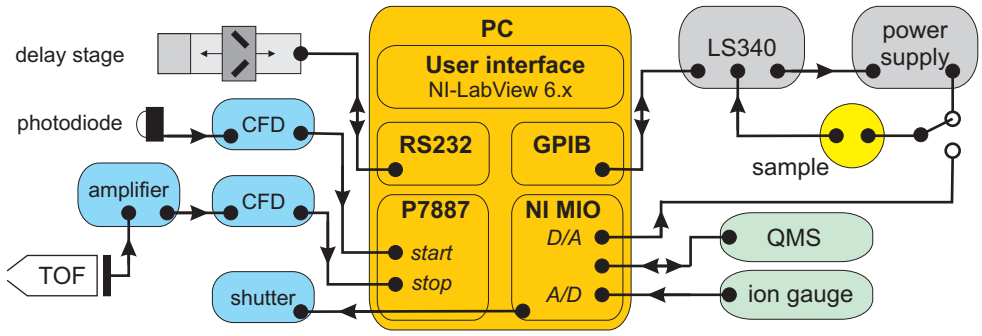

Figure 3.10: Schematic depiction of the data acquisition components used within the framework of this thesis. The arrows along the connecting wires indicate the direction of the communication.

digitizer both signals first pass through a constant fraction discriminator (Canberra CFD2126) which eliminates the timing error due to statistical fluctuations of the peak intensities.

The delay stage for time-resolved measurements is operated by a Physics Instruments motor controller (Mercury C-844). It is connected to the main computer via a RS-323 interface and can conveniently be operated within the LabView programmed 2PPE environment. While the stage is in motion the acquisition is stopped by an implemented software routine. This prevents the simultaneous accumulation of 2PPE data from different pump-probe delays. In addition mechanical shutters are used to block the laser beams. They are also employed to separately record the one-color background spectra needed to retrieve the pure cross correlation signal. The shutters are controlled by a 12bit multifunction DAQ card from National Instruments (PCI-MIO-16E-1).

The DAQ card also offers an analog-to-digital (A/D) converter. It converts the output of the ion gauge and the quadrupol mass spectrometer which provide an analog signal of 0 to 10V proportional to the measured value. Here a calibrated transformation sequence is implemented into the LabView routines. In the opposite direction the mass of the QMS can be set using the D/A converted signal which is fed into its modified control unit. The analog output also adjusts the sample potential (bias) required for a field free 2PPE measurement.

A crucial part of the experiments is the control of the temperature. The read out of the thermocouples and the heating are handled separately by a temperature controller (LakeShore 340). It is connected to the external input of a power supply (Delta Elektronica SM 35-45) used for the resistive sample heating. The ramping and stabilization of the temperature is controlled done by the LakeShore internal PID algorithm. Bi-directional communication with the computer is established through a GPIB-bus interface. In the remote mode all functions of the LakeShore can be directly accessed from the LabView program.

3.5 Sample preparation

In order to achieve a good clean surface quality for the gold and silver crystals used we employ the sputter and annealing technique. Samples that have been exposed to ambient conditions are first annealed to desorb the residual gas contaminating the surface. The subsequent sputtering is done with Argon (purity 5.0) at a background pressure of $2 \cdot 10^{-6} mbar$. A Specs ion gun accelerates the rare gas with 1.5 keV to hit the sample under an incident angle of 30°. Due to the large beam diameter (>1cm) it is not necessary to scan the sample. The sputtering cycles of 5 min length are followed by a 30 min annealing at $T = 800K$ for the gold and $T = 740K$ for the silver substrate. The quality of the surface preparation is checked with 2PPE. This allows to monitor the progress as well as comparison of the work function and surface state linewidth with results published by other groups. A sample stored under clean ambient condition usually requires 5 to 20 cycles of preparation to meet the corresponding criteria.

The above preparation is repeated at least once on a daily basis to remove residual gas and durable contaminations prior to a new experiment. At the same time the doser is heated to 350K to clean the molecule container from loosely adsorbed materials. This is done at a closed gate valve to preserve the low pressure in the main chamber. Subsequent to the preparation the crystal is cooled down with either LN or LHe depending on the experimental requirements. Again the quality is checked with 2PPE and the sample flashed one more time at $T = 800K$ ($T = 740K$) prior to the deposition of the molecules. Simultaneously the doser is brought to its final temperature. The experimental parameter for the adsorption differ for each of the molecules and the desired coverages. An overview is giving in table 3.1. Note that due to the complex behavior of the TBI molecules we have to distinguish between molecules adsorbed onto a cold and a warm substrate (for details see section 6.1).

After reaching the respective temperatures the doser is inserted into the chamber. At this point, with the shutter in front of the container still closed, the pressure in the main chamber increases by roughly one order of magnitude. Turning the shutter unblocks the path of the heated molecules onto the sample. It is closed again after

molecule	T_{doser}	T_{sample}	$time_{dose}$	resulting coverage
TBA	370K	260K	>2min	multilayer
		350K	2min	monolayer
		410K	2min	0.9 monolayer
TBI	380K	40K	>0min	submonolayer
		260K	>2min	multilayer
		320K	2min	monolayer
TBS	360K	260K	2min	monolayer
		320K	>2min	multilayer

Table 3.1: Experimental parameter for the preparation of the different molecule-metal samples investigated within the framework of this thesis.

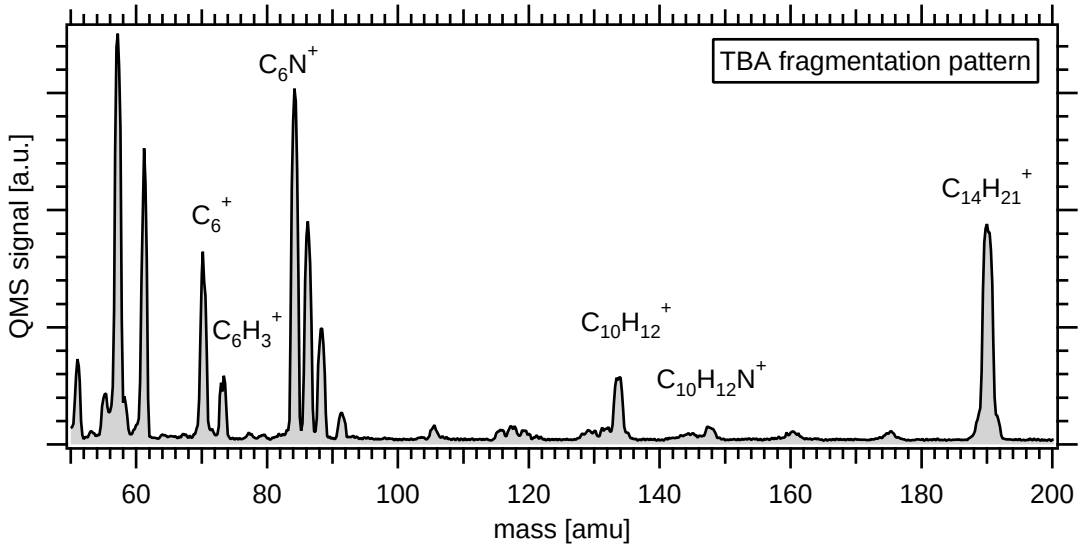

Figure 3.11: Fragmentation pattern of TBA recorded for an inserted doser at $T = 370K$. The main peaks have been labeled according to the molecular fragments. Smaller satellite peaks are mostly attributed to a varying number of hydrogen atoms. For a temperature dependence of the signal intensities see [Ley07].

the coverage dependent dosing time has expired. Retracting the doser and shutting the gate valve allows to reach the initial base pressure of $p < 2 \cdot 10^{-6} mbar$ within a few minutes.

The preparation of a well defined coverage is achieved by employing thermal desorption spectroscopy (TDS). Here the partial pressure of the desorbed molecule is recorded as a function of the sample temperature (see section 2.5). The used quardupol mass spectrometer (QMS) can resolve particles up to a mass of 200amu which is still below the mass of the three molecules studied in this thesis. However the detection process of the QMS requires an initial ionization of the molecule which, as a side effect, dissolves some of them into smaller fragments. Here the fragments of $m < 200amu$ can be conveniently detected with the current setup. For the case of TBA a fragmentation pattern is depicted in figure 3.11. Traces of all major fragments can be identified and have been labeled in the graph. The heaviest particle clearly resolvable has a mass of $m = 190amu$. It can be assigned to a benzene ring with both its tert-butyl groups. This fragment is also present in the other two molecules TBI and TBS and thus will be our primary choice for monitoring the desorption.

In general the precise coverage of the sample can only be determined after the 2PPE measurements by means of TDS. Here the area underneath the temperature dependent desorption yield is proportional to the amount of previously adsorbed molecules. As will be shown in the following chapters the multilayer of each adsorbate used can clearly be distinguished from the monolayer based on the TDS peak structure. Since a complete monolayer consist of a distinct amount of molecules its constant area can be used to express any coverage as a multiple of a single layer.

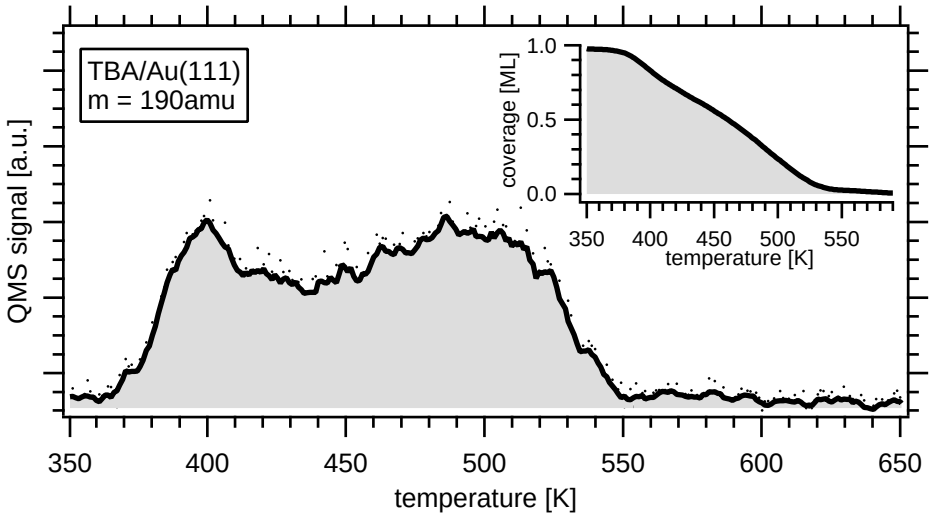

Figure 3.12: Sample TDS spectra of 1ML TBA/Au(111). The area underneath the peak is proportional to amount of desorbed molecules. Correspondingly the integration will yield a temperature dependent coverage (see inset) which can conveniently be used for gauging desorption experiments where TDS data is not available. Respective curves for all molecules used within this thesis are given in appendix G.

For an effective investigation it is very convenient to choose the layer thickness prior to the measurements. In a first approach this can be done by varying the exposure time, t_{dose} of the sample to the molecular beam. Under stable experimental conditions the coverage proved to be linearly dependent on t_{dose}. The error is, depending on the actual rate of adsorption, in the range of 0.1 to 0.5ML. While this is the only option to pre-determine the multilayer coverage there is a second, more accurate method available for the mono and submonolayer regime. It takes advantage of the broad monolayer peak shown on the example of TBA/Au(111) in figure 3.12. By carefully heating the sample the number of adsorbed molecules can be gradually decreased. The temperature can, in good approximation, be linked directly to the remaining coverage through integration of the monolayer signal. In this case the error is only in the range of 0.05 to 0.1ML. A sample of the corresponding integration is presented in the inset of graph 3.12. The respective calibration curves for all the remaining molecules is given in appendix G. Note, for the experiments it is irrelevant whether a high coverage is prepared and subsequently heated of at T_{anneal} or if the dosing is conducted at elevated substrate temperatures, $T_{dose} = T_{anneal}$. In principle both procedures proved to yield the same coverage.

4 Isomerization of TBA adsorbed on Au(111)

Within the framework of this thesis 3,3',5,5'-tetra-*tert*-butyl-azobenzene (TBA) adsorbed on Au(111) has been the first system to investigate the properties of surface confined photochromic molecules. Its four bulky tert-butyl substituents are intended to increase the distance between the azobenzene core and the substrate thereby reducing the attractive interaction between the surface and phenyl rings. In addition this leads to an electronic decoupling making TBA/Au(111) promising candidate to maintain its isomerization ability.

The occupied and unoccupied electronic structure of TBA/Au(111) has been investigated using 2-photon photoemission (2PPE). Based on coverage dependent measurements three occupied and one unoccupied molecular states can be identified. Also the existence of two isomer specific interface states is revealed. To initiate a photoisomerization TBA/Au(111) was cooled to temperature as low as 35K and continuously irradiated at photon energies in the range from 2.1 to 6eV. Simultaneously recorded 2PPE spectra exhibit saturating changes in the work function and the photoemission yield of the interface states. Upon annealing at room temperature these changes can be reverted completely. Cycles of illumination and annealing prove the robustness of this isomerization process.

In order to elucidate the excitation mechanism of the photoinduced switching its efficiency is determined as a function of the photon energy. Interestingly the dominant channel is a charge transfer from the substrate rather than an intramolecular transition. It drives the isomerization in both directions, from trans to cis (forward) and vice versa (revers), leading to a non-unity reaction yield in the photostationary state. The time dependent concentrations of trans- and cis-TBA are obtained analyzing of the photoemission signal from the corresponding interface states. This also allows to separate the contributions of the forward and reverse photoisomerization channels to the reaction kinetics.

Heating the sample increases the efficiency of the photoinduced switching and simultaneously leads to a non-monotonic change of the isomerization yield. A detailed investigation indicates a correlation to the thermal excitation of vibrational modes. At temperatures above 120K the isomerization of TBA/Au(111) is governed by the thermally induced cis-to-trans reaction. Due to the elevated ground state energy of the cis isomer this process is unidirectional. An analysis of the temperature dependent reaction kinetics yields the height of the energy barrier which significantly deviates from the TBA in solution.

4.1 Absorption behavior

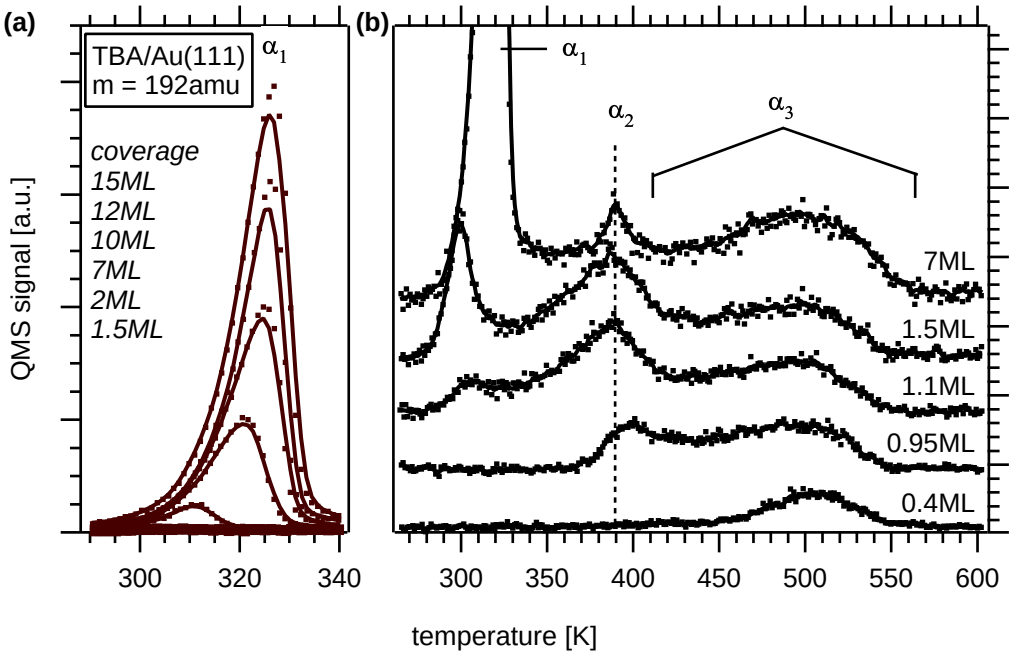

Figure 4.1: Thermal desorption spectra for different coverages of TBA adsorbed on Au(111). **(a):** Single phase mulitlayer signal exploiting a common zero order desorption kinetic. **(b):** Depiction of the monolayer regime. Two peaks are observed corresponding to a compressed (α_2) and a relaxed phase (α_3).

In order to study the adsorption behavior and to quantify the coverage of the tetra-*tert*-butyl-azobenzene on Au(111) thermal desorption spectroscopy (TDS) is employed. Here the adsorbate-covered surface was heated with a rate of $\beta = 1\frac{K}{s}$. Simultaneously the amount of desorbed molecules was monitored on one of its main fragments, a tert-butyl substituted phenyl ring, as a function of temperature. The results for different initial coverages are plotted in figure 4.1. Graph 4.1(b) displays the high temperature regime in which an evolving three peak structure is found. For small amounts of adsorbed molecules a broad peak, α_3, appears with a maximum around 500K. It spreads to lower temperatures as the coverage is gradually increased. A second, sharp peak, α_2 arises around 390K. Like α_3 it saturates upon further desorption and a new, more weakly bound peak α_1 emerges at temperatures around 300K.

Graph 4.1(a) focuses on the evolution of α_1 at high coverages. We assign this peak to the multilayer desorption of the TBA/Au(111) as its intensity grows with increasing amount of molecules. Moreover it shows a zero order desorption behavior indicated by the equal slopes and the shifting maxima of the traces. Due to the obvious saturation of the remaining spectral features they will be assigned to the

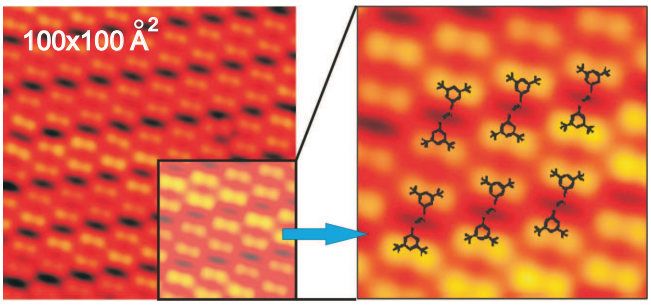

Figure 4.2: STM images of TBA/Au(111). Upon adsorption the molecules form large well-ordered islands of strictly trans isomers which are oriented parallel to the surface. Image reproduced from [Ale08].

monolayer regime. From their distinct structure exploiting two peaks we deduce the existence of multiple phases. The evolution of the low coverage phase (α_3) is very much akin to results obtained for other aromatic molecules like benzene or pyridine adsorbed on Cu(111) [Xi94][Zho02]. Its broad shape can be explained with repulsive intermolecular interactions. Those typically reduce the overall binding energy and shift the peak onset to lower temperatures as the amount of adsorbate is increased. The second phase α_2 appears only for densely packed regimes. It requires a minimum monolayer coverage of ≈90% and can be attributed to a different ordering. In this compressed phase the repulsive interaction between the molecules can be assumed stronger and the the binding to the substrate weakened. Consequently the desorption occurs at lower temperatures leading to the observed preceding peak .

Dealing with molecule confined to metal substrates we address an interplay of various physical phenomena. The investigation and the understanding of elementary processes in those systems is challenged by their complexity. In this respect the experiments greatly benefit from the existence of well-defined structures. At the full monolayer coverage this cannot be presumed as the stronger molecular interactions of the compressed phase may lead e.g. to steric hinderance or a modification of the electronic structure. Evidence is given by NEXAFS[3] measurements suggesting that TBA in the relaxed phase is oriented parallel to the substrate whereas in the compressed phase its functional group is tilted with respect to the surface. Therefore the system of choice is the relaxed monolayer of the α_3-phase with coverages up to 0.9ML. Additional supporting information is supplied by high resolution electron energy loss spectroscopy (HREELS) [Ova07] and scanning tunneling microscopy experiments (STM) [Com08][Ale06]. An STM image from a low coverage regime (<0.6ML) TBA/Au(111) is presented in figure 4.2 [Ale08]. It shows a large, well-ordered island of the molecules. In agreement with NEXAFS and HREELS the TBA appears to lie flat on the substrate. No deviations in the height can be observed from which the authors conclude that all molecules are adsorbed in the trans configuration. This can be attributed to the deposition process. Here the molecules are heated to ≈380K, a temperature at which the free TBA efficiently performs a thermally induced unidirectional cis-to-trans isomerization.

[3]near edge X-ray absorption fine structure, see section 4.3.1

4.2 Switching properties

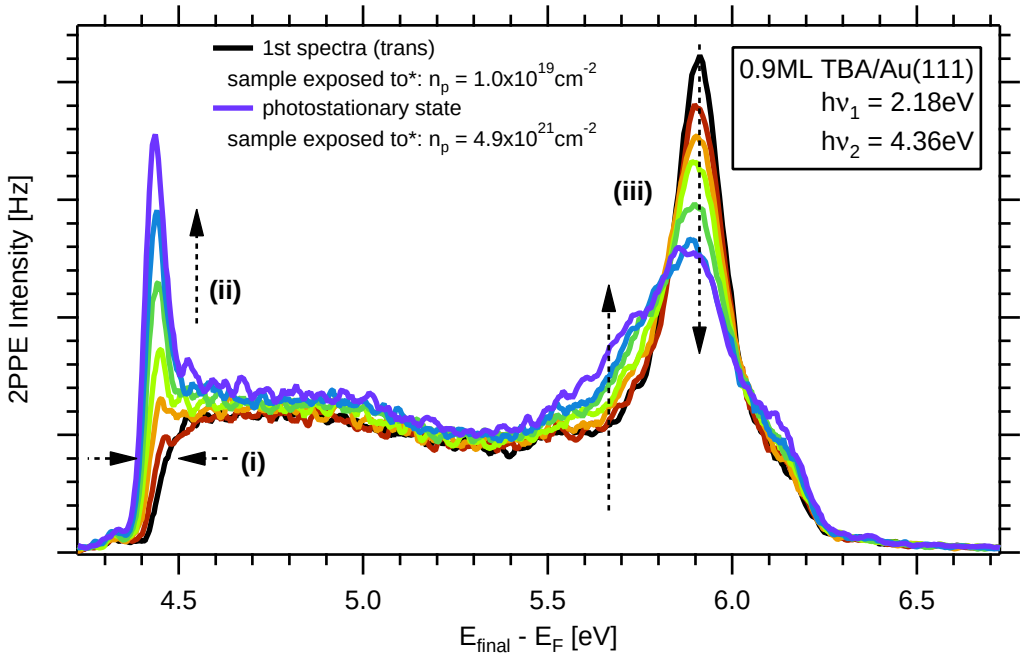

Figure 4.3: Light induced evolution of 2PPE spectra from 0.9ML TBA/Au(111). Three major changes are observed: (i) A decrease of the work function, (ii) an increase of the low-energy secondary electron yield, and (iii) a shift of spectral weight in the peak structure close to the Fermi cutoff edge. *(*): Photon dose of the UV light ($h\nu = 4.36eV$), the visible photons are neglected as they do not significantly contribute to the isomerization. For details see section 4.5*

In the following we present a general introduction to the observed photoisomerization of TBA/Au(111). This will motivate the investigations of the underlying excitation mechanisms and furthermore yield important considerations for the analysis of the electronic structure.

Figure 4.3 depicts a series of subsequent 2PPE spectra from 0.9ML TBA/Au(111) using $h\nu_1 = 2.18eV$ and $h\nu_2 = 4.36eV$. Each trace has been recorded with a UV-photon dose of $N_{ph} = 1 \cdot 10^{19} cm^{-2}$ followed by an illumination interval of $N_{ph} = 1.1 \cdot 10^{20} cm^{-2}$ at the same photon energies. Without going into detail we can clearly observe three photon induced changes in the spectra: (i) The position of the vacuum cutoff edge, which can be directly linked to the sample work function Φ, is shifted to lower energies. Hence Φ is lowered due to the illumination. (ii) The photoemission signal at the vacuum cutoff edge experiences a dramatic increase. (iii) A sharp peak close to the Fermi edge of the spectra broadens upon illumination and loses intensity.

At a sample temperature of $T = 40K$ this evolution saturates after an exposure to approximately $N_{ph} = 2 \cdot 10^{21} cm^{-2}$ and the shape of the spectra remains constant

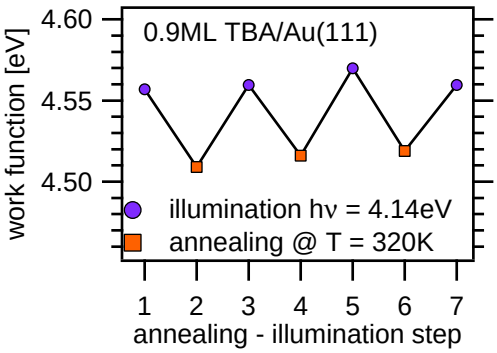

Figure 4.4: Work function shift due to cycles of light induced forward and thermally activated reverse isomerization of 0.9ML TBA/Au(111). The series demonstrates the reversibility of the switching which rules out a decomposition of the molecule.

over several hours even in the absence of the laser light. Annealing the sample at room temperature on the other hand reverses the changes completely. A second illumination series shows the same changes as the initial one. We repeated this experiment at an increased sample temperature of 90K and with a photon energy of $h\nu = 4.14eV$. Here we monitor the work function over several illumination and annealing cycles as shown in figure 4.4. The data clearly proves that we are able to reversibly change the electronic structure of the investigated system which we interpret as a signature of the TBA/Au(111) trans-cis isomerization.

From the above experiment we can draw some preliminary conclusions regarding the switching properties of TBA/Au(111). Most importantly the system exploits two thermodynamically stable states at temperatures $\leq$90K. Those can be assigned to different configurations of the molecules. Since STM and XPS measurements show that TBA absorbs in the trans configuration we will henceforth correlate the initial spectra to this isomer. The conversion to the cis form is triggered by illumination with our femtosecond laser pulses causing the above mentioned changes in the electronic structure. Heating the sample creates a second isomerization channel of opposite direction similar to the molecule in solution. A depiction of this process in terms of a simple 1D potential energy landscape is presented in figure 4.5. In addition to the discussed switching pathways the graph also includes a photon induced cis-to-trans (reverse) isomerization. Its existence is not a priori deducible from our

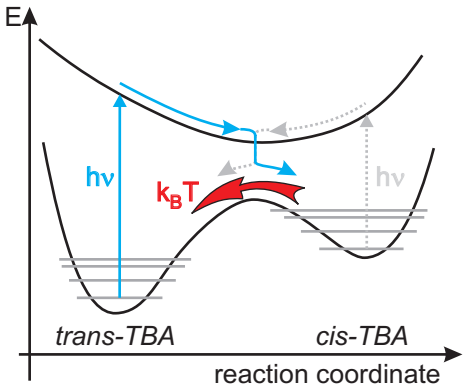

Figure 4.5: Schematic depiction of the potential energy landscape of TBA/Au(111) and the observed isomerization pathways. Light induced processes (blue and gray) lead to switching in both directions whereas the thermal channel (red) initiates an unidirectional conversion of the cis isomers. A detailed analysis, including the influence of the vibrational level, will be given in the course of this chapter.

preliminary experiment. Evidence however will be found when analyzing the isomer ratios in section 4.6.3. Consequently the continuous illumination of TBA/Au(111) will not yield a purely cis configuration. Instead a photostationary state is reached in which the light induced forward and reverse isomerizations occur at an equal rate.

In order to elucidate the underlying excitation mechanism, being either a direct intramolecular or a substrate mediated excitation, detailed knowledge of the electronic structure is required. A powerful tool in this respect is the 2PPE which provides an access to the energetic positions of the occupied and unoccupied states of TBA/Au(111). The corresponding results will be presented in section 4.3. In a second step the isomerization process will be quantified as a function of the wavelength and the intensity of the laser light. Connecting this data with the electronic structure will help us to identify the underlying excitation mechanism. Prior to the analysis however a detailed analytic description of the switching has to be obtained to ensure the proper interpretation of the experimental data. An introduction to the reaction kinetics and the discussion of the photon induced excitation will be given in sections 4.4 and 4.5.3 respectively.

Returning to figure 4.5 a barrier in the ground state separates the two isomers. As we have seen from our preliminary experiment it can be overcome thermally in the cis-to-trans direction. This behavior is in agreement with the results of TBA in solution where the barrier height is ≈1eV [Hag08b]. The adsorption of the molecule onto the gold substrate can well be assumed to alter the geometry and thus also the potential energy landscape. Here the height of the barrier is very well suited to compare the adsorbed with the solvated species. The corresponding measurements will be discussed in section 4.6.1.

Having determined the influence of the thermally induced reverse channel we were able to extract the temperature dependence of the photoisomerization from the experimental data. In sections 4.6.4 and thereafter evidence will be presented that the efficiency of the photon induced switching is strongly enhanced via heating the substrate. In addition the trans-cis isomer ratio in the photostationary state is shifted as a function of the temperature. Both observations can be associated with the excitation of vibrational modes which therefore are already indicated in the isomerization sketch 4.4.

4.3 The electronic structure of TBA/Au(111)

The discussion of the electronic structure of TBA/Au(111) has to be treated with care as we have witnessed a number of obvious, light induced changes. To avoid inconsistencies all measurements are referenced to the photostationary state at a sample temperature of 90K unless otherwise stated. The justification of this approach will become obvious when examining the switching properties of TBA/Au(111) in sections 4.5ff.

A common behavior of adsorbate-covered metals is the change of the sample work function Φ due to the creation of a dipole layer at the surface [DR05]. For the case of the TBA/Au(111) the corresponding values are plotted versus the coverage in figure 4.6. We see an approximately linear decrease of Φ from $5.45 \pm 0.05eV$ of the bare gold surface to $4.45 \pm 0.05eV$ for a full monolayer. Upon further deposition this value is stabilized and does not change in the range of investigated coverage up to 6ML.

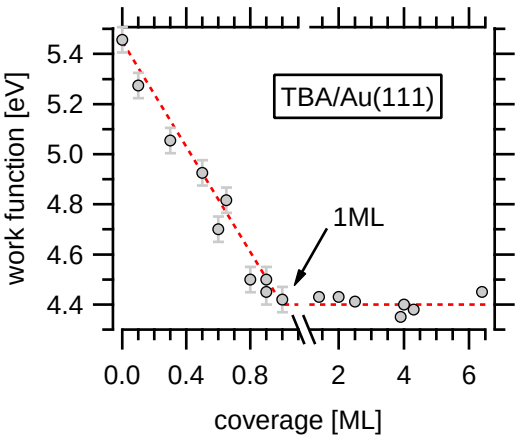

Figure 4.6: Coverage dependent work function of the TBA/Au(111) in the photostationary state.

Access to the energy region of occupied states is given by direct photoemission. For this purpose we use the pulsed 6eV beam of our laser system. A coverage dependent series of spectra is shown in figure 4.7. The spectra of the clean surface is dominated by the peak labeled as SS which we assign to the gold surface state at $E_B = -0.47eV$. It is quenched with increasing TBA coverage but retains its initial binding energy. Simultaneously a second feature, SSx, appears at $E_B = -0.23eV$. Contrary to the SS its intensity seems to be independent of the coverage. In case of a molecular state however one would expect a decrease as the monolayer is desorbed. Hence this option can be ruled out. A similar state, derived from the substrate, has been observed by Forster *et al.* adsorbing xenon onto a Au(111) crystal [For03]. They assign it to a split off from the surface state which is shifted in energy due to the Xe absorption. It exploits the same dispersion and spin orbit splitting as the SS of the clean surface which substantiates this proposal. Due to the agreement of the energetic position and the coverage dependence we adopt this assignment for the SSx peak found in our spectra. Further evidence is given in sections 6.1.2 and 6.2.2 where we discuss the electronic structure of similar switch/metal systems. In this context data will be presented proving that the surface state and SSx indeed have the same dispersion (see section 6.1.2).

Returning to figure 4.7 we see that in agreement with the work function change the width of the spectra increases with the amount of adsorbed molecules. At 0.9ML

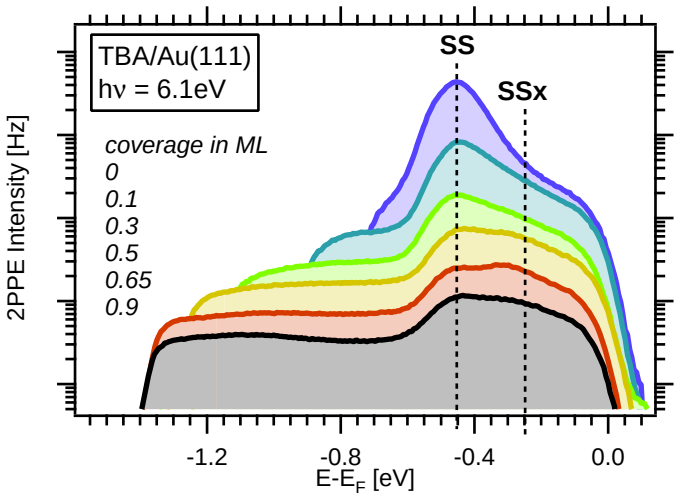

Figure 4.7: Coverage dependent series of direct photoemission spectra from TBA/Au(111). The traces are governed by the gold surface state (SS) and its split-off (SSx). No molecular states have been observed.

we are able to probe up to ≈1.2eV below the Fermi level. Within this region no molecular states can be found. Note however that at this coverage, which will be used to elucidate the excitation mechanism of the photoisomerization, the gold features are still present and cannot be neglected.

To extend the probed region and to include the unoccupied states 2-photon photoemission is employed. Exemplary spectra for 0.9ML TBA/Au(111) are presented in figure 4.8. The one-color trace has been recorded using UV light at $h\nu = 4.37eV$. It shows two molecule induced states A and B which are located on top of the broad background signal of the gold d-bands. In the corresponding two-color spectra recorded at $h\nu_1 = 2.18eV$ and $h\nu_2 = 4.37eV$ we observe two additional peaks (C and D) close to the Fermi cutoff edge. Carefully analyzing the data we will find those states in the UV spectra as well indicating that they are either initial or UV-light pumped intermediate states. In order to properly assign the peaks to the corresponding molecular or metal states we have to investigate their coverage and photon energy dependence.

Figure 4.9 exploits the results of the respective measurements for peaks A and B. From the photon energy dependance ($h\nu$) in graph 4.9(b) we see that the final state energy of both features shifts with $2\Delta h\nu$. According to the 2PPE excitation mechanisms discussed in section 2.4.2 this is the case for peaks originating from occupied initial states. Graph 4.9(a) depicts the evolution of the peaks for different coverages ranging from 2ML to the almost clean gold substrate. Here A and B decrease in intensity as molecules are desorbed. Hence the initial classification as molecular induced features is validated. The spectra also show a third peak E which likewise can be assigned to an occupied molecular state (see 4.9(b)). From the data we determine the binding energies of peaks A, B and E to $E_B = -2.65 \pm$

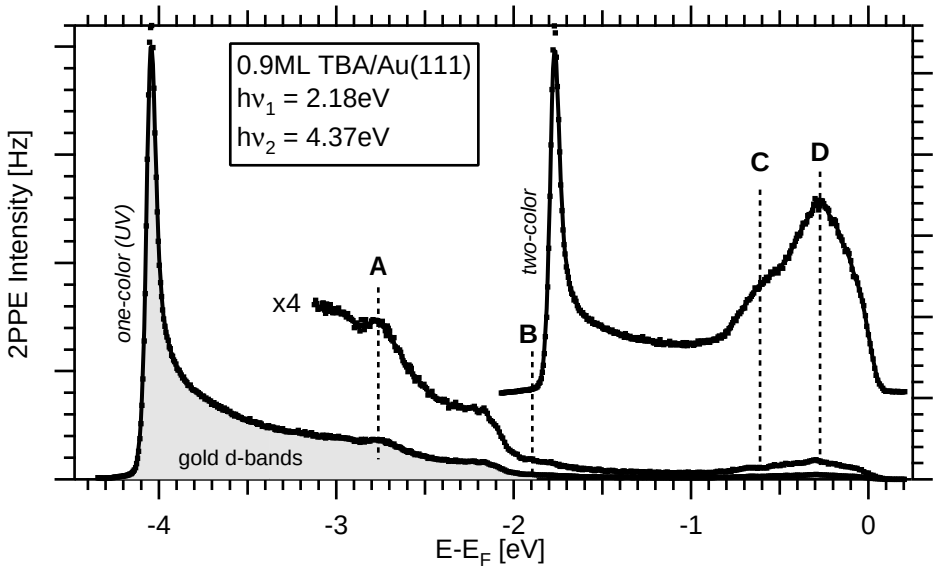

Figure 4.8: One and two-color 2PPE spectra of 0.9ML TBA/Au(111). Four molecule related states (A-D) have been identified. The occupied features A and B are masked by the large background consisting of the Au(111) d-bands and secondary electrons. For a more detailed depiction see figure 4.9(b) where the existence of an additional occupied peak is revealed.

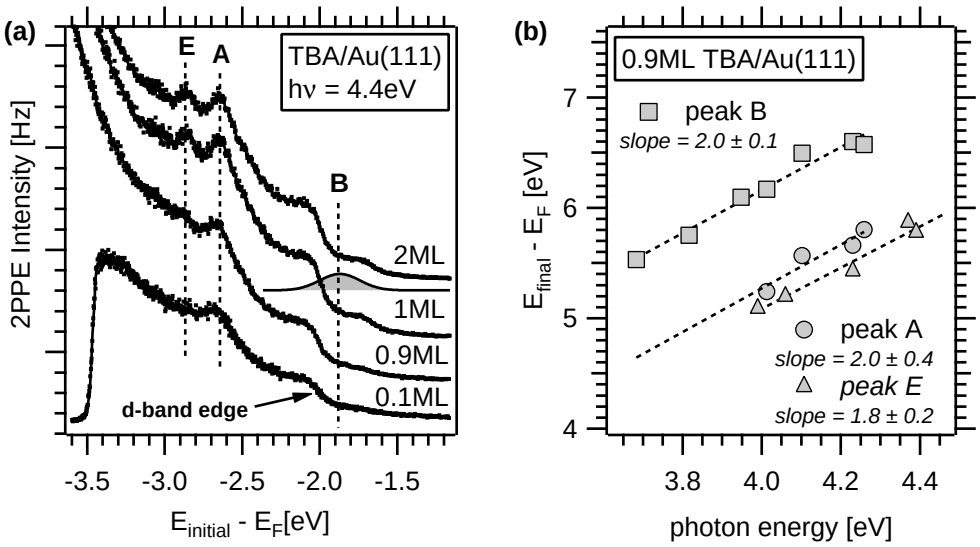

Figure 4.9: (a): Selected spectra from a coverage dependent one-color 2PPE series. Peaks A,B and E loose intensity upon desorption of the TBA suggesting a molecular origin. The signal of peak B is spread across the edge of the gold d-band. To illustrate its position the result of a Gaussian peak fitting is appended (gray area). **(b):** Photon energy dependence for peaks A, B and E. According to their slopes all three peaks have to be assigned to occupied initial states.

$0.08eV$, $E_B = -1.88 \pm 0.08eV$ and $E_B = -2.87 \pm 0.08eV$, respectively. B indeed coincides with the first rising edges of the d-band as can be nicely seen in the coverage dependence. To mark its position we added the trace of a gaussian peak (gray shaded area) obtained from fitting the spectra.

The above discussed states will remain the only occupied states accessible within the used photon energy range. Since all of them display a molecular character we assign the in descending order of their binding energy to the HOMO, HOMO-1 and HOMO-2 of the adsorbed TBA. For the free azobenzene it is known that the first and second occupied orbital belong to the free electron pair and the π-bond of the azo-group respectively [Näg97]. However XPS measurements performed in cooperation with Martin Weinelt and coworkers (MBI Berlin) show that this order is reversed or at least degenerate for TBA adsorbed on Au(111)[4]. Such a detailed site specific correlation of the orbitals cannot be given based on the 2PPE data.

We proceed the discussion of the electronic structure by analyzing the peaks labeled C and D in figure 4.8. A photon energy dependent series of two-color 2PPE spectra is obtained to elucidate the energetic position of the corresponding states. In figure 4.10 the final state energies of peaks C and D are plotted versus the energy of the visible light. Here the slopes of $m = 1.1 \pm 0.2$ (D) and $m = 1.1 \pm 0.3$ (C) suggest an assignment to UV light pumped, unoccupied intermediate states. A detailed analysis of their energetic positions yields values of $E_B = 3.80 \pm 0.08eV$ (C) and $E_B = 4.05 \pm 0.08eV$ (D) with respect to the Fermi level. This is strongly supported by data from one-color 2PPE measurements (not shown here). To clarify the origin of those unoccupied states we again have to investigate their coverage dependence.

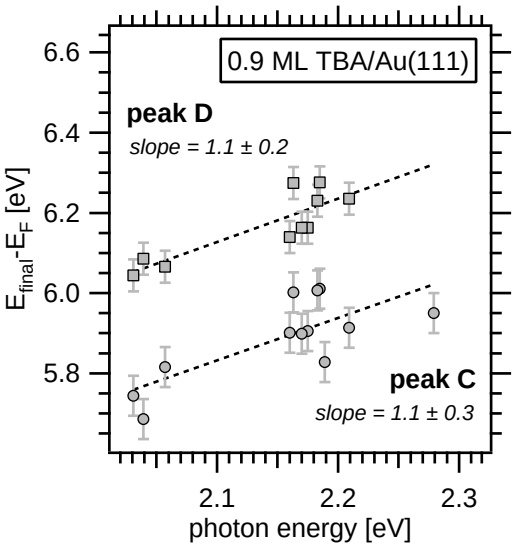

Figure 4.10: Photon energy dependence of peaks C and D measured on 0.9ML TBA/Au(111).

Figure 4.11(a) depicts a series of two-color 2PPE spectra taken at varying adsorbate thicknesses. Here the peak positions of C and D are masked by three contributions from the Au(111) substrate: The surface state (SS) which, as observed in direct photoemission experiments, is reduced upon adsorption of the TBA. The split off state SSx appearing as a weak shoulder to the main peaks D and SS. And finally peak SPB which is present in all traces but becomes obvious only at coverages <0.4ML where peak C is almost extinct from the spectra. It originates from a

[4] a brief description of the experiments and their results will be given in section 4.3.1

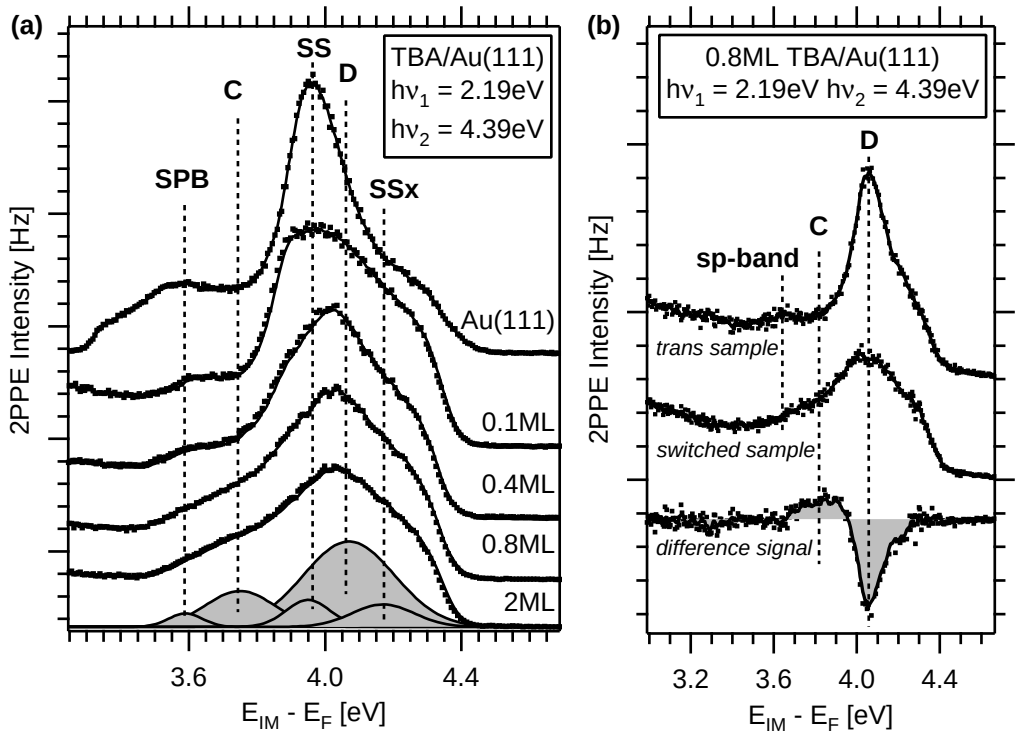

Figure 4.11: (a): Two-color 2PPE spectra from different TBA/Au(111) coverages. Desorption of the molecule leads to a reduction of the signal induced by the molecular features C and D. Simultaneously the adsorbate quenched gold surface state, SS, regains intensity. **(b):** Comparison of 2PPE spectra from an initial (trans) and a partially switched sample. The difference spectra clearly shows opposing behavior for states C and D justifying an assignment to a cis-TBA and trans-TBA state, respectively.

direct transition between the gold sp-bands and has been previously been identified in the direct photoemission spectra. A detailed discussion of this state and its appearance in the 2PPE spectra is given in appendix C presenting data from the clean gold surface. Due to the large number of participating states the photoemission signal is rather broad an one can hardly distinguish the individual contributions. To illustrate them the 0.8ML TBA/Au(111) spectra has been analyzed employing a Gaussian peak fit function and the respective results are appended in form of gray shaded areas. A comparison of the different coverages shows that the intensities of peaks C and D increase with the amount of deposited molecules. Hence we can assign them to adsorbate induced states.

A peculiarity of the two intermediate peaks (C and D) is their evolution under the influence of laser irradiation as has briefly been described in the previous section. For a more detailed analysis we turn to graph 4.11(b). It depicts three spectra from a 0.8ML TBA/Au(111) sample obtained in a two-color 2PPE measurement. The top trace represents the electronic structure of the trans isomer. It is recorded

with a photon dose of $N_{ph} = 1 \cdot 10^{19} cm^{-2}$ which is negligible for the isomerization process considering the dose of $N_{ph} = 2 \cdot 10^{21} cm^{-2}$ needed to reach the photostationary state (PSS). The middle trace represents the 2PPE signal of the switched sample. To highlight the illumination induced changes the difference signal is visualized by the lower trace. It clearly shows an increase of peak C and a decrease of peak D as the sample is switched from a purely trans state to the PSS. Hence C and D can be assigned to states of the cis and trans isomers, respectively. This gives us the extraordinary advantage not only to observe the relative changes in the isomer concentration as a function of time but also to determine an absolute value of the reaction yield. A detailed description of this issue will be given in section 4.6.3. The second important information retrieved from the difference spectra is deduced from the peak ratio. Although the sample consists of ≈66% cis molecules[5] the corresponding peak C is still significantly smaller than the trans peak D. This can be explained by the differences in the wave function overlap between adsorbate induced states and the Au(111) band structure [Lin07]. Key criteria in this respect are the availability (density) of metal states and the spatial and energetic location of the molecular state. Here state C is located close to the projected band gap at $E_B = 3.6eV$ whereas state D is well within the region of the unoccupied sp-band [Woo86]. Hence we can assume that peak D experiences a stronger electronic coupling which leads to a enhanced population and thus to a larger photoemission signal.

In a next step we want to determine the actual origin of the intermediate states. A first indication is given by their dispersion presented in figure 4.12. Here we performed angle-resolved 2PPE measurements using $h\nu_1 = 2.23eV$ and $h\nu_2 = 4.32eV$ photons on 0.9ML TBA/Au(111) in the photostationary state. A quadratic fit of the energetic position as a function of the parallel momentum $k_{\|}$ (dashed lines) yields the effective mass m_{eff}. The values of $m_{eff} = 1.3 \pm 0.2 m_e$ (C) and $m_{eff} = 1.2 \pm 0.3 m_e$ (D) point to a free electron like dispersion of both states. Hence they are delocalized in the plane parallel to the surface.

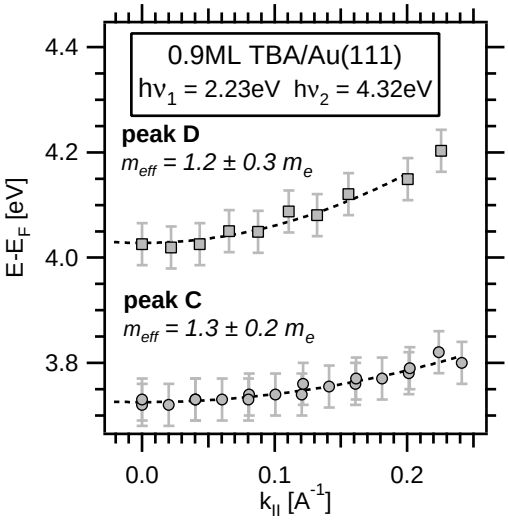

Figure 4.12: Dispersion of the interface states C and D. With effective masses close to the value of the free electron they appear delocalized parallel to the surface.

States with similar binding energies and dispersions can usually be assigned to the image potential at the metal-

[5] The analysis of the isomer concentration and thus the origin of this value is discussed in section 4.6.3.

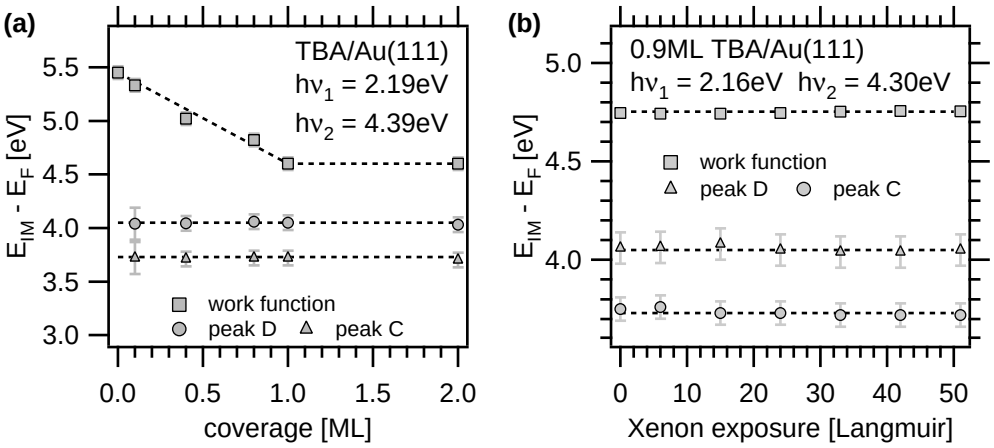

Figure 4.13: Modification of the adsorbate layer thickness to elucidate the origin of the intermediate states C and D. **(a):** Coverage dependent binding energies of peak C and D in comparison to the TBA/Au(111) work function. No pinning to the vacuum level is observed. **(b):** Xenon titration experiment. The work function and binding energies of peak C and D remain constant even upon extended exposure to Xe. For details see text.

vacuum interface. This has e.g. been shown for alkane layers on Ag(111)[Lin96], benzene on Cu(111) [Vel98] and naphthalene on Cu(111) [Wan00]. The properties of the image potential states (IPS), viz. their binding energies and lifetimes, are influenced by the electron affinity of the molecules and the thickness of the adsorbate layer. In a simple picture the adsorption of molecules: (i) creates a barrier which pushes the electrons further away from the surface and (ii) modifies the potential at the vacuum site [Hot07]. (i) leads to a decoupling of the image state wave function from the substrate which increases e.g. its lifetime whereas (ii) will result in a shift of the binding energy. This has been observed as a function of coverage in the above mentioned examples.

For TBA/Au(111) however the binding energies of the cis(C) and the trans(D) state are clearly coverage independent as can be seen from figure 4.13(a). In contrast to the expected behavior of an image potential state they are not pinnend to the sample work function indicated by the quadratic markers. At coverages of $\leq$0.9ML the separation between peak C and E_{vac} even exceeds 0.85eV. This value represents an upper theoretical limit, derived from the lowest state of the corresponding Rydberg series (see section 2.3), for an IPS binding energy [Hot07]. Consequently we have to look for an alternative origin of the intermediate states C and D.

To verify this observation we perform an alternative measurement increasing the size of the molecular layer by co-adsorption of xenon. This method has been employed previously to determine the image states properties of various systems [Wol96] [Mer93] [Ber00]. The use of a rare gas is assumed to have a negligible impact on the underlying TBA molecules. Results from a measurement performed on 0.9ML TBA/Au(111) are presented in figure 4.13(b). Here xenon was adsorbed via

a background pressure of $p = 1 \cdot 10^{-7} mbar$. Based on the exposure time we estimate the final Xe coverage at the end of this measurement to be $\gg$1ML. Throughout the experiment subsequent spectra were taken to observe the evolution of the binding energies of states C and D. Independent of the coverage both remained at their initial energetic positions.

For the final assignment of the two states (cis and trans) we have to include a discussion of their lifetimes. Figure 4.14 depicts time resolved 2PPE data from 0.9ML TBA/Au(111) in a 2-dimensional false color plot. As can be seen from a 1D spectra at zero delay the measurement has been obtained in the photostationary state, thus exploiting an overlapping signal of the trans(D) and the cis(C) intermediate state (right side graph). In the 2D spectra this can be witnessed as a bright spot. It shows an obvious asymmetry towards lower binding energies. For a detailed analysis we cut the spectra at the corresponding peak positions of C and D to obtain the temporal evolution of their intensity (lower graph). The cross-correlation curve of the trans state (D) at $E_B = 4.05eV$ is completely symmetric. Thus the signal is the simple convolution of both laser pulses and a state with a lifetime below the resolution limit of ≈10fs. For the cis state at $E_B = 3.80eV$ on the other hand we can retrieve a short lifetime as indicated by the deviating cross correlation trace in the direction of positive delays. An exponential fit yields a lifetime of $\tau = 30 \pm 10 fs$ which reflects upon the above mentioned asymmetry in the 2D plot. The difference in the lifetimes can again be explained by the difference in coupling to the substrate. In agreement with the photoemission intensities the cis related peak (C) exploits a weaker interaction which leads to a slower decay. Additional time resolved measurement on 0.6, 1.0 and 3.0ML TBA/Au(111) display equal times for the respective decays of the trans and cis state. Hence the electron dynamics, in agreement with the constant binding energy, is independent of the coverage.

The results of the coverage dependence, the xenon co-adsorption and the lifetime measurements strongly suggest that the two states C and D are located not at the vacuum interface but at or close to the metal/molecule interface. On the other hand the free electron like dispersion contradicts the assignment to a molecular state. Hence we propose an origin derived from the potential created at the metal/molecule interface. Thus far only two systems have been reported to exhibit such states. They were first observed in bulk argon adsorbed on a Ag(111) crystal [Roh05]. In contrast to image potential states (IPS) they require a minimum layer thickness to appear in the spectra [Güd05]. Little attention has been given to such systems as one usually is interested in thin adsorbate films and the resulting effects on the IPS. For argon however a minimum coverage of 4ML is needed and calculations show that this number is even larger for other rare gas adsorbates [Güd05]. Therefore it is not surprising that only limited knowledge about interface states is available. Evidence for their existence in more complex systems has been found investigating alkanethiolate self-assembled monolayers on Au(111) [Mun06]. This species however is chemisorbed onto the surface. In the case of TBA/Au(111) on the other hand they exist within the first monolayer of a physisorbed system which to our knowledge has not been observed before. We will reencounter those states

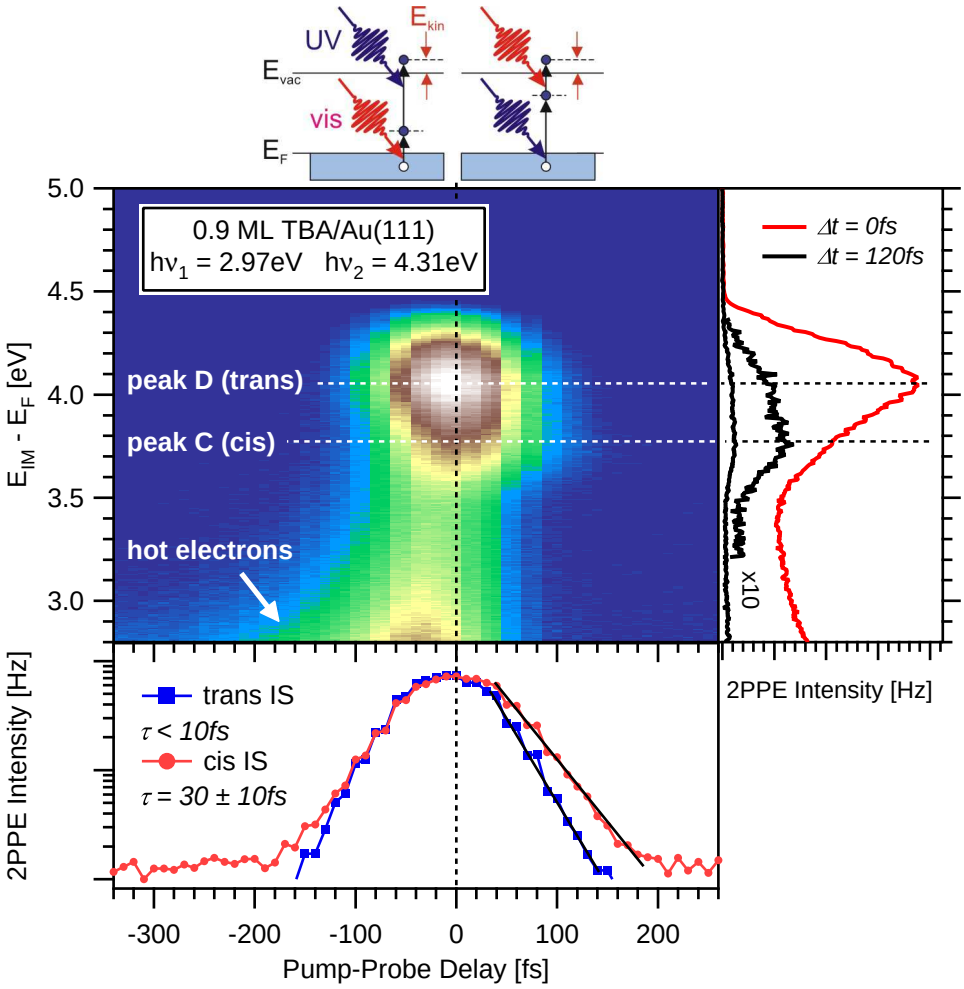

Figure 4.14: Time-resolved 2PPE data of 0.9ML TBA/Au(111) presented in a 2D false color plot. The laser sequences are depicted in the top sketch. For negative time delays probing occurs via the visible and probing via UV light, for positive time delays the order is vice versa. The lifetime of the trans related state (D) is below the experimental resolution. Peak C on the other hand exhibits a decay of 30fs. Extracting a one dimensional 2PPE spectra at a delay of 120fs (right graph) we can now clearly distinguish its contributions from peak D which governs the spectra at the zero delay.

for further molecule/metal systems investigated in the framework of this thesis (see sections 6.1.2 and 6.2.2).

In the previous discussion of the electronic states we have not yet found an obvious signal from the lowest unoccupied molecular orbital which is expected in the energetic region closely above the Fermi level. Carefully analyzing the two-color 2PPE data we indeed find a third unoccupied state. To elucidate its energetic positioning we present a photon energy dependence recorded on 0.9ML TBA/Au(111)

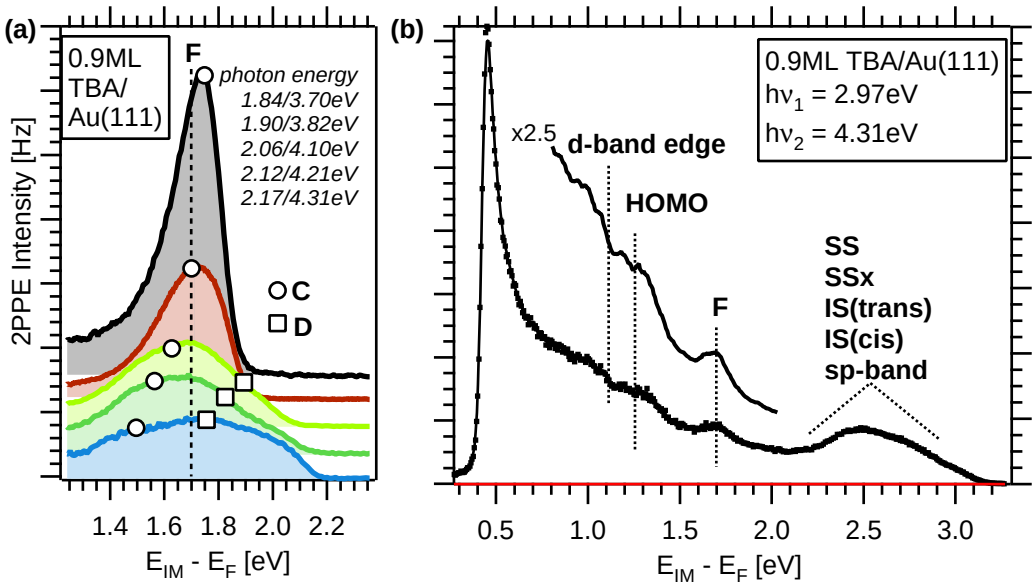

Figure 4.15: Intermediate state F observed in 2-color 2PPE spectra on 0.9ML TBA/Au(111). **(a):** Photon energy dependence using a common setup with fundamental (visible) and frequency doubled (UV) light. Here peak F moves in between the two UV light pumped intermediate states C and D (indicated by circles and squares) which mask its position. **(b):** Peak F appears well resolved in a spectra using separately tuned photon energies of 2.97 and 4.31eV.

in figure 4.15(a). All traces have been plotted versus the intermediate state energy of states pumped with visible light. This depiction allows us to identify similarities in the different spectra. Here we find indications of a peak labeled F pumped by photons of the visible (fundamental) beam. It moves in between the peaks of the cis and trans interface states (C and D) indicated by circles and boxes in the graph. Due to its low intensity it is barely distinguishable from the neighboring features. Thus to verify the existence of F we cannot retain the common 1:2 ratio of pumping and probing photon energies. Instead we use a combination of $h\nu_1 = 2.97eV$ and $h\nu_2 = 4.31eV$ yielding the spectra depicted in figure 4.15(b). A clear peak at a binding energy of $E_B = 1.7 \pm 0.1eV$ proves our previous assumptions to be correct. Furthermore we find a strong signal 1.9eV below the Fermi edge which can confidently be assigned to the HOMO seen in the one-color 2PPE spectra before. The broad feature at the right end of the spectra can be explained as the overlapping signal from various gold and TBA induced features as labeled in the graph.

Based on the binding energy a correlation of this state to the interface or vacuum potential seems unlikely. Instead we assign it to the LUMO of the TBA since it is clearly not a feature of the clean gold surface. This assignment is in very well agreement with data from STS measurements which report the LUMO of the trans molecule at $E_B = 1.67eV$ [Ale07][Ale08]. There also the existence of a spectral

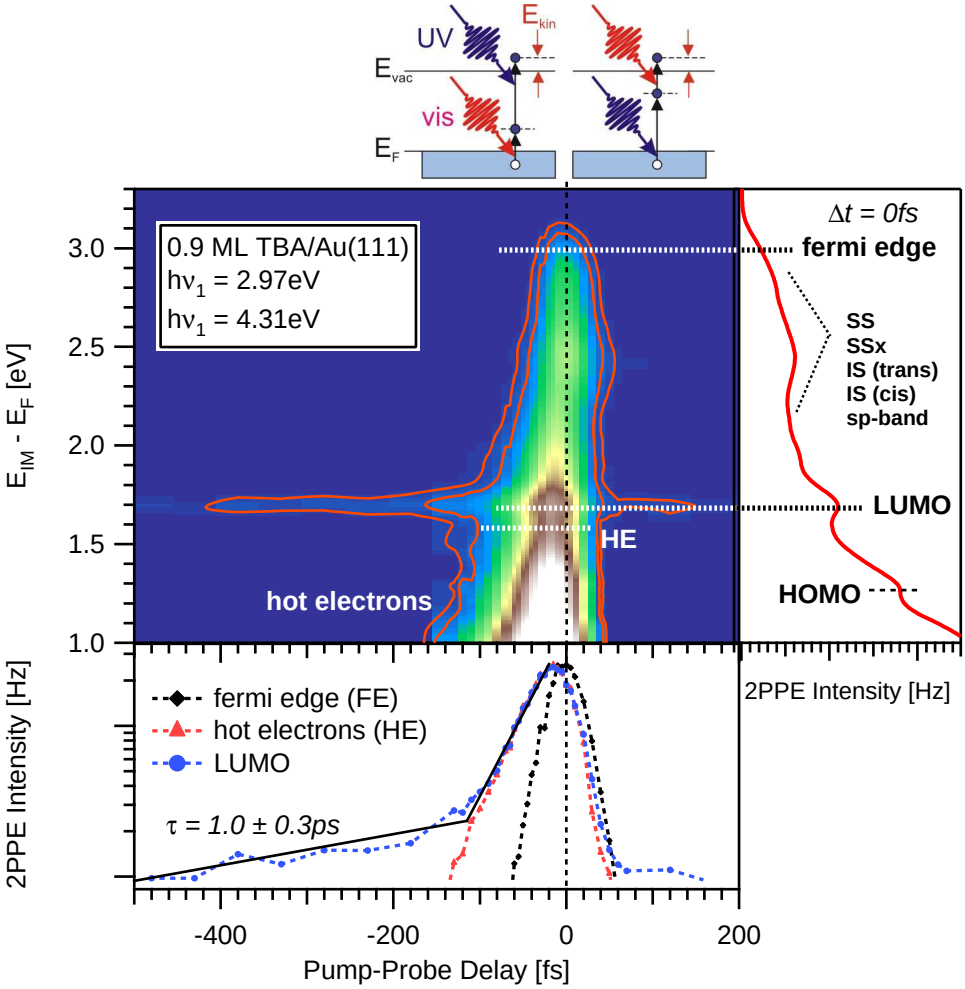

Figure 4.16: Time-resolved 2PPE data of 0.9ML TBA/Au(111) presented in a 2D false color plot. Using separately tuned photon energies we obtain access to the weak signal of the LUMO which is superimposed on a large hot electron background (for details see text). To highlight the extraordinary long lifetime of approximately 1ps selected contour traces (red) are appended to the plot.

feature from the cis-LUMO at $E_B = 1.35eV$ is reported. We however find no corresponding signal in our spectra which could be due to a very weak electronic coupling between the molecular state and the gold substrate.

Preliminary data for the lifetime of the LUMO has been acquired using time resolved 2PPE at the above mentioned photon energies. The corresponding 2D plot is depicted in figure 4.16. A cut along the zero delay axis yields an energy spectra identical to the one presented in figure 4.15. Hence we can directly focus on the investigation of the LUMO peak at $E_B = 1.7eV$. It sits on top of a large exponentially decaying background originating from hot electrons crated by an intense

$h\nu = 2.97eV$ beam. The magnitude of this background becomes obvious when cutting the spectra along the binding energy as shown in the blue trace of the lower graph. Here we see a presumably bi-exponential decay of the LUMO. Fitting the slower component we obtain a lifetime of $\tau = 1.0 \pm 0.3ps$. This is an astonishingly long value pointing to a weak electronic coupling between the LUMO and the gold substrate. An obvious reason is its energetic location within the projected band gap. In return this suggests a scattering of hot electrons as the main population channel which should be reflected in the electron dynamics in terms of a delayed rise of the LUMO peak intensity. Due to the preliminary character of the data we unfortunately cannot distinguish such a behavior.

4.3.1 XPS/NEXAFS

Within the framework of this thesis a fruitful collaboration has been started with the group of Martin Weinelt[6] from the Max Born Institute Berlin. It allowed us to investigate the geometric and electronic structure of TBA/Au(111) with near edge X-ray adsorption fine structure (NEXAFS) and X-ray photoemission spectroscopy (XPS). The experiments have been performed at the synchrotron beam lines of BESSY II[7]. A detailed description and analysis of the obtained data will be given in the PhD thesis of Roland Schmidt [Sch09]. Here we will limit ourselves to a brief discussion of results relevant for this work which have previously been presented at various meetings.

Photoisomerization of TBA/Au(111) Core level spectroscopy has successfully been employed to demonstrate the photoisomerization of 1ML TBA/Au(111). Two traces, one of an annealed/pristine sample and one of an illuminated and thus switched sample are presented in figure 4.17(a). The former exhibits a single peak indicating a similar chemical environment for all nitrogen atoms within the TBA. The latter shows two peaks which are assigned to different chemical environments due to the tilting of one of the phenyl rings upon isomerization (see also figure 4.18). From the peak ratio an isomerization yield of ≈73% is determined.

In order to induce the switching the sample has been illuminated using a 405nm continuous wave laser diode. This indicates that the underlying process is not limited to short pulse lasers and thus is presumably not based on higher order phenomena. Synchrotron radiation on the other hand had no effect on the isomerization of TBA/Au(111).

Absorption geometry The absorption geometry of TBA has been elucidated using NEXAFS spectra from the carbon 1s and the nitrogen 1s edge. Here the π^*-resonances of the phenyl rings (carbon) and the azo double bond (nitrogen)

[6] and here in particular I would like to thank Roland Schmidt!

[7] Helmholtz-Zentrum (formerly known as Berliner Elektronenspeicherring - Gesellschaft für Synchrotronstrahlung mbH)

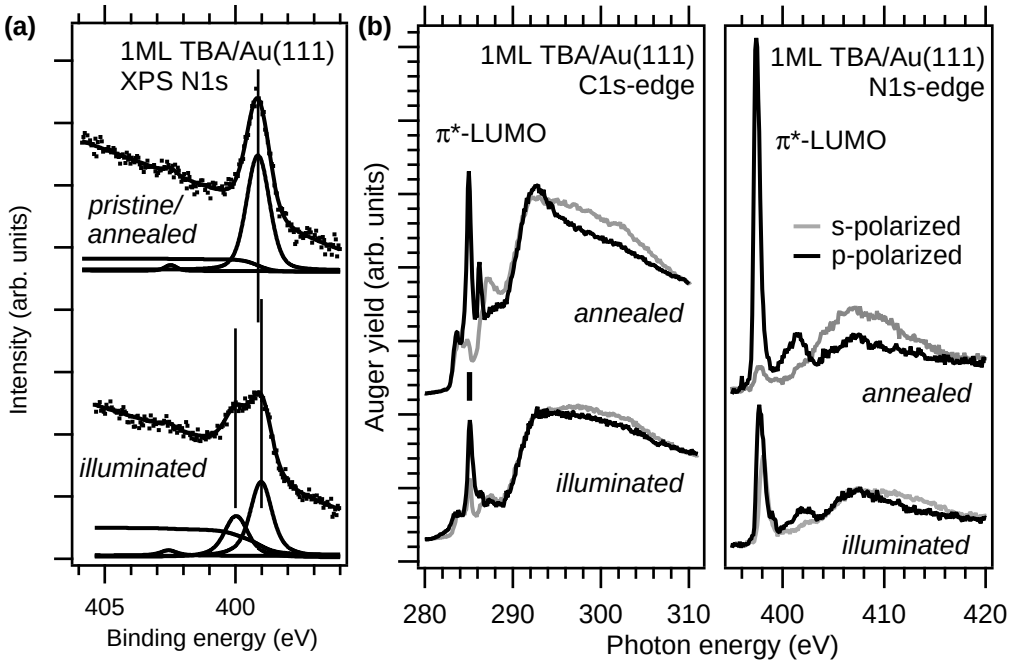

Figure 4.17: **(a):** XPS spectra of 1ML TBA/Au(111). The upper trace corresponds to a non-switched sample whereas the lower is the result of extended illumination at a wavelength of 405nm. Based on the induced spectral changes an isomerization yield of ≈73% can be determined. **(b):** NEXAFS spectra of different polarizations obtained from 1ML TBA/Au(111). The strong π^*-resonances yield valuable information on the geometry of the adsorbed molecules (see text and figure 4.18). *Graphs courtesy of Roland Schmidt, MBI Berlin.*

are ideal markers as they are highly directional. Thus the corresponding excitations (C1s-π^* and N1s-π^*) are very sensitive to the electric field of the synchrotron radiation. This can be seen in figure 4.17(b) where annealed (trans) and illuminated (switched) samples of 1ML TBA/Au(111) are investigated using s- and p-polarized synchrotron light. Without going into further detail one clearly observes an intensity difference in the resonances of the switched and the annealed sample.

The analysis of the data in conjunction with the XPS data yields a monolayer geometry as depicted in figure 4.18. In the trans configuration the TBA is slightly bend out of the plane parallel to the surface. This is contrasted by the geometry in the 0.9ML coverage (not shown here) where the molecule appears to lie flat on the surface. In this respect the NEXAFS experiments corroborate our classification of the monolayer into a compressed and a relaxed phase. Returning to the monolayer TBA/Au(111) we observed that the cis isomer is twisting one of its phenyl rings away from the substrate. This is in well agreement with STM data from submonolayer coverages [Ale08] [Com07].

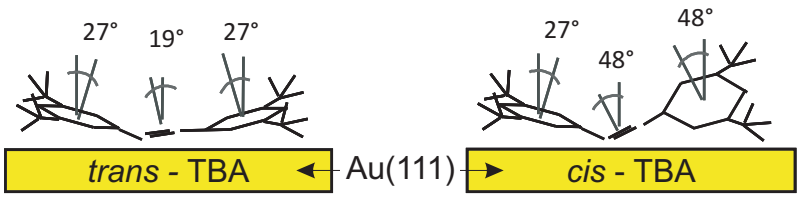

Figure 4.18: Absorption geometry of trans and cis-TBA in the monolayer phase. The given values represent the tilting of the phenyl ring normal and the azo-bridge normal in respect to the surface normal. *Sketch courtesy of Roland Schmidt, MBI Berlin.*

Electronic structure A last important point is the electronic structure obtained from XPS measurements (not shown here). Two conclusions have been drawn from those experiments: (i) The order of the occupied orbitals of TBA/Au(111) is degenerate if not reversed in comparison to the free azobenzene. Thus in the present case the HOMO can be assigned to the delocalized π-system extending over the phenyl rings and the azo group. (ii) An occupied electronic state is found approximately 4.4eV below the Fermi level, a region which cannot be reached with the 2PPE. It will be of great interest for the substrate mediated photoisomerization discussed in section 4.5.3.

4.3.2 *Conclusions*

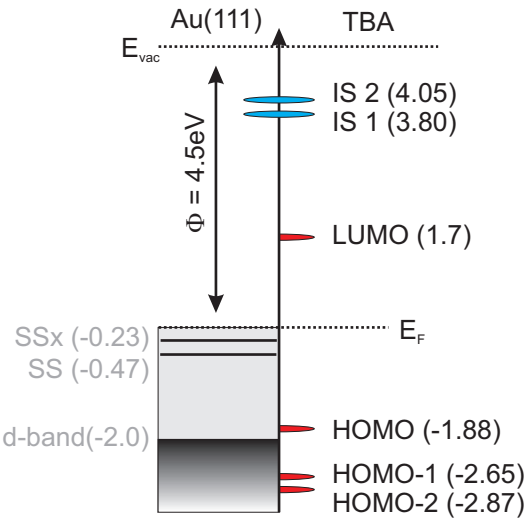

Figure 4.19: Summary of the TBA/Au(111) electronic states discussed in this work. Interface states are depicted in blue, molecular states in red. Binding energies are given in eV with respect to the Au(111) Fermi level.

We will close the discussion of the electronic structure with a brief summary. A graphical depiction of the main results for TBA/Au(111) is given in figure 4.19. All binding energies are given with respect to the Fermi level. No coverage dependent deviations of those values could be observed in the range from 0 to 6ML. Besides the apparent gold states we find six states which can clearly be linked to the presence of the molecule. Four of those have been identified as the lowest unoccupied (LUMO) and the three highest occupied molecular orbitals (HOMO, HOMO-1 and HOMO-2). The HOMO-LUMO gap of 3.58eV is close to the theoretical value of 3.9eV for the free TBA[Teg07] indicating that the surface confinement has only a limited effect on its electronic structure. A more detailed comparison is given in section 6.4. Two additional states observed in

the spectra (IS 1 and IS2) have been assigned to the interface potential arising due to the adsorption of the the molecules. Such interface states, to our knowledge, have not yet been reported for low coverage physisorbed systems. Experimental evidence has been restricted to chemisorbed molecules [Mun06] and bulk rare gas systems adsorbed on a metal substrate[Roh05]. Interface states hold a great potential for the investigation of transfer dynamics in layered systems. They grant access to an interesting region at the metal/molecule interface which in conventional methods cannot be addressed directly [Güd05]. However in the context of this thesis the value of the IS is clearly determined by their isomerization specific behavior. Since we can assign the two interface states to the cis and the trans isomer respectively we are enabled to determine the TBA isomer concentrations and consequently the reaction yield based on the electronic structure.

4.4 Analytical description of the switching

To analyze the photoisomerization of TBA/Au(111) the corresponding reaction kinetics have to be correlated to the changes in the electronic structure. The required fundamental theoretical and experimental considerations will be presented in the following section. We start with a general description of the isomerization reaction which is subsequently evaluated by implementing the experimentally accessible variables. The resulting formalism will enable an analytical separation of the different isomerization channels based on: (i) their excitation mechanism, considering either light or temperature induced reactions. (ii) their direction, viz. either the trans-to-cis or the cis-to-trans pathway. In addition the photoinduced evolution of the isomer concentrations will be related to an effective cross section. It expresses the probability of a single photon to induce the isomerization of a molecule and thus is of eminent importance for the determination of the underlying excitation mechanism.

In order to properly combine the analytical description with the experimental data the observed changes have to be directly proportional to the respective isomer concentration. Since this can not be assumed a priori we will use the second part of this section to discuss the origin of the three switching signatures introduced in section 4.2.

4.4.1 Reaction kinetics

The isomerization of the surface adsorbed TBA is a reversible chemical reaction

$$TBA_{trans} \rightleftharpoons TBA_{cis} \tag{4.17}$$

Depending on the stimuli it can occur in either direction leading to a change in the respective isomer population. Since the isomerization neither creates nor destroys molecules the concentration of trans $[trans]$ and cis $[cis]$ obeys the simple relationship

$$[cis] = 1 - [trans] \tag{4.18}$$

The change in the trans concentration is the sum of the trans-to-cis (forward) and the respective cis-to-trans (reverse) isomerization reactions:

$$\frac{d[trans]}{dt} = -k_{TC}[trans] + k_{CT}(1 - [trans]) \tag{4.19}$$

Here the "velocity" of the reaction in the two direction is expressed by the rate constants k_{TC} (forward) and k_{CT} (reverse). This term can now be evaluated

$$\frac{d[trans]}{dt} = k_{CT} - [trans](k_{TC} + k_{CT}) \tag{4.20}$$

$$\frac{d[trans]}{k_{CT} - [trans](k_{TC} + k_{CT})} = dt \tag{4.21}$$

and finally integrated

$$\log[\frac{k_{CT} - [trans](k_{TC} + k_{CT})}{k_{CT} - [trans]_0(k_{TC} + k_{CT})}] = -(k_{TC} + k_{CT})t \tag{4.22}$$

We thus can express the concentration $[trans]$ as function of the time and the initial concentration $[trans]_0$:

$$[trans](t) = \frac{k_{CT}}{k_{CT} + k_{TC}} + ([trans]_0 - \frac{k_{CT}}{k_{CT} + k_{TC}})e^{-(k_{CT}+k_{TC})t} \tag{4.23}$$

A consistency check shows that for $t = 0$ the exponential term yields unity, reducing the equation $[trans](0) = [trans]_0$ which is the initial population prior to the switching. For infinite times the system will end up in a stationary equilibrium defined by the forward and backward switching rates as:

$$[trans]_{eq} = [trans](\infty) = \frac{k_{CT}}{k_{CT} + k_{TC}} \tag{4.24}$$

The above equations yield some useful consequences for the analysis of the data. Based on the equilibrium concentration $[trans]_{eq}$ we can separate and quantify the contributions of forward and reverse isomerization. This is essential for the discussion of bi-directional channels like the photoisomerization. On the other hand the temporal evolution of the concentration, which is determined by the exponential term in equation 4.23, allows us to separate the different isomerization channels, viz. the photo and the thermally induced channel. Therefore we have to correlate the experimental signal, e.g. the intensity of a peak or the work function, to the amount of switched molecules. This is possible if the obtained signal exhibits a direct proportionality according to:

$$N_T(t) \propto I(t) = A + Be^{-(k_{CT}+k_{TC})t} \tag{4.25}$$

Here A and B are free fitting parameter scaling the number of trans molecules to the retrieved (photoemission) signal $I(t)$. It is important to note that they do not affect the exponential saturation of the isomerization process. Due to the transformation the equilibrium concentration has been eliminated from equation 4.25. Thus the time dependent experimental signal cannot be used to separate the forward and reverse reactions. However it enables, as mentioned above, a convenient regrouping of the reaction rates based on the thermal ($k_{thermal}$) and light induced (k_{light}) excitations:

$$I(t) = A + Be^{-(k_{thermal}+k_{light})t} \tag{4.26}$$

In order to elucidate the photoisomerization we have to experimentally separate its contributions to $I(t)$. As we have shown before (see section 4.2) the thermal reverse isomerization is negligible at temperatures $\leq$90K. Hence in the corresponding temperature regime the saturation function can be reduced to:

$$I(t) = A + Be^{-k_{light}t} \tag{4.27}$$

The progress of the reaction depends on the interaction of the single photons with the molecules and the substrate. Thus we have to express the isomerization rate as

the efficiency of each photo to trigger an isomerization. This is done introducing an effective cross section σ_{eff} which is related to the reaction rate k according to:

$$k_{light} = \sigma_{eff} * f^n \tag{4.28}$$

f denotes the fluence of the laser pulse, viz. the number of photons impinging on the sample per unit area and time. Since it is not a priori obvious whether the photoisomerization is a linear or a nonlinear optical process an exponential variable n is implemented into the relationship. It can be determined by fluence dependent measurements as will be shown for the case of TBA/Au(111) in section 4.5.1.

At his point we have to emphasize two important characteristics of the effective cross section: (i) It expresses the probability of a photon to induce a successful isomerization event. This contrasts its general use in which the cross section refers to the probability of a photon induced excitation. (ii) In agreement with the above evaluation of the analytical description σ_{eff} can be separated based on the light induced forward (σ_{TC}) and revers (σ_{CT}) isomerization channels:

$$\sigma_{eff} = \sigma_{CT} + \sigma_{TC} \tag{4.29}$$

Access to those separate contributions can only be obtained through investigation of the equilibrium concentration in the photostationary state (see section 4.4.2). However for the discussion of the excitation mechanism leading to the isomerization the analysis of σ_{eff}, which is only a function of the photon energy, will be sufficient. It is retrieved from the changes in the electronic structure according to:

$$I(t, h\nu, f) = A + Be^{-\sigma_{eff}(h\nu)f^n t} \tag{4.30}$$

The above equation will be the main building block of our fitting routines describing the light induced evolution of the TBA-isomer concentration. However it has to be adapted to match the experimental conditions by considering the beam profile of the laser spot. Its spatial intensity distribution follows a Gaussian profile which consequently causes a likewise distribution of fluences. A detailed presentation of the resulting modified fitting procedures is given in appendix D.

4.4.2 Photoinduced spectral changes

The above introduced formalism is suitable for any modification in the 2PPE spectra which can be directly linked to the photoisomerization process. Thus far we have only briefly mentioned the tree observed changes for TBA/Au(111). In the following we are going to discuss their origin and elucidate their compliance with the analytical description.

Vacuum cutoff edge Upon photoisomerization of TBA/Au(111) the intensity of the 2PPE signal from the vacuum cutoff edge increased dramatically. Based on the photon energy and coverage dependent experiments (see section 4.3) we can exclude electronic states to be the origin of this behavior. Instead we attribute

the signal to an increasing number of secondary electrons. Their creation has to be discussed in respect to the morphology of the adsorbate covered surface. In case of a non-illuminated sample only flat lying trans isomers have been reported by NEXAFS and STM experiments [Ale07]. Assuming a vanishing dipole moment as observed for the free TBA [Fuc06] the surface layer exhibits an approximately homogenous potential. This is contrasted by the geometry and the large dipole moment (3.6Debye) of the cis isomers. Their appearance upon switching introduces local distortions which interact with the surrounding electrons in terms of defect scattering thereby creating additional secondary electrons.

Although the secondary electrons can be related to the photoisomerization they are not suitable for an analytical description. Here three reason are presented: (i) Without further investigation it is not clear whether the increase in the signal intensity is directly proportional to the TBA isomer concentration. (ii) Due to the simultaneous shift of the work function the potential between the sample and the time-of-flight spectrometer is modified. This is known to change the detection efficiency for electrons with low kinetic energy [Gah04]. (iii) For photon energies close to the work function the isomerization induced shift will cause a transition from two-photon to direct photoemission leading to a strong, non-linear signal increase as the latter is much more efficient.

Work function The use of the work function (Φ) to monitor the isomerization process has several advantages. First of all it is an easy accessible quantity in photoemission spectroscopy methods since it is intrinsic to every spectra and thus its occurrence is independent of the photon energy. This is in contrast to the spectroscopy of electronic states which has certain limits imposed as we will see below when discussing the interface states. Moreover Φ is determined only by the potential acting on the escaping electron. Therefore it is not affected by variations in the photoemission yield due to detection intrinsic properties. A corresponding example has been given in the above discussion of the vacuum cutoff edge intensity.

As mentioned above we expect a similar behavior of the dipole moment for the free and the adsorbed TBA, thus a neutral trans and a polarized cis configuration. Therefore we conclude that the observed shift is a direct result of the photoisomerization caused by the different dipole moments of the two isomers. Evidence is given by a recently published work reporting an identical behavior for asymmetric azobenzene dithiol self-assembled monolayers on gold [Qun08]. In addition there are several papers commenting on the general impact of the dipole moment on the work function [DR05][Cri02].

The picture of having two work functions, one for the trans and one for the cis isomer, needs some clarification as to why they are not separated in the spectra. Here a photo-emitted electron can well be assumed to experience an averaged work function as it passes the surface region. Consequently the illumination induced progression of the isomerization will lead to a gradual shifting of Φ. This can be directly witnessed in 2-photon photoemission based on the shift of the vacuum cutoff edge. The result of a corresponding isomerization series for 0.9ML TBA/Au(111)

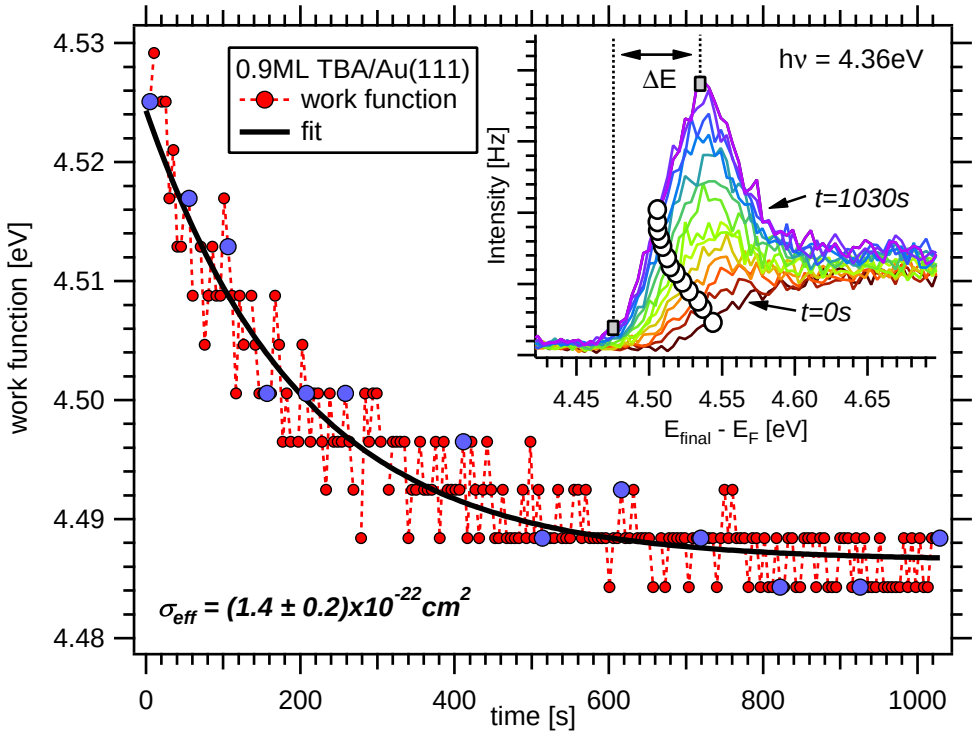

Figure 4.20: Work function shift of TBA/Au(111) as a function of the illumination time. The inset shows the vacuum cutoff edge of selected spectra (blue dots) from which the work function values have been retrieved. White circles mark the corresponding center of the edge. It is shifted upwards due to the isomerization induced increase in secondary electrons. Fitting has been performed according to equation 4.30. For details see text.

is depicted in figure 4.20. It has been obtained by continuously recording single spectra with a photon dose of $N_{ph} = 5 \cdot 10^{19} cm^{-2}$ each. Details regarding the data acquisition, including the retrieval of Φ, are discussed in appendix E.

The main graph displays the saturating work function shift in dependence of the illumination time and hence the photon dose. It has been fitted based on equation 4.30 yielding an effective cross section of $\sigma_{eff} = (1.4 \pm 0.2) \cdot 10^{-23} cm^2$. The trace of the fit is in well agreement with the experimental data. This indicates that the work function shift behaves according to the exponential saturation function discussed in the previous section. A magnification of the vacuum cutoff edge for selected spectra is presented in the inset graph. The center of the edge, which is directly related to the work function, clearly shifts to lower final state energies as the illumination progresses. The width of the vacuum cutoff edge (ΔE) is influenced by to aspects: the energy resolution of the 2PPE spectrometer and the homogeneity of the work function. For a clean Au(111) crystal ΔE is in the order of 40 to 50meV. This is comparable to the width of a spectra from TBA/Au(111) in the photostationary state which in the here presented case is 57meV. The initial spectra

of the isomerization series on the other hand has a width of 77meV. However in the beginning of the switching process the signal is the average of a rapidly changing electronic structure as can be witnessed by the steep slope of the work function change for small times (see figure 4.20). Thus there is no significant broadening of the vacuum cutoff edge due to the switching of TBA/Au(111). This indicates a rather homogenous work function despite the fact that the mixture of cis and trans molecules can be expected to create a "rough" surface. Hence the assumption of an averaged work function is corroborated. Based on the above we conclude that the work function is directly proportional to the isomer concentration and thus can be conveniently used for the analysis of the photoisomerization.

Trans and cis interface states The third isomerization induced change in the electronic structure is related to the appearance of two unoccupied interface states (IS) which can be exclusively assigned to either of TBA isomers. Due to their energetic position a minimum photon energy of 4.05eV is required to excite both of them. Consequently the the application range is strongly limited. Nevertheless they are of crucial importance for the determination of the absolute isomer concentrations. Before discussing the correlation between this quantity and the experimental data we first have to demonstrate that both peaks evolve at the same rate.

Figure 4.21 depicts the results of a spectra series recording the illumination induced changes in the region of the interface states. Graph 4.21(a) presents data from a two-color 2PPE measurement using photons of $h\nu_1 = 2.18eV$ and $h\nu_2 = 4.36eV$. The spectra are governed by the strong signal of IS(trans) at $E_B = 4.05eV$ which masks the weak contributions of IS(cis). The latter can be derived by carefully fitting the spectra with Gaussian peak functions as has been demonstrated . An alternative method is to record the spectra changing the polarization[8](p-pol to s-pol) of the pumping UV light by 90°. This eliminates the electric field components of the laser which are oriented perpendicular to the substrate surface. In agreement with the NEXAFS experiments (see section 4.3.1) this quenches the pumping of the trans-isomer interface state as it exhibits a parallel orientation. The tilted geometry of the cis-isomer on the other hand leads to the weak but distinguishable 2PPE signal presented in graph 4.21(b)). To illustrate the influence of the isomerization the differences to the initial "un-swithced" spectrum have been indicated by shaded areas.

In a next step we evaluate the peak intensities and the work function for each data set. Due to the different photoemission efficiencies of IS(trans) and IS(cis) they cannot be compared directly. Thus we have to scale the results which, according to 4.30 of the analytical description, can be done without altering the information about the reaction kinetics. The modified traces are depicted in graph 4.21(c) exploiting an identical saturation behavior and coinciding with the isomerization induced shift of the work function. Therefore we conclude that the intensity change in the 2PPE signal of the interface states is directly related to the isomer concentration.

[8]Orientation of the polarization given with respect to the laser table

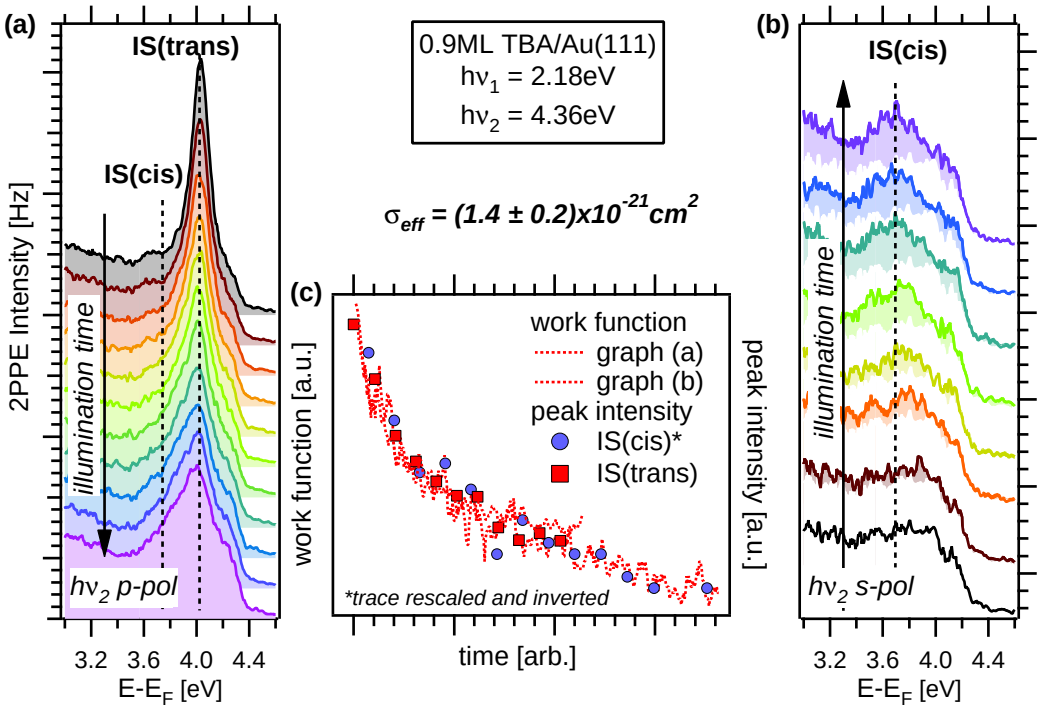

Figure 4.21: Evolution of the trans- and cis-TBA induced interface states as a function of illumination. **(a):** Excitation of the interface states using p-polarized UV-photons. The strong signal of IS(trans) masks the contributions of IS(cis). **(b):** Using s-polarized UV-light the trans feature is expelled from the spectra granting access to the peak intensities of IS(cis). **(c):** Comparison of the scaled peak intensities and the work functions derived from graphs (a) and (b). All traces exploit an similar saturation indicating a direct proportionality to the isomer concentration. For details see text.

Based on the above results the absolute isomer concentration can be obtained from the IS(trans) peak alone since its initial intensity I_0^{trans} for a non-illuminated sample corresponds to $[trans] = 1$. A comparison with the peak intensity $I^{trans}(t)$ after illuminating the sample for a time interval t yields the remaining trans molecules according to:

$$[trans](t) = \frac{I^{trans}(t)}{I_0^{trans}} \tag{4.31}$$

Of course the analysis can be extended to include the cis interface state as well. In this case the respective peak intensities have to be scaled again to compensate for the different photoemission yields. This method is commonly used to verify the experimental results.

4.5 Photon induced isomerization

We will now turn to the investigation of the photoisomerization of TBA/Au(111). To reveal the underlying excitation mechanism it is necessary to determine the reaction rate as a function of the fluence and the photon energy. The former will give detailed information on the order of the excitation process, viz. whether it is linear or non-linear. The latter is required to analyze the electronic excitations involved in the photoisomerization. For this purpose we will use the effective cross section as introduced in the analytical description of the switching reaction. The presentation of the experimental results will be followed by a detailed discussion of the possible excitation mechanisms.

4.5.1 Fluence dependence

A critical aspect in the discussion of photoinduced processes is the reaction order n of the underlying excitation. In the present case it determines the number of photons required for a trans-cis isomerization and thus yields complementary information on the excitation pathway. A simple yet effective way to determine n is the investigation of the reaction rate as a function of the laser fluence (see equation 4.28).

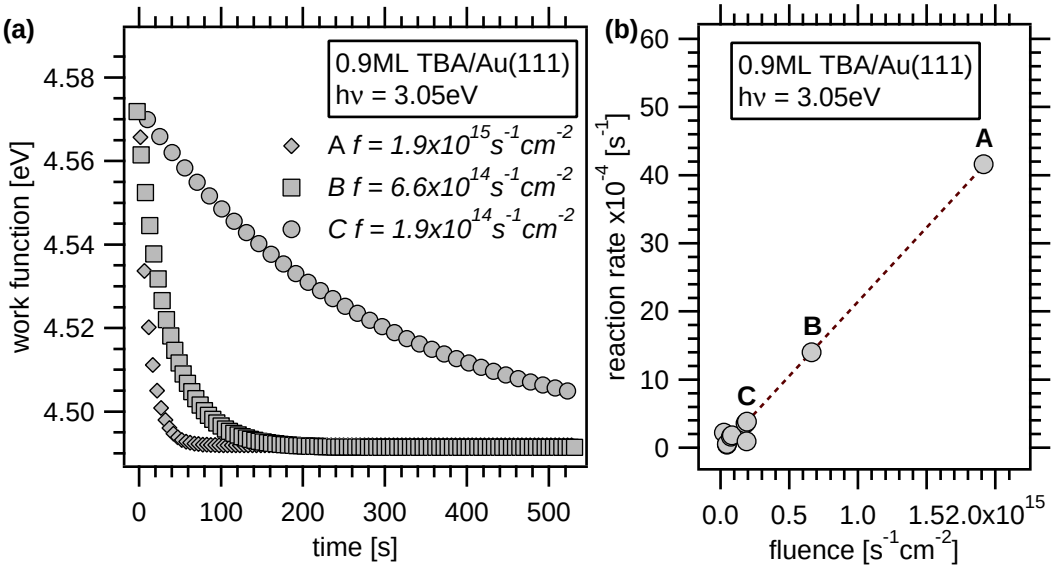

Figure 4.22: Fluence dependence of the TBA/Au(111) switching rate. **(a):** Selected traces of the light induced work function shift observed for three different fluences. In agreement with the reaction kinetics, exposure to a higher photon flux accelerates the isomerization. The equilibrium concentration in the photostationary state on the other hand remains constant. **(b):** The isomerization (reaction) rate as a function of the fluence. The values of the graph (a) have been marked by their corresponding letter. The linear relationship points to a 1st order optical excitation process.

For this purpose we illuminated 0.9ML TBA/Au(111) using a 3.05eV beam of variable power. The resulting spectra were analyzed in respect to the light induced work function shift (see appendix E) and fitted according to equation. 4.30. Figure 4.22(a) exhibits the corresponding fit traces of three selected data sets. In agreement with the theoretical picture the reaction rate increases proportional with the fluence. Thus less time is required to reach the photostationary state (PSS). Furthermore the reaction yield derived from the PSS work function is constant for all spectra and thus independent of the fluence. This indicates that only light driven isomerization is present under the current experimental conditions (see equilibrium condition, equation 4.24). Graph 4.22(b) displays the reaction rates derived from the fitting as a function of the fluence. Here a clear linear relationship can be witnessed over a range of more than two orders of magnitude. Similar results have been obtained for photon energies in the range of 2.1 to 4.9eV. Therefore we conclude that the photoisomerization of TBA/Au(111) is a first order process ($n = 1$).

4.5.2 Photon energy dependence

To determine the excitation mechanism of the TBA/Au(111) photoisomerization we investigate the photon energy dependence of the effective cross section. Samples with a coverage of 0.9ML TBA were illuminated at different photon energies in the range of 1.8 to 6.1eV. In agreement with the temperature restrictions imposed by the analytical description all measurements have been performed at 90K. For each spectra the work function shift has been analyzed as described in appendix E and was subsequently fitted according to equation 4.30. The retrieved effective cross section σ_{eff}, describing the efficiency of the photoisomerization, is plotted as a function of the photon energy in figure 4.23. The graph can be divided in five different regions labeled as I-V. Investigations of region I in the low energy range of $1.8 < h\nu < 2.1eV$ showed no light induced changes in the electronic structure. Thus at these wavelength no isomerization occurs. The second region, $2.1 < h\nu < 2.5eV$, is governed by an increase of the cross section. Within this range the switching efficiency increases by more than one order of magnitude from $\sigma_{eff} = (5 \pm 2) \cdot 10^{-23}cm^2$ to $\sigma_{eff} = (1.0 \pm 0.5) \cdot 10^{-21}cm^2$. In the subsequent region III, extending from $h\nu = 2.5eV$ to $h\nu = 4.4eV$, we observe a constant cross section as indicated by the blue dotted line. It increases again in the photon energy range from $h\nu = 4.4eV$ to $h\nu = 4.7eV$. The corresponding values show an enhancement of roughly one order of magnitude. At $h\nu = 4.7eV$ the cross section appears to reach a second plateau like region (V). Here an approximately constant switching efficiency of $\sigma_{eff} = (1.0 \pm 0.5) \cdot 10^{-20}cm^2$ is observed in a small region up to 4.95eV. A further reference point has been recorded in direct photoemission at $h\nu = 6.1eV$ which, within its error, supports the assumption of an almost constant cross section.

The results of our experiment are supported by a recently published low temperature STM measurement [Com08]. Within this work TBA/Au(111) has been successfully switched using UV-light of 2.8 and 3.3eV at ≈30K. The corresponding reported cross section of $5 \cdot 10^{-23}cm^2$ is a factor of 20 smaller compared to the here

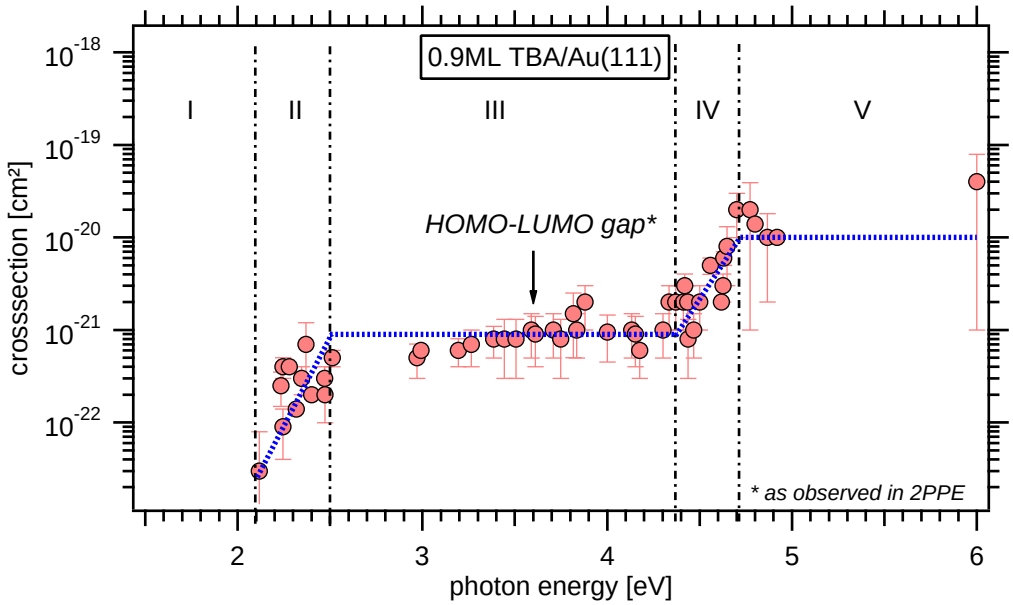

Figure 4.23: Photon energy dependence of the effective cross section. The threshold for the TBA/Au(111) photoisomerization is 2.1eV. For higher photon energies two distinct plateaus but no resonant behavior is observed. The HOMO-LUMO gap which is expected to participate in a possible direct excitation has been marked in the spectra. Based on this graph the excitation mechanism of the photoisomerization will be discussed in section 4.5.3.

presented values. This can be attributed to the different sample temperatures. Evidence will be given in section 4.6.2 where we investigate the temperature dependence of the photoisomerization.

Returning to the analysis of the data depicted in figure 4.23 we find that TBA adsorbed on Au(111) can be switched over a wide range of photon energies with a low energy threshold of 2.1eV. This is in contrast to TBA in solution where distinct resonances are observed [Hag07] and indicates a different excitation mechanisms. A second difference is the isomerization efficiency which, depending on the photon energy, is one to three orders of magnitude larger in solution ($\sigma \approx 10^{-19} cm^2$) [Rau03]. Here three possible explanations are presented: (i) The coupling to substrate reduces the lifetimes of the electronically excited molecule and thus decreases the isomerization probability. (ii) Steric hinderance due to the surface confinement and the interaction with neighboring molecules suppresses certain molecular motions. The isomerization has to take a "detour" using a slower pathway. (iii) A direct comparison does not account for thermal effects. Those may play an important role especially since the experiments in solution were commonly performed at room temperature. (iv) A completely different excitation channel is used. In this case it is difficult to directly compare the cross sections of TBA in solution and the effective cross section of TBA/Au(111). To clarify the excitation mechanism we shall proceed with a discussion of the available channels.

4.5.3 Excitation mechanism of the TBA/Au(111) photoisomerization

In the following we are going to elucidate the isomerization mechanism based on the previously discussed properties of the effective cross section. Two principle excitation channels are available for the photo induced switching of TBA/Au(111): a direct intramolecular transition or a charge transfer from the metal substrate.

The intramolecular channel is based on the excitation mechanism of the free molecule where an electron from the HOMO or HOMO-1 is excited into the LUMO of the TBA [Näg97]. Consequently the size of the gap between those orbitals determines the suitable photon energies and the respective resonant absorption. In the case of TBA/Au(111) the HOMO-LUMO gap as retrieved from the 2PPE experiments has a value of 3.6eV (see section 4.3). Within this region the photon energy dependence (figure 4.23) of the isomerization displays a constant cross section which contradicts the expected resonant behavior for an intramolecular excitation. In fact the data exhibits no resonances at all in the investigated photon energy range. Therefore intramolecular transitions can be ruled out as the primary excitations mechanism leading to the photoisomerization of TBA/Au(111). Moreover we presume that it is completely suppressed since the quantum yield of the dominant switching process is already very low.

For the quenching of the intramolecular excitation pathway we propose the following possible explanations: (i) Due to the electronic coupling to the substrate new decay channels are available. The lifetime of the excited molecular states is reduced such that the system relaxes before an isomerization occurs. (ii) The adsorption of the molecule onto the metal substrate alters the excited state potential energy landscape creating a barrier along the isomerization pathway. This can be caused by modifications of the molecular electronic structure. It can also be a result of intermolecular or molecule-substrate interactions which suppress certain molecular motions. In the limit of strong interactions (chemical) bond is created which "glues" the molecule to the surface. This last option however seems rather unlikely since this would generally suppress the isomerization. In addition STM measurements have shown that TBA only weakly binds with the Au(111) surface [Com07].

Since the experimental results contradict a dominant intramolecular excitation channel we proceed with the discussion of the different available substrate-molecule charge transfer pathways. A first well known concept is the creation of a so called negative ion resonance (NIR). Here an electron is excited within the metal substrate and subsequently tunnels into an unoccupied orbital of the adsorbate. NIRs have been observed for a large number of systems, playing an initial role in the desorption and dissociation of molecules. [Dai95][Zhu94][Zho91][Zim95][Guo99]. In order to switch TBA/Au(111) a NIR would have to be created by injecting an electron into the LUMO at $E_B = 1.6eV$. According to the Au(111) band structure this molecular state is located within the surface projected band gap [Eck84]. Thus its occupation has to occur via a scattering of hot electrons. The hot electron distribution however strongly depends on the exciting photon energy. In particular

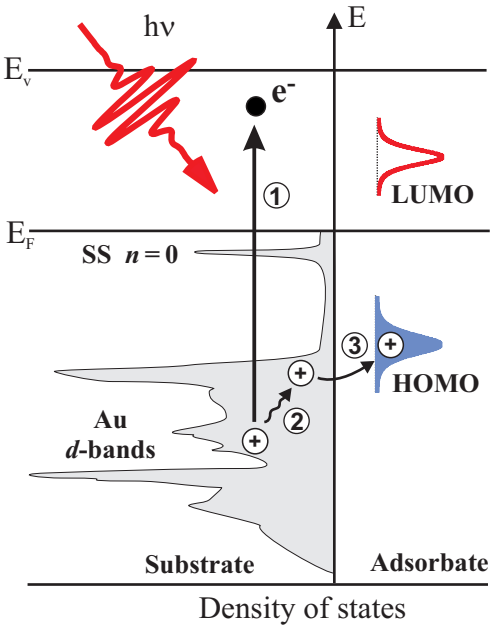

Figure 4.24: Schematic depiction of the excitation mechanism leading to the photoisomerization of TBA/Au(111). (1) An electron of the d-band is photoexcited leaving a hole behind. (2) Through scattering this hole relaxed towards the upper edge of the band. (3) In the final step the charge is transferred to the HOMO of the molecule creating a positive ion resonance. This excited state enables the molecule to conduct the isomerization (Sketch adapted from reference [Hag08a]).

the number of electrons available for scattering into the LUMO can be assumed to increase nonlinearly. Consequently the photon energy dependence of the effective cross section should exhibit a likewise nonlinear and moreover non-constant behavior. This opposes our experimental results and thus we also exclude this pathway to be involved in the photoisomerization of TBA/Au(111). A second argument contradicting the participation of an NIR is the observed energy threshold of 2.1eV. For a switching mechanism induced via a substrate mediated excitation of the LUMO this value would be expected to coincide or at least be close to the corresponding binding energy (1.6eV).

In a second charge transfer scenario we consider excitations of ground state electrons from the molecule into the gold substrate creating a positive ion resonance. Here the transition has to occur between an occupied adsorbate orbital and an unoccupied metal state in front of the surface. This seems rather unlikely as the metal wave functions exponentially decay into the interface region if they are not surface states themselves. In the latter case we again would expect a resonant excitation behavior of the photoisomerization which already has been ruled out based on our experimental data. In order to excite the electron into a bulk state its momentum has to be changed. However the probability for a scattering event is rather low inside a molecule due the limited phase space available. Thus a contribution from this excitation pathway is not expected.

Instead we propose a photoisomerization based on a hole transfer from the metal substrate into the HOMO of the molecule. Such processes are well known from the photochemistry of adsorbate covered semiconductors [Tho06] [Osg06] [Du07]. It is also believed that they occur at metal surfaces e.g. in the case of laser induced desorption of molecular oxygen from Pd(111) [Mis96]. However no clear evidence could

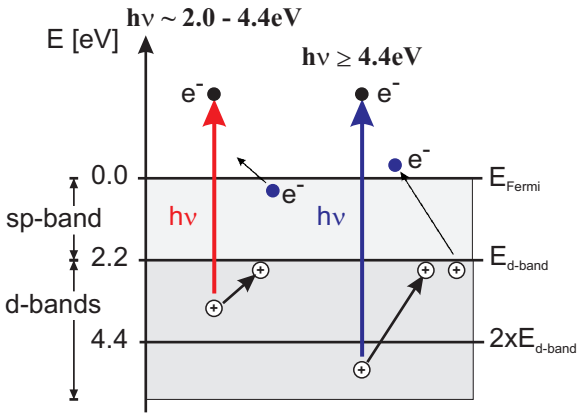

Figure 4.25: Schematic drawing of a multiple hole creation. For photon energies larger than the upper d-band edge binding energy E_{d-band} a single hole is created. It can relax by interaction with electrons of the Fermi sea as shown on the left side. For photon energies twice the E_{d-band} and larger the created hole can participate in an auger decay creating a second electron-hole pair. Thus the number of positive charges for transfer to the molecule is increased (Sketch adapted from reference [Hag08a]).

be presented thus far. The proposed excitation pathway is schematically depicted in figure 4.24: A hole in the Au(111) d-band is created through photoexcitation of an electron (1). Due to the subsequent Auger decay the hole relaxes rapidly towards the upper edge of the d-band (2). From there it is transferred to the HOMO of the TBA creating a positive ion resonance (3).

The energetic overlap of the HOMO with the d-bands of the gold can be witnessed in the electronic structure retrieved from the 2PPE experiments (see figure 4.19). Hence it can well be assumed that the corresponding wave functions at least partially overlap and an electronic coupling is present. The crucial part of this excitation mechanism however is the decay of the hole toward the upper band edge. Such processes have been the subject of several dynamics and lifetime studies performed on different noble metal surfaces [Pet99][Mat99]. It is demonstrated that the relaxation trough scattering within the d-band is very fast resulting from the high density-of-states (DOS) in the corresponding energy region. In case of Cu(111) this electronic decay is reported to occur on a timescale of a few fs [Kno98]. At the top of the d-band on the other hand, the phase space for particle interaction is significantly reduced due to the much lower density-of-states (DOS) in the energetically higher lying sp-band. This leads to an increase in the hole lifetimes up to 25fs (Au(111)) [Cam00].

Having presented a reasonable scenario for a substrate mediated excitation mechanism we now want to discuss its consequences in respect to the switching efficiency. Based on the photon energy dependence of the photoisomerization we have excluded switching for excitation energies below $hv = 2.1eV$. This lower threshold coincides with the energetic position of the upper d-band edge around 2eV [Eck84]. By increasing the photon energy we start to probe deeper into the emerging d-band structure. Correspondingly a larger number of positive charge carriers will be created and thus be available for tunneling into the TBA molecule. Consequently a sudden increase in the isomerization efficiency can be expected which is in agreement with the experimental data. For $hv > 2.5eV$ most of the energy of the laser pulse is adsorbed in the d-bands [Pet97]. Thus in first approximation the number of created holes

becomes independent of the photon energy. Due to the rapid decay an almost constant amount of positive carriers is piled up the the upper d-band edge. This nicely explains the observed plateau in the photon energy dependence of the switching cross section. The here presented excitation mechanism is also in agreement with the linear fluence dependence (see section 4.5.1) of the isomerization rate since the number of created holes should scale likewise linearly with the number of photons.

While the motivation of the first cross section plateau (figure 4.23) has been obvious, the reasons for the second increase at photon energies above 4.4eV are ambiguous. Here we introduce two schemes suitable to explain this observation: The first is based on a 2PPE intrinsic increase of d-band holes. This is illustrated using the sketch in figure 4.25 depicting possible electronic decay processes for different excitation energies. The lower limit of a d-band hole creation is naturally given by the band edge around 2eV below the Fermi level. In the energy range of -2.1 to -4.4eV the positive charge carriers relax under simultaneous excitation of a weakly bound electron. For photon energies >4.4eV on the other hand, the hole is additionally enabled to participate in an Auger decay, creating a second electron-hole pair. Consequently the number of positive charges at the upper d-band edge is increased and will lead to an enhancement of the isomerization rate. A second possible explanation is obtained from the results of the XPS experiments introduced in section 4.3.1. Those revealed an occupied molecular orbital at a binding energy of $E_B = -4.4 \pm 0.5eV$ which energetically coincides with the observed cross section increase. Assuming that the corresponding orbital exhibits a stronger electronic coupling[9] to the substrate than the HOMO it is well suitable to open a new even more efficient hole induced excitation channel.

Due to the revelation of a substrate mediated excitation mechanism which triggers the photoisomerization of TBA/Au(111) it is obvious that the establishment of an electronic coupling between metal and molecule is of crucial importance. This however has to be critically discussed as the charge transfer cannot be assumed unidirectional. Moreover we have to presume that the back transfer of the hole into the substrate is equally efficient as its injection into the molecule. A reasonable explanation for the occurrence of the isomerization can be derived from an examination of the corresponding timescales. According to experiments in solution the conversion from one isomer to the other usually takes place within 170fs [Näg97]. This is a long time considering the above argument of equal transfer rates in both directions which is essentially determined (or limited) by the d-hole lifetime of 25fs. However the probability of a molecule to reside in an excited state decays exponentially. Thus there is a small but not negligible chance for an isomerization even in case of a strong coupling and respectively short charge transfer timescales.

Even without sufficient lifetimes the isomerization can be successful if we consider a stepwise excitation of vibrational levels. Such processes are e.g. participating in the well known case of desorption induced by multiple electronic transitions (DIMET)

[9] Preliminary results from autoionization experiments confirm this assumption, however data analysis is still in progress.

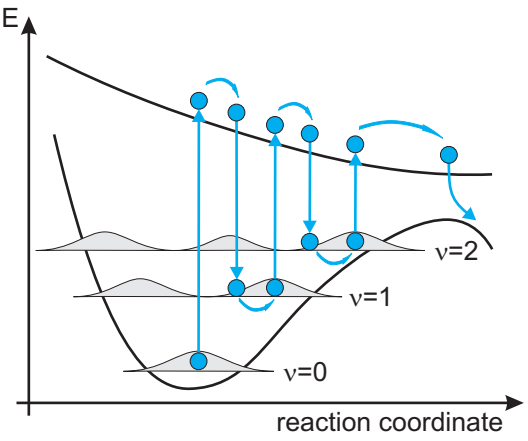

Figure 4.26: Sketch of a ladder climbing process as suggested for the hole induced photoisomerization process. Subsequent excitations lead to a movement of the system along the reaction coordinate. Vibrational modes serve as intermediate states conserving the progress. Each step enhances the possibility of jumping the energy barrier separating the isomers.

[Mis92]. A corresponding mechanism for the TBA/Au(111) photoisomerization is sketched in figure 4.26: The ground state molecule is excited by the hole injection from the substrate. In its excited state it relaxes towards the minimum of the potential energy surface by initiating a conformational change along the isomerization pathway. Due to the coupling with the metal a back transfer of the charge takes place. This leads to a vibrationally activated molecule based on a Franck-Condon transition from the excited to the ground state potential. A subsequent excitation repeats this procedure resulting in the occupation of a yet higher vibrational level. Continuing this ladder climbing process will reduce the relative barrier height and eventually enable an isomerization event even in case of short electronic lifetimes.

Based on the above considerations we conclude that the molecule-substrate coupling obviously influences the probability of: (i) the molecular excitation via a charge transfer, (ii) the switching which is determined by the competing timescales of molecular motion and electronic relaxation. In this respect the coupling is beneficial only for substrate mediate processes as it is naturally required for the charge transfer. Here the balance between (i) and (ii) is expected to be a key factor for a successful switching. Strong evidence will be presented in chapter 5 where we discuss the influence of the substrate. Intramolecular excitation on the other hand suffer from a faster decay without experiencing an increase in the quantum yield. Therefore it seems reasonable that they do not contribute to the photoisomerization of TBA/Au(111).

4.6 Thermal contributions to the isomerization

In the previous sections we have gained valuable information on the photoexcited isomerization pathway of TBA/Au(111) which is clearly affected by the presence of the substrate. The next essential step is to investigate the impact of the adsorption onto the ground state of the molecule. Therefore we have to examine the thermally driven reaction converting the less stable cis isomer into the trans isomer. This will yield fundamental properties of the ground state barrier which can be compared with TBA in solution and calculations for the free molecule. Subsequently we will address the temperature dependence of the photoisomerization. Here in particular the changing efficiency, in terms of the cross section, and its correlation to the vibrational modes of the TBA will be discussed. Finally we include the analysis of the isomer concentrations which enables us to separate the rates of the photo induced forward and reverse switching.

4.6.1 Thermally induced cis-to-trans isomerization

In order to analyze the thermodynamics of the ground state TBA/Au(111) we have to experimentally resolve the changes in the isomer concentrations as a function of the temperature. Due to the unidirectional character of the thermally induced (cis-to-trans) isomerization it is more convenient to conduct this discussion based on the concentration of cis-isomer $[cis]$. According to the reaction kinetics introduced in section 4.4 its value can be expressed as a function of time:

$$[cis](t) = [cis]_0 e^{-kt} \tag{4.32}$$

Here the temperature dependence is implemented in the rate constant k which is commonly expressed in terms of the Arrhenius law:

$$k(T) = k_0 e^{-\frac{E_A}{k_B T}} \tag{4.33}$$

with k_B the Boltzmann factor, k_0 the frequency factor and E_a the activation energy required to overcome the barrier. The latter two quantities are intrinsic values of the investigated system and can be retrieved by analyzing the saturation function:

$$[cis](t) \propto I(t) = I_\infty \left(1 - e^{-e^{-\frac{E_A}{k_B T} t}}\right) \tag{4.34}$$

$I(t)$ again is the experimental signal, e.g. the work function, and I_∞ the respective asymptotic value reached at large times. This approach monitors the concentration of the cis-TBA as a function of time for different temperatures. A second, more elaborate way to determine the energy barrier is by investigating $[cis]$ as a function of temperature. Therefore we have to transform equations 4.32 and 4.33 resulting in:

$$k = -\frac{\ln([cis])}{t} \tag{4.35}$$

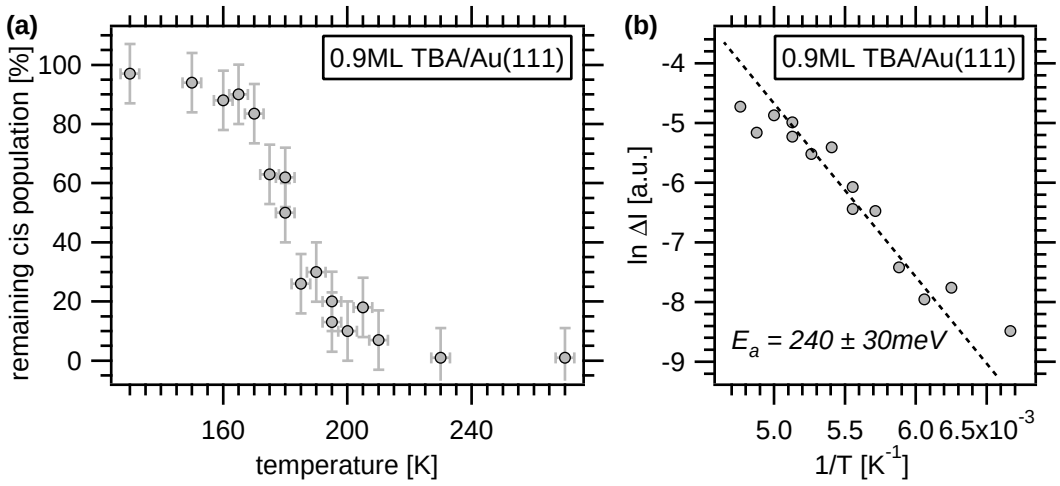

Figure 4.27: Temperature dependent isomer ratio of non-illuminated 0.9ML TBA/Au(111). **(a):** Cis-isomer concentration as a function of annealing temperature. Prior to the measurements the sample is switched into the PSS via illumination. Note, the amount of initial cis molecules is derived from the isomerization yield and does not equal the total number of molecules. **(b):** Depiction of the same results based on equation 4.37. Here the adsorption of TBA reduces the energy barrier by a factor of four. For details see text.

and

$$ln(k) = E_A - \frac{1}{k_B T} + ln(k_0) \tag{4.36}$$

Their combination yields:

$$\ln(\ln([cis])) = -\frac{E_A}{k_B}\frac{1}{T} + c \tag{4.37}$$

with

$$c = \ln(k_0) + \ln(t) \tag{4.38}$$

In order to eliminate the time dependence all measurements have to be performed employing the same annealing time t. The results of such an experiment are depicted in figure 4.27. Here a series of sample with a 0.9ML TBA coverage has been illuminated with UV light until the photostationary state (PSS) was reached. In subsequent annealing intervals of 5min at different temperatures the cis-to-trans isomerization is activated. Comparing the electronic structure before and after the annealing we retrieve the concentration of non-converted cis molecules[10]. It is plotted in graph 4.27(a) versus the respective annealing temperature. In agreement with our initial results no back reaction is observed for $T < 100K$. At $T = 240K$ on the other hand an annealing time of 5min is sufficient to revert the entire population of the formerly switched TBA isomer. For the analysis of the energy barrier we

[10] A detailed description of the data acquisition and the retrieval of the isomer concentrations is given in appendix F

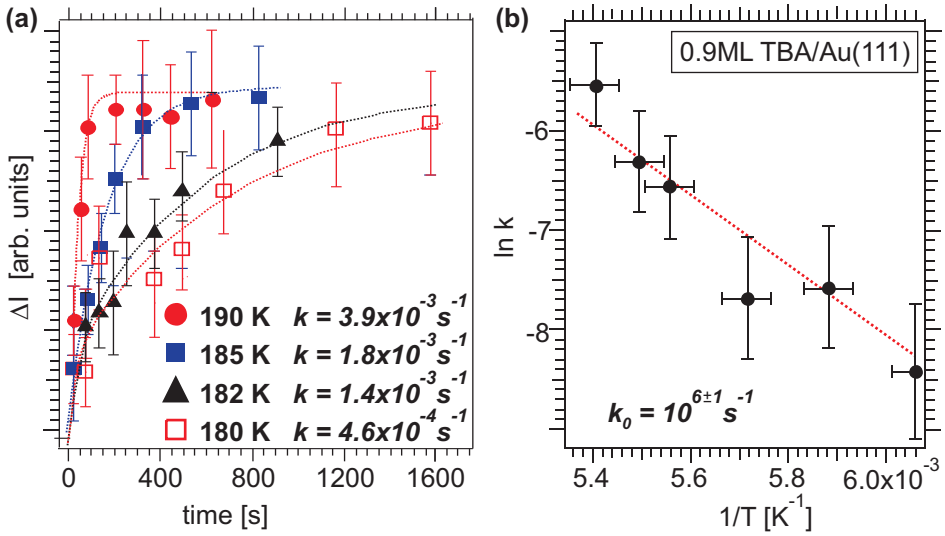

Figure 4.28: Thermally activated cis-to-trans isomerization. **(a):** Saturation curves for selected measurements at different heating temperatures. **(b):** Arrhenius plot of the corresponding reaction rates k. Here the slope yields the frequency factor which indicates a restriction of molecular degrees of freedom due to the surface confinement.

plotted the results according to equation 4.37 which is shown in graph 4.27(b). The linearly fitted slope of the experimental data yields a value of $E_a = 240 \pm 30meV$ for 0.9ML of TBA/Au(111). In contrast, measurements of TBA in a cyclohexane solution [Hag08b] and quantumchemical calculations of the free molecule [Dok09b] yield values of $E_a = 1eV$ and $E_a = 1.02eV$, respectively. Hence the height of the cis-to-trans isomerization barrier is reduced by a factor of 4 upon adsorption onto the gold surface.

To determine the frequency factor k_0 we return to the time dependent cis isomer concentration according to equation 4.34. As in the previous case we prepare 0.9ML TBA/Au(111) in the PSS by illumination with UV light. In a subsequent step the sample is quickly heated to the desired annealing temperature and a series of 2PPE spectra are recorded to observe the temporal evolution [*cis*]. To reduce the error of photoinduced isomerization processes the applied photon doses for the data acquisition are much smaller (at least a factor of hundred) than the photon dose needed to reach the photostationary state (PSS). Exemplary spectra from selected measurements at different annealing temperatures are depicted in graph 4.28(a). One nicely sees the increasing slope of the saturation function as the temperature is increased. The fitted reaction rates are inserted into the Arrhenius plot shown in graph 4.28(b). Using the energy barrier retrieved in the above experiment we obtain a frequency factor of $k_0 = 10^{6\pm1}s^{-1}$ upon linearly fitting the data. Again the confinement to the substrate leads to large deviations from the experimental values of TBA in solution yielding $k_0 = 1.6 \cdot 10^{10}s^{-1}$ and theoretical calculations yielding $k_0 = 4 \cdot 10^{13}s^{-1}$.

The above results clearly demonstrate that the binding of the TBA to Au(111) evokes significant changes in its potential energy surface and in particular in its ground state energy barrier. In this we attribute the differences to the steric effects induced by the substrate. Thus it can be assumed that the range of motion is limited by the interaction with the surface and the neighboring molecules which is witnessed based on the comparably small frequency factor. Similar low values of k_0 have been reported for the rotation of phenyl endgroups in chiral molecules [Wei06]. Here the authors argue in the same fashion, claiming that the confinement to the surface reduces the agility of the molecule and changes the potential energy landscape.

4.6.2 Temperature dependence of the photoisomerization efficiency

In the next step we investigated the temperature dependence of the effective photoisomerization cross section (σ_{eff}). A direct experimental access is prevented by the simultaneous occurrence of the thermally activated cis-to-trans isomerization. Therefore we have to eliminate the corresponding contributions from the experimental data based on the results obtained in the previous section. This can be accomplished by a rather simple analytical transformation. According to the reaction kinetics introduced in section 4.4 the combined isomerization rate of the light and thermally induced processes is given by:

$$k(T) = \sigma_{eff} f + k_0 e^{-\frac{E_A}{k_B T}} \tag{4.39}$$

Here f in agreement with its former assignment is the laser fluence. We now introduce a new combined effective cross section σ'_{eff}:

$$k(T) = \sigma'_{eff}(T) f \tag{4.40}$$

with

$$\sigma'_{eff}(T) = \sigma_{eff}(T) + \frac{k_0}{f} e^{-\frac{E_A}{k_B T}} \tag{4.41}$$

Thus we can employ the already established fitting routines and subtract the influence of the thermal cis-to-trans isomerization to obtain the temperature dependent effective cross section.

For the respective experiment we adsorbed 0.9ML TBA onto the Au(111) surface and gradually changed the substrate temperature in the range from 35 to 200K. At each intermediate step the sample has been illuminated with UV light of $h\nu = 2.99eV$ and the evolution of the work function was recorded as a function of the photon dose. The obtained saturating traces were fitted according to equation 4.30 of the reaction kinetics to retrieve the above introduced combined effective cross section σ'_{eff}. Figure 4.29 depicts the corresponding temperature dependent values. Within this logarithmic plot $\sigma'_{eff}(T)$ increases exponentially in the range of 35K to 200K. Including the results obtained in a LT-STM measurement by Comstock et al. [Com08] it can be extend to $T = 30K$. The appended data point nicely fits into the trend exploited by the 2PPE experiment. In the graph we have marked the contributions of

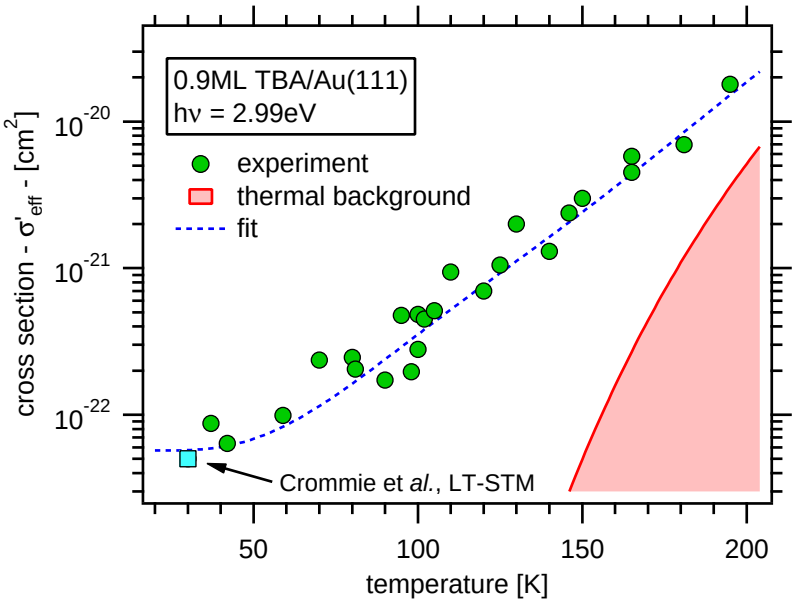

Figure 4.29: Temperature dependance of the effective cross section. The experimental values incorporate the thermal cis-to-trans switching channel as a constant background. Its contribution to the slope is illustrated by the red shaded area. The data point at 30K has been obtained by Crommie *et al.* using a LT-STM [Com08]. It continues the obvious trend of a temperature enhanced photoisomerization. Details regarding the fit are presented in section 4.6.4.

the thermally induced cis-to-trans isomerization by a red shaded area. It contributes only slightly to the cross section in the here depicted temperature range (note the exponential scale!). Thus $\sigma'_{eff}(T)$ increases by over two orders of magnitude between 30K and 200K. Two explain this significant change we have to discuss two possible scenarios: (i) The existence of an energy barrier along the excited potential energy surface. (ii) An efficiency enhancement through the excitation of vibrational levels.

In order to show that the first scenario does not properly describe the experimental results we attempted to fit the data assuming a common barrier yielding:

$$\sigma_{eff}(T) = e^{-\frac{E_a}{k_B T}} \sigma_0 \tag{4.42}$$

with $\sigma_0 = \sigma_{eff}(0)$ the isomerization cross section in the limit of 0K. For the modeling we arbitrarily choose three activation energies E_a of 20meV, 37meV and 63meV. The experimental data together with the respective fit curves is depicted in figure 4.30. Here the blue shaded areas represent the solutions with the least deviation from the measurement. Depending on the activation energy E_a of the used barrier they are obviously capable of reproducing either the low, middle or high temperature regime of the experimental data but fail to properly describe the whole range. Thus a single barrier approach cannot explain the thermally induced increase of the photoisomerization cross section and is therefore ruled out.

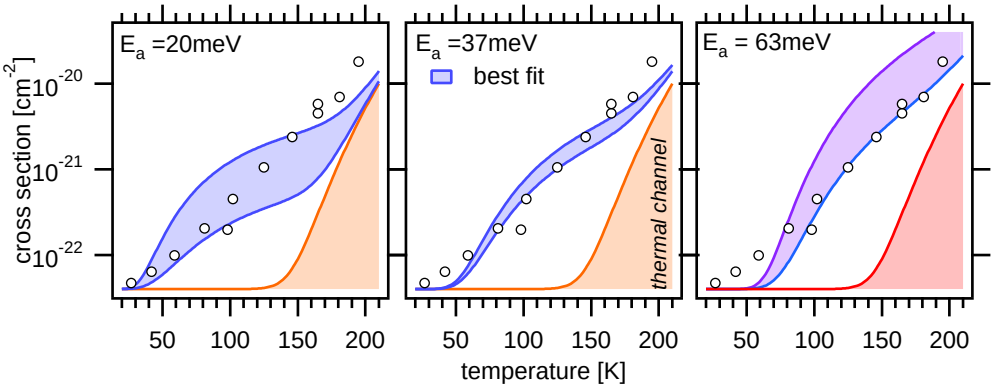

Figure 4.30: Fitting of the temperature dependent cross sections using a single energy barrier E_a. The best fit areas are determined for the given values, including the separately shown contributions of the thermally induced cis-to-trans channel (red). The single barrier approach clearly fails to correctly describe the experimental data. Instead we propose an enhancement of the photoisomerization due to excitation of vibrational modes. For details see text.

A more promising attempt in this respect is the to consider a participation of excited vibrational level. Those are well known to enhance surface reactions as for example in the case of phonon assisted desorption [Xin97][Krö08][Arn03]. The vibrational modes of TBA/Au(111) have be analyzed by Óvári *et al.* using HREELS [Óvá08]. For a fundamental description of the temperature dependent cross section we focus on vibrations assigned to the low frequency modes involved in the isomerization of the free molecule. These are the bending modes of the bond between the nitrogen and the *tert*-butyl substituted phenyl rings at energies of 25meV, 37meV, 63meV and 147meV [Ova07].

The temperature dependent population of i different vibrational level is commonly described by a Boltzmann distribution. Hence the total effective cross section $\sigma_{eff}(T)$ becomes the sum of the partial effective cross sections from the ground state (σ_0) and the different vibrationally excited states (σ_i) according to

$$\sigma_{eff}(T) = (1 - \sum e^{(-\frac{E_i}{k_B T})})\sigma_0 + \sum e^{(-\frac{E_i}{k_B T})}\sigma_i \tag{4.43}$$

with $i = 1..4$ denoting the order of the vibrations according to their ascending energies. This approach enables us to properly describe the experimental data as is demonstrated by the fit which has been appended to figure 4.29. The respective values of the partial cross section for each vibrational level are listed in table 4.1. This approach appears to be very well suited to explain the temperature dependence of the cross section. However we have to be cautious with its interpretation since due to the large number of free fit parameters multiple solutions can be obtained yielding an equally well coinciding theoretical curve. In order to narrow down the

i	0	1	2	3	4
σ_i $[cm^2]$	5.7e-23	1.4e-21	5.9e-21	1.5e-19	4.0e-17

Table 4.1: Fitted cross sections of four selected vibrational modes participating in the photoisomerization of TBA/Au(111). For details see text.

solution space we have to determine the isomer concentration ($[trans]_{eq}$) in the photostationary state. The results, presented in the next section, will corroborate the here proposed correlation between the cross section and the vibrational level of the TBA/Au(111). At this point we shall briefly return to the details of the proposed hole induced excitation of the photoisomerization and discuss the implementation of the vibrational modes. In a first scenario we considered the probability of the TBA excited state lifetime τ_{exc} to exceed the timescale of the switching process. Of great importance in this respect is the electronic coupling to the substrate which has an essential impact on τ_{exc}. The coupling itself on the other hand, in terms of a wave function mixing, is dependent on the molecule metal distance. This of course is subjected to changes in case of a vibrating molecule. Here we can create a simple picture where the vibration continuously changes the wave function mixing of the HOMO and the gold d-bands. Thus at close distances and respective high transfer probabilities a hole can be "picked up" by the TBA (see figure 4.31(a)). Subsequently the molecule continues its motion away from the surface reducing the probability of the charge tunneling back into the substrate and thus leading to an elongated lifetime (figure 4.31(b)).

A second scenario discussed in respect to the photoisomerization mechanism has been a ladder climbing process due to subsequent excitations of the TBA. In this scheme we already used the vibrational level for the different intermediate steps (see figure 4.26). By thermal excitation of these level we reduce the size of the ladder and consequently each step spared enhances the probability of a successful switching. This evokes an efficiency increase of the cross section following the ascending order of the vibrational modes. More supporting evidence will be presented in section 4.6.4.

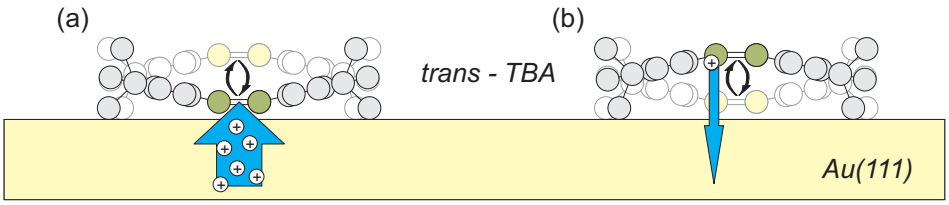

Figure 4.31: Schematic depiction of a simplified, possible scenarios explaining the vibration induced raise of the isomerization efficiency. **(a):** The vibration brings the functional group closer to the substrate which enhances the charge transfer. **(b):** At the opposite end of the vibrational motion the coupling to the Au(111) is reduced leading to a longer lifetime of the hole "picked up" in (a) and thus increasing the isomerization probability.

4.6.3 Isomer ratio in the equilibrium state

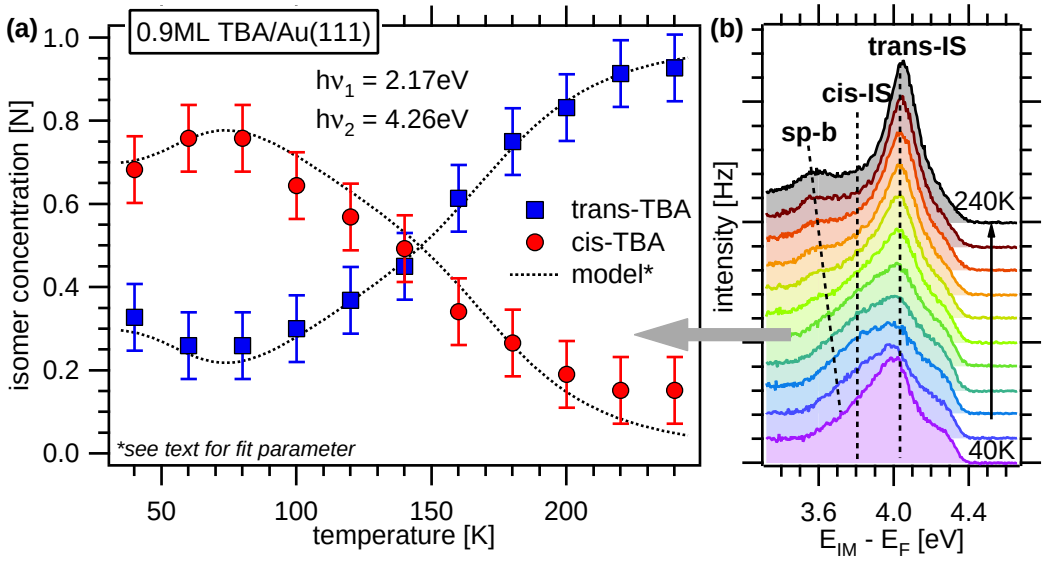

Figure 4.32: Temperature dependence of the TBA/Au(111) isomerization yield. **(a):** Isomer concentrations of trans and cis isomers as a function of the sample temperature. The values are retrieved from the analysis of the corresponding interface states. Note the increase of the cis isomers in the region up to 75K. For details see text. **(b):** Two-color 2PPE spectra set used to retrieve the temperature dependent isomer concentrations.

Thus far the experimental results have been discussed in terms of the combined forward and reverse photoisomerization. In the following we will extend our understanding of the underlying processes by analyzing the temperature dependent isomer concentrations. This enables a separation of the photo induced trans-to-cis and cis-to-trans isomerization processes on one hand and on the other delivers additional information on the temperature dependence of the cross section. Access to the absolute isomer concentration is given by the analysis of the trans- and cis-TBA induced interface states. An introduction to their properties and details regarding the evaluation of the data have been given in sections 4.3 and 4.4 respectively.

Figure 4.32 presents data of the 0.9ML TBA/Au(111) isomer concentrations evolving as a function of the substrate temperature. It is obtained from a series of two-color 2PPE spectra recorded in the photostationary state (PSS) using photon energies of $h\nu_1 = 2.17eV$ and $h\nu_2 = 4.26eV$. The corresponding traces, showing the two interface states (IS), are plotted on an intermediate state energy scale in graph 4.32(b). We assign the sp-b labeled peak on the left side to the sp-band of the Au(111) substrate. Its energetic position in the spectra is strongly temperature dependent. This is well known from investigations of the bare gold sample (see appendix C). Based on the peak intensities of the IS(trans) and the IS(cis) we obtain the respective trans and cis isomers concentrations as depicted in graph 4.32(a).

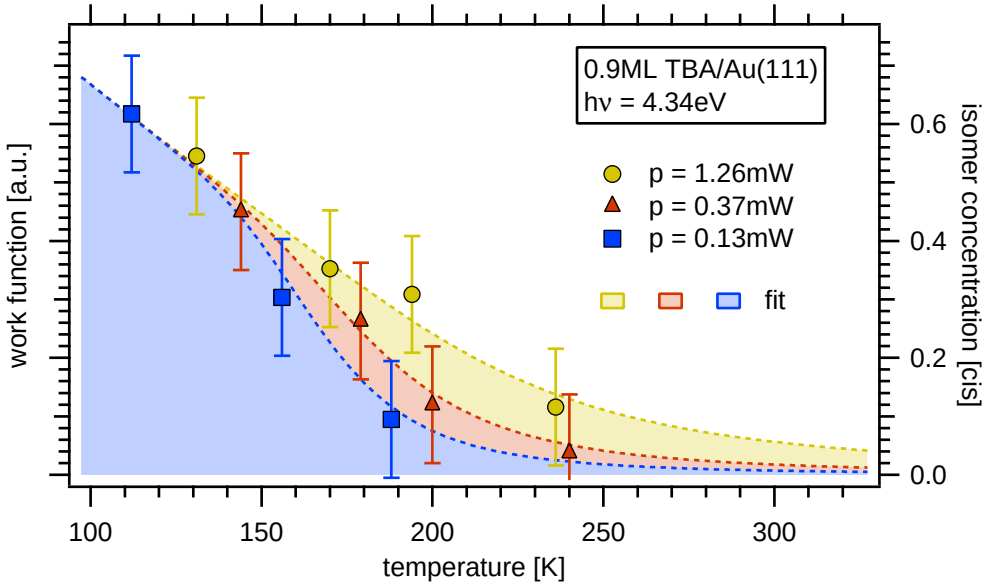

Figure 4.33: Concentration of cis-TBA for three different fluences. In the depicted temperature range it is determined by the competition between the photoinduced bi-directional and the thermally induced cis-to-trans isomerization channels. Increasing the laser power enhances the forward switching and thus the isomerization yield. The experimental values are in good agreement with the equilibrium condition (equation 4.24) as is demonstrated by the fit traces.

In agreement with the analytical description (see section 4.4) the sum of the individually determined isomer concentrations $[trans]$ and $[cis]$ is approximately equal to one. At 40K the sample consists of ≈65% switched molecules. As we increase the temperature the influence of the trans-to-cis isomerization starts to grow until a maximum of ∼75% is reached around 75K. From this point on the concentration slowly evolves back to a purely trans sample. At $T = 240K$ the amount of switched molecules is less than 10%. The data points have been fitted according to the vibration enhanced photoisomerization channel introduced in the previous section. A thorough discussion of the fit (dotted lines) and its interpretation will be given in the next section.

In the low temperature regime ($T < 120K$) the thermally induced back switching can be neglected and the isomer concentration is governed only by photoinduced processes. Since the reaction yield is below unity the data clearly demonstrates the existence of a light driven cis-to-trans isomerization. A likewise behavior is observed for various photon energies in the range from 2.1 to 4.8eV[11]. Therefore we conclude that both photoisomerization channels (forward and reverse) are driven by the same hole transfer mechanism proposed in section 4.5.

[11]For most photon energies the analysis has been based on the work function shift which based on the above results can now be directly linked to absolute concentrations.

Interestingly the isomer concentration shows a distinct temperature dependence in the low temperature regime. This observation has partially been corroborated by STM [Com08] and XPS measurements. The latter have been briefly introduced in section 4.3.1 exploiting a cis concentration of ≈73% at a substrate temperature of 90K in a presumably photostationary state. The former report a cis concentration of ≈50% at 30K. Considering the declining reaction yield going from 70K to 40K this value appears to continue the trend observed in figure 4.32. The most obvious explanation for this extraordinary behavior of the isomer concentration is a correlation to the differences in the trans- and cis-TBA vibrational structure. Based on the experimental results we can draw two conclusions: (i) According to the respective activation energies no vibrational modes can be excited at very low temperatures (<30K) [Ova07]. In this limit the cis-to-trans isomerization efficiency appears to be higher or at least of equal magnitude compared to the trans-to-cis direction. (ii) The efficiency enhancement due to thermal activation is more pronounced for the trans-to-cis isomerization channel as can be witnessed by the increasing reaction yield in the range from 45 to 75K.

In the high temperature regime ($T > 120K$) on the other hand the isomer concentration is clearly governed by the thermally induced cis-to-trans channel. However it can be influenced to some extend by the forward photoisomerization. Here increasing the fluence will lead to a faster trans-to-cis isomerization shifting the equilibrium concentration in the photostationary state towards the higher cis concentrations. This effect can be observed in the spectra presented in figure 4.33. The corresponding measurements have been obtained illuminating 0.9ML TBA/Au(111) alternating between three different fluences of a $h\nu = 4.34eV$ laser beam. They nicely agree with the theoretical predictions indicated by the shaded areas. Here again a detailed discussion of those fits will be given in the next section.

4.6.4 Kinetic analysis of the vibrationally assisted photoisomerization

In the following we will introduce and discuss the results of a complete analytical description of the vibrationally assisted photoisomerization. For this purpose we combine the different aspects investigated in the previous sections, viz. different isomerization channels and their temperature dependencies. Based on the obtained set of vibration specific cross sections we will be able to determine the equilibrium concentration in the photostationary state and the temporal evolution and of the TBA/Au(111) isomer concentrations for any given temperature and fluence in the photon energy range of 2.4 to 4.4eV

Fit equations and input parameter For the fitting we used a single set of parameters to describe (A) the temperature dependence of the photoisomerization efficiency (cross section), (B) the temperature dependent isomer concentration in the photostationary state and (C) the fluence dependence of the isomer concentration at elevated temperatures where the thermally induced cis-to-trans channel is

active. The corresponding data has been presented in figures 4.29, 4.32 and 4.33, respectively. (A) has been fitted combining equations 4.43 and 4.41 to:

$$\sigma'_{eff}(T) = \sigma_{TC} + \sigma_{CT} + \frac{k_0}{f} e^{-\frac{E_A}{k_B T}} \tag{4.44}$$

with

$$\sigma_{TC}(T) = \left(1 - \sum e^{(-\frac{E_i}{k_B T})}\right) \sigma_{i=0} + \sum e^{(-\frac{E_i}{k_B T})} \sigma_i \tag{4.45}$$

$$\sigma_{CT}(T) = \left(1 - \sum e^{(-\frac{E_j}{k_B T})}\right) \sigma_{j=0} + \sum e^{(-\frac{E_j}{k_B T})} \sigma_j \tag{4.46}$$

Here k_0 and E_A denote the frequency factor and the activation energy of the thermally induced cis-to-trans isomerization. The photoinduced contributions are split into their trans-cis (TC) and cis-trans (CT) contributions. Correspondingly i and j denote the vibrational modes, E_i and E_j the respective activation energies of the different isomers. The values for these variables will be adapted from the previously obtained results presented in section 4.6.1 ($E_a = 240meV$, $k_0 = 10^6 s^{-1}$) and the HREELS measurements of TBA/Au(111) [Ova07] as discussed in section 4.6.2 ($E_i = E_j$ =25meV, 37meV, 63meV and 147meV). Hence the free fitting parameter of the analytical description are the cross sections of each considered vibrational level (σ_i and σ_j).

Likewise the temperature and fluence (f) dependence of the trans isomer concentration $[trans](T, f)$ in (B) and (C) will be modeled using:

$$[trans](T, f) = \frac{1}{1 + \frac{k_{TC}}{k_{CT}}} \tag{4.47}$$

with

$$k_{TC} = \sigma_{TC}(T) * f \tag{4.48}$$

$$k_{CT} = \left(\sigma_{CT} + \frac{k_0}{f} e^{-\frac{E_A}{k_B T}}\right) * f \tag{4.49}$$

Results and discussion The results of the fitting procedure are presented in table 4.2 and for visual comparison illustrated in figure 4.34. Although the model traces of the fitting routines nicely agree with the experimental data we have to critically discuss the considered vibrational modes. Those have been assumed to exhibit equal activation energies for both TBA isomers which clearly is a rough approximation and cannot be expected to reflect the actual properties of the molecule. However the energetic separation of the subsequent modes is rather small which compensates for this inadequacy. Correspondingly the individual error of the fitted cross sections is rather large with an estimated size of 40%. On the other hand the retrieved values extend over several orders of magnitude and thus allow a fairly accurate comparison. In this respect the results of the analytical description are suitable to determine the relative photoisomerization enhancement induced by thermal activation of vibrational modes. This will be elucidated in the following.

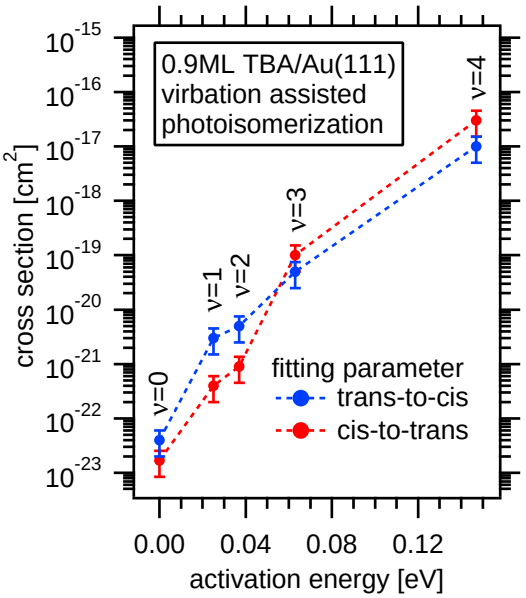

Figure 4.34: Fitted cross sections of different vibrational modes participating in the photoisomerization TBA/Au(111). For details see text.

From the obtained values we see that the efficiency of the hole transfer induced photoisomerization increases in ascending order of the vibrational level. This clearly supports the idea of a ladder climbing process as proposed in sections 4.5 and 4.6.4. Similar temperature assisted (initial state) effects have been thoroughly discussed for the desorption initiated by (single) electronic transitions (DIET) [Xin97][Arn03][Vaz07a] and also for multiple electronic transitions (DIMET) [Saa08]. In case of methyl radicals photo-desorbing from a GaAs substrate Zhu *et al.* report an efficiency increase within the first three excited vibrational level of 1:4:30:500 [Xin97]. In comparison the photoisomerization of TBA/Au(111) exhibits ratios of 1:24:53:5900 for the trans-to-cis channel and 1:75:125:1250 for the cis-to-trans-channel. Here again, the deviations clearly have to be attributed the differences in the respective vibrational structures. Nevertheless the fundamental idea of a process enhancement can be applied to the here presented system as well. Consequently the results of the analytical description corroborate the proposed vibration assisted photoisomerization of TBA/Au(111).

$\nu = i = j$	0	1	2	3	4
E_ν in meV	0	25	37	63	147
mode	$\delta^*(C-N)$	$\delta^*(C-N)$	$\delta^*(C-N)$	$\delta^*(C-N)$	$\delta^*(C-N)$
σ_i^{**} in cm^2	4e-23	1e-21	5e-21	5e-20	1e-17
σ_j^{**} in cm^2	1.7e-23	4e-22	9e-22	1e-19	3e-17

Table 4.2: Parameter set for the analytical description of the virbrationally assisted photoisomerization of 0.9ML TBA/Au(111). Activation energies for the vibrational level have been obtained from [Ova07]. The cross sections for the trans-to-cis (i) and cis-to-trans (j) channels result from fitting of the experimental data. For details see text.* *C-N bending mode of the t-phenyl group.* ** *i = trans-to-cis, j =cis-to-trans*

4.7 *Conclusions*

In conclusion we have demonstrated the reversible isomerization of tetra-*tert*-butylazobenzene adsorbed onto a Au(111) crystal. To determine the underlying excitation mechanisms the electronic structure has been investigated using 2-photon photoemission. It revealed three of the highest occupied molecular orbitals, viz. the HOMO, HOMO-1 and HOMO-2, as well as the lowest unoccupied molecular orbital (LUMO). Upon initiating a trans-to-cis isomerization the dipole moment of the TBA is increased causing a modification of the potential at the substrate-adsorbate interface. This leads to the decrease of the average work function which can thus be used to monitor the switching. Moreover the different potentials give rise to two clearly distinguishable interface states (IS) which can be assigned to the cis and the trans isomer, respectively. Based on the ratio of their photoemission signal direct access to the absolute isomer concentrations and the reaction yield is granted. The observation of interface states has previously been limited to chemisorbed and high coverage adsorbate/metal systems. Here we present a first evidence for their existence in a low coverage regime of a physisorbed molecule.

The isomerization of TBA/Au(111) can either be initiated via illumination or through thermal activation. A detailed analysis of the photon energy dependent isomerization efficiency suggest that (i) the switching due to an intermolecular transition is suppressed and instead (ii) a substrate mediated charge transfer is the dominant excitation channel. Here we proposed a laser induced photoexcitation of Au(111) d-band electrons creating positive charges (holes) which subsequently tunnel into the HOMO of the TBA. Due to the energetic position of the upper d-band edge a minimum excitation energy of 2.1eV is required to initiate the switching. Above this threshold the substrate mediated isomerization process of TBA/Au(111) is bi-directional and exhibits a photon energy independent isomerization yield. This is in strong contrast to the wavelength selective intramolecular excitation channel of TBA in solution.

The reaction rate of the photoisomerization is strongly temperature dependent, increasing by more than two orders of magnitude over a range of 160K. This is attributed to a thermal activation of successive vibrational modes which exhibit an ascending switching efficiency. Due to differences in the vibronic structure the enhancement for the two isomerization directions is asynchronous. Consequently the reaction yield of the photoisomerization a function of the temperature too. It can be tuned between the low temperature (ground state) limit of $\approx$50% and a maximum of $\approx$75% at 75K.

The thermally activated isomerization channel of TBA/Au(111) is unidirectional. Based on the reaction kinetics we were able to determine the height of the ground state barrier which is, compared to the molecule in solution, reduced by a factor of four. Likewise the range of molecular motion is significantly limited. Both effects can clearly be correlated to the interaction with the substrate. Consequently the cis-TBA is not stable at room temperature and thus cooling is required for the investigation as well as a possible functionalization of TBA/Au(111).

5 Influence of the substrate on the photoisomerization: TBA/Ag(111)

Investigating tetra-*tert*-butyl-azobenzene adsorbed on Au(111) we found that the intramolecular isomerization channel has been quenched in the presence of the substrate. Instead a new channel via a hole transfer from the d-band into the HOMO of the TBA could be employed to switch the molecule. A question of interest resulting form this observation is the role of the substrate. In case of TBA/Au(111) the photoisomerization obviously benefits from the the energetic overlap of the involved molecular state with metal bands exhibiting a high density-of-states. However the interaction between an adsorbate and a substrate is not limited to an electronic coupling. It is rather a combination of different contributions like e.g. the binding of the molecule leading to a deformation of the geometric and electronic structure, steric hinderance due to the local confinement or even the modification of intermolecular forces as in densely packed (mono-)layers. To understand how the substrate properties influence the (substrate mediated) switching mechanism it is necessary to carefully tune those and analyze the response of the system.

In a first attempt we realize this approach by exchanging the Au(111) with a Ag(111) crystal. A main difference between these two noble metals is their work function. It can assumed to influence the binding to the substrate and also the alignment of the TBA energy level. We elucidated the resulting changes by investigating the adsorption behavior and the electronic structure of TBA/Ag(111) using thermal desorption spectroscopy and 2-photon photoemission respectively. In both cases only minor deviations from the TBA/Au(111) properties could be identified. This is attributed to the inertness of the noble metal substrate.

A second striking difference is the electronic structure of the substrate and here in particular the energetic position of its d-bands. The corresponding upper band edge has a binding energy of 4eV with respect to the Fermi level and thus does not overlap with the HOMO of the TBA. Consequently we expect a quenching of the substrate mediated photoisomerization as the low density-of-states in the sp-band is assumed to be insufficient to drive such a reaction.

5.1 Absorption

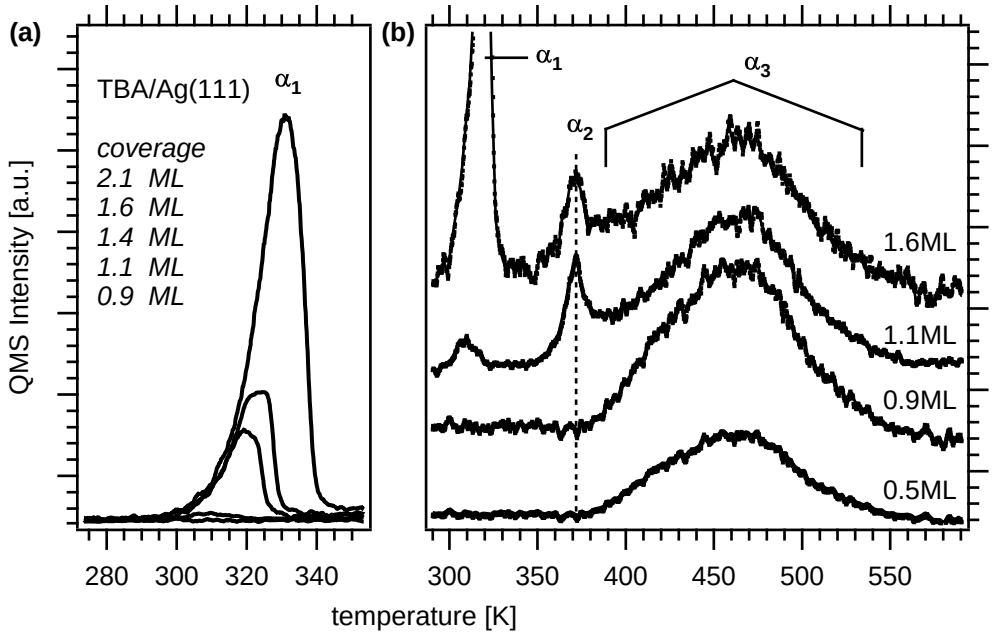

Figure 5.1: Thermal desorption spectra of TBA/Ag(111) for different coverages. **(a):** Evolution of the α_1-multilayer peaks due to increasing layer thickness. **(b):** The monolayer regime with the compressed α_2 and the relaxed α_3-phase.

The first step in investigating TBA/Ag(111) is the analysis of the adsorption behavior and the quantification of the coverage. For this purpose thermal desorption spectroscopy (TDS) is employed. Data from different initial coverages recorded at a heating rate of $\beta = 1Ks^{-1}$ is presented in figure 5.1. Three peaks, α_1, α_2 and α_3 corresponding to different phases have been identified in the spectra. At low coverages only α_3 is visible in the spectra. Continuously increasing the amount of adsorbed molecules the peak grows and starts to spread to lower temperatures. Upon reaching 370K the second, sharp peak α_2 develops. Further adsorption leads to a saturation of both peaks which justifies their assignment to the monolayer of TBA/Ag(111). The corresponding two phase structure has been previously observed in the case of TBA/Au(111). In agreement we correlate them to a compressed (α_2) and a relaxed phase (α_3). The α_2-phase, having its maximum at 370K, accounts for ≈10% of the monolayer. It is governed by repulsive intermolecular forces which reduce the binding to the substrate and leads to desorption at lower temperatures. The maximum of α_3 is located at 470K. In this regime the interactions between the molecules can be assumed much weaker and the interaction with the substrate dominates the desorption behavior.

Increasing the coverage beyond the monolayer a third peak,α_1, appears in the spectra starting at ≈300K. It displays the typical zero order desorption kinetics

known from the multilayer. This can be witnessed by the equal slopes of the spectra and the peak maxima shifting to higher temperatures with increasing initial coverage.

Comparing TDS data of the silver and the gold substrate the overall shape is very similar. The multilayer peaks are identical as their binding is not influenced by the metal surface. Small deviations are found in the position of the peak maxima for the compressed and the relaxed phase. For both cases the TBA/Ag(111) values are shifted to lower values by approximately 30 to 40K. This implies that the molecule-substrate interaction is slightly reduced for the silver substrate.

5.2 The electronic structure

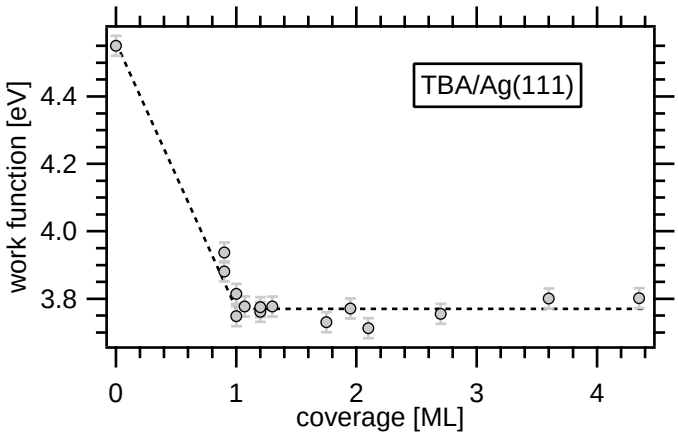

Figure 5.2: Work function of TBA/Ag(111) as a function of coverage.

The clean Ag(111) sample has a work function of $\Phi = 4.56 \pm 0.05eV$. Upon adsorption of the TBA molecules it is lowered to $\Phi = 3.9 \pm 0.05eV$ for a 0.9ML coverage. This is the respective value for the uncompressed α_3 phase found in the TDS spectra. It continues to decrease until the full monolayer coverage is reached. The corresponding minimum work function of $\Phi = 3.77 \pm 0.05eV$ remains constant under the adsorption of further layers which can be seen in figure 5.2. No data is available for submonolayer coverages <0.9ML. However, from the initial slope of the change and in agreement with the TBA/Au(111) data we assume an approximately linear relationship as is indicated by the dotted line in the work function graph.

To investigate the occupied band structure we performed measurements using direct photoemission. The data for different TBA coverages recorded at $h\nu = 6eV$ is shown in figure 5.3. We observe three strong peaks labeled as HOMO, SPB and SS. The HOMO is visible only for the TBA covered substrate. In addition band structure calculations and experiments on the clean surface reveal no Ag related states at this position [Mil96][Fus90]. Hence we assign this peak to the highest occupied molecular orbital (HOMO) of the adsorbed TBA at $E_B = -1.85 \pm 0.05eV$

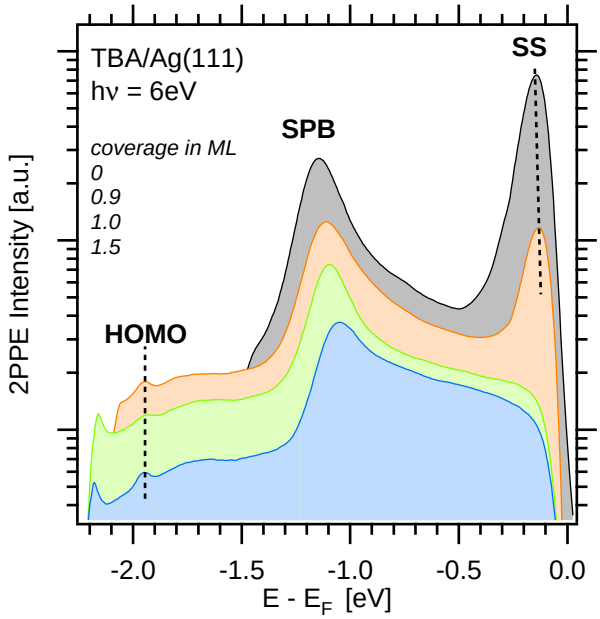

Figure 5.3: Coverage dependent 6eV (direct photoemission) spectra of the TBA/Ag(111).

with respect to E_F. The peak SPB 1eV below the Fermi cutoff edge originates from the sp-bands of silver. Similar to the gold sp-band the initial state energy of the corresponding peak shifts with the photon energy [Mil96]. It is determined by the direct transition between the strongly dispersing occupied and unoccupied parts of the band along the ΓL-line of the Brillouin zone. The shoulder of the SPB-peak towards the Fermi edge is a result of simultaneous indirect transitions [Mil96]. Peak SS is assigned to the surface state of the clean Ag(111) surface at a binding energy of $E_B = -0.07 \pm 0.05eV$ with respect to the Fermi level. Upon adsorption of the molecules the SS is slightly shifted to lower binding energies. Here a detailed analysis is prevented due to the partial cutting of the peak at the edge of the spectra. For mono- and multilayer coverages the SS is completely quenched.

Switching to 2PPE we find a series of TBA induced states. Figure 5.4 depicts the corresponding spectra recorded at a photon energy of $h\nu = 2.99eV$. In graph 5.4(a) we find a pronounced peak from the silver sp-band and the two adsorbate induced peaks A and B. To determine whether they originate from occupied or unoccupied states we have to investigate their photon energy dependence. From graph 5.4(b) we see that both states exploit a constant kinetic energy regardless of the excitation energy $h\nu$. Hence both peaks are derived form unoccupied final states of the TBA which are located above the vacuum level. Their binding energies have been determined as $E_B = 3.95 \pm 0.05eV$ (A) and $E_B = 4.20 \pm 0.05eV$ (B) with respect to E_F. The excitation of such states occurs via transient scattering followed by an autodetachment of the electron which leads to its detection [Plu07]. The final states A and B are clearly visible at the 0.9ML but expose a slightly reduced intensity

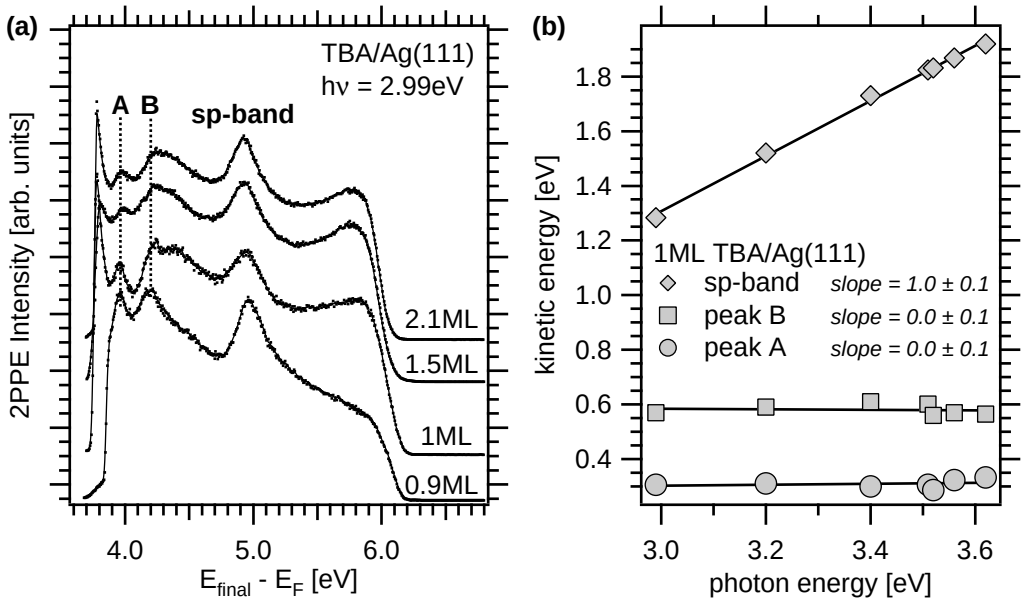

Figure 5.4: One-color 2PPE spectra of TBA/Ag(111). **(a):** Coverage series taken at $h\nu = 2.99eV$. The spectra exploits two molecular states, A and B, and the silver sp-band. **(b):** Photon energy dependence of the peaks found in the 2PPE spectra.

at the monolayer and multilayer coverages. Simultaneously a broad shoulder rises at the right side of state B. A possible explanation is given by electronic structure calculations for the free TBA [Teg07]. These reveal a large number of unoccupied states in the corresponding energy region which have to be considered as contributors to the photoemission signal. The change in the signal intensities on the other hand reflects upon a change in the coupling of the molecular states to the substrate. This has been discussed before in the case of the gold interface states (see section 4.3). Here a possible origin can be found in the transition from the relaxed to the compressed monolayer phase which apparently occurs increasing the coverage above 0.9ML.

In the photon energy dependence (fig. 5.4(b)), we also show data of the sp-band which exploits a slope of $m = 1.1 \pm 0.1$. This is a result of its previously mentioned dispersion in which direct excitations take place along the ΓL-line of the Brillouin zone. It has not to be mistaken as indication for the photon energy dependence pointing to an intermediate state.

Thus far we discussed only the initial and final states of the TBA/Ag(111). To investigate the intermediate state region we revert to a 2-color 2PPE setup. Figure 5.5 displays three sample spectra at 1.5ML, 1.0ML and 0.9ML coverages recorded with $h\nu_1 = 1.80eV$ and $h\nu_2 = 3.62eV$. The spectra are dominated by two peaks labeled C and IS. From the photon energy dependence depicted in graphs 5.5(b) and 5.5(c) we are able to determine the energetic position of the corresponding states. The IS feature is pumped using UV light and thus is located at $E_B =$

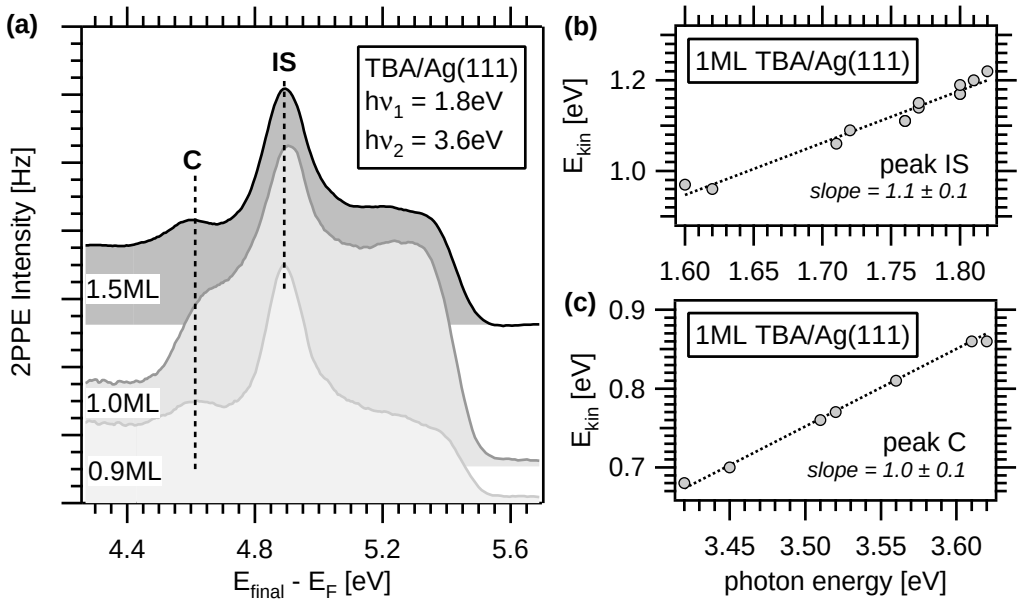

Figure 5.5: 2-color 2PPE spectra of TBA/Ag(111). **(a):** Coverage series taken at $h\nu_1 = 1.8eV$ and $h\nu_2 = 3.6eV$. The spectra is governed by the two molecule induced peaks C and IS. For state assignment see text. **(b) and (c):** Photon energy dependence of IS and C at a 1.0ML coverage. The kinetic energy of IS scales directly with the vis-beam ($h\nu_1$) energy hence it is pumped by the UV-beam($h\nu_2$). For peak C the behavior is vice-versa.

$3.23 \pm 0.06eV$. Peak C is pumped by the visible light yielding a binding energy of $E_B = 1.00 \pm 0.06eV$ with respect to E_F. In this energy region we can exclude the existence of image potential states hence we assign this feature to the LUMO of the adsorbate. This again is supported by the calculations for the free molecule placing the LUMO at ≈1.6eV above the Fermi level. Together with the first occupied molecular state the resulting HOMO-LUMO gap of TBA/Ag(111) has a width of 2.85eV. The above mentioned model calculations on the other hand yield a gap of 3.77eV with the HOMO at $E_B = -2.21eV$ in contrast to our value of $E_B = -1.85eV$. This discrepancy can related to two effects. (i) A modification of the energetic structure due the adsorption. However in the present case of physisorption these changes can be assumed rather small. (ii) The excitation mechanism of the 2PPE. Here the population of the LUMO is most likely not the result of an intramolecular transition but of the scattering from hot substrate electrons. This has been discussed before in the case of the TBA/Au(111) LUMO (see section 4.3). Therefore we resolve the energetic position of a negatively charged (negative ion resoncance) molecule which is shifted down in energy with respect to the results of the calculations. For the HOMO the situation is vice versa. The 2PPE process first excites the electron from the HOMO into an intermediate state from where it is emitted. Thus the detected electron reflects the energetic position of a state with a missing charge which is shifted up in energy [Teg07].

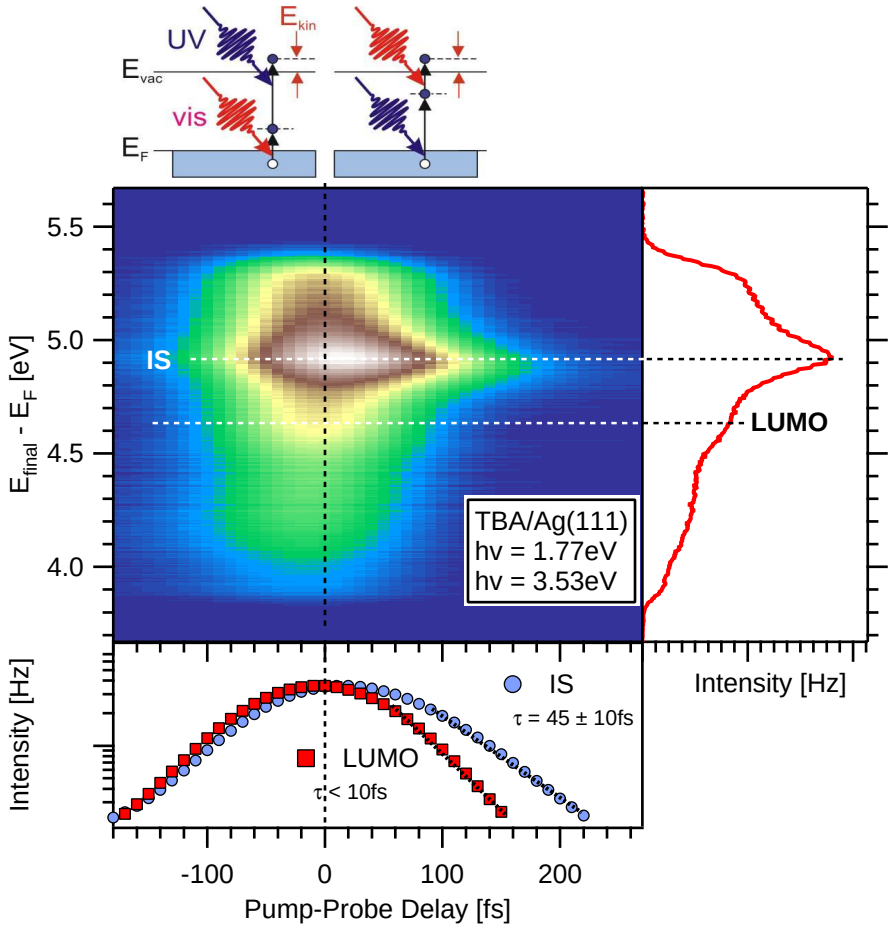

Figure 5.6: Time-resolved 2PPE data of 1ML TBA/Ag(111) presented in a 2D false color plot. Cross correlation curves exploiting the lifetimes of the interface state (IS) and the LUMO are depicted in the lower panel.

We now return to the assignment of the IS peak. Its energetic position indicates a possible origin from the image potential of the substrate. This leads to the question whether this is a classical image potential state or another of the molecule/metal interface states discussed for the gold surface (see section 4.3). A final answer cannot be given at this point as experimental evidence is limited. Our strongest argument is retrieved from the coverage dependence in figure 5.5(a). There the binding energy of peak IS is constant in all three traces while the work function shifts about 150meV going from 0.9 to 1.0ML. In case of an image potential state one would expect a coupling to the vacuum level and thus a shift in agreement with the work function [Hot07]. Therefore we favor the assignment to an interface state (IS). Supporting evidence is given by experiments investigating the electronic structure of the isoelectronic molecues TBS and TBI adsorbed on Au(111).

In a last step we use time resolved 2PPE to elucidate the lifetime of the LUMO and the interface state. The measurement has been performed on a monolayer TBA/Ag(111) using photon energies of $h\nu_1 = 1.77eV$ and $h\nu_2 = 3.53eV$. Figure 5.6 displays the result in a 2-dimensional false color plot. The spectra is governed by the strong peak of the interface state IS. This is the only feature which shows an obvious lifetime. To analyze the decay times we cut the spectra along the respective final state energies of the IS and the LUMO peak. While we observe a lifetime of $\tau = 45 \pm 10fs$ for the former, the latter relaxes on a timescale below our temporal resolution of 10fs. This fast decay of both states indicates a rather strong electronic coupling to the substrate.

A summary of the TBA/Ag(111) electronic structure is given in figure 5.7. Here we linked the two final states A and B to the LUMO+1 and LUMO+2 respectively. This is motivated by the absence of further electronic states in the intermediate region. Consequently the states are labeled in an ascending order.

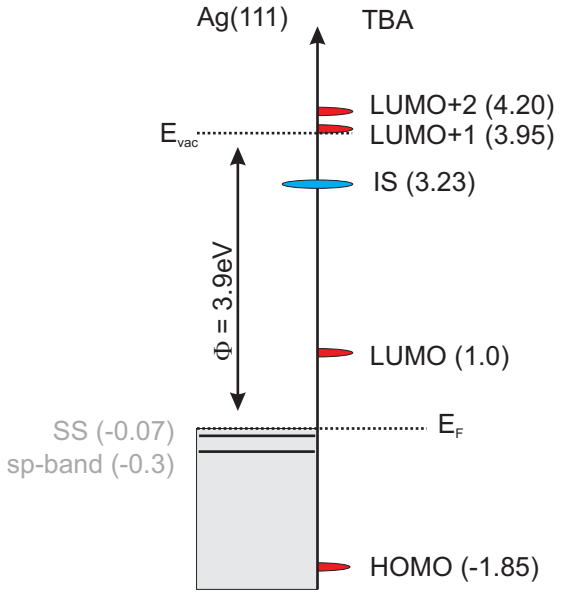

Figure 5.7: Energy diagram of the TBA/Ag(111) states found in direct photoemission and 2PPE. Molecular states are shown in red, states arising from interface potentials in blue. Binding energies are given in eV with respect to the Fermi level.

5.3 Quenched photoisomerization

In order to induce a possible isomerization of the TBA/Ag(111) we illuminated the sample at photon energies in the range of 1.8 to 3.9eV and at 6eV. Special attention has been given to the HOMO-LUMO excitation energy 2.85eV. According to the here presented electronic structure this is the most promising channel for an intramolecular transition leading to an isomerization. However upon illumination we did not observe any changes in the electronic structure. This is in agreement with the TBA/Au(111) experiment where the intramolecular channel is quenched as well. Two explanations can be presented for this observation. (i) The relaxation of the photoexcited molecular state occurs on a timescale faster than the isomerization. This can be attributed to the electronic coupling of the LUMO to the substrate which opens up new decay channels. (ii) The adsorption of the TBA leads to changes in the electronic structure which impose a barrier along the isomerization pathway of the photoexcited state. As for the case of the gold substrate this may be attributed to modifications of the electronic structure or steric hinderance due to the interaction with the substrate.

Having ruled out an intramolecular excitation we continue our investigation with the substrate mediated channels, viz. the creation of a negative or positive ion resonance. The former can be achieved via the creation of hot electrons which subsequently scatter into the LUMO of the molecule. A positive ion resonance on the other hand requires the injection of positive charge carriers (holes) into the HOMO. In the corresponding energy region of silver a hole can only be donated by the hybridized sp-band since the upper d-band edge is located 4eV below the Fermi level. However it is well known that in noble metals the decay of charge carriers is much faster in the sp-band than in the d-band [Cam00]. Thus the chances of a charge transfer from the silver to the TBA HOMO can be expected very low if not impossible.

The investigated photon energy range is sufficient to create charge carriers for either of the above described scenarios. Nevertheless no isomerization could be witnessed based on changes in the electronic structure. Hence we conclude that also no substrate mediated channels are present for the TBA/Ag(111) system. In case of the negative ion resonance we can again argue with the decay of the excited state electron back into the substrate or a barrier along the corresponding isomerization pathway. The latter applies for the positive ion resonance as well but here a much more probable cause is the low charge transfer rate. This is clearly in contrast to the gold substrate where we observe an energetic overlap of the HOMO and the d-bands. Those do not only adsorb a large part of the laser light but also their density-of-states and the respective long lifetimes of excited charges evoke a sufficient tunneling probability into the molecule. Due to a binding energy of -4eV with respect to the Fermi level the Ag(111) d-bands cannot couple to the HOMO of the TBA and thus do not contribute to a substrate mediated excitation channel.

5.4 *Conclusions*

Thermal desorption spectroscopy has been employed to characterize the adsorption behavior of TBA/Ag(111) showing good agreement with the results obtained for the Au(111) substrate. In both cases a single phase multilayer and a monolayer consisting of a compressed and a relaxed phase have been identified. However the results also indicate that the binding to the gold crystal is slightly stronger. In a subsequent step the electronic structure of TBA/Ag(111) has been analyzed using 2-photon photoemission. Here the adsorption reduces the work function by 0.79eV to 3.77eV. A series of molecule induced states are observed viz. the highest occupied (HOMO) and the lowest unoccupied molecular orbital (LUMO) as well as the LUMO+1 and LUMO+2. In addition we have shown the existence of an interface state at 3.23eV above the Fermi level.

In a photon energy range of 1.8 to 4.5 and at 6eV we find no evidence for a photo induced trans-cis isomerization. In compliance with TBA/Au(111) the intramolecular excitation channel appears to be suppressed due to the molecule-substrate coupling. As expected the previously proposed substrate mediated hole driven isomerization process is not accessible which can be related to the energetic position of the Ag d-bands since these do not energetically overlap with the HOMO of the TBA.

6 Influence of the functional group: TBI & TBS on Au(111)

One of the great advantages of molecular switches is the tunability of their properties due to substitution and attachment of atoms or atomic groups. These changes inevitably lead to a modification of the intermolecular interactions and in case of adsorbed molecules of the adsorbate-substrate interactions. The latter has been demonstrated for the case of different azobenzene derivatives adsorbed on Au(111) [Com07]. Here Comstock et al. compared the isomerization behavior of the "four legged" tetra-*tert*-butyl-azobenzene with a "two legged" and a bare azobenzene showing that only TBA could be switched reversibly. The apparent suppression of the photoisomerization channel in the other two molecules is explained by the differences in the electronic coupling which corroborates the results of the previous chapters.

In retrospect, the azobenzene related molecules have greatly contributed to the understanding of surface confined molecular switches and in particular to their sensitivity regarding electronic coupling. However the increase of knowledge will be limited as the functional group responsible for the isomerization remains unaltered by most of the substituents. Thus in order to elucidate further adsorption related phenomena, e.g. alternative excitation channels, it is of crucial importance to extend the investigations to different switches. Correspondingly the following chapter presents the results of experiments performed on tetra-*tert*-butyl-imine (TBI) and tetra-*tert*-butyl-stilbene (TBS) adsorbed onto an Au(111) substrate. Together with TBA these two represent a subgroup of molecules which differ only by the composition of the functional group. The initial N=N azo-group is subsequently replaced by a N=CH (TBI) and a HC=CH group (TBS). This is assumed to leave the interaction of the large tert butyl substituted phenyl rings with the substrate unchanged whereas the isomerization properties based on the functional group can be modified.

The main question is of course whether there is an isomerization channel available for the surface confined TBI and TBS. In order to discuss the occurrence or the absence of the different possible excitation mechanisms we again require a detailed knowledge of the adsorption behavior and the electronic structure of the molecules. As in the previous cases access to those properties will be given by thermal desorption spectroscopy and 2-photon photoemission.

Another key focus within this chapter are the intermolecular interactions of the surface confined molecules. Their impact on the adsorption behavior, the electronic structure and the coupling to the surface can be nicely monitored in case of the TBI/Au(111) since it has, in contrast to TBA and TBS, a non vanishing dipole moment. Moreover the data indicates an apparent competition between intramolecular and substrate-adsorbate interactions leading to different adsorption phases. This situation has some interesting consequences for states arising at the metal/molecule interface which appear to be affected by the molecular orientation.

6.1 Adsorption behavior and electronic structure of TBI/Au(111)

Tetra-*tert*-butyl-imine exploits a non-vanishing dipole moment in its ground state of 1.8 Debye [Wei71]. This gives rise to strong Coulomb interactions with the surrounding molecules and the surface. In addition the twisted geometry and the asymmetry of the functional N=CH group suggest an adsorption behavior which should contrast the case of the planar and almost neutral TBA. This can indeed be witnessed in thermal desorption spectroscopy (TDS) used to analyze the adsorption of the molecule and the coverage of the substrate. As we will show in the following different meta-stable and stable phases occur in the multi and in the monolayer regime. Here we will address their thermally induced conversion and elucidate the possible underlying processes.

In addition access to the adsorption behavior is granted by the electronic structure investigated with 2-photon photoemission (2PPE). Due to the non-vanishing dipole moment of the TBI its phase transitions can be well resolved based on a shift of the work function. Simultaneously the electronic coupling between the molecules and the substrate is modified resulting in changes of the photoemission yield from molecular induced states. The combined picture of TDS and 2PPE data indicates a strong intermolecular and molecule-substrate interaction in terms of: (i) The coverage hindered relaxation of the monolayer molecules. (ii) A temperature activated improvement of electronic coupling in the low coverage regime.

A peculiarity which cannot go unmentioned is the existence of an interface state which, as a consequence of the phase transition, experiences a binding energy shift. It starts at a position within the substrates projected band gap and is moved into a region where it overlaps with the unoccupied sp-bands of the Au(111). According to the theory of electron scattering this opens up new channels for electronic relaxations. Evidence is clearly given by the observed lifetime decrease from 110 to <10fs.
We will close the discussion of TBI/Au(111) by analyzing its suppressed cis-trans photoisomerization. In this respect we will also elucidate why the observed phase transitions, based on our data, cannot be interpreted as a switching.

6.1.1 Adsorption

Thermal desorption spectra of different TBI/Au(111) coverages are depicted in figure 6.1. For the present system we have to distinguish between an ordered and a disordered multilayer configuration. Graph 6.1(a) shows the multilayer region of samples prepared at $T = 40K$. Two peaks, α_1 and α_2, corresponding to different phases can be identified. Their spectra exhibit the usual zero order desorption kinetics with a homogenous slope starting below $T = 280K$ (α_1) and a peak maximum shifting to higher temperatures as the coverage increases. Peak α_1 is dominant for higher coverages. Its respective phase is converted into the α_2-phase as we heat the sample. Evidence is given by the spectra depicted in graph 6.1(b). Here the multi-

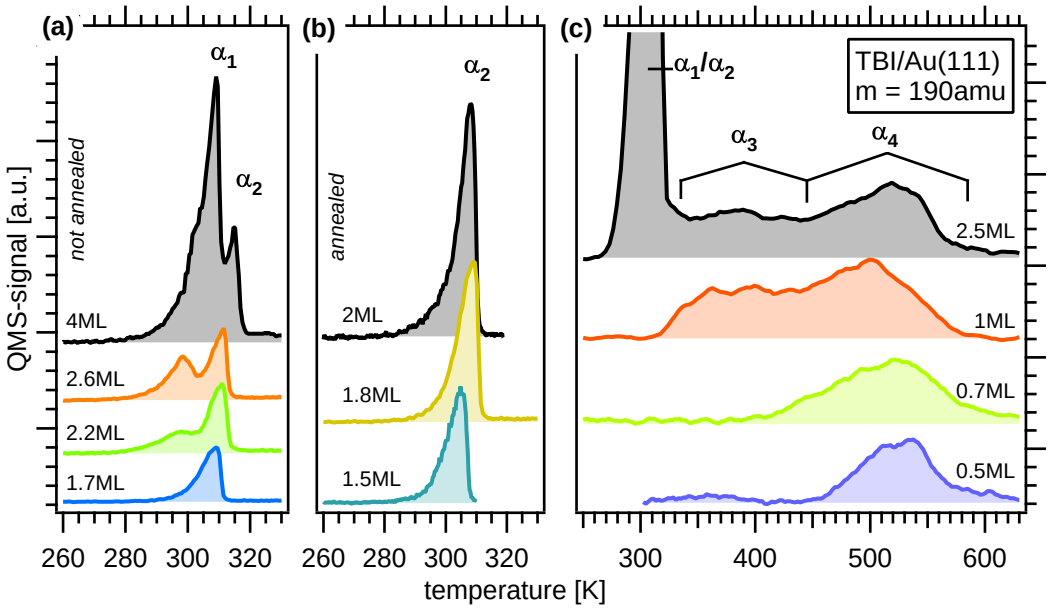

Figure 6.1: Thermal desorption spectra of TBI/Au(111) for different coverages. **(a):** Double peak structure of the two phases α_1 and α_2 found in multilayer regimes adsorbed at sample temperatures of $T = 40K$. **(b):** Upon sample annealing at $T = 260K$ the α_1 converts into the α_2 phase. The subsequently taken spectra show only a single peak. Dosing at higher substrate temperatures leads to the same behavior. **(c):** The monolayer regime with the two phases α_3 and α_4.

layer TBI/Au(111) has been annealed for 10min at 260K prior to the measurement. The α_1 peak has vanished and only a single α_2-phase is observed.

The amount of desorbed molecules is shown to be independent of the annealing procedure. Therefore two samples were prepared at a substrate temperature of 40K with one of them being heated at 260K for 10min prior to the TDS measurement. For both cases the area underneath the multilayer peak structure, which is a direct measure of the coverage, is equal. Thus no molecules have been desorbed in the annealing process.

Taking into account the observed phase transition we can extend the interpretation of the multilayer spectra. Since there is a finite heating rate of $\beta = 1Ks^{-1}$ for the TDS measurement we have to assume a partial conversion (α_1 to α_2) before the desorption temperature of the multilayer is reached. Indeed the height of peak α_1 increases rapidly with the coverage whereas α_2 remains almost constant. This implies that the α_2 feature is induced by the annealing effect of the temperature ramp. Consequently we can assume that TBI at low temperatures adsorbs predominantly in the α_1-phase.

We now turn to the high temperature regime of the TDS spectra depicted in graph 6.1(c). Here we observe two peaks with almost identical width which saturate for large amounts of adsorbed molecules. One possible explanation for this structure

is the existence of a bi-layer system in which not only the first but also the second layer is influenced by the interaction with the substrate. A classical example in this respect is the adsorption of benzene on Cu(111) [Vel98]. This is clearly not the case for TBI/Au(111) as will be obvious when discussing its electronic structure. Thus we assign the region in between 320 and 585K to a monolayer regime with two phases α_3 and α_4. The latter appears in the range from 450 to 585K and can be associated with low monolayer coverages of up to 60%. As in the case of the multilayer we have to consider a thermally induced phase transition for TBI films prepared at low substrate temperatures ($T = 40K$). A detailed comparison of the respective spectra shows no indication of such behavior, instead a constant α_3 to α_4 peak ratio is maintained. However the detection of the phase transition could be masked by the annealing effect of the heating ramp as seen for the multilayer regime. This presumption is strongly supported by temperature induced changes in the electronic structure which will be discussed in the next section.

According to the TDS data the adsorption of TBI on Au(111) is very complex with meta-stable phases which can be thermally converted. Similar behavior has been observed for several other molecule/metal systems like multilayers of benzene on Ru(001) [Jak89], pyridine [Yan01] and naphthalene [Hua04] on Ag(111) or cyclooctatetraene on Ru(001) [Teg05]. This adsorption behavior is explained by a competition between molecule-substrate and intermolecular forces. At low coverages the interaction with the substrate is dominant and hence it will be the main influence on the structure upon absorption. Increasing the amount of molecules emphasizes the intermolecular forces which leads to a meta-stable phase. Eventually the adsorption reaches a threshold coverage where those interactions become dominant and lead to the formation of a bulk structure. This conversion away from the substrate influenced phase can also be thermally activated and leads to a 3D growth in form of islands or clusters as observed in the above examples. A similar scenario can be imagined for the case of TBI/Au(111) as it implements the assumed intermolecular dipole interaction. Again, more evidence and a thorough discussion will be presented based on the thermally induced changes in the electronic structure in the next section.

6.1.2 The electronic structure

Work function Due to the annealing effects observed in the the TDS spectra it is preferable to start the investigation of the electronic structure using samples prepared at 40K and thereafter monitoring the temperature induced changes. Figure 6.2 shows the evolution of the work function for such an experiment upon cycles of illumination and annealing. Here we prepared 0.5ML TBI/Au(111) at a substrate temperature of 40K. As a result of the adsorption process the work function of the clean gold, $\Phi = 5.45 \pm 0.05eV$ is lowered to $\Phi = 4.90 \pm 0.07eV$. During the first illumination period using a photon energy of $h\nu = 2.99eV$, Φ drops again by approximately 40meV to $\Phi = 4.86eV$ (1). The corresponding trace exploits an exponential saturation similar to the switching induced changes of the TBA. In a

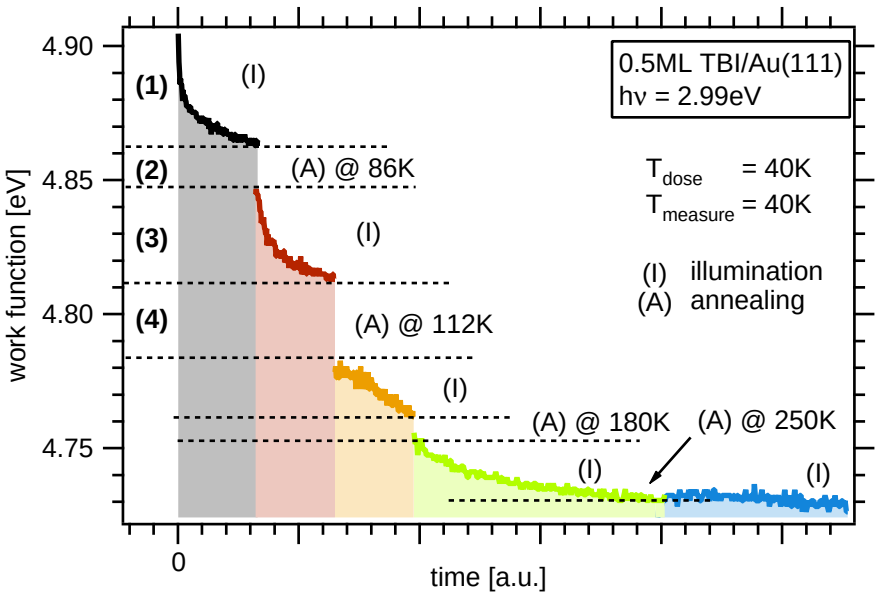

Figure 6.2: Work function shift of 0.5ML TBI/Au(111) induced by cycles of illumination and annealing. Each sequence is taken on a fresh sample spot. The light driven changes decrease in magnitude as the annealing temperature rises. Around 260K the work function saturates. A similar behavior is found for coverages up to 3ML. For details on the different steps (1 to 4) see text.

subsequent annealing step to $T = 86K$ the work function is further reduced by 15meV (2). A second illumination series taken on a fresh sample spot again shows the exponential change found in the first step only this time with a smaller magnitude of 35meV (3). This trend continues as we anneal the sample at a higher temperature of 112K (4). After 5 cycles and a maximum annealing temperature of $T_{max} = 320K$ the work function saturates 170meV below its initial value. The 2PPE spectra for the above experiment have all been obtained at a temperature of 40K. This way we can assign the observed changes to a thermally induced transition. In contrast a temperature dependent effect without a conversion of some kind, e.g. a binding energy shift due to lattice expansion[12], would in this case lead to identical spectra.

We repeat this experiment under altering conditions, individually changing the substrate temperature during TBI deposition ($T = 260K$), the coverage (0.5 to 3ML). This give us a consistent picture about the behavior of the work function Φ:

(i) Heating the sample leads to a decrease of Φ which converges to a coverage dependent final value. Here it is not important whether a cold sample is annealed or the adsorption is performed at higher temperatures. As for any thermally activated process the timescale on which saturation is reached depends on the maximum annealing temperature T_{max}.

[12] this is e.g. observed for the Au(111) surface state, see appendix C

(ii) The illumination of the sample results in a work function shift as well. The induced changes progress in the same direction (to a reduced work function) but have a smaller magnitude. In addition each spot can only be converted once. Hence a previously illuminated area will not exploit a further exponential work function decrease even after a subsequent heating cycle.

(iii) An annealing of the sample prior to the illumination reduces the light induced changes. The higher the corresponding annealing temperature the smaller the shift due to the illumination.

(iv) The observed evolution is irreversible. Neither heating nor a change of the photon energy within the available range of 1.8 to 4.7eV resulted in a work function increase.

(v) In a first approximation the rate of the light induced change is independent of the wavelength and the fluence.

(vi) The work function shift has qualitatively been observed for all investigated coverages (0.5 to 3ML). Its magnitude however is still a function of the layer thickness.

Before discussing the origin of the light and temperature induced changes we have to consider the actual coverage dependence of the work function which is superimposed on the above introduced work function shift. Therefore we prepared a series of samples at a substrate temperature of 40K which were annealed at 260K prior to the measurement. The results for different initial coverages are presented in figure 6.3. Within the first layer the work function decreases almost linearly with the coverage. It starts at a clean gold surface value of $\Phi = 5.45 \pm 0.05eV$, and reaches $\Phi = 4.1 \pm 0.07eV$ at the full monolayer. For coverages >1.3ML we observe a constant work function of $\Phi = 4.55eV$. The most unusual part found in this graph is the region between 1.0 and 1.3ML. Here the work function drops significantly (450meV) desorbing only a small amount of molecules. The linearity in the submonolayer regime contradicts the assignment of the TDS peaks α_3 and α_4 to a bilayer system. In such systems the first and second layer can well be assumed to have a different impact on the sample work function which would result in a non homogeneous slope as e.g. seen for benzene on Cu(111) [Vel98].

To explain the observed temperature, light and coverage induced changes we employ a variation of the scenario proposed in the discussion of the TDS experiments: Adsorption on a cold substrate creates randomly oriented molecules. For low coverages this leads to the monolayer phase α_3. Subsequent heating initiates a reorientation (ordering) of the molecules increasing the interaction with the substrate. This is in agreement with the further decreasing work function shown in figure 6.2. Also it is suitable to explain the α_4-phase of increased binding energy in the TDS spectra.

For higher coverages, close to a monolayer, the picture is essentially the same, only here the relaxation of the molecules is quenched by the intermolecular inter-

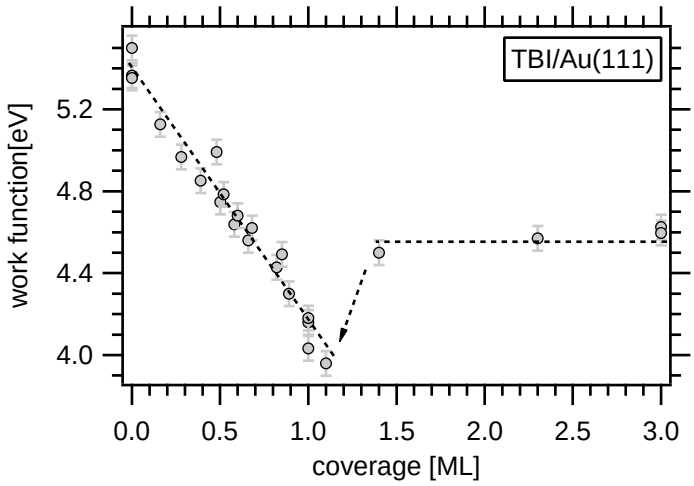

Figure 6.3: Coverage dependence of the TBI/Au(111) work function. All values have been obtained after annealing the samples at 260K. For details see the text.

actions which become dominant as the distance between neighboring molecules is reduced. Hence we observe two effects on the work function: (i) the total value decreases further as more molecules are adsorbed (ii) the work function shift upon annealing is reduced because the relaxation is hindered. This is in agreement with the the occurrence of the α_3-phase as witnessed in the monolayer TDS spectra (see figure 6.1).

Increasing the coverage to the multilayer regime leads to a blocking of the relaxation. Evidence is given by the kink in the coverage dependence of the work function. It can be explained based on two observations. First, Figure 6.3 showed a constant Φ in the region from 1.3 to 3ML. From this we conclude that the work function of TBI/Au(111) is mostly determined by the first layer and its corresponding phase. Second, a phase transition has also been witnessed for the multilayer. Here a shift of 100meV resulted in a final work function value of $\Phi = 4.55eV$. This is a comparably weak shift if one considers that it reflects upon the transition of a fully covered surface. In contrast a change of 170meV has been observed for only 0.5ML TBI/Au(111). From these two arguments we conclude that the relaxation in the multilayer regime is not completed and can only be achieved upon its desorption which eventually leads to the tremendous drop in the work function.

Finally we want to comment on the light driven effects. Due to the observed spectral changes they appear to induce the same processes as the annealing procedures only with a limited magnitude. One possible explanation is the heating of the sample under laser irradiation. This however seems rather unlikely as the excitation is locally restricted[13] and the energy should be dissipated quickly into the bulk of the substrate. Moreover the increase of the fluence should lead to a stronger heating and thus a larger work function shift which is contradicting our observations. A sec-

[13]the penetration depth of the light is in the order of few Å[Sea79]

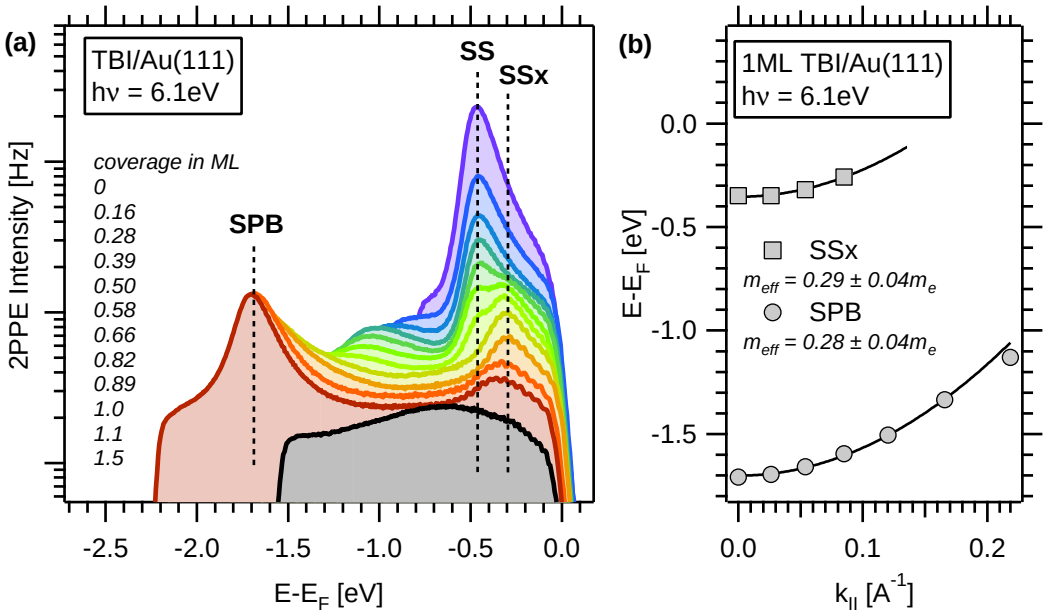

Figure 6.4: **(a):** Coverage dependence of the gold surface states at $E_B = -0.43eV$ and $E_B = -0.21eV$ recorded in direct photoemission. In the monolayer regime a peak resulting from a direct transition between the sp-bands can be observed at $E_B = -1.6eV$. **(b):** Dispersion of the gold sp-band and surfaces state feature SSx at a monolayer coverage.

ond possibility is the light induced intramolecular or substrate mediated excitation of vibrational modes. Although steric hinderance from the neighboring molecules can be expected this approach allows at least for minor changes in the substrate-adsorbate interaction. This is in agreement with the small magnitude of the work function shift observed only at the "unordered" sample. The light induced channel would thus be contrasted by the thermal channel which can be assumed to supply sufficient energy to also overcome the intermolecular interaction.

In summary we suggest a thermally and light induced phase transition of the first TBI layer adsorbed on Au(111) which is partially suppressed in dependence of the coverage. Further evidence will be presented when discussing the electronic states. This will also provide information necessary to prove that the observed transition is not a cis-trans isomerization as seen for TBA/Au(111).

Electronic states Spectra from a $h\nu = 6eV$ experiment in direct photoemission are shown in figure 6.4. To monitor the changes induced by the TBI molecules a 1.5ML coverage is prepared and stepwise heated off. We can distinguish three features in the spectra (SPB, SS and SSx). For the clean surface a large peak (SS) at $E_B = -0.43 \pm 0.05eV$ appears which we identify as the gold surface state. As previously observed for the TBA its intensity is reduced with increasing coverage. For a monolayer the signal of the SS is completely quenched and the spectra is governed

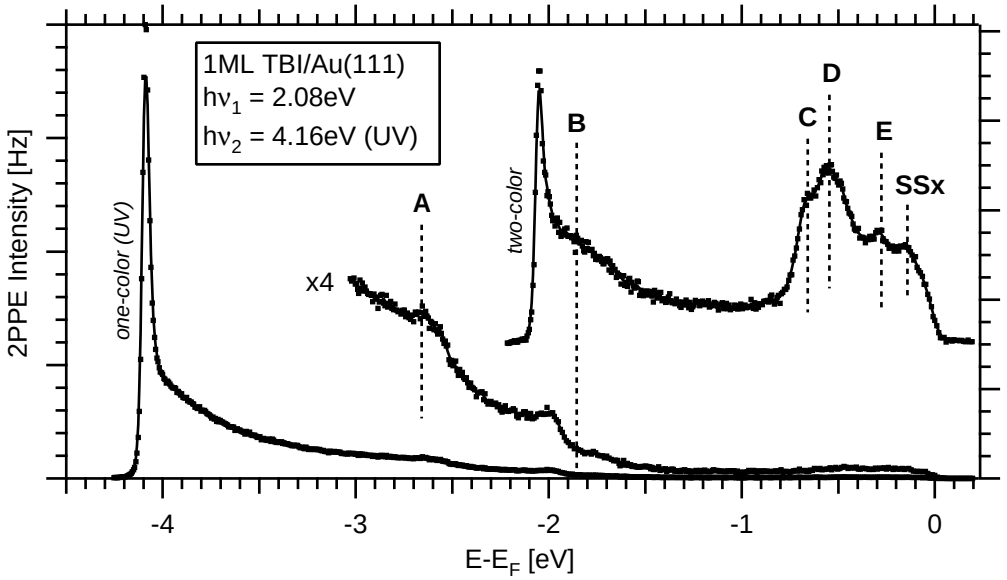

Figure 6.5: Sample one and two color 2PPE spectra of a monolayer TBI/Au(111). The spectra are plotted vs. the initial state energy to identify states which appear in both of them. A detailed discussion and high resolution spectra of the labeled peaks will be given in the text and the following figures, respectively.

by the two peak SPB and SSx. The former is assigned to a direct transition between the strongly dispersing sp-bands of the Au(111). At $h\nu = 6eV$ the corresponding excitations take place at a suitable point along the ΓL-line of the Brillouin zone. This leads to the respective initial state position of $E - E_F = 1.7eV$. A similar occurrence has been reported for the case of the Ag(111) sp-band [Pon05].

The SPB-peak is also strongly dispersing in the directions parallel to the surface. This can be seen in the angle resolved measurement depicted in graph 6.4(b) yielding an effective mass of $m_{eff} = 0.28 \pm 0.04 m_e$. The second peak, SSx, is located at $E_B = -0.27 \pm 0.05eV$ having an effective mass of $m_{eff} = 0.29 \pm 0.04 m_e$. This value is essentially equal to the surface state value of $m_{eff} = 0.25 m_e$ [Hoe04]. The peak SSx has been previously observed for TBA/Au(111) as well where it has been associated with an adsorbate induced surface state split off. This assignment is copied for the case of TBI/Au(111) which is strongly supported by the above shown dispersion curve.

Molecular induced states are observed in 2PPE as shown in the exemplary spectra in figure 6.5. Here we identify 5 peaks, A-E, on a monolayer TBI/Au(111) using photon energies of $h\nu_1 = 2.08eV$ and $h\nu_2 = 4.16eV$. In the (one color) UV spectra two peaks, A and B, are found at the edge of the gold d-bands. According to their photon energy dependence (see fig. 6.6) both originate from initial states with binding energies of $E_B = -2.65 \pm 0.07eV$ and $E_B = -1.9 \pm 0.07eV$ in respect to the Fermi level. Since no further occupied states can be identified in the spectra we assign A and B to the HOMO-1 and the HOMO respectively.

The molecular character of the HOMO-1 is supported by a coverage dependent experiment. A selection of submonolayer spectra taken at $h\nu = 4.56eV$ is depicted in figure 6.7. Surprisingly the maximum peak intensity is not observed at high coverages but approximately on a 0.5ML sample. This roughly coincides with the results of the TDS measurements were the α_3-phase accounted for 40% of the monolayer. Hence the photoemission signal from the occupied states seems to quench in the presence of the α_3-phase.

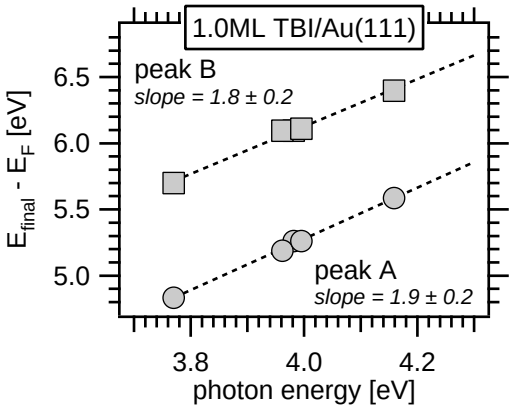

Figure 6.6: Photon energy dependencies of the TBI/Au(111) initial states as function of the probing wavelength.

A comprehensive picture can be obtained using the argument of Lindstrom et al., describing the 2PPE signal intensity as a function of the adsorbate states mixing with substrate states [Lin07]. Correspondingly we can attribute the small signal in the monolayer regime to a weak molecule-substrate coupling in the α_3-phase. It is increased upon desorption of the molecules which according to the description of the TBI absorption behavior leads to a relaxation into the α_4-phase exhibiting an enhanced coupling. A correlation to the adsorption geometry can be made by including quantum chemical calculations of the molecular orbitals. Those

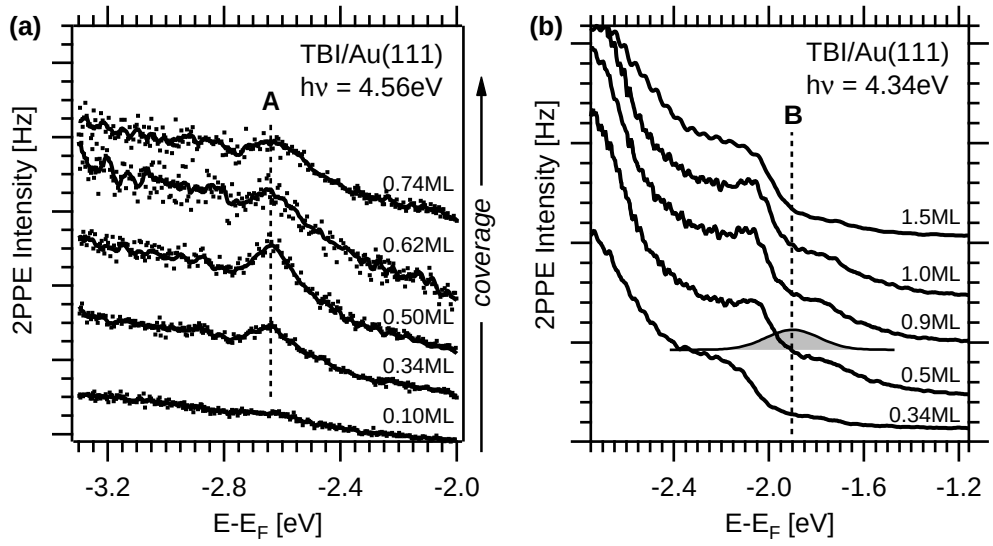

Figure 6.7: Coverage dependence of the occupied molecular states A (a) and B (b). Reducing the coverage leads to a signal increase down to 0.5ML. This gives supporting evidence for a phase transition which increases the electronic coupling. For details see text.

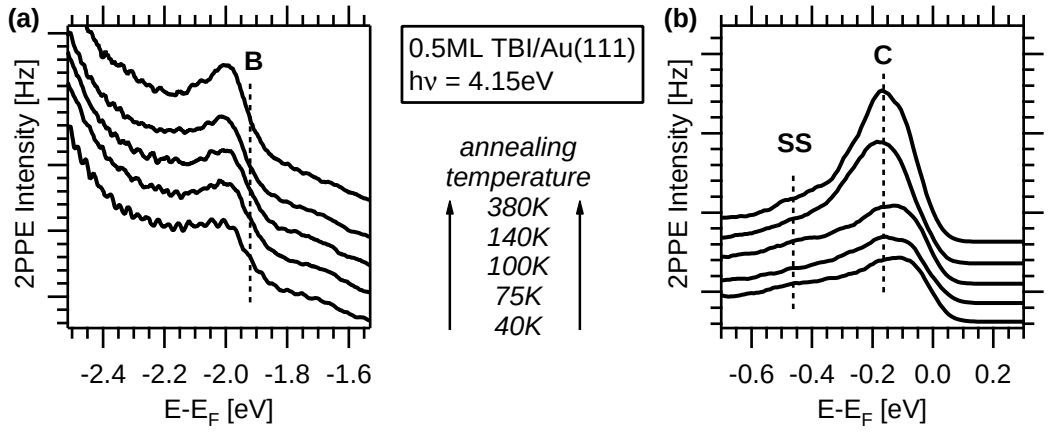

Figure 6.8: Peak intensities of the TBI induced states B (a) and C (b) as a function of sample annealing. TBI has been adsorbed at substrate temperatures of 40K. Subsequent heating leads to a phase transition which increases the electronic coupling leading to an increased signal.

have been kindly supplied by the group of Peter Saalfrank, University Potsdam. A graphical depiction of selected results is given in appendix B. In case of the HOMO-1 the electron density is largest at the phenyl ring attached to the nitrogen atom. Hence the orbital distribution is highly asymmetric and one can explain the increasing photoemission signal with its reorientation (phase transition) in respect to the surface plane. In contrast, the HOMO is delocalized almost symmetrically across the whole molecule. Therefore any reordering effects should have only little impact on its 2PPE signal. This can nicely be witnessed in graph 6.7(b).

We previously proposed that the phase transition of the TBI/Au(111) is thermally activated but partially suppressed for large amounts of adsorbed molecules. Thus, based on the above results, one should also observe a change in the intensity resulting from gradually heating a low coverage sample. To elucidate such annealing effects we performed a series of measurements on 0.5ML TBI/Au(111) which has been prepared at $= 40K$. The spectra taken at $h\nu = 4.15eV$ are depicted in figure 6.8(a). They show a rising signal intensity of the HOMO peak as a function of the increasing annealing temperature.

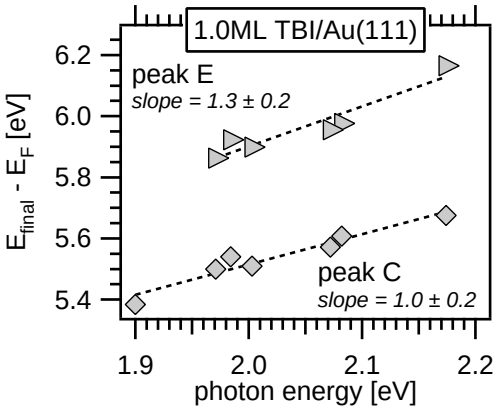

Figure 6.9: Photon energy dependencies of the TBI/Au(111) intermediate states as function of the probing wavelength.

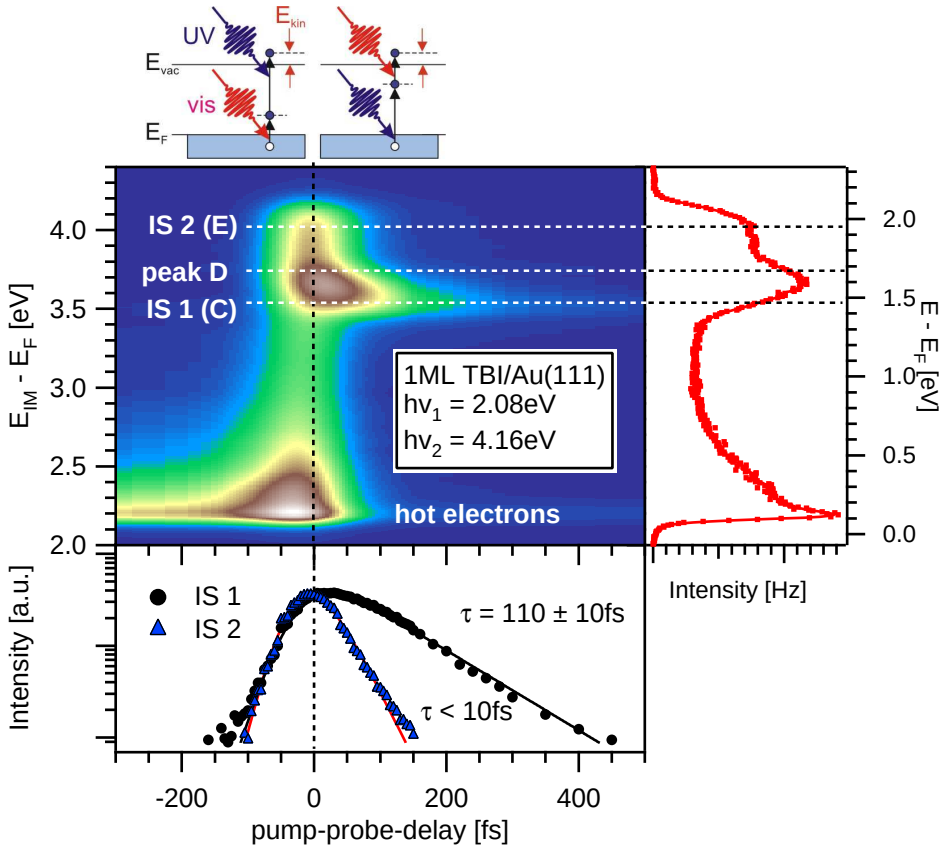

Figure 6.10: Time resolved 2PPE measurement on a monolayer TBI coverage. The three major contributions to the spectra, A,B and C originate from the hot electrons, the lower and the higher lying intermediate states respectively. A 1D cut along the zero delay axis shown on the right side. To evaluate the lifetimes the temporal evolution of the peak intensities is retrieved by a constant energy mapping at the corresponding binding energies.

The same dependence is observed for peak C which appears in this spectra close to the Fermi edge. Thus heating of sample indeed leads to a stronger coupling as proposed by our picture of a thermally induced phase transition. Note, due to the smaller magnitude of the illumination induced changes their impact could not be distinguished within the spectra. This however does not rule out their existence.

Returning to the sample spectra in figure 6.5 three more states, C-E, can clearly be seen in the 2-color 2PPE spectra. From their respective photon energy dependencies all of them can be identified as unoccupied intermediate states (see fig. 6.9). Peak C is found at an energetic position of $E_B = 3.55 \pm 0.05eV$ in respect to the Fermi level. This is supported by time resolved measurements on a monolayer sample using photons of $h\nu_1 = 2.08eV$ and $h\nu_2 = 4.16eV$. The resulting 2-dimensional false color plot is presented in figure 6.10 and shows an obvious lifetime for the UV pumped feature C. At large positive delays ($\Delta T = 200fs$) it is the only remaining

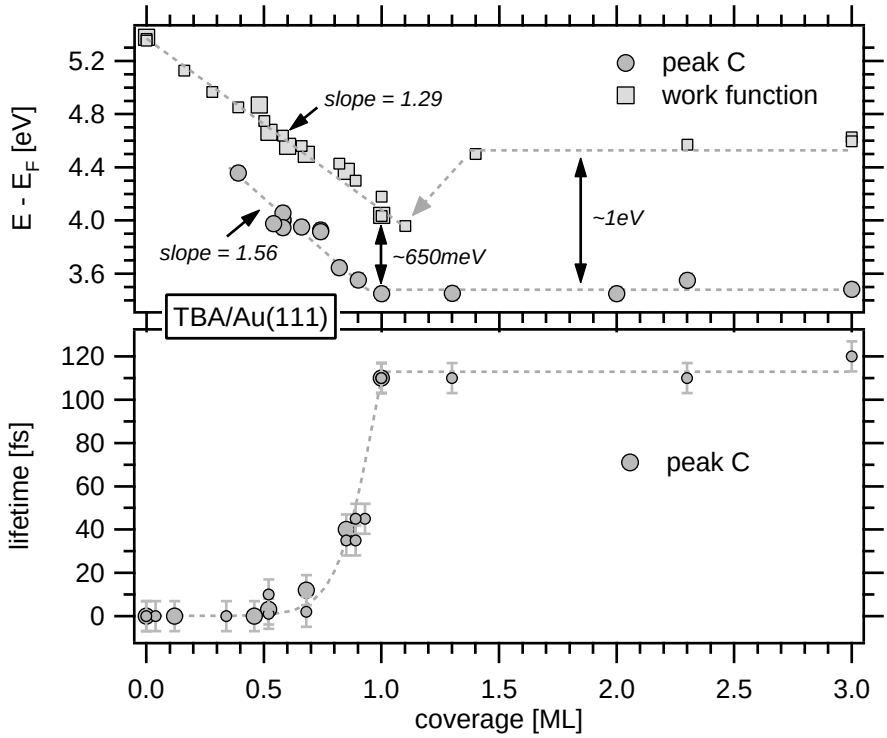

Figure 6.11: Lifetime (bottom) and energetic position (top) E_B of the first intermediate state (peak C) as a function of the coverage. Note that for submonolayer coverages peak C appears to pin to the work function (plotted in the top graph). At the transition to the multilayer regime however it remains constant whereas Φ experiences a sudden increase of 350meV.

feature in the spectra. Therefore its binding energy can be evaluated without the influence of neighboring peaks.

An analysis of the temporal evolution taken along the constant energy axis of peak C yields a decay of $\tau = 110 \pm 10 fs$. As we have mentioned before the electronic structure is sensitive to the TBI coverage. In case of the occupied features A and B the desorption of the first half monolayer lead to an increase in the signal intensity. Peak C in addition experiences a shift in binding energy which is accompanied by a reduction of its lifetime. Both quantities are plotted versus the coverage in figure 6.11. From 0.5ML to 1ML we witness an approximately linear relationship between the amount of adsorbed molecules and the energetic position of peak C with a slope of $\Delta E = 1.5 eV/\text{ML}$. At coverages below 0.5ML peak it is masked by the rising signal of the gold surface state. Time resolved 2PPE spectra from corresponding samples indicate no decaying states. Therefore we have no possibility to determine the binding energy of peak C in the range of 0 to 0.5ML. However, assuming that the slope of the shift does not increase, we can predict that its lifetime remains below the resolution limit of 10fs.

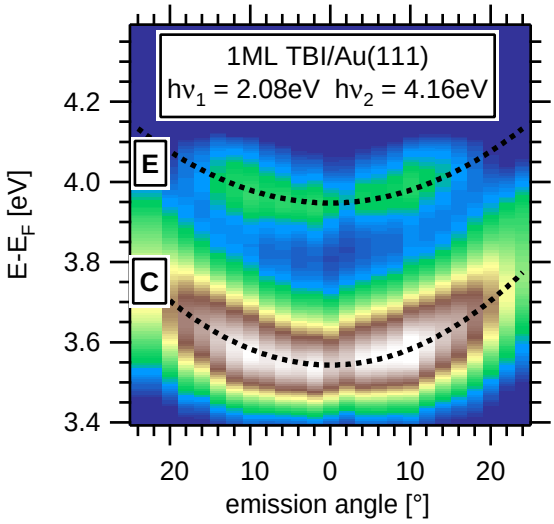

Figure 6.12: The dispersion of the UV pumped intermediate states C and E recorded in a 2-color 2PPE setup. A parabolic fit yields effective masses of $m_{eff} = 1.33 \pm 0.05 m_e$ and $m_{eff} = 1.6 \pm 0.1 m_e$, respectively. *Experimental note: The spectra have been recorded twice, turning the sample to positive angles and on the way back. The two series are depicted to the left and to the right of the normal emission angle!!!*

The relationship between the lifetime of the state and its energetic position in figure 6.11 can be brought into good agreement with the theory of electronic relaxation from adsorbate states. The major channel of this relaxation is the inelastic scattering of electrons into lower lying bulk bands [Chu06][Ech04]. One of the key parameters determining the decay rate is the available phase space. The energetic position of the molecular state shifts from the band gap region of the gold substrate into the conduction band region starting at $E_{CBM} = 3.6eV$ [Woo86]. Hence at the multilayer binding energy of $E_B = 3.55eV$ there is little overlap with the gold bands leading to a substantially long lifetime. It decreases rapidly as peak C shifts to energies above the conduction band minimum where the phase space for the scattering is significantly enlarged.

Comparing the decay behavior of the TBI induced peak C with the TBA/Au(111) experiments we find a striking similarity with the therein found trans and cis interface states. At energetic positions of $E_B = 4.05eV$ (trans) and $E_B = 3.73eV$ (cis) they exploit lifetimes of $\tau < 10fs$ and $\tau = 20fs$. This suggest not only that these states appear in the same binding energy region but also that their coupling to the substrate is of comparable magnitude. Hence the question is raised whether the TBI induced molecular state C is an interface state as well.

Before discussing this matter we shall introduce the second intermediate state, peak E, which exploits similar properties. Peak E, as seen in figure 6.5, is found at $E_B = 3.95 \pm 0.05eV$ having a lifetime of $\tau = 20 \pm 10fs$ (see fig. 6.10). Within the region of 0.8ML to 1ML its binding energy shifts according to the slope found for state C ($1.5eV/ML$). At lower coverages peak E also suffers from the competing contributions of the uprising gold surface states SS and SSx.

To investigate the origin of the peaks C and E we performed an angle resolved measurement on a monolayer TBI/Au(111). The resulting 2-color spectra using $h\nu_1 = 2.08eV$ and $h\nu_2 = 4.16eV$ are plotted in a 2-dimensional graph in figure 6.12. The brighter feature at the bottom corresponds to peak C having an effective mass of

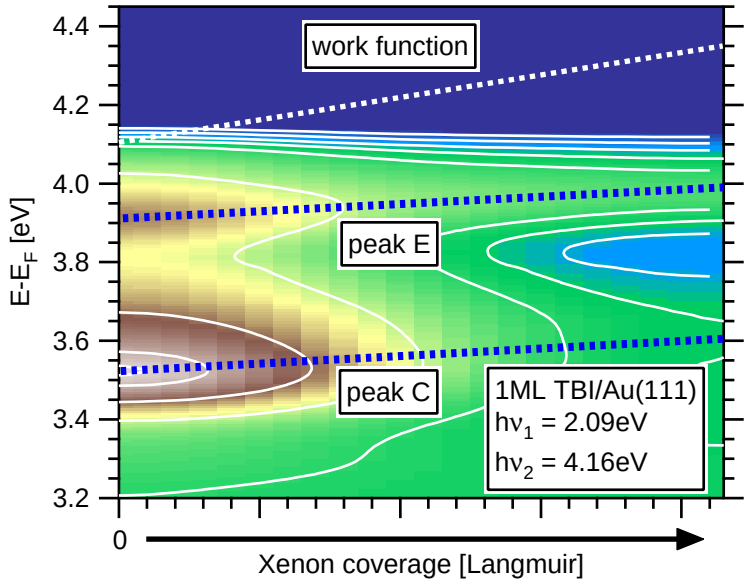

Figure 6.13: 2PPE spectra of a xenon co-adsorption experiment depicted in a 2-dimensional false color plot. The blue dashed lines indicate the maxima and thus the binding energies of peaks C and E (plotted with respect to E_F). They shift to higher values as more Xe is adsorbed. Likewise the work function of the sample (white dashed line) increases with the coverage. We attribute those changes to the interaction between the TBI and the xenon molecules. For details see text.

$m_{eff} = 1.33 \pm 0.05 m_e$. For peak E in the upper region we retrieve $m_{eff} = 1.6 \pm 0.1 m_e$. Thus both peaks are fairly delocalized with effective masses close to the free electron mass m_e. This cannot be expected in case of a strictly molecular state which at this point can be ruled out.

A second option which is rather unlikely is the formation of molecular bands as e.g. shown for C_6F_6 on Cu(111) [Zhu02][Gah00]. Here a binding energy shift would be expected going from a monolayer to the multilayer regime. Furthermore the occurrence of the signal even at low coverages (0.5ML) and the observed phase transition behavior contradict such an assignment. This reduces the possible options to either an image potential or the afore mentioned interface states.

In a last experiment to determine the origin of peaks C and E we co-adsorbed xenon onto a monolayer TBI. The Xe coverage was continuously increased via a background dosing at $p_{Xe} = 1 \cdot 10^{-8} mbar$ and the changes monitored in a 2-color 2PPE setup with $h\nu_1 = 2.09eV$ and $h\nu_2 = 4.16eV$. Figure 6.13 displays the resulting shifts of the binding energy in a false color 2D-plot. On the left edge we start with the pure TBI/Au(111) sample. The binding energy of both peaks shifts to higher values and their intensities decrease as the xenon coverage increases. A comparison with the work function, depicted in the top graph, shows that C and E are neither pinned to the vacuum level nor to the Fermi level of the sample.

Although the above evidence seems ambiguous we prefer the assignment to an interface state for the following reasons: (i) The coverage dependence clearly shows that in case of a TBI multilayer an increasing film thickness affects neither the lifetime nor the energetic position of the peaks. This is very unlikely for states located at the vacuum interface [Hot07]. The situation is different for the submonolayer regime. In this case , as can be seen in figure 6.11, the peak positions shift with a slope almost identical to the work function. An explanation for this scenario is given by the witnessed phase transition and the respective reorientation of the molecules. (ii) In the multilayer regime the gap between state C and the vacuum level is approximately 1eV. According to the well established model of image potential states this value exceeds the theoretical limit of 0.85eV for the separation [Hot07]. It is, on the other hand, a reasonable value for an interface state. (iii) The shift of E_B and the work function Φ caused by the xenon co-adsorption can be explained by the interaction of the rare gas with the TBI molecules. In principle Φ is determined by the first adsorbate layer and thus adding atoms of neutral charge should have no effect on its value. This has e.g. been the case for the xenon co-adsorption on TBA/Au(111) (see section 4.3). Therefore we propose a scenario where the small rare gas atoms sit in between the large TBI molecules altering their interaction and consequently influence the potential at the substrate/adsorbate interface.

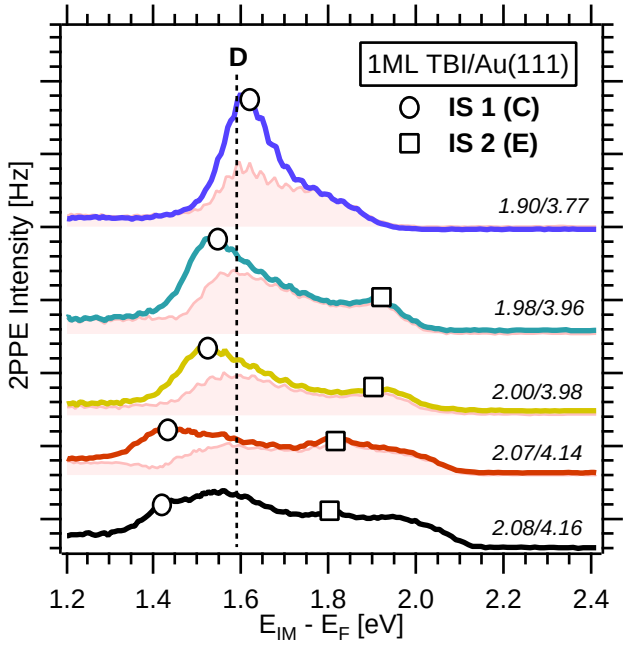

Figure 6.14: Photon energy dependence of the peak D plotted versus the intermediate state energy for pumping by visible light. For better identification the positions of the interface states are marked with circles and squares. Subtracting the contributions of IS 1 yields the shaded spectra allowing a better resolution of peak D. For details see text.

In the last part of this section we want to discuss peak D which has initially been observed in graph 6.5. A series of 2-color 2PPE spectra taken at different photon energies is displayed in figure 6.14. All spectra show a broad feature consisting of several peaks close to the Fermi cutoff edge. To mark the position of the visible light pumped peak D they are plotted versus the corresponding intermediate state energy. D is clearly distinguishable only for the combination of $h\nu_1 = 2.08eV$ and $h\nu_2 = 4.16eV$. At lower photon energies it merges into the peak of the interface state IS 1 whose energetic position is indicated by the white circles. The width and intensity of IS 1 can be estimated fairly well from the analysis of time resolved measurements. Therefore we are able to subtract its contributions from the spectra. The resulting traces are indicated by the shaded areas in the graph. They indeed corroborate the existence of a third unoccupied intermediate state at $E_B = 1.6 \pm 0.1eV$. Following the arguments of TBA/Au(111) (see section 4.3) we assign peak D to the LUMO of the TBI molecule.

6.1.3 *Conclusions*

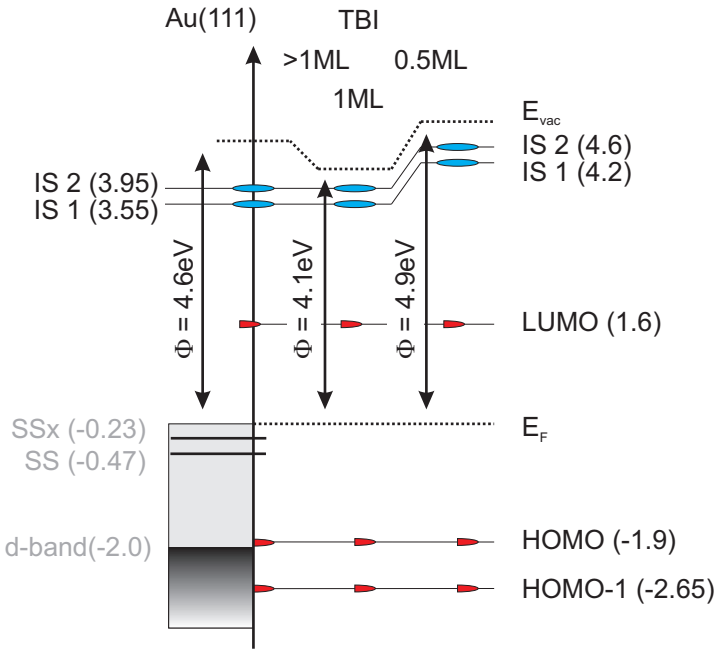

Figure 6.15: Energy diagram of TBI/Au(111) states from different coverages found in direct photoemission and 2PPE. Molecular states are shown in red, states arising from interface potentials in blue. Binding energies are given in eV with respect to the Fermi level.

In summary we have investigated the adsorption and the electronic structure of TBI on Au(111) with thermal desorption spectroscopy and 2-photon photoemission. Combining the results of these two techniques we were able to draw a self-consistent picture of its very complex behavior which is characterized by a competition between intermolecular and molecule/substrate interactions. At low temperatures TBI adsorbs in an unordered phase which can be converted into an ordered phase via thermal activation. A partial transition has even been induced by illumination with photon energies in the visible and UV range. For thin films (<0.5ML) the arrange-

ment of the molecules is dominated by the interaction with the surface. For higher coverages on the other hand the intermolecular forces gain influence which is observed in terms of an attenuated phase transition. This behavior is most obvious at the border between the mono and the multilayer regime. Here the desorption of only few molecules leads to a tremendous reorientation of the molecules as is witnessed by a work function change of >0.5eV.

The phase transition of the TBI/Au(111) is also affecting the electronic structure. A schematic depiction for three different coverages, >1ML, 1ML and 0.5ML, is given in figure 6.15. Two distinct effects can be observed: The first is a change of the electronic coupling which is directly linked to the phase transition and thus a respective reorientation of the TBI. This has been demonstrated based on the photoemission signal from the occupied molecular states. The second effect is a shift in the binding energy of the molecule induced interface states IS 1 and IS 2. In the monolayer regime it almost linearly increases with decreasing coverage. For the multilayer however the energetic position becomes independent of the molecular film thickness. Again this behavior supports a modification of the molecular geometry in respect to the gold surface.

A special role is given to the first interface state IS 1. Due to its coverage dependent shift in binding energy it can be tuned from a position within the projected band gap to a position which allows to tune the wave function mixing with the unoccupied sp-bands. This can be directly monitored based on the lifetime of the respective excited electrons.

6.2 Adsorption behavior and electronic structure of TBS/Au(111)

The third investigated molecule known for its cis-trans isomerization is tetra-*tert*-butyl-stilbene . Its corresponding HC=CH functional group displays a symmetric character with an almost planar ground state configuration and a vanishing dipole moment. Consequently it exhibits an adsorption behavior which is closely related to the results of TBA/Au(111). On the other hand thermal desorption experiments indicate a stronger interaction with the substrate. This is supported by the analysis of the electronic structure. It exploits the previously observed occupied molecular states but lacks evidence for an unoccupied state. Again we find no signature of a photoinduced isomerization.

6.2.1 Absorption of TBS on Au(111)

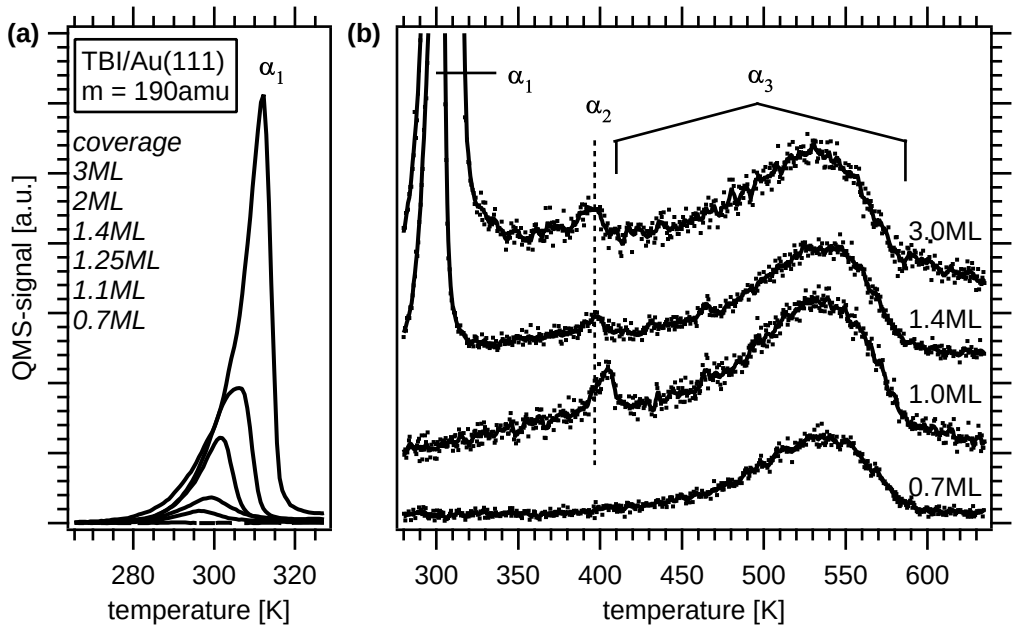

Figure 6.16: Thermal desorption spectra of TBS/Au(111) for different coverages. **(a):** Evolution of the α_1-multilayer peaks in dependence of the amount of adsorbed molecules. **(b):** The monolayer regime with the compressed α_2 and the relaxed α_3-phase.

As for the previously investigated systems we will use thermal desorption spectroscopy (TDS) to evaluate the adsorption behavior of the TBS. Figure 6.16 depicts the results for different initial coverages prepared at a sample temperature of 260K. The multilayer peak α_1 is found to start around 280K. It shows the usual zero order desorption kinetics with the spectra having equal slopes and maxims shifting to higher temperatures with increasing coverage. The desorption behavior of TBS is

independent of the initial sample temperature during the dosing procedure. Thus there is no evidence for a multilayer phase transition as has been observed in the case of TBI/Au(111). The shape of the monolayer spectra is similar to the one obtained for TBA on Au(111) and Ag(111) (see figures 4.1 and 6.1, respectively). Consequently we assign the two phases α_2 and α_3 to a compressed and a relaxed phase respectively. The α_2 phase peaks at $T = 395K$ whereas the α_3 phase shows a comparably high binding energy with a maximum at 540K. Analyzing the area of the traces we conclude that the relaxed phase is present up to a monolayer coverage of 90%.

For TBS/Au(111) the overall width of the TDS spectra is the largest of all three investigated molecules extending to almost $T = 600K$. This increase in the binding strength from TBA to TBI to TBS can be directly correlated to the exchange of the functional group. Apparently the attractive interaction towards the substrate increases going from N=N to N=CH to HC=CH.

6.2.2 The electronic structure of TBS/Au(111)

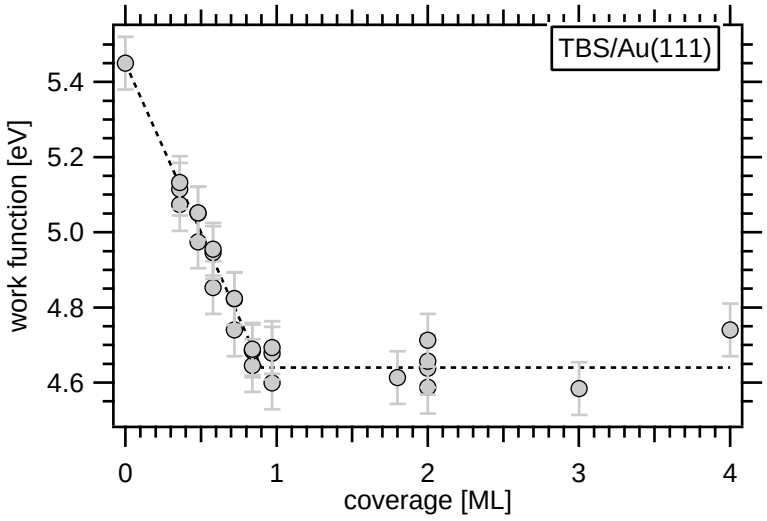

Figure 6.17: Work function of TBS/Au(111) as a function of coverage.

Like the previously used molecules TBS initiates a work function shift of almost 1eV. Figure 6.17 shows a detailed mapping of the coverage dependent values. The work function starts at $\Phi = 5.4 \pm 0.05eV$ on the bare surface and is continuously decreased to $\Phi = 4.65 \pm 0.05eV$ which is reached at the full monolayer. This value is not changed upon further adsorption. In the thermal desorption spectra evidence was given that the system is not obliged to a thermally induced phase transition. Work function measurements on a sample prepared at $T = 40K$ support this result as they show a invariance towards heating and annealing procedures.

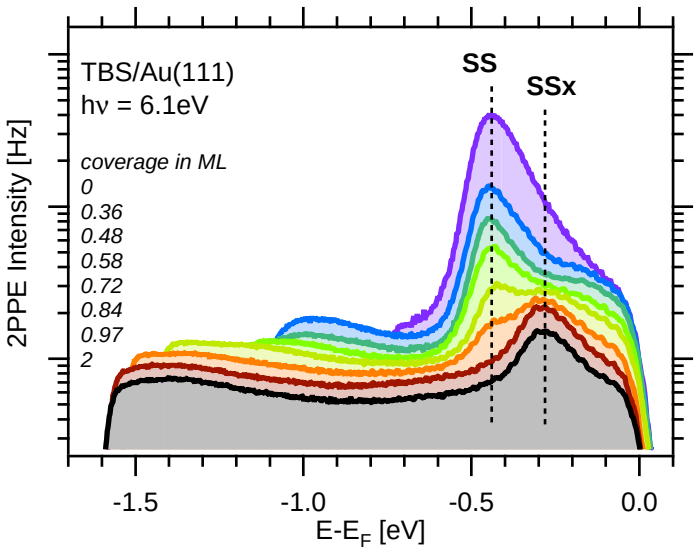

Figure 6.18: Coverage dependent direct photoemission spectra of the TBA/Ag(111) sample at $h\nu = 6.1eV$. To obtain different coverages a monolayer sample was prepared and subsequently annealed at increasing temperatures. All measurements were taken at $T = 40K$.

The 6eV spectra of the TBS/Au(111)taken in a direct photoemission experiment are presented in figure 6.18. They show the evolution of the gold gold surface state (SS) and the gold surface feature (SSx) as a function of the TBS coverage. Both have been witnessed in the TBA/Au(111) and TBI/Au(111) spectra as well and their assignment is motivated in the corresponding sections 4.3 and 6.1.2. Here again the quenching of the surface state progresses with an increasing amount of molecules until it is completely suppressed in the monolayer regime. The surface feature (SSx) on the other hand shows no substantial change in is initial intensity, even upon absorption of a second layer. Due to the minimum work function of $\Phi = 4.6eV$ the spectral width is limited to 1.5eV. Within this region we observe no further states.

Spectra from a 2PPE measurement on a monolayer TBS/Au(111) are depicted in figure 6.19. In the monochromatic spectrum recorded at $h\nu = 4.57eV$ we find two strong peaks, A and B, on top of the gold d-band structure. Additional peaks are found in the energy region up to 2eV below the Fermi cutoff edge. These features become more obvious in the 2-color 2PPE spectrum which is appended to the figure. In this trace we find four more features, C, D, SSx and SPB. All these peaks can be identified in the monochromatic spectrum as well, thus we can exclude a correlation to intermediate states pumped by visible light.

For the proper assignment of the electronic states we monitor the shift of the peak kinetic energy as a function of the photon energy. The corresponding slope indicates the actual energetic position of the respective state (figure 6.20(b)). In addition coverage dependent experiments were performed to elucidate the gold or molecular origin of the states. To change the amount of adsorbed molecules we

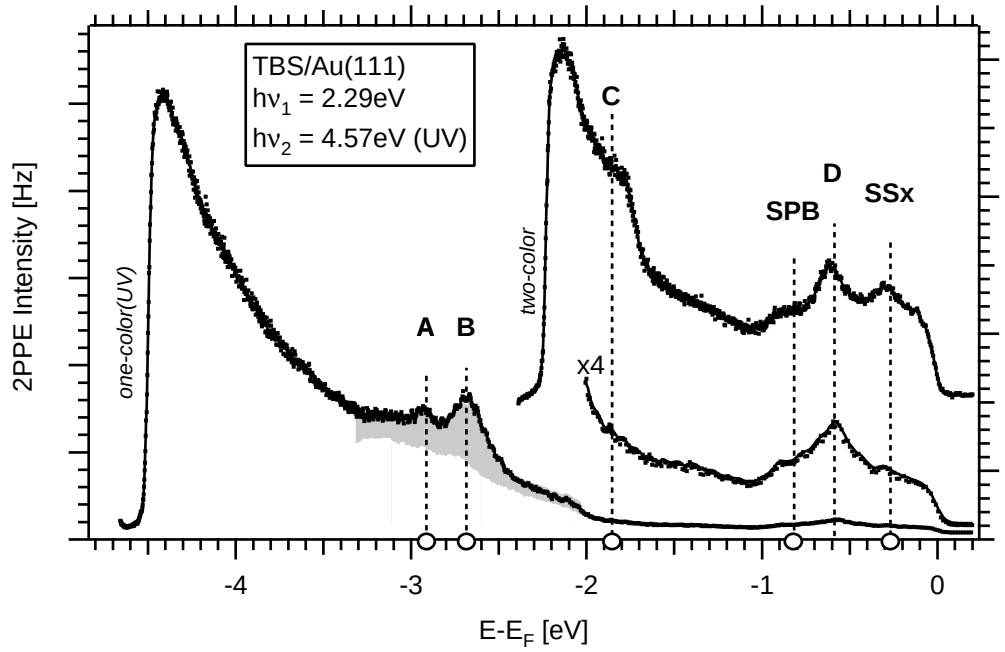

Figure 6.19: 2PPE spectra of 1ML TBS/Au(111) using $h\nu_1 = 2.29eV$ and $h\nu_2 = 4.57eV$. The one-color (UV) spectra exploits two molecular states A and B at the top of the d-band. Deviations from the signal of the clean Au(111) surface in the region of those states are marked by the gray shaded area. Further molecular (C and D) and substrate (SPB and SSx) states are found close to the Fermi cutoff edge which are better resolved in the corresponding 2-color spectra. Due to their simultaneous appearance in both spectra we can exclude their origin from visible($h\nu_1$) pumped intermediate states. For peak assignment see text.

prepare a multilayer sample and heat it stepwise at increasing temperatures. Figure 6.20(a) displays the spectra of such a desorption series in the energy range of the peaks A and B. All traces have been obtained from a monochromatic measurement at $h\nu = 4.43eV$. The maximum intensity for both peaks is observed at a monolayer. It drops as the coverage is reduced towards the bare gold surface. Thus we assign both peaks to molecular states. The photon energy dependence of peaks A and B is depicted in graph 6.20(b). According to the respective slopes of $m = 1.9 \pm 0.2$ and $m = 2.0 \pm 0.2$ both peaks are occupied initial states. From the data we obtain binding energies of $E_B = -2.87 \pm 0.05eV$ for state A and $E_B = -2.65 \pm 0.05eV$ for state B with respect to the Fermi level.

A third molecular state is found in the C labeled peak. The signal of this state is rather weak in the monochromatic spectra. However it does clearly appear in the 2-color spectra as well (see fig. 6.19). For this reason we extended the photon energy dependence to include those spectra as follows: In the usual case the change in kinetic energy ΔE_{kin} is plotted versus the probing photon energy. Combining one- and two color 2PPE experiments we have to consider the total energy, pump

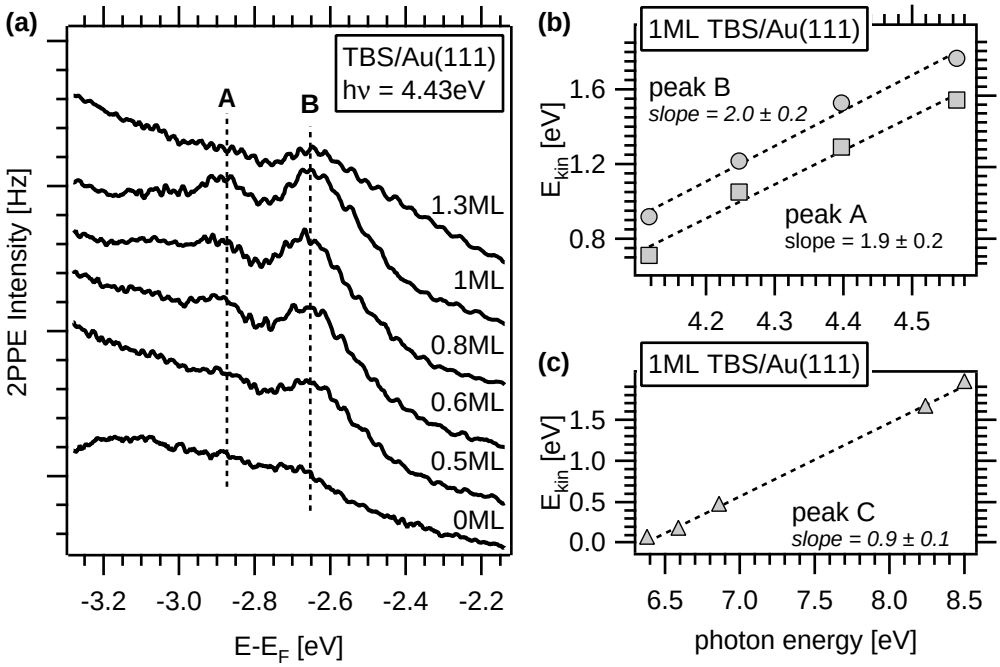

Figure 6.20: One-color 2PPE spectra of states A and B. **(a):** Coverage dependence of both peaks taken at $h\nu = 4.43eV$. **(b):** Photon energy dependence of the peaks A and B revealing an initial state character. **(c):** Photon energy dependence of the peak C plotted versus the joint pump and probe photon energy. See text for details.

and probe, transferred to the electron[14]. The results of this procedure are depicted in graph 6.20(c). The slope of $m = 0.9 \pm 0.1$ associates peak C to an occupied initial state at $E_B = -1.9 \pm 0.1eV$ in respect to the Fermi level. Since there are no further occupied molecular states we assign the peaks C, B and A to the HOMO, HOMO-1 and HOMO-2 of the TBS/Au(111) respectively.

For the discussion of states SPB, D and SSx a 2-color 2PPE coverage series taken at $h\nu = 2.23eV$ and $h\nu = 4.43eV$ and depicted together with the photon energy dependencies in figure 6.21. The 2PPE spectra in graph 6.21(a) are shown in the region of interest close to the Fermi cutoff edge. For peak SPB no change in intensity is observed as the TBS coverage decreases. Thus it is a part of the gold band structure and we assign this peak to the sp-band. Due to its strong dispersion along the ΓL-direction of the Brillouin zone the initial state energy of the state shifts with the UV photon energy as seen in graph (c) of figure 6.21. Therefore the corresponding slope of $m = 0.99 \pm 0.03$ shall not be mistaken as evidence for an intermediate state. This extraordinary behavior has been observed for TBI and TBA on Au(111) as well and is also known from the equally dispersing sp-band of Ag(111) [Pon05].

[14] $\Delta E_{kin} = \Delta 2h\nu_{UV}$ for one-color, $\Delta E_{kin} = \Delta(h\nu_{UV} + h\nu_{vis})$ for two-color spectra

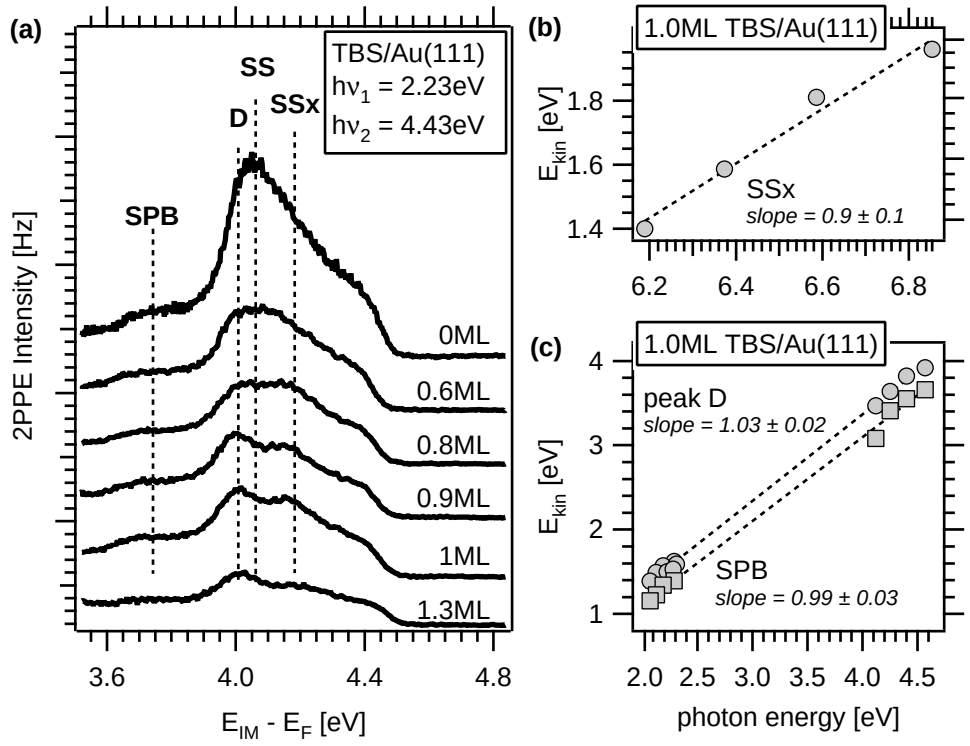

Figure 6.21: Two-color 2PPE spectra of the gold and molecular states close to the Fermi cutoff edge. **(a):** Coverage dependence of the peaks taken at $h\nu_1 = 2.23eV$ and $h\nu_2 = 4.43eV$. In the submonolayer regime the previously quenched gold surface state (SS) reappears in the spectra. **(b):** Photon energy dependence of the peak SSx plotted versus the joint pump and probe photon energy. See text for details. **(c):** Photon energy dependence of the peaks D and SPB plotted versus the probe photon energy.

The evolution of the features D and SSx as function of coverage is partially masked by the rise of a new peak labeled SS. Based on its binding energy and the appearance upon desorption it can be convincingly assigned to the Au(111) surface state. Neglecting the SS contributions to the spectra the intensity of peak D decreases together with the coverage. Peak SSx on the other hand appears to maintain its monolayer height. A photon energy dependence of SSx yields a slope of $m = 0.9 \pm 0.1$ thus it is an initial state from the Au(111) with a binding energy of $E_B = -0.27 \pm 0.05eV$. We already identified this state in the direct photoemission as a gold surface state split off which is shifted in the presence of an adsorbate (see section 6.1.2 and [For03]).

As can be seen from graph 6.21(c) the kinetic energy of the obviously molecule induced state D shifts with a slope of $m = 1.03 \pm 0.02$. This implies an UV light pumped intermediate state which is in agreement with its above mentioned simultaneous appearance in the one-color (UV) spectra. The energetic position at $E_B = 4.0 \pm 0.1eV$

is in a region where the previously studied systems TBA/Au(111) and TBI/Au(111) revealed metal/molecule interface states. Additional possible origins one has to consider are molecular states or image potential states. The latter can be ruled out based on the coverage invariance of the binding energy. Also an energetic difference of 950meV to the vacuum level at 0.6ML TBA/Au(111) clearly contradicts such an assignment as it again exceeds the theoretical limit of 850meV [Hot07].

To further clarify the origin a angle resolve measurement is performed. The results for a monolayer coverage are shown in figure 6.22, yielding an effective mass of $m_{eff} = 3.4 \pm 0.4 m_e$. This value is a roughly a factor of 3 larger than for interface states observed at TBA and TBI samples and suggest an increased localization of the state D in the plane parallel to the surface. This has previously been observed for case of molecular bands in C_6F_6/Cu(111) [Zhu02] [Gah00]. However in those studies a coverage dependent shift of the binding energy is reported. It is attributed to a band formation within the molecular bulk rather than at the interface to the metal substrate. Since the coverage independence of the peak C binding energy contradicts such a molecular origin we instead assign it to an interface state. An alternative scenario for the strong local confinement could be the corrugation of the interface potential which limits the excited electrons range of motion. This may be attributed e.g. to a bending of the functional group towards the surface which would reflect upon the high binding energy observed in the TDS spectra.

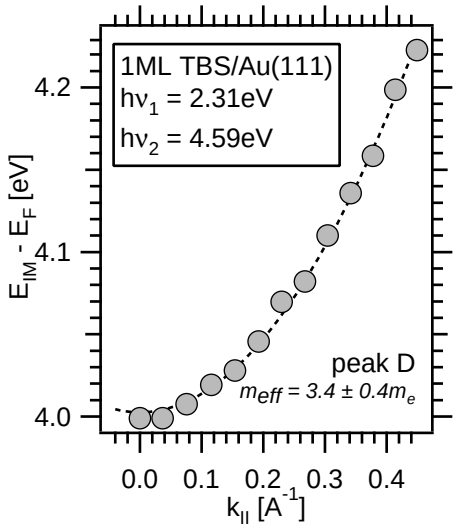

Figure 6.22: Dispersion of the TBS/Au(111) interface state at $E_B = 4.0eV$

In a final step we want to analyze the lifetime of the interface state D. A 2-dimensional false color plot of a time resolved 2PPE spectra is presented in figure 6.23. Here we used photon energies of $h\nu = 2.29eV$ and $h\nu = 4.57eV$ to observe the decay of the intermediate state on a monolayer TBS/Au(111). Cutting the spectra along the zero delay line yields a spectrum identical to the initially presented 2-color 2PPE spectra (see figure 6.19). To obtain the decay times of the different states we cut the spectra at their respective binding energies. As generally expected for occupied states, the SSx and SPB features display a symmetric shape with an infinitesimal short lifetime. The interface state in contrast shows a decay of $\tau = 15 \pm 8fs$ which agrees nicely with the values obtained from TBA/AU(111) and TBI/Au(111) (see section 4.3 and 6.1.2). At the low energy end of the spectra we see the slowly relaxing tail of the hot electron distribution.

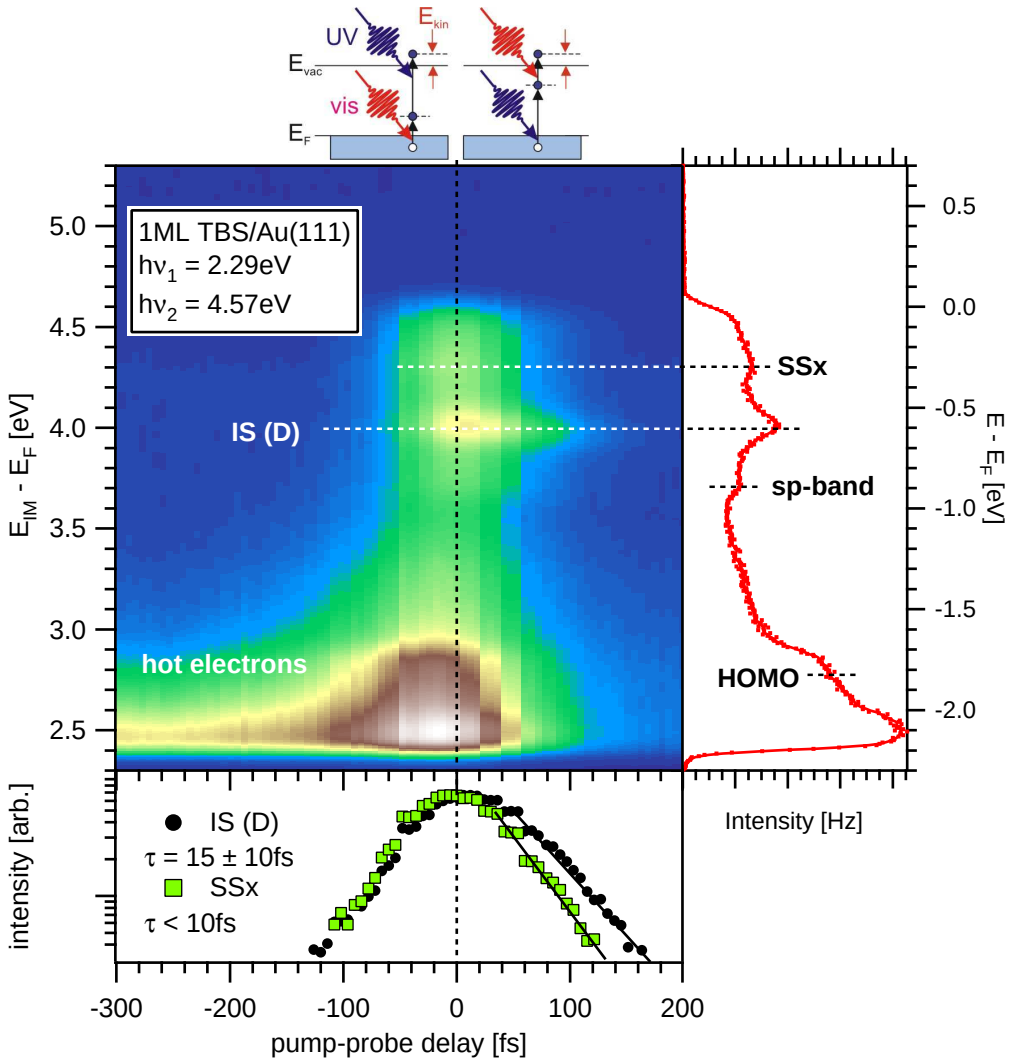

Figure 6.23: Time-resolved 2PPE data of 1ML TBS/Au(111) presented in a 2D false color plot. The laser sequences are depicted in the top sketch. For negative times probing occurs via the visible and probing via UV light, for positive times the order is vice versa. The lifetime of the surface state split off (SSx) is below the experimental resolution. The interface state (IS) on other hand exhibits a short lifetime of 15fs. At the bottom of the 2D-plot the strong background signal of the slowly decaying hot electron population is visible.

Figure 6.24 summarizes the electronic structure of the TBS/Au(111) system which we analyzed with direct photoemission and 2PPE. Next to the well known gold substrate contributions we find 3 occupied and one unoccupied state induced by the molecular presence. The former are assigned to the three highest lying occupied molecular orbitals (HOMO, HOMO-1 and HOMO-2) whereas the latter is an interface state resulting from the potential at the metal/molecule junction. In contrast to the TBA and TBI molecules we cannot identify a second of these interface states.

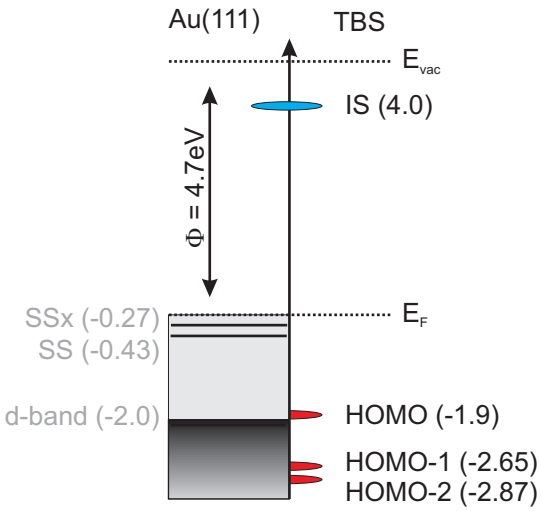

Figure 6.24: Energy diagram of the TBS/Au(111) states found in direct photoemission and 2PPE. Molecular states are shown in red, states arising from interface potentials in blue. Binding energies are given in eV with respect to the Fermi level.

Neither do we observe a signal which can be related to an unoccupied molecular orbital (LUMO). A possible explanation for the missing LUMO is a weak coupling to the substrate. This has been seen in TBA and TBI experiments where the main population channel in case of non-resonant excitation is through scattering of hot electrons. Correspondingly the intensity of their respective LUMOs peaks has been very weak. It can be assumed that in case of a further decoupling a signal is likely to be suppressed. A similar argumentation is given by Lindstrom et al. discussing differences between inverse photoemission and 2PPE experiments [Lin07].

6.3 Substrate quenched photoisomerization

6.3.1 TBI/Au(111) isomerization experiments

To elucidate the possibilities of a trans-cis isomerization we investigate optically induced changes in the previously introduced electronic structure of TBI/Au(111). In contrast to the TBA/Au(111) the choice of well defined system is complicated by the fact that TBI exploits different phases which are coverage dependent. In order to reduce the intermolecular interactions the investigations would have to be restrained to the α_4-phase found for coverages <0.6ML. On the other hand it cannot be a priori excluded that the α_3-phase is more favorable for a photoisomerization. It obviously exhibits a completely different coupling to the substrate, a property which has proven to play an important role in the underlying excitation mechanism. Therefore we investigated two sets of samples, one having a monolayer coverage with a mixture of both phases and the second having a 0.5ML coverage with only the relaxed α_4-phase. Prior to the measurements these were annealed at 260K to ensure that no phase transition is superimposed on the photoemission signal.

All illumination experiments were performed at a substrate temperature of 40K in order to suppress the magnitude of a possible thermally induced reverse reaction. We employed photon energies between 1.8 to 4.7eV and at 6eV to stimulate optical transitions. Within this range no photoinduced changes of the electronic structure could be observed. This can be attributed to either a suppression of photoisomerization or a signal change below our energetic resolution. The latter has to be considered since the ground state molecule already exhibits a strong dipole moment. If this is not significantly changed, as in the case of TBA/Au(111), a detection based on a work function shift may be impossible. On the other hand a molecular switch requires two distinguishable states. It can well be assumed that in this case also the electronic structure is distinguishable. Thus it appears more likely that indeed the photoisomerization is quenched.

Several possible reasons can be given for the absence of a switching: (i) As presumed for the intramolecular excitation mechanism of TBA/Au(111) the coupling to the substrate could be too strong to allow sufficiently long lifetimes for an isomerization. (ii) The ground state energy barrier separating the cis and trans isomer of the free imine is significantly lower as for azobenzene. In good approximation the influence of the tert-butyl ligands can be neglected. However the barrier can be lowered upon adsorption (see section 4.6.1). This could lead to a vanishing or at least very small barrier in the case of TBI/Au(111). Consequently the system cannot fulfill the requirement of two stable states. (iii) Steric hinderance creates an energy barrier which cannot be overcome by the pathways created upon optical excitation.

The absence of an intramolecular channel is not surprising as this has been witnessed for TBA/Au(111) before. On the other hand the electronic structure of TBI/Au(111) clearly shows an overlap between the gold d-bands and the highest occupied molecular orbital (HOMO) of the TBI. Thus in principle this should enable a charge transfer of a hole which creates a positive ion resonance. Again we can

present different explanations why this channel appears inactive for TBI/Au(111): (iv) There is a mismatch in the electronic coupling, viz. it is either too strong: a rapid back transfer suppresses the isomerization, or too weak: the probability of the excitation is not high enough. (v) In agreement with (ii), there are no clearly distinguishable states. (vi) The excited state potential energy surface inherits an energy barrier which cannot be overcome, e.g. a sterically hindered motion.

Based on the experimental evidence it is not possible to determine which of the given explanations is the most likely. Here clearly additional information is needed. At this point we shall return to the initially observed light and temperature induced changes which we assigned to a phase transition. Clearly this transition can be assumed to affect the geometry and the electronic structure of the molecule to some extend. Nevertheless there are two reasons why we do not consider this as an isomerization: First, the electronic structure changes gradually in terms of the work function and the energetic position of the interface states. Thus we are able to observe intermediate steps of this conversion. In case of an isomerization we would rather expect two different signals of a changing intensity ratio then a simple shifting of the peak. Second, the change, using the available excitation sources (laser light, temperature), is not reversible. Hence there is no evidence that the molecule actually changed its conformation in terms of crossing the ground state energy barrier between the cis and the trans isomer.

6.3.2 TBS/Au(111) isomerization experiments

To elucidate the possibilities of a trans-cis isomerization we investigate optically induced changes in the previously introduced electronic structures of TBS/Au(111). For an elaborate analysis it is preferable to perform the measurements on a well defined system. In case of TBS the choice can be made in agreement with the TBA/Au(111) experiments using a 0.9ML coverage. This ensures that the results are not influenced by the contributions of the compressed α_2-phase. In addition the molecular electronic states showed no coverage dependence of their binding energy suggesting a stable molecule-substrate interaction dominating over intermolecular forces.

The investigation of a possible isomerization in the photon energy range of 1.8 to 6eV yields the same negative results as for the case of TBI/Au(111). To explain the suppression of the intramolecular excitation pathway we again have to consider the influence of the electronic coupling and steric effects (see also sections 4.5.3 and6.3.1). Due to the energetic position of the HOMO the TBS, like the TBI, should in principle be able to engage in a charge transfer with gold d-bands. However we again do not observe a corresponding substrate mediated photoisomerization. In the present case this is most likely not due to a degeneracy of the isomers since the ground state barrier of the free molecule is comparably high. Consequently a complete elimination due to the surface confinement is not expected. Instead an alternative possibility has to be considered in which the hydrogen atoms of the functional group attenuate the steric effects imposed by the adsorbate/substrate interactions. This can well lead to a barrier along the reaction pathway, suppressing a hole induced isomerization.

6.4 Electronic structure of TBA, TBI and TBS on Au(111): comparison and conclusions

In the framework of this thesis the electronic structures of three different molecular switch/Au(111) systems have been studied to elucidate a possible isomerization and determine the underlying excitation mechanism. Valuable information can also be retrieved from a comparison of the individual results. Here we will present the most obvious similarities of TBA, TBI and TBS adsorbed on Au(111) and discuss their relevance in respect to the isomerization, binding and electronic coupling.

6.4.1 Highest occupied molecular orbitals

ΔE in [eV]	TBA/Au(111)		TBI/Au(111)		TBS/Au(111)	
	exp.	cal.	exp.	cal.	exp.	cal.
LUMO - HOMO	3.6	3.9	3.5	4.2	—	3.9
E_F - HOMO	1.9	—	1.9	—	1.9	—
HOMO - HOMO-1	0.7	0.7[a]	0.8	0.7	0.8	1.1
HOMO-1 - HOMO-2	0.2	0.5[b]	—	—	0.2	0.4[c]

Table 6.1: Orbital separation for TBA, TBS and TBI adsorbed on Au(111) investigated by 2PPE (exp.). The values are compared to the results of quantum chemical calculations of the free molecules (cal.) [Teg07][Dok09a]. For TBA and TBS some orbital assignments differ between experiment and theory. This is due to degeneracies which can not be resolved by 2PPE. In those cases the next lower lying orbital is used to determined the energetic spacing: (a): HOMO - HOMO-2, (b): HOMO-2 - HOMO-4, (c):HOMO-1 - HOMO-3

In table 6.1 the energetic separations of the most prominent molecular states are summarized and compared with quantum-chemical calculations for the respective free molecules [Teg07][Dok09a]. Although we have generally found good agreement between the experimental and theoretical values there is an apparent discrepancy in the assignment. Based on their binding energies the states observed in 2PPE have been correlated in descending order to the HOMO, HOMO-1 and HOMO-2. The calculations for the free molecule however exhibit an energetic degeneracy for some of the orbitals which cannot be resolved in our photoemission spectra. Thus, for further discussion of the results we will associate the experimentally determined states to the theoretical orbitals given in the above table. The corresponding similar energy separations suggest that the electronic structure of the molecules remains almost unchanged upon adsorption to the noble metal substrate. Therefore we assume a weak binding of the adsorbate which is supported e.g. by STM measurements investigating the mobility of TBA molecules on Au(111) [Com07].

Another interesting aspect is the striking similarity of the HOMO-X binding energies for all three switch/metal systems. This indicates that the corresponding states are omnipresent in each molecule. Since the functional group is varied this leaves only the *tert*-butyl substituted phenyl rings as a possible origin. Here

strong evidence is given by Kohn-Sham orbitals derived from quantum-chemical calculations [15]. Each of the orbitals which can be associated with a molecular state observed in the 2PPE spectra, shows a significant probability density located at the phenyl rings. A special case in this respect is the HOMO-1 of the TBI. It exhibits an asymmetric shape, being limited to the phenyl ring bound to the nitrogen of the functional group. As we have shown in section 6.1.2 the photoemission signal from this orbital can be used to elucidate relative changes in the absorption geometry of the molecules.

Finally the binding energy of the HOMO is, in agreement with the above, equal for TBA, TBI and TBS on Au(111). Hence, in all three cases, we can expect a wave function overlap with the d-band of the substrate and consequently a substrate mediated excitation via a hole transfer should be possible. Nevertheless a photoisomerization based on this reaction pathway is only observed for the TBA molecules indicating that the functional group and its corresponding switching properties are of crucial importance as well.

6.4.2 Lowest unoccupied molecular orbital

According to the theoretical HOMO-LUMO gaps of the used molecules (see table 6.1) the lowest unoccupied molecular orbital will for each case be located within the projected band gap of the Au(111) substrate. Therefore the electronic coupling to the metal is expected to be weak as no states for a wave function mixing are available. In return a substrate mediated excitation of the LUMO has to occur via scattering of hot electrons. With increasing energetic separation from the Fermi level the excitation probability decreases since the corresponding charge carrier density exponentially decays towards higher binding energies. This will consequently affect the photoemission yield of the respective 2PPE process as witnessed e.g. for TBA and TBI on Au(111) (see 4.3 and 6.1.2). In addition the former example exhibited an extraordinarily long lifetime of the excited LUMO of approximately 1ps corroborating the proposal of a weak coupling. Yet there has been no sign of a photoisomerization based on intramolecular transitions. This can be understood considering the actual switching mechanism. It requires either a breaking of the double bond of the functional group or a hybridization of the orbitals involved in the bonding to the phenyl rings. Hence the necessary condition for the isomerization is the electron vacancy in an occupied orbital. Therefore it is very likely that the switching probability is not primarily affected by the decay timescale of the LUMO but by the charge transfer times between the substrate and the involved HOMO which fills the hole created by the intramolecular transition.

6.4.3 Interface states

An essential result of this thesis is the detection of the interface states(IS) created by the potential arising from the molecule/metal interaction. Although the main focus of the investigations have been concerned with the isomerization behavior of

[15] For a graphical depiction of the results see appendix B

mol./Au(111)	trans-TBA	TBS	0.59ML TBI	cis-TBA	0.73ML TBI
$E - E_F$ in [eV]	4.05	4.0	4.00	3.80	3.80
Φ in [eV]	4.55	4.65	4.60	4.40	4.43
τ in [fs]	0	15	2	30	15

Table 6.2: Basic properties of the interface states. The table has been split into two groups of approximately equal binding energy. Similarities are also found in the respective work functions and lifetimes. Here a correlation to the dipole moment of the molecules and its influence on the surface potential can be assumed.

TBA, TBI and TBS on Au(111) we were able to obtain valuable information about some general aspects of the IS. First of all they appeared in each of the investigated systems. Their properties are very much alike as can be seen by a comparison of their respective binding energies, work functions and lifetimes in table 6.2. Here we have split the interface states in two groups according to their binding energy. The first group with the IS ≈4eV above the Fermi level includes the trans-TBA, the TBS and the 0.59ML TBI states. Interestingly their work functions and lifetimes are of approximately equal values as well. The same trend is observed in the second group consisting of the cis-TBA and the 0.73ML TBI interface states. It appears that the there is not only a distinct correlation between the work function and the dipole moment of the molecule but also between the binding energy of the IS and the dipole moment. Consequently these states are very sensitive probes in respect to the molecular geometry. We have already taken advantage of this aspect determining the isomer concentrations of the TBA/Au(111) isomerization (see section 4.4.2) and the adsorption behavior of TBI/Au(111) (see section 6.1.2).

6.5 *Conclusions*

We have investigated the adsorption and the electronic structure of tetra-*tert*-butyl-imine and tetra-*tert*-butyl-stilbene on a Au(111) substrate in order to compare their isomerization behavior with the successfully switched TBA/Au(111). The results show a large differences in the basic properties between the two symmetric molecules, TBA and TBS, and the asymmetric TBI. For the former the adsorption behavior, analyzed with thermal desorption spectroscopy, exploits a single phase multilayer peak with an underlying two phase monolayer. Those can be divided into a relaxed phase up to a coverage of 0.9ML and a compressed phase of the remaining 10%. In contrast TBI shows two multilayer phases and two monolayer phases of almost equal size. By employing 2-photon photoemission we could show that the multilayer and the monolayer phases undergo a a thermally induced phase transition. Moreover it could be activated by illumination in a photon energy range of 1.8 to 4.7eV. Here the phase transition is associated to a reorientation of the molecular geometry resulting in an increased coupling to the substrate.
The adsorption behavior of TBI and TBS is reflected in their electronic structure. While the molecule induced states of TBS/Au(111) exhibit a constant binding energy independent of the coverage the TBI induced states are greatly influenced by the competing phases of the monolayer. Two peculiarities can be observed in the spectra. The first is the existence of interface states (IS) for either molecule. Hence we found evidence for those states in four[16] different molecule/metal systems. This creates the opportunity to deepen the understanding of interface states which have previously only been observed for thick argon layers on Cu(100) [Güd05] and alkanethiolate self-assembled monolayer/Au(111) [Mun06]. Of particular interest is the overlap of those states with the substrate bands. Concerning this issue we presented magnificent data showing the lifetime dependence of a TBI interface state as function of its energetic position. Due to the annealing induced phase transition of this system it can be continuously tuned from the surface projected band gap into the region of the unoccupied sp-band. In agreement with the available relaxation channels the IS lifetime decreased from 110 to <10fs.
Returning to the general observation of the electronic structure we find the highest occupied molecular orbital (HOMO) for all three stereo isomers at approximately 1.8 to 1.9 eV below the Fermi level. This position close to the onset of the gold d-bands has been the key factor for the hole induced photoisomerization of the TBA/Au(111). Thus the same excitation channel is available for the other two molecules as well. However from our experiments we have to exclude a photoisomerization in the photon energy range of 1.8 to 4.7eV and at 6eV.
For the quenched photoisomerization of TBI and TBS adsorbed on Au(111) we suggested two explanations. The first can be summarized as the effect of the electronic substrate-molecule coupling. The second discusses a substrate induced barrier along the reaction pathways of the intramolecular and substrate induced excitations. In both cases the functional group and its interaction with the substrate can be held responsible. Hence the results of TBI and TBS clearly show that the crucial impact of the functional group on the isomerization behavior of adsorbed molecules.

[16] an interface states has also been reported for TBA/Ag(111)

7 Conclusion and Outlook

In conclusion we have investigated the isomerization ability of the three photochromic molecules tetra-*tert*-butyl-azobenzene (TBA),tetra-*tert*-butyl-imine (TBI) and tetra-*tert*-butyl-stilbene (TBS) upon their adsorption onto a Au(111) substrate. While the switching is suppressed for TBI and TBS, reversible light and temperature induced processes could be observed for TBA/Au(111). Based on the changes in its electronic structure which have been analyzed using 2PPE, we were able gain fundamental knowledge of the underlying excitation mechanisms and the interactions between substrate and molecule. The main results can be summarized as follows:

- In contrast to TBA in solution, light induced intramolecular transitions do not contribute to the isomerization of the adsorbed molecules. Main reasons are either a fast decay of the excited state via channels created by the presence of the substrate or a suppression of switching relevant molecular motions due to steric effects.

- Instead a temperature assisted, substrate mediate process has been identified to induce a bi-directional switching. Here electrons from the Au(111) d-bands are photoexcited creating a positive charge (hole) which is subsequently transferred to the highest occupied molecular orbital (HOMO) of the TBA. For this excitation channel the reaction yield is photon energy independent. To our knowledge this is the first time that a hole induced chemical reaction on a metal surface has been witnessed.

- The photoinduced switching can be reversed through a thermally activated cis-to-trans isomerization. Due to the interaction with the surface the ground state energy barrier separating the two TBA-isomers is lowered by a factor of four. Likewise the analysis of the reaction kinetics yields evidence for the influence of the substrate indicating a strong steric hinderance which limits the range of molecular motion.

According to the above it is obvious that the electronic coupling, as initially assumed, is a critical factor to the success of the photoisomerization. In this respect two aspects have to be considered: The first one is the probability of an excited molecule to switch. It is in principle a competition between the timescales of the molecular motion and the electronic relaxation. The latter is clearly influenced by the electronic coupling. It is thus a combined property of the molecule metal system which depends, amongst others, on the available density-of-states in the metal and the molecule-substrate distance. The minimum isomerization time on the other hand is an intrinsic property of the molecule. However it is determined by the available reaction pathways or in a more simple picture on the available range of molecular motions. Here it cannot be excluded that steric effects due to the geometric confinement to the surface will hinder certain molecular motions and thereby alter the potential energy landscape of the excited state. Hence the interaction with the substrate not

only creates additional decay channels but also may influence the timescales of the isomerization process. These arguments can well be applied to explain the suppression of the photoisomerization initiated by intramolecular excitations as witnessed for all molecules studied in this thesis.

A second aspect besides the enhanced decay which is influenced by the electronic coupling is the probability of the excitation process via a substrate mediated charge transfer. In fact this is the initial and therefore a required step of the photoisomerization. Here the coupling enables a charge transfer to the molecule and thus the excitation. A limiting factor in this case is the available number of suitable charge carriers having the right energy. This has been demonstrated comparing the photoisomerization ability of TBA adsorbed on different noble metal substrates, viz. Au(111) and Ag(111). In contrast to the gold substrate the d-bands of the silver are separated from the HOMO of the TBA by approximately 2eV. Consequently only few, fast decaying sp-band holes can contribute to the excitation process. We propose that this is the main reason why no substrate mediated, photoinduced switching is observed for TBA/Ag(111).

Depending on the adsorption geometry of the molecule steric effect can become another critical factor in regard to the isomerization ability. Here again we have to distinguish two contributions. The first is the range of molecular motion which in case of TBA/Au(111) is proven to be significantly reduced. This can lead to the creation or amplification of barriers along the reaction pathways of the isomerization. If these cannot be overcome, e.g. through thermal excitation or by using an alternative motion, the switching will be quenched. This presents a possible explanation why no substrate mediated isomerization is observed for TBS/Au(111) although its occupied electronic structure is very similar to TBA/Au(111). Here supporting evidence is given by a comparison of the respective free molecules. While the switching of TBS is limited to a rotational motion TBA can in addition use an inversion pathway. In this case the initial molecular properties are decisive for a successful switching.

The second contribution of the geometric confinement of the molecules to the surface is a distortion of the potential energy landscape. It can be regarded as a hindered electronic relaxation which consequently elevates the ground state energies of the isomers. This in return can be regarded as a relative reduction of the ground state energy barrier. Again evidence has been found in the analysis of the TBA/Au(111) isomerization kinetics. Those show that the thermal stability of the switched state is significantly reduced upon adsorption. In the limit of strong interactions an extinction of the barrier can be assumed trapping the adsorbed molecule in an intermediate configuration. Likewise a small initial energy barrier of the free molecule can lead to such a scenario. Thus it represents a possible explanation for the suppressed substrate mediated isomerization of TBI/Au(111) although this molecule as well exhibits an occupied electronic structure similar to TBA/Au(111)

The results of this work clearly show that the adsorption of a molecule to a substrate changes its initial properties almost completely. This makes it a difficult task to predict the switching ability of such systems and also to determine the detailed reasons for a suppressed photoisomerization as seen in the cases of TBS and

TBI on Au(111). Access to the answers is given only by a fundamental understanding of the underlying interactions between the molecules and the substrate. This on the other hand requires systems which can be successfully switched. In this respect the investigation of TBA/Au(111) has been a major step forward. Especially since it has demonstrated that the interaction of the molecules with the substrate is not simply quenching the isomerization based on intramolecular excitations but indeed is capable of creating new excitation pathway via charge transfer reactions.

At this point we would like to stress the great advantages of the 2PPE regarding the analysis of isomerization processes of surface adsorbed molecular switches. It allows to simultaneously access the occupied as well as the unoccupied sates of the substrate-adsorbate system. Those have been essential for the determination of the underlying excitation mechanism but also to identify changes in the electronic structure due to the adsorption. As has been shown in this thesis, 2PPE is very well suitable to resolve the reaction kinetics of light and temperature induced isomerization processes. Here a key role has been given to the analysis of the isomer specific unoccupied interface states which allowed us to retrieve absolute isomer concentrations. Moreover 2PPE is an ideal tool to resolve phenomena of low cross sections since the corresponding non-linear photoemission process naturally requires high photon densities. Nevertheless a successful investigation of molecular switches requires to employ different experimental methods. This can be witnessed in this work as well, as many observations have been supported and understanding has been extended by incorporating results from vibrational spectroscopy (HREELS), core level spectroscopy and imaging techniques (STM).

Quo vadis? Although the current work has contributed significantly to the knowledge about the switching of TBA/Au(111) there are still many unresolved questions. E.g. it is not yet completely understood whether sterical hinderance or a strong electronic coupling leads to the quenching of the isomerization induced by intramolecular excitations. Here the exchange of the *tert*-butyl substituents can be used to alter the substrate-molecule interaction. In the ideal case this can be done gradually to resolve the transition from the substrate mediated to the intramolecular excited switching mechanism. This would be a huge motivation to further investigate the isomerization ability of stilbene and imine derivatives. Another major challenge of near future experiments will be the search for ways to control the isomerization yield via the photon energy. This is a basic requirement for a possible functionalization of surface confined switches. Promising processes in this respect are alternative charge transfer reactions involving isomer specific unoccupied states of the molecule.

Having demonstrated a substrate mediated, photoinduced switching is a first important step towards the functionalization of the surface itself. Here a broad field of research is opened where not only switches exploiting a cis-trans isomerization but also alternative molecules can be used to modify the property of the substrate. In this respect sensor applications can be envisioned. Moreover the geometric confinement to the surface allows to study cooperate effects in molecular ensembles and thus the lateral interaction between the molecules.

A Abbreviations

1C	one-color
2C	two-color
2D	two-dimensional
2PPE	two-photon photoemission
a.u.	arbitrary units
amu	atomic mass units
AR	angle resolved
BS	beam splitter
CBM	conduction band minimum
CFD	constant-fraction-discriminator
DFT	density functional theory
DOS	density-of-states
e-e	electron-electron
e-ph	electron-phonon
fcc	face centered cubic
LUMO	lowest unoccupied molecular orbital
LT	low temperature
hcp	hexagonal close packed
HOMO	highest occupied molecular orbital
HREELS	high resolution electron energy loss spectroscopy
IPS	image potential state
IR	infrared
IS	interface state
NEXAFS	near edge X-ray adsorption fine structure
OPA	optical parametrical amplifier
PD	photodiode
RegA	regenerative amplifier
QMS	quadrupol mass spectrometer
STM	scanning tunneling microscopy
TBA	tetra-*tert*-butyl-azobenzene
TBI	tetra-*tert*-butyl-imine
TBS	tetra-*tert*-butyl-stilbene
TDS	thermal desorption spectroscopy
TOF	time-of-flight
TR	time resolved
UHV	ultra high vacuum
UV	ultra-violet
VBM	valance band maximum
vis	visible
XPS	X-ray photoemission spectroscopy

B Kohn-Sham orbitals of TBA, TBI and TBS

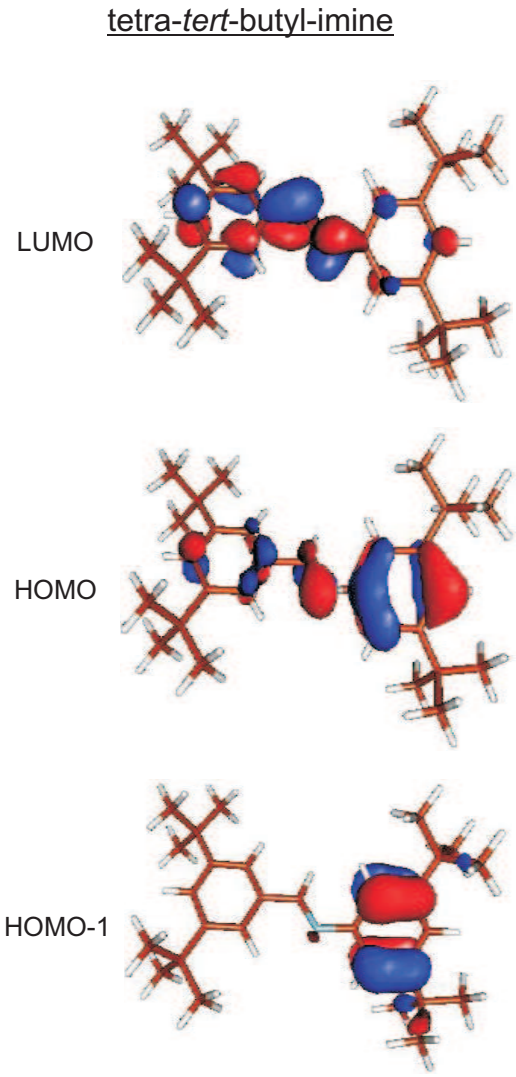

Figure B.1: Kohn-Sham orbitals of tetra-*tert*-butyl-imine. Courtesy of P.Saalfrank and coworkers, Universität Potsdam.

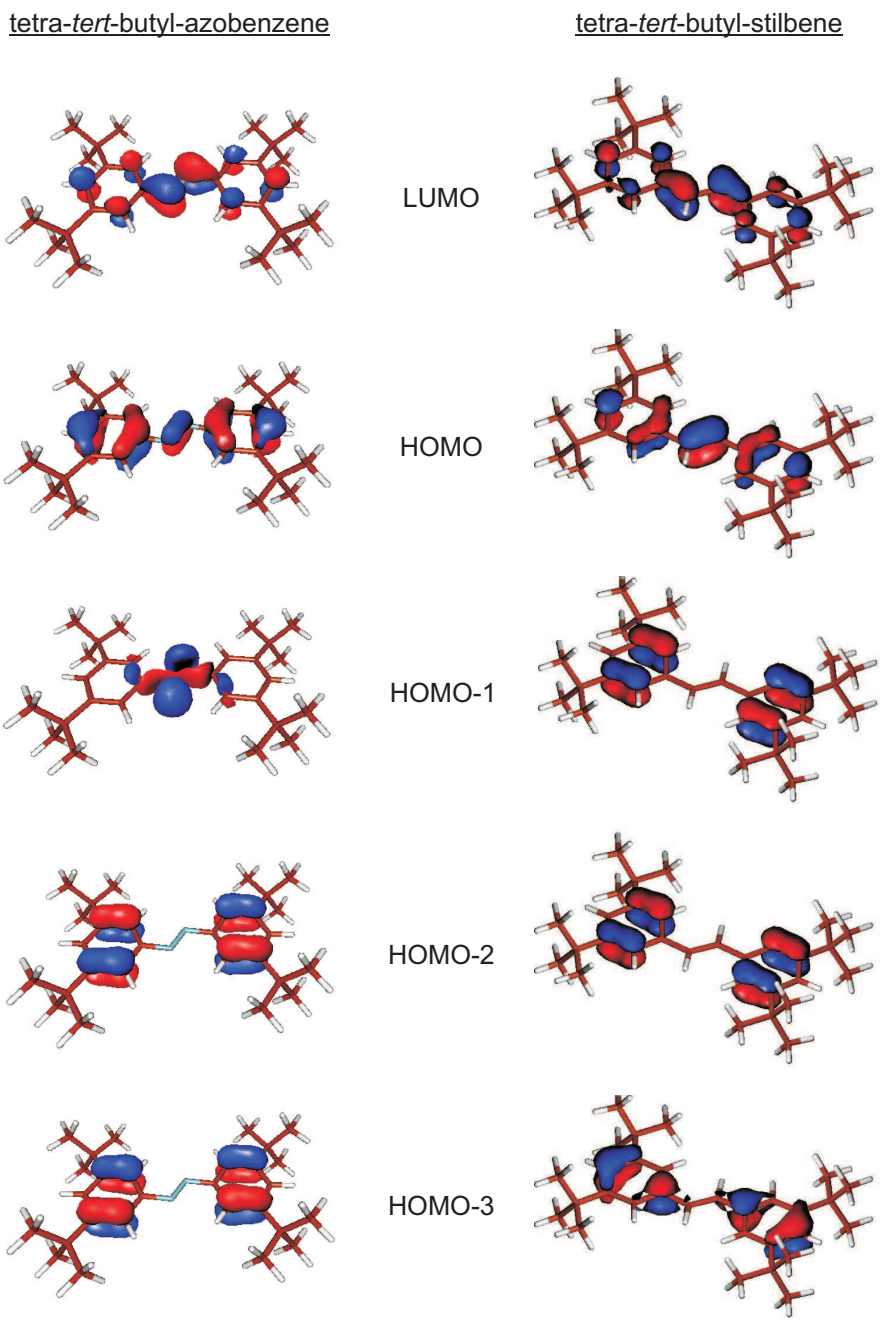

Figure B.2: Kohn-Sham orbitals of tetra-*tert*-butyl-azobenzene and tetra-*tert*-butyl-stilbene. Courtesy of P.Saalfrank and coworkers, Universität Potdam.

C 2PPE of the Au(111) substrate

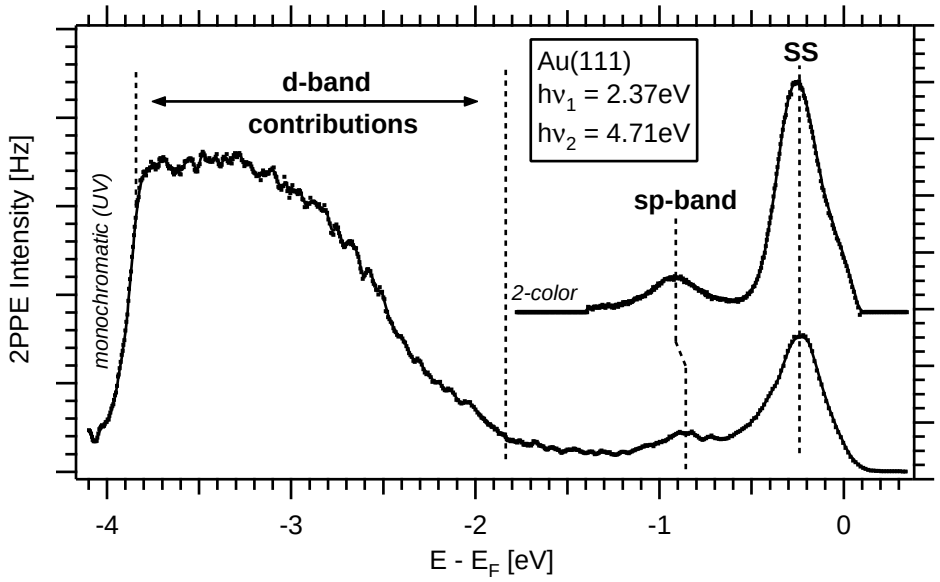

Figure C.1: One and two-color 2PPE spectra of the clean Au(111) substrate. The former is dominated by the broad peak structure of the d-bands. In both spectra contributions from the surface state (SS) and the hybridized sp-band are observed. A detailed analysis of the sp-band shift is given in the text.

Investigating the electronic structure of organic/metal interfaces requires a detailed understanding of the substrate. The theoretical background for the measurements has been given in section 2.2.1. Moreover it is essential to have a solid experimental knowledge which will be presented in the following. Based on the results we (i) have the possibility to compare the quality of our sample and preparation to other work and (ii) have access to required information for distinguishing substrate from adsorbate induced photoemission features.

2PPE spectra from a freshly prepared Au(111) crystal are presented in figure C.1. The lower trace has been recorded in a one-color setup using strictly UV photons of $h\nu = 4.71eV$. The upper trace on the other hand exploits a spectrum from 2-color measurements combining the UV beam with a vis beam of $h\nu = 2.37eV$. This method is especially useful for the investigation of unoccupied intermediate states. From the data we determine a work function of $\Phi = 5.45 \pm 0.05eV$ which is in agreement with results from other groups [Han78][Pan95][Reu96]. At the low energy end of the UV spectra we see a broad increasing signal. It is attributed to photoemission from the bulk d-bands which are well known to lie in this region with an upper edge at ≈2.0eV below the Fermi level [Eck84].

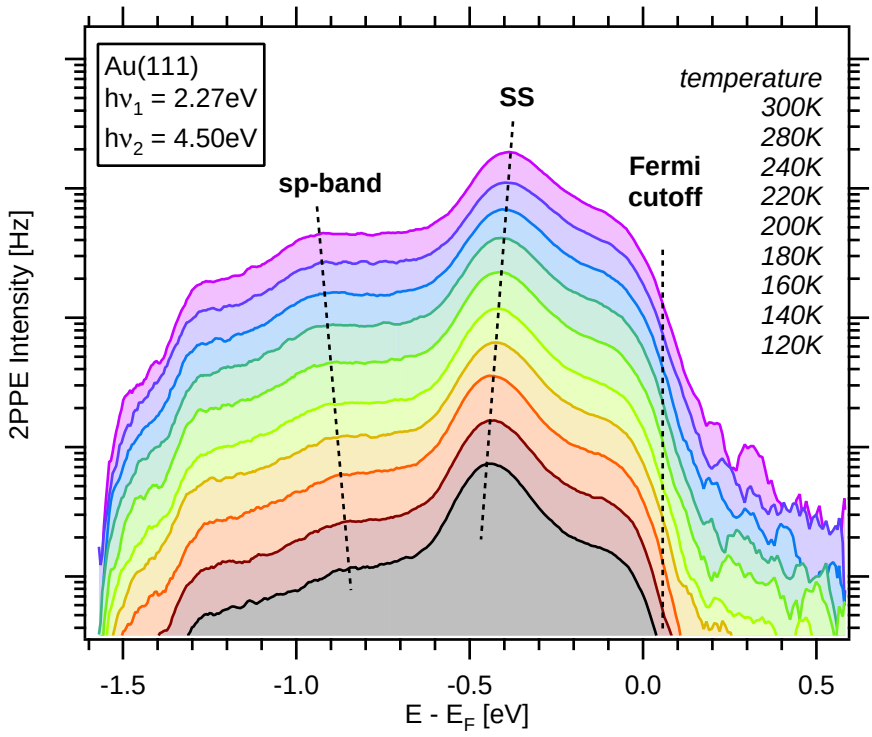

Figure C.2: Temperature dependent shift of the gold surface state and the bulk sp-band. For details on the origin see text.

In the region close the the Fermi cutoff edge two more peaks are found. The larger feature SS at $E = -0.3eV$ agrees very well with the surface state thoroughly discussed in the literature [Cou86]. It can be found in the two-color spectra as well. The second peak which we assign to the sp-band of the gold substrate appears to be shifted in the different spectra. This is a consequence of the favored direct excitations and the strong dispersion of the band. Consequently transitions will occur at a point along the ΓL-line of the Brillouin zone which enables a resonant transition and thus the initial state energy becomes photon energy dependent. Similar observations have been reported for 2PPE spectra of the Ag(111) sp-band [Pon05].

A second peculiarity of the gold substrate is the temperature dependence of the sp-band and surface state binding energies. Figure C.2 displays a series of 2-color 2PPE spectra taken at different sample temperatures. Heating the sample obviously lowers the binding energy of the sp-band whereas the surface state moves closer to the Fermi level. In the following we will give a detailed analysis of these observed shifts.

The sp-band The temperature dependent initial state energies of the gold sp-band are plotted for two different photon energies in figure C.3. From the two obtained data sets we retrieve temperature dependent initial state energies of $\Delta E_B(T) = -0.60 - 3.8 \cdot 10^{-4} eVK^{-1}$ and $\Delta E_B(T) = -0.77 - 3.6 \cdot 10^{-4} eVK^{-1}$ in order of increasing photon energy.

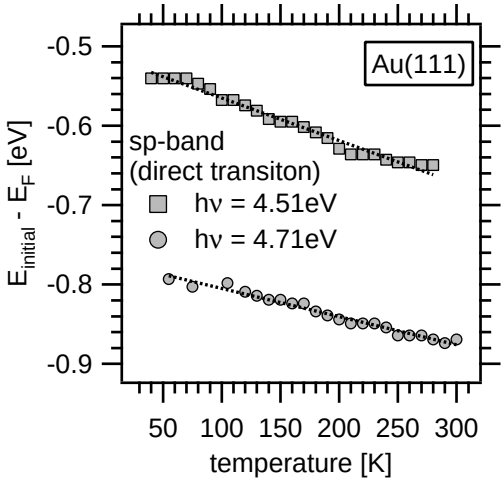

Figure C.3: Initial state energy of the Au(111) sp-band as a function of temperature. Experimental data from measurements using two different photon energies.

To explain the respective shifts a schematic drawing of occupied and unoccupied gold sp-bands along the ΓL-Line of the Brillouin zone at two temperatures T_1 and T_2 is presented in figure C.4. The red and blue arrows, representing different photon energies ($h\nu_1$ and $h\nu_2$), depict the direct transitions between the occupied and unoccupied band. These are known to account for the majority of the photoemission signal [Pon05]. Thus depending on the photon energies used different regions across the k-space will be probed, thus leading to a shift ΔE_2 in the observed initial state energy. A change of the substrate temperature on the other hand is known to alter the distance between the occupied and unoccupied band [Win76]. Consequently the direct transitions will take place at a different position in the k-space. The magnitude of the initial state energy shift (ΔE_1) depends on the specific slope of the sp-band. For Au(111) we observed stronger shifts when probing transitions close to the Γ-point of the Brillouin zone.

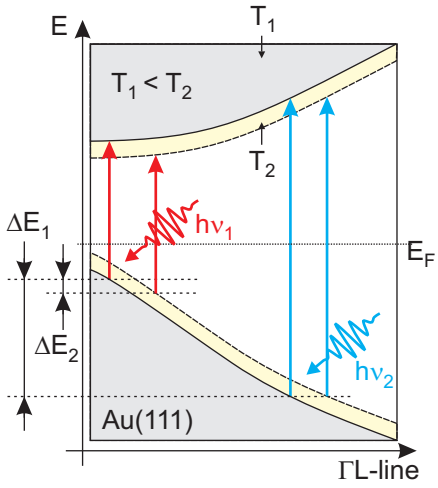

Figure C.4: Schematic depiction of the Au(111) sp-band. Electronic excitation processes favors direct transitions. Consequently a change in photon energies will lead to a shift of initial state energy (ΔE_2). A likewise effect (ΔE_1) is induced upon heating the sample which increases the band gap size.

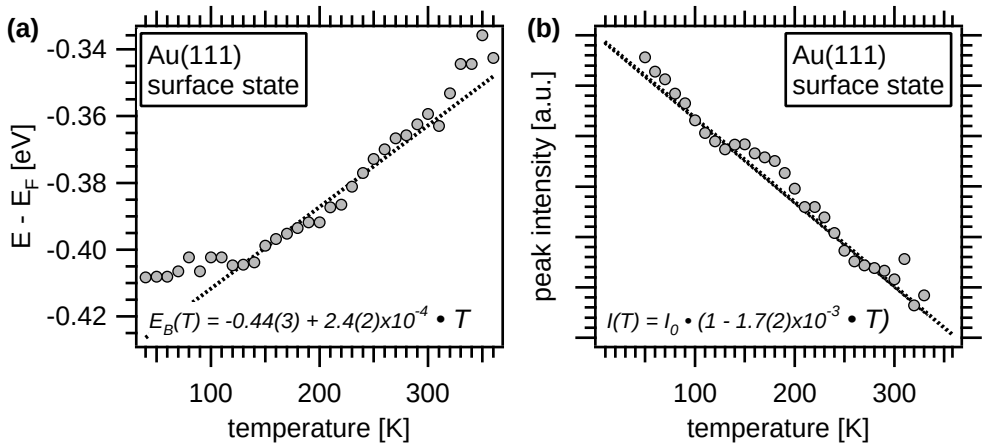

Figure C.5: Temperature dependence of the Au(111) surface state properties. **(a):** Experimental values for the SS binding energy with respect to the Fermi level. **(b):** SS peak intensity as a function of sample temperature.

The surface state The thermally induced shift of the Au(111) surface state has been previously investigate by different groups [Pan95][Kow06]. Within the framework of this thesis it is required for the accurate analysis of temperature dependent 2PPE measurements on molecule covered Au(111) surfaces. Figure C.5 depicts the binding energy and the relative peak intensity of the surface state as a function of the temperature. Linearly fitting the data we obtain $E_B(T) = 0.44 - 2.4 \cdot 10^{-4} eVK^{-1}$ and $I(T) = I_0(1 - 17 \cdot 10^{-4} K^{-1})$ with I_0 the peak intensity at 0K. This is in very well agreement with values of $\Delta E_B(T) = 2.6 \cdot 10^{-4} eVK^{-1}$ and $I(T) = 1 - 14 \cdot 10^{-4} eVK^{-1}$ reported by Paniago *et al.* [Pan95]. Therein the authors correlate the shift of the surface state to the above discussed temperature dependent variation of the bulk band gap.

The here presented results have been used to properly analyze the 2PPE spectra recorded for various molecules (TBA, TBI, TBS) adsorbed on the Au(111) surface. They have proven to be very useful especially in respect to the temperature dependent cis-trans concentration of the photoisomerized TBA/Au(111) (see section 4.6.3) where the peaks of the molecule induced states partially overlap with the sp-band features.

D Laser accommodated fitting of the isomerization rates

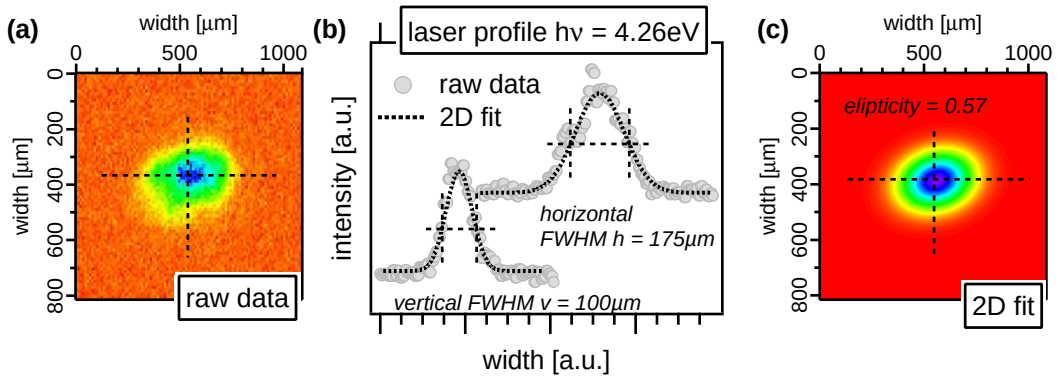

Figure D.1: Analysis of the laser beam profile. **(a):** Laser image recorded with a 8-bit CCD-camera. **(b):** Horizontal and vertical cuts of the laser intensity profile as indicated by the dotted lines. The data has been fitted using a 2-dimensional Gaussian function. **(c):** 2D-plot of the fitted beam image

In section 4.4 we introduced an analytical description of the TBA/Au(111) isomerization kinetics. It correlated the efficiency of the photoinduced process, in terms of an effective cross section, to the changes in the experimental signal (equation 4.30). Those are also a function of the fluence, viz. the number of photons impinging on a unit area of the sample. Figure D.1(a) shows the intensity profile of sample laser pulse as commonly used in our measurements. It exhibits a spatial variation of the power and hence of the fluence with a maximum value in the center of the laser spot. This aspect is of tremendous importance for the analysis of the experimental signal. In the inner, high fluence, regions the isomerization occurs on a faster timescale as in the outside regions leading to a non-homogenous distribution of the time dependent concentrations. Those on the other hand determine the electronic structure observed in 2PPE which represents the average of all local contributions. This effect can be neglected in the limit of $t \rightarrow \infty$ where each area within the laser spot reaches the same final isomer concentration (photostationary state). However to deduce the cross section of the photoisomerization we have to analyze the temporal evolution of the signal. Therefore it is necessary to implement the laser profile into our fitting routines. This requires an integration of the saturation function 4.30 over the spatial distribution of the fluences which unfortunately yields an expression that cannot be solved analytically. To avoid this problem we instead use a summation in the form of:

$$I_{exp} = \sum I_i(t, f) = \sum f_i^m A_i (B + Ce^{-\sigma f_i^n t}) \tag{D.50}$$

Here the experimental signal I_{exp} is summed over i patches of equal fluence f_i. Each patch has to be weighted according to its area A_i. The influence of the fluence on

the I_{exp} is denoted by the power m and depends on the used investigation method. E.g. the 2PPE is a 2nd order nonlinear process an therefore its photoemission intensity has to weighted quadratically ($m = 2$). In contrast the intensity of the direct photoemission scales linearly with the fluence ($m = 1$). The most common approach used in this thesis however is the determination of the work function. It is completely independent of signal intensity and thus the fluence ($m = 0$) as it is derived from the width of the spectra. Finally the observed changes lead to an exponential saturation which is also has a distinct fluence dependence accounted for be the exponent n. It determines the order of the isomerization process, viz. whether it is linear or nonlinear.

The above equation with its free parameters B and C is used to fit our experimental data. In order to obtain i, f_i and A_i we have to analyze the corresponding laser beam profiles as will be explained in the following. The spatial intensity distribution of the laser pulse is recorded with a camera in front of the chamber (for details see section 3.1.3). It is subsequently fitted with a 2-dimensional Gaussian function. The respective result for our sample beam is presented in figure D.1 (c). Implementing the photon energy and the total power the fitted intensity mapping of the CCD-camera can be converted into a fluence mapping.

A critical issue is the fluence binning, hence the number of different fluence levels f_i required to properly describe the isomerization kinetics. In the limit of $i \to \infty$ the fit function is expected to converge towards the accurate solution. However for large i this will lead to inconveniently long computational times. To determine a sufficient limit we observe the convergence of a model system for increasing i. Here we use $B = C = 1$, $m = 0$ according to an analysis of the work function and $n = 1$ as observed in the fluence dependence measurement (see section 4.5.1). The constant fluence areas A_i can be calculated based on the Gaussian fit function. Traces for a slicing into 10, 100, 1000 and 10000 levels can be seen in figure D.2. As predicted we observe a convergence which yields almost identical values for $i = 1000$ and $i = 10000$. The relative deviations of both values remain below 1% (note the logarithmic scale). Hence we have to use a minimum binning into 1000 equally spaced fluence levels to obtain sufficiently accurate results from the fitting routines.

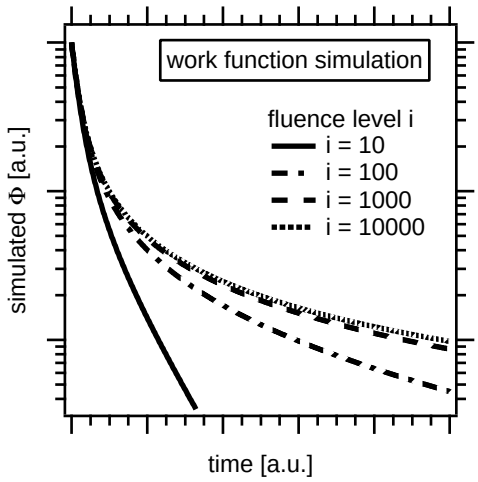

Figure D.2: Temporal evolution of the work function modeled using different fluence slicing parameter (i). For details see text.

E Analysis of the work function shift

According to the discussion in section 4.4.2 the TBA/Au(111) photoisomerization kinetics will be analyzed based on the corresponding work function changes. In the following we will present basic considerations regarding the data acquisition and evaluation which yields the saturation curves (see equation 4.30) necessary for the determination of the switching efficiency (cross section). The work function in a 2PPE experiment is given by the photon energy dependent width of the spectra. It can be deduced by analyzing the energy of the vacuum and the Fermi cutoff edges:

$$\Phi = h\nu_{pump} + h\nu_{probe} - (E_{Fermi} - E_{vacuum}) \tag{E.51}$$

with $h\nu_{pump}$ and $h\nu_{probe}$ the energies of the pumping and the probing photons respectively.

Upon illumination the work function of TBA/Au(111) decreases (see section 4.4.2). Consequently the potential between the analyzer and the sample is changed (see section 3.3). Due to the small magnitude of the variation (∼100meV) we can neglect the effects of the corresponding electric field on the energy resolution. Therefore we restrain from altering the sample potential (bias voltage) during the measurement. As a result of the isomerization induced work function change the vacuum cutoff edge shifts towards lower kinetic energies whereas the Fermi edge remains constant. Here we encounter a first experimental restriction. The initial potential (bias voltage) has to be chosen in a way which enables the analysis of the vacuum cutoff edge when reaching the final (photostationary) state.

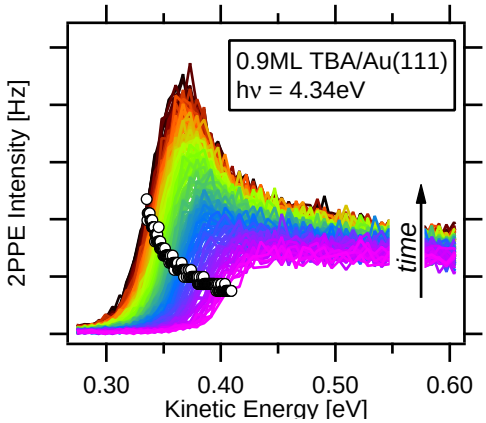

Figure E.1: 2PPE illumination series of the photoisomerization. The switching induced work function change can be directly witnessed based on the shift of the vacuum cutoff edge. White circles mark the respective energetic positions at the half maximum intensity.

In agreement with the above, the evaluation of the isomerization induced changes can be reduced to the observation of the vacuum cutoff edge shift. As mentioned in section 4.4.2 the width of the edge is mainly determined by the energy resolution of the (time-of-flight) analyzer, the surface homogeneity and the accumulation of isomerization induced work function changes. Sample spectra from an actual 2PPE illumination dependent experiment are presented in figure E.1. Here we see 200 traces subsequently recorded at a photon dose of $N_{ph} = 5 \cdot 10^{18} cm^{-2}$ each. The shifting of the vacuum cutoff edge due to the photoisomerization can nicely be observed in this graph. Its energetic position is deduced from the half maximum

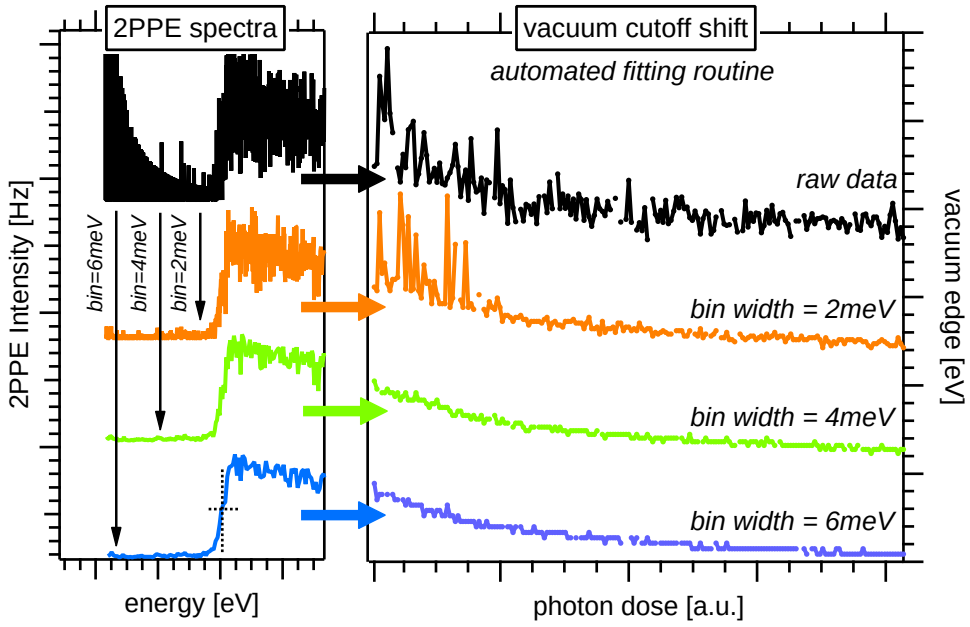

Figure E.2: Saturating work function change as a function of illumination. The traces in graph (b) are obtained from an automated fitting routine analyzing the position of the vacuum cutoff edge. (a) shows a sample spectra of the corresponding illumination series (see figure E.1). The signal-to-noise ratio of the fitting routines can be improved by binning of the 2PPE traces.

value of the total cutoff intensity as indicated by the white circles. Due to the large amount of spectra it is inevitable to use automated fitting routines. Since this is a delicate method selected data sets were cross checked on a regular basis to validate the results.

The quality of the (automated) edge fit depends on the statistics of the 2PPE spectra. Here we encounter a second experimental restriction. Since the probing laser light is simultaneously driving the isomerization mechanism we have to record the individual spectra at a photon dose which is small compared to the dose needed to reach the stationary state. This in return reduces the statistics of the measurement. To illustrate this problem we pick a sample trace from the above 2PPE series. The raw data, as displayed in the top trace of figure E.2, exhibits a very noisy edge. As can be seen from the corresponding automated fit of all 200 traces (appended on the right side) the error margin is very large. To resolve this problem of bad statistics the data is energetically binned as described in section 3.3.1. Here the three bottom traces show the results for bin width of 2,4 and 6meV, respectively. Employing the automated fitting routines we see that in the resulting saturation curves exhibit an improved signal-to-noise ratio. The price for this automated data evaluation is a reduction in the energy resolution. It respective value of usually 4 to 6meV however is still suitable to properly fit the data according to the procedures discussed in appendix D.

F cis isomer concentration in thermal experiments

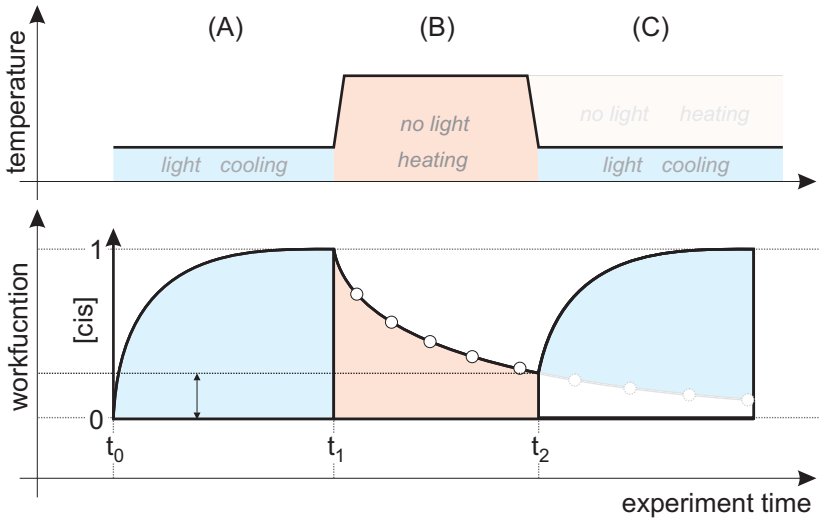

Figure F.1: Data acquisition scheme for the investigation of the thermally induced cis-to-trans isomerization. For details see text.

For the discussion of the thermally induced cis-to-trans isomerization discussed in section 4.6.1 we have to analyze the TBA cis-isomer concentration as a function of the temperature. Experimental access to this quantity is obtained as depicted in figure F.1. (A): At first the sample (usually 0.9ML TBA/Au(111)) is brought into the photostationary state (PSS) via illumination at a suitable photon energy (2.2-6eV). The corresponding saturation is monitored based on the work function shift discussed in section 4.4.2 and appendix E. (B): The sample is quickly heated to the desired temperature which is then stabilized by a thermo-controller. In this step the laser is blocked to avoid a simultaneous photonisomerization. At the end of the heating interval (t_1 to t_2) the sample temperature is ramped down quickly to prevent further thermally activated switching processes. (C): In the final step the work function change is again monitored. Depending on the progress of the thermal back switching there is a deviation between the values at t_0 (unswitched sample) and t_2 (backswitched sample). The relative changes in the work function can be correlated to the heating induced changes in the cis population by referencing the maximum and minimum values to $[cis] = 1$ and $[cis] = 0$, respectively.

An alternative method to investigate the thermal isomerization is to take single spectra of low photon doses during the heating period. This is indicated by the white circles. Here again we can determine the cis concentration based on the work function.

G Coverage Gauging

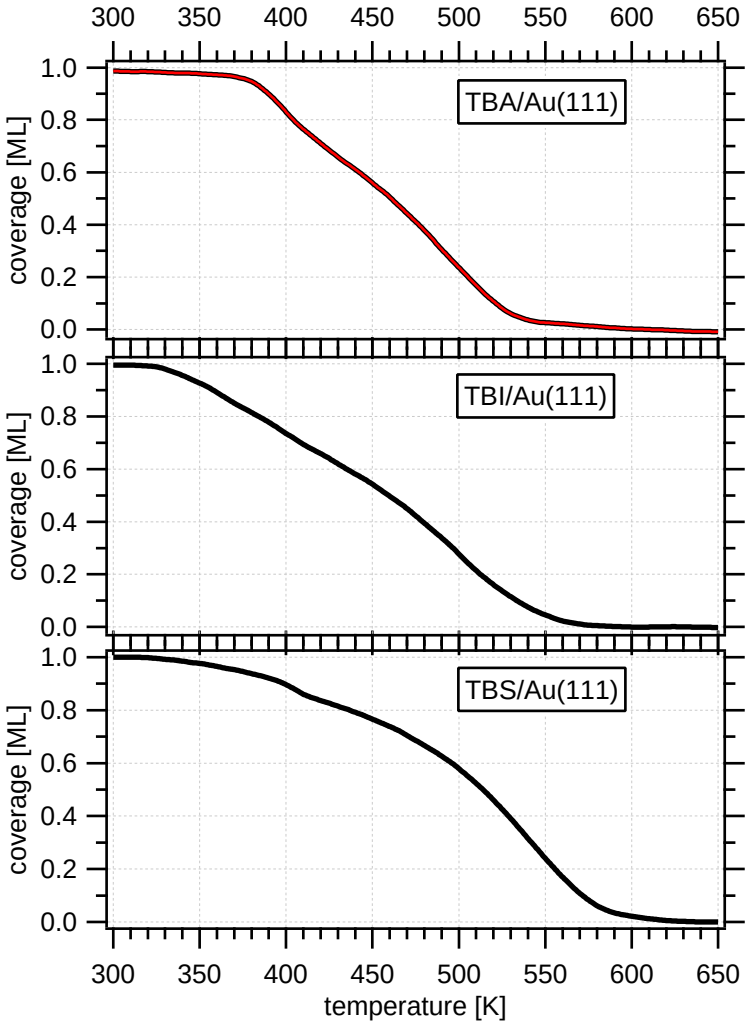

Figure G.1: Coverage gauging as a function of the annealing temperature for tetra-*tert*-butyl-azobenzene , tetra-*tert*-butyl-imine and tetra-*tert*-butyl-stilbene on Au(111). The curves have been obtained from integrating the monolayer signal of the thermal desorption spectra. The here presented values have been used to determine the coverage in case of partial desorption due to annealing of the sample.

References

[Ale06] Micol Alemani, Maike V. Peters, Stefan Hecht, Karl-Heinz Rieder, Francesca Moresco, & Leonhard Grill. *Electric Field-Induced Isomerization of Azobenzene by STM.* Journal of the American Chemical Society **128**, 45, 14446 (2006). DOI: 10.1021/ja065449s.

[Ale07] M. Alemani. *Low Temperature STM Investigation of Molecular Manipulation, Decoupling and Switching.* PhD Thesis, Freie Universität Berlin (2007). URL `http://www.diss.fu-berlin.de/2007/238/index.html`.

[Ale08] Micol Alemani, Sofia Selvanathan, Francisco Ample, Maike V. Peters, Karl-Heinz Rieder, Francesca Moresco, Christian Joachim, Stefan Hecht, & Leonhard Grill. *Adsorption and Switching Properties of Azobenzene Derivatives on Different Noble Metal Surfaces: Au(111), Cu(111), and Au(100).* The Journal of Physical Chemistry C **112**, 28, 10509 (2008). DOI: 10.1021/jp711134p.

[And65] Daniel G. Anderson & Gunnar Wettermark. *Photoinduced Isomerizations in Anils.* Journal of the American Chemical Society **87**, 7, 1433 (1965). DOI: 10.1021/ja01085a004.

[Arm95] D. R. Armstrong, J. Clarkson, & W. E. Smith. *Vibrational Analysis of trans-Azobenzene.* The Journal of Physical Chemistry **99**, 51, 17825 (1995). DOI: 10.1021/j100051a005.

[Arn03] Heike Arnolds, Robert J. Levis, & David A. King. *Vibrationally assisted DIET through transient temperature rise: the case of benzene on Pt(111).* Chemical Physics Letters **380**, 3-4, 444 (2003). DOI: 10.1016/j.cplett.2003.09.017.

[Avi74] Arieh Aviram & Mark A. Ratner. *Molecular rectifiers.* Chemical Physics Letters **29**, 2, 277 (1974). DOI: DOI: 10.1016/0009-2614(74)85031-1.

[Bag08] Paul S. Bagus, Daniel Kafer, Gregor Witte, & Christof Woll. *Work Function Changes Induced by Charged Adsorbates: Origin of the Polarity Asymmetry.* Physical Review Letters **100**, 12, 126101 (2008). DOI: 10.1103/PhysRevLett.100.126101.

[Bar90] J. V. Barth, H. Brune, G. Ertl, & R. J. Behm. *Scanning tunneling microscopy observations on the reconstructed Au(111) surface: Atomic structure, long-range superstructure, rotational domains, and surface defects.* Phys. Rev. B **42**, 15, 9307 (1990). DOI: 10.1103/PhysRevB.42.9307.

[Bar05] Johannes V. Barth, Giovanni Costantini, & Klaus Kern. *Engineering atomic and molecular nanostructures at surfaces.* Nature **437**, 7059, 671 (2005). http://dx.doi.org/10.1038/nature04166.

[Ber41] Ernst. Bergmann & Anna. Weizmann. *Dipole Moments as a Tool in the Determination of Structure.* Chemical Reviews **29**, 3, 553 (1941). DOI: 10.1021/cr60094a010.

[Ber00] W. Berthold, U. Höfer, P. Feulner, & D. Menzel. *Influence of Xe adlayer morphology and electronic structure on image-potential state lifetimes of Ru(0001).* Chemical Physics **251**, 1-3, 123 (2000). DOI: 10.1016/S0301-0104(99)00329-8.

[Ble04] A. A. Blevins & G. J. Blanchard. *Effect of Positional Substitution on the Optical Response of Symmetrically Disubstituted Azobenzene Derivatives.* The Journal of Physical Chemistry B **108**, 16, 4962 (2004). DOI: 10.1021/jp037436w.

[Boy92] R. W. Boyd (Ed.). *Nonlinear Optics.* Academic Press, San Diego, USA (1992).

[Bru07] L. W. Bruch, R. D. Diehl, & J. A. Venables. *Progress in the measurement and modeling of physisorbed layers.* Reviews of Modern Physics **79**, 4, 1381 (2007). DOI: 10.1103/RevModPhys.79.1381.

[Cam00] I. Campillo, A. Rubio, J. M. Pitarke, A. Goldmann, & P. M. Echenique. *Hole Dynamics in Noble Metals.* Phys. Rev. Lett. **85**, 15, 3241 (2000). DOI: 10.1103/PhysRevLett.85.3241.

[Cat99] Paola Cattaneo & Maurizio Persico. *An abinitio study of the photochemistry of azobenzene.* Phys. Chem. Chem. Phys. **1**, 4739 (1999). DOI: 10.1039/a905055h.

[Che03] P. C. Chen & Y. C. Chieh. *Azobenzene and stilbene: a computational study.* Journal of Molecular Structure: THEOCHEM **624**, 1-3, 191 (2003). DOI: 10.1016/S0166-1280(02)00783-2.

[Chu06] E.V. Chulkov, A. Leonardo, I.A. Nechaev, & V.M. Silkin. *Decay of electronic excitations in bulk metals and at surfaces.* Surface Science **600**, 18, 3795 (2006). DOI: 10.1016/j.susc.2006.01.091.

[Com07] Matthew J. Comstock, Niv Levy, Armen Kirakosian, Jongweon Cho, Frank Lauterwasser, Jessica H. Harvey, David A. Strubbe, Jean M. J. Frechet, Dirk Trauner, Steven G. Louie, & Michael F. Crommie. *Reversible Photomechanical Switching of Individual Engineered Molecules at a Metallic Surface.* Physical Review Letters **99**, 3, 038301 (2007). DOI: 10.1103/PhysRevLett.99.038301.

[Com08] Matthew J. Comstock, Niv Levy, Jongweon Cho, Luis Berbil-Bautista, Michael F. Crommie, Daniel A. Poulsen, & Jean M. J. Frechet. *Measuring reversible photomechanical switching rates for a molecule at a surface.* Applied Physics Letters **92**, 12, 123107 (2008). DOI: 10.1063/1.2901877.

[Cou86] R. Courths, H. G. Zimmer, A. Goldmann, & H. Saalfeld. *Electronic structure of gold: An angle-resolved photoemission study along the Lambda-line.* Phys. Rev. B **34**, 6, 3577 (1986). DOI: 10.1103/PhysRevB.34.3577.

[Cri02] Xavier Crispin, Victor Geskin, Annica Crispin, Jerome Cornil, Roberto Lazzaroni, William R. Salaneck, & Jean-Luc Bredas. *Characterization of the Interface Dipole at Organic/ Metal Interfaces.* Journal of the American Chemical Society **124**, 27, 8131 (2002). DOI: 10.1021/ja025673r.

[Cun05] Gianaurelio Cuniberti, Giorgos Fagas, & Klaus Richter. *Introducing Molecular Electronics*, Vol. 680 of *Lecture notes in physics.* Springer, Berlin (2005).

[Dai95] H.-L. Dai & W. Ho. *Laser Spectroscopy and Photochemistry at Metal Surfaces.* World Scientific, Singapore (1995).

[Dem03] W. Demtröder (Ed.). *Laser Spectroscopy.* Springer, Berlin (2003).

[Dok09a] Jadranka Dokic. private communications (2009).

[Dok09b] Jadranka Dokic, M. Gothe, J. Wirth, Maike V. Peters, Jutta Schwarz, Stefan Hecht, & Peter Saalfrank. *Quantum chemical investigation of thermal cis-to-trans isomerization of azobenzene derivatives: substituent effects and comparison to experimental data.* Jounal of Physical Chemistry **to be published**, 0 (2009).

[Dür03] Heinz Dürr & Henri Bouas-Laurent (Eds.). *Photochromism: Molecules and Systems.* Elsevier Science (2003).

[DR05] V. De Renzi, R. Rousseau, D. Marchetto, R. Biagi, S. Scandolo, & U. del Pennino. *Metal Work-Function Changes Induced by Organic Adsorbates: A Combined Experimental and Theoretical Study.* Phys. Rev. Lett. **95**, 4, 046804 (2005). DOI: 10.1103/PhysRevLett.95.046804.

[Du07] Mao-Hua Du, Jun Feng, & S. B. Zhang. *Photo-Oxidation of Polyhydroxyl Molecules on TiO_2 Surfaces: From Hole Scavenging to Light-Induced Self-Assembly of TiO_2-Cyclodextrin Wires.* Physical Review Letters **98**, 6, 066102 (2007). DOI: 10.1103/PhysRevLett.98.066102.

[Ech89] P.M. Echenique & J.B. Pendry. *Theory of image states at metal surfaces.* Progress in Surface Science **32**, 2, 111 (1989). DOI: 10.1016/0079-6816(89)90015-4.

[Ech00] P. M. Echenique, J. M. Pitarke, E. V. Chulkov, & A. Rubio. *Theory of inelastic lifetimes of low-energy electrons in metals.* CHEM.PHYS. **251**, 1 (2000).

[Ech04] P. M. Echenique, R. Berndt, E. V. Chulkov, Th. Fauster, A. Goldmann, & U. Höfer. *Decay of electronic excitations at metal surfaces.* Surface Science Reports **52**, 7-8, 219 (2004). DOI: 10.1016/j.surfrep.2004.02.002.

[Eck84] H Eckardt, L Fritsche, & J Noffke. *Self-consistent relativistic band structure of the noble metals.* Journal of Physics F: Metal Physics **14**, 1, 97 (1984). http://stacks.iop.org/0305-4608/14/97.

[Ehr61] Gert Ehrlich. *Kinetic and Experimental Basis of Flash Desorption.* Journal of Applied Physics **32**, 1, 4 (1961). DOI: 10.1063/1.1735956.

[Fan90] D Fanghänel, G. Timpe, & V. Orthman. *Organic Photochromes.* Consultants Bureau: New York (1990).

[Fer01] Ben L. Feringa. *Molecular Switches.* Wiley-VCH (2001).

[Feu78] B. Feuerbacher, B. Fitton, & R. F. Willis. *Photoemission and the electronic properties of surfaces / edited by B. Feuerbacher, B. Fitton, R. F. Willis.* Wiley, London ; New York : (1978).

[Fig90] K. Figueroa, M. Campos-Vallette, & Madeleine Rey-Lafon. *Vibrational study of p, p'-disubstituted N-benzylideneanilines.* Spectrochimica Acta Part A: Molecular Spectroscopy **46**, 11, 1659 (1990). DOI: 10.1016/0584-8539(90)80278-7.

[For03] F. Forster, G. Nicolay, F. Reinert, D. Ehm, S. Schmidt, & S. Hüfner. *Surface and interface states on adsorbate covered noble metal surfaces.* Surface Science **532-535**, 160 (2003). DOI: 10.1016/S0039-6028(03)00151-1.

[Fuc06] Gernot Fuchsel, Tillmann Klamroth, Jadranka Dokic, & Peter Saalfrank. *On the Electronic Structure of Neutral and Ionic Azobenzenes and Their Possible Role as Surface Mounted Molecular Switches.* The Journal of Physical Chemistry B **110**, 33, 16337 (2006). DOI: 10.1021/jp060969v.

[Fus90] G. Fuster, J. M. Tyler, N. E. Brener, J. Callaway, & D. Bagayoko. *Electronic structure and related properties of silver.* Phys. Rev. B **42**, 12, 7322 (1990). DOI: 10.1103/PhysRevB.42.7322.

[Gae07] Alexander Gaenko, Ajitha Devarajan, Laura Gagliardi, Roland Lindh, & Giorgio Orlandi. *Ab initio DFT study of Z-E isomerization pathways of N –benzylideneaniline.* Theoretical Chemistry Accounts: Theory, Computation, and Modeling (Theoretica Chimica Acta) **118**, 1, 271 (2007). http://dx.doi.org/10.1007/s00214-007-0319-1.

[Gah00] C. Gahl, K. Ishioka, Q. Zhong, A. Hotzel, & M. Wolf. *Structure and dynamics of excited electronic states at the adsorbate/metal interface: C6F6/Cu(111).* Faraday Discussions **117**, 191 (2000). DOI: 10.1039/b003308l.

[Gah04] Cornelius Gahl. *Elektronentransfer- und Solvatisierungsdynamik in Eis adsorbiert auf Metalloberflächen.* PhD Thesis, Freie Universtiät Berlin (2004).

[Güd05] J. Güdde & U. Höfer. *Femtosecond time-resolved studies of image-potential states at surfaces and interfaces of rare-gas adlayers.* Progress in Surface Science **80**, 3-4, 49 (2005). DOI: 10.1016/j.progsurf.2005.10.003.

[Gie85] K. Giesen, F. Hage, F. J. Himpsel, H. J. Riess, & W. Steinmann. *Two-photon photoemission via image-potential states.* Phys. Rev. Lett. **55**, 3, 300 (1985). DOI: 10.1103/PhysRevLett.55.300.

[Gri08] Leonhard Grill. *Functionalized molecules studied by STM: motion, switching and reactivity.* Journal of Physics: Condensed Matter **20**, 5, 053001 (19pp) (2008). http://stacks.iop.org/0953-8984/20/053001.

[Gro93] Coherent Laser Group (Ed.). *Operator's Manual, The Coherent Mira 900-B Laser.* Coherent Inc., Santa Clara (1993).

[Gro94] Coherent Laser Group (Ed.). *Operator's Manual, The Coherent Modell 9800 Optical Parametric Amplifier.* Coherent Inc., Santa Clara (1994).

[Gro07] Coherent Laser Group (Ed.). *Operator's Manual, Verdi V-18 Diode-Pumped Lasers.* Coherent Inc., Santa Clara (2007).

[Guo99] Hua Guo, Peter Saalfrank, & Tamar Seideman. *Theory of photoinduced surface reactions of admolecules.* Progress in Surface Science **62**, 7-8, 239 (1999). DOI: 10.1016/S0079-6816(99)00013-1.

[Hag07] Sebastian Hagen, Felix Leyssner, Dhananjay Nandi, Martin Wolf, & Petra Tegeder. *Reversible switching of tetra-tert-butyl-azobenzene on a Au(111) surface induced by light and thermal activation.* Chemical Physics Letters **444**, 1-3, 85 (2007). DOI: 10.1016/j.cplett.2007.07.005.

[Hag08a] Sebastian Hagen, Peter Kate, Felix Leyssner, Dhananjay Nandi, Martin Wolf, & Petra Tegeder. *Excitation mechanism in the photoisomerization of a surface-bound azobenzene derivative: Role of the metallic substrate.* The Journal of Chemical Physics **129**, 16, 164102 (2008). DOI: 10.1063/1.2997343.

[Hag08b] Sebastian Hagen, Peter Kate, Maike Peters, Stefan Hecht, Martin Wolf, & Petra Tegeder. *Kinetic analysis of the photochemically and thermally induced isomerization of an azobenzene derivative on Au(111) probed by two-photon photoemission.* Applied Physics A: Materials Science & Processing **93**, 2, 253 (2008). http://dx.doi.org/10.1007/s00339-008-4831-5.

[Hai95] Richard Haight. *Electron dynamics at surfaces.* Surface Science Reports **21**, 8, 275 (1995). DOI: 10.1016/0167-5729(95)00002-X.

[Ham95] B. Hammer & J. K. Norskov. *Why gold is the noblest of all the metals.* Nature **376**, 6537, 238 (1995). http://dx.doi.org/10.1038/376238a0.

[Han78] G. V. Hansson & S. A. Flodström. *Photoemission study of the bulk and surface electronic structure of single crystals of gold.* Phys. Rev. B **18**, 4, 1572 (1978). DOI: 10.1103/PhysRevB.18.1572.

[Han02] Wen-Ge Han, Timothy Lovell, Tiqing Liu, & Louis Noodleman. *Density Functional Studies of the Ground- and Excited-State Potential-Energy Curves of Stilbene cis-trans Isomerization.* ChemPhysChem **3**, 2, 167 (2002). http://dx.doi.org/10.1002/1439-7641(20020215)3:2<167::AID-CPHC167>3.0.CO;2-G.

[Har97] C. B. Harris, N.-H. Ge, R. L. Lingle, J. D. McNeill, & C. M. Wong. *Femtosecond dynamics of electrons on surfaces and at interfaces.* Annual Review of Physical Chemistry **48**, 1, 711 (1997). DOI: 10.1146/annurev.physchem.48.1.711.

[Has90] Z. F. Liu K. Hashimoto & A. Fujishima. *Photoelectrochemical information storage using an azobenzene derivative.* Nature **347**, 658 (1990). DOI: 10.1038/347658a0.

[Hen06] Jörg Henzl, Michael Mehlhorn, Heiko Gawronski, Karl-Heinz Rieder, & Karina Morgenstern. *Reversible cis-trans Isomerization of a Single Azobenzene Molecule.* Angewandte Chemie International Edition **45**, 4, 603 (2006). http://dx.doi.org/10.1002/anie.200502229.

[Her96] T. Hertel, E. Knoesel, M. Wolf, & G. Ertl. *Ultrafast Electron Dynamics at Cu(111): Response of an Electron Gas to Optical Excitation.* Phys. Rev. Lett. **76**, 3, 535 (1996). DOI: 10.1103/PhysRevLett.76.535.

[Hüf95] S. Hüfner. *Photoelectron Spectroscopy.* Springer, Heidelberg (1995).

[Hoe04] M. Hoesch, M. Muntwiler, V. N. Petrov, M. Hengsberger, L. Patthey, M. Shi, M. Falub, T. Greber, & J. Osterwalder. *Spin structure of the Shockley surface state on Au (111).* Phys. Rev. B **69**, 24, 241401 (2004). DOI: 10.1103/PhysRevB.69.241401.

[Hof97] U. Hofer, I. L. Shumay, Ch. Reuss, U. Thomann, W. Wallauer, & Th. Fauster. *Time-Resolved Coherent Photoelectron Spectroscopy of Quantized Electronic States on Metal Surfaces.* Science **277**, 5331, 1480 (1997). DOI: 10.1126/science.277.5331.1480.

[Hot99] Arthur Hotzel. *Elektronendynamik der adsorbatbedeckten Cu(111)-Oberfläche.* PhD Thesis, Freie Universität Berlin (1999).

[Hot07] Arthur Hotzel. *Electron dynamics of image potential states in weakly bound adsorbate layers: A short review.* Progress in Surface Science **82**, 4-6, 336 (2007). DOI: 10.1016/j.progsurf.2007.03.009.

[Hua04] W. X. Huang & J. M. White. *Growth and Orientation of Naphthalene Films on Ag(111).* The Journal of Physical Chemistry B **108**, 16, 5060 (2004). DOI: 10.1021/jp0378384.

[Iri00] M. Irie. *Photochromism: Memories and Switches Introduction.* Chemical Reviews **100**, 5, 1683 (2000). DOI: 10.1021/cr980068l.

[Jak75] R. C. Jaklevic & John Lambe. *Experimental study of quantum size effects in thin metal films by electron tunneling.* Phys. Rev. B **12**, 10, 4146 (1975). DOI: 10.1103/PhysRevB.12.4146.

[Jak89] P. Jakob & D. Menzel. *Benzene multilayers: A model for their anisotropic growth from vibrational spectroscopy and thermal desorption.* Surface Science **220**, 1, 70 (1989). DOI: 10.1016/0039-6028(89)90464-0.

[Jun97] T. A. Jung, R. R. Schlittler, & J. K. Gimzewski. *Conformational identification of individual adsorbed molecules with the STM.* Nature **386**, 6626, 696 (1997). http://dx.doi.org/10.1038/386696a0.

[Kaw08] Eiji Kawabe, Hiroyuki Yamane, Ryohei Sumii, Kenji Koizumi, Yukio Ouchi, Kazuhiko Seki, & Kaname Kanai. *A role of metal d-band in the interfacial electronic structure at organic/metal interface: PTCDA on Au, Ag and Cu.* Organic Electronics **9**, 5, 783 (2008). DOI: DOI: 10.1016/j.orgel.2008.05.017.

[Kin75] David A. King. *Thermal desorption from metal surfaces: A review.* Surface Science **47**, 1, 384 (1975). DOI: 10.1016/0039-6028(75)90302-7.

[Kir09] Patrick Kirchmann. *Ultrafast Electron Dynamics in Low-Dimensional Materials.* PhD Thesis, Freie Universität Berlin (2009).

[Kno98] E. Knoesel, A. Hotzel, & M. Wolf. *Ultrafast dynamics of hot electrons and holes in copper: Excitation, energy relaxation, and transport effects.* Phys. Rev. B **57**, 20, 12812 (1998). DOI: 10.1103/PhysRevB.57.12812.

[Kor06] J. D. Koralek, J. F. Douglas, N. C. Plumb, Z. Sun, A. V. Fedorov, M. M. Murnane, H. C. Kapteyn, S. T. Cundiff, Y. Aiura, K. Oka, H. Eisaki, & D. S. Dessau. *Laser Based Angle-Resolved Photoemission, the Sudden Approximation, and Quasiparticle-Like Spectral Peaks in* $Bi_2Sr_2CaCu_2O_{8+\delta}$. Physical Review Letters **96**, 1, 017005 (2006). DOI: 10.1103/PhysRevLett.96.017005.

[Kow06] P. Kowalczyk, W. Kozlowski, W. Olejniczak, & P.K. Datta. *STS investigations of temperature dependence of Au(111) surface state*

energy position. Surface Science **600**, 8, 1604 (2006). DOI: 10.1016/j.susc.2005.11.044.

[Koz93] L. I. Kozhevina, E. B. Prokopenko, V. I. Rybachenko, & E. V. Titov. *The vibrational spectra and force constants of benzylideneaniline and its fluoroderivatives.* Journal of Molecular Structure **295**, 53 (1993). DOI: 10.1016/0022-2860(93)85007-H.

[Krö08] Dominik Kröner, Stefan Klinkusch, & Tillmann Klamroth. *Enhanced photodesorption by vibrational pre-excitation: Quantum model simulations for Cs/Cu(1 1 1).* Surface Science **602**, 20, 3148 (2008). DOI: 10.1016/j.susc.2007.04.260.

[Lew82] J. W. Lewis & C. Sandorfy. *An infrared study of the photoisomerization of N-benzylideneaniline.* Canadian Journal of Chemistry **60**, 1720 (1982).

[Ley07] Felix Leyssner. *Adsorption und elektronische Struktur des molekularen Schalters tetra-tert-butyl-Azobenzol auf Ag(111) und Au(111).* Diploma Thesis, Freie Universität Berlin (2007).

[Lin96] R. L. Lingle, N. H. Ge, R. E. Jordan, J. D. McNeill, & C. B. Harris. *Femtosecond studies of electron tunneling at metal-dielectric interfaces.* Chemical Physics **205**, 1-2, 191 (1996). DOI: 10.1016/0301-0104(95)00375-4.

[Lin06] C. D. Lindstrom & X.-Y. Zhu. *Photoinduced Electron Transfer at Molecule-Metal Interfaces.* Chemical Reviews **106**, 10, 4281 (2006). DOI: 10.1021/cr0501689.

[Lin07] C. D. Lindstrom, M. Muntwiler, & X.-Y. Zhu. *Electron Dynamics at Polyacene/Au(111) Interfaces.* The Journal of Physical Chemistry B **111**, 24, 6913 (2007). DOI: 10.1021/jp0662505.

[Lis05] M. Lisowski. *Elektronen- und Magnetisierungsdynamik in Metallen untersucht mit zeitaufgelöster Photoemission.* PhD Thesis, Freie Universität Berlin (2005).

[Lou00] Rodney Loudon. *The Quantum Theory of Light.* Oxford University Press (2000).

[Lüt93] Hans Lüth. *Surfaces and Interfaces of Solids.* Springer-Verlag Berlin (1993).

[Mah70a] G. D. Mahan. *Angular Dependence of Photoemission in Metals.* Phys. Rev. Lett. **24**, 19, 1068 (1970). DOI: 10.1103/PhysRevLett.24.1068.

[Mah70b] G. D. Mahan. *Theory of Photoemission in Simple Metals.* Phys. Rev. B **2**, 11, 4334 (1970). DOI: 10.1103/PhysRevB.2.4334.

[Mat99] R. Matzdorf, A. Gerlach, F. Theilmann, G. Meister, & A. Goldmann. *New lifetime estimates for d-band holes at noble metal surfaces.* Applied Physics B: Lasers and Optics **68**, 3, 393 (1999). http://dx.doi.org/10.1007/s003400050637.

[Mer93] W.R. Merry, R.E. Jordan, D.F. Padowitz, & C.B. Harris. *Electrons at metal-insulator interfaces: I. The effect of Xe monolayers on the image potential states of Ag(111).* Surface Science **295**, 3, 393 (1993). DOI: 10.1016/0039-6028(93)90286-S.

[Mil96] T. Miller, W. E. McMahon, & T.-C. Chiang. *Interference between Bulk and Surface Photoemission Transitions in Ag(111).* Phys. Rev. Lett. **77**, 6, 1167 (1996). DOI: 10.1103/PhysRevLett.77.1167.

[Mis92] J. A. Misewich, T. F. Heinz, & D. M. Newns. *Desorption induced by multiple electronic transitions.* Phys. Rev. Lett. **68**, 25, 3737 (1992). DOI: 10.1103/PhysRevLett.68.3737.

[Mis96] J. A. Misewich, S. Nakabayashi, P. Weigand, M. Wolf, & T. F. Heinz. *Anomalous branching ratio in the femtosecond surface chemistry of O_2/Pd(111).* Surface Science **363**, 1-3, 204 (1996). DOI: 10.1016/0039-6028(96)00138-0.

[Mon82] Sandra Monti, Giorgio Orlandi, & Paolo Palmieri. *Features of the photochemically active state surfaces of azobenzene.* Chemical Physics **71**, 1, 87 (1982). DOI: 10.1016/0301-0104(82)87008-0.

[Mor01] Francesca Moresco, Gerhard Meyer, Karl-Heinz Rieder, Hao Tang, André Gourdon, & Christian Joachim. *Conformational Changes of Single Molecules Induced by Scanning Tunneling Microscopy Manipulation: A Route to Molecular Switching.* Phys. Rev. Lett. **86**, 4, 672 (2001). DOI: 10.1103/PhysRevLett.86.672.

[Mun06] M. Muntwiler, C. D. Lindstrom, & X.-Y. Zhu. *Delocalized electron resonance at the alkanethiolate self-assembled monolayer/Au(111) interface.* The Journal of Chemical Physics **124**, 8, 081104 (2006). DOI: 10.1063/1.2171437.

[Nar92] Shobhana Narasimhan & David Vanderbilt. *Elastic stress domains and the herringbone reconstruction on Au(111).* Phys. Rev. Lett. **69**, 10, 1564 (1992). DOI: 10.1103/PhysRevLett.69.1564.

[Näg97] T. Nägele, R. Hoche, W. Zinth, & J. Wachtveitl. *Femtosecond photoisomerization of cis-azobenzene.* Chemical Physics Letters **272**, 5-6, 489 (1997). DOI: 10.1016/S0009-2614(97)00531-9.

[Nic01] G. Nicolay, F. Reinert, S. Hüfner, & P. Blaha. *Spin-orbit splitting of the L-gap surface state on Au(111) and Ag(111).* Phys. Rev. B **65**, 3, 033407 (2001). DOI: 10.1103/PhysRevB.65.033407.

[Osg06] Richard Osgood. *Photoreaction Dynamics of Molecular Adsorbates on Semiconductor and Oxide Surfaces.* Chemical Reviews **106**, 10, 4379 (2006). DOI: 10.1021/cr050175x.

[Ova07] Laszlo Ovari, Martin Wolf, & Petra Tegeder. *Reversible Changes in the Vibrational Structure of Tetra-tert-butylazobenzene on a Au(111) Surface Induced by Light and Thermal Activation.* The Journal of Physical Chemistry C **111**, 42, 15370 (2007). DOI: 10.1021/jp075274o.

[Pan95] R. Paniago, R. Matzdorf, G. Meister, & A. Goldmann. *Temperature dependence of Shockley-type surface energy bands on Cu(111), Ag(111) and Au(111).* Surface Science **336**, 1-2, 113 (1995). DOI: 10.1016/0039-6028(95)00509-9.

[Pet97] H. Petek & S. Ogawa. *Femtosecond time-resolved two-photon photoemission studies of electron dynamics in metals.* Progress in Surface Science **56**, 4, 239 (1997). DOI: 10.1016/S0079-6816(98)00002-1.

[Pet99] H. Petek, H. Nagano, & S. Ogawa. *Hole Decoherence of d-Bands in Copper.* Phys. Rev. Lett. **83**, 4, 832 (1999). DOI: 10.1103/PhysRevLett.83.832.

[Pis74] Cesare Pisani, Giovanni Rabino, & Franco Ricca. *Statistical analysis and model determination for thermal desorption spectra: Nitrogen on tungsten.* Surface Science **41**, 1, 277 (1974). DOI: 10.1016/0039-6028(74)90309-4.

[Plu07] E. W. Plummer & W. Eberhardt. *Angle-Resolved Photoemission as a Tool for the Study of Surfaces.* In Stuart A. Rice I. Prigogine (Ed.), *Advances in Chemical Physics*. Wiley InterScience (2007) 533–656. URL `http://dx.doi.org/10.1002/9780470142691.ch8`.

[Pon05] N. Pontius, V. Sametoglu, & H. Petek. *Simulation of two-photon photoemission from the bulk sp-bands of Ag(111).* Phys. Rev. B **72**, 11, 115105 (2005). DOI: 10.1103/PhysRevB.72.115105.

[Qun08] Lloyd F. N. Ah Qune, H. Akiyama, T. Nagahiro, K. Tamada, & Andrew T. S. Wee. *Reversible work function changes induced by photoisomerization of asymmetric azobenzene dithiol self-assembled monolayers on gold.* Applied Physics Letters **93**, 8, 083109 (2008). DOI: 10.1063/1.2969468.

[Rau03] H. Rau. *Photochromism – Molecules and Systems.* Elsevier, Amsterdam (2003).

[Red62] P.A. Redhead. *Thermal desorption of gases.* Vacuum **12**, 4, 203 (1962). DOI: 10.1016/0042-207X(62)90978-8.

[Ree97] M. A. Reed, C. Zhou, C. J. Muller, T. P. Burgin, & J. M. Tour. *Conductance of a Molecular Junction.* Science **278**, 5336, 252 (1997). DOI: 10.1126/science.278.5336.252.

[Rei00] G.D. Reid & K. Wynne. *Ultrafast laser technology and spectroscopy.* Encyclopedia of Analytical Chemistry, RA Meyers ed.(John Wiley & Sons Ltd, Chichester, UK. 2000) **1**, 26 (2000). DOI: 10.1002/9780470027318.a8104g.

[Rei01] F. Reinert, G. Nicolay, S. Schmidt, D. Ehm, & S. Hüfner. *Direct measurements of the L-gap surface states on the (111) face of noble metals by photoelectron spectroscopy.* Phys. Rev. B **63**, 11, 115415 (2001). DOI: 10.1103/PhysRevB.63.115415.

[Rei04] F. Reinert & G. Nicolay. *Influence of the herringbone reconstruction on the surface electronic structure of Au(111).* Applied Physics A: Materials Science & Processing **78**, 6, 817 (2004). http://dx.doi.org/10.1007/s00339-003-2436-6.

[Reu96] C. Reuß, W. Wallauer, & T. Fauster. *Image States of Ag on Au(111).* Surface Review and Letters **3**, 1547 (1996). DOI: 10.1142/S0218625X96002539.

[Roh05] M. Rohleder, W. Berthold, J. Güdde, & U. Höfer. *Time-Resolved Two-Photon Photoemission of Buried Interface States in Ar/Cu(100).* Phys. Rev. Lett. **94**, 1, 017401 (2005). DOI: 10.1103/PhysRevLett.94.017401.

[Rul98] Claude Rulliere (Ed.). *Laser Spectroscopy.* Springer, Berlin (1998).

[Saa08] Peter Saalfrank, Tijo Vazhappilly, Stephanie Beyvers, G.K. Paramonov, & Tillmann Klamroth. *Controlling the photodesorption of adspecies from surfaces.* Surface Science **602**, 20, 3153 (2008). DOI: 10.1016/j.susc.2007.07.037.

[Sat03] H. Satzger, S. Spörlein, C. Root, J. Wachtveitl, W. Zinth, & P. Gilch. *Fluorescence spectra of trans- and cis-azobenzene - emission from the Franck-Condon state.* Chemical Physics Letters **372**, 1-2, 216 (2003). DOI: 10.1016/S0009-2614(03)00364-6.

[Sch03] Wolfgang Schattke. *Solid-State Photoemission and Related Methods.* Wiley-VCH, Berlin (2003).

[Sch04] B. Schmidt, C. Sobotta, S. Malkmus, S. Laimgruber, M. Braun, W. Zinth, & P. Gilch. *Femtosecond Fluorescence and Absorption Dynamics of an Azobenzene with a Strong Push-Pull Substitution.* The Journal of Physical Chemistry A **108**, 20, 4399 (2004). DOI: 10.1021/jp0495747.

[Sch08a] Roland Schmidt, Erik McNellis, Wolfgang Freyer, Daniel Brete, Tanja Gießel, Cornelius Gahl, Karsten Reuter, & Martin Weinelt. *Azobenzene-functionalized alkanethiols in self-assembled monolayers on gold.* Applied Physics A: Materials Science & Processing **93**, 2, 267 (2008). http://dx.doi.org/10.1007/s00339-008-4829-z.

[Sch08b] F. Schmitt, P. S. Kirchmann, U. Bovensiepen, R. G. Moore, L. Rettig, M. Krenz, J.-H. Chu, N. Ru, L. Perfetti, D. H. Lu, M. Wolf, I. R. Fisher, & Z.-X. Shen. *Transient Electronic Structure and Melting of a Charge Density Wave in $TbTe_3$.* Science **321**, 5896, 1649 (2008). DOI: 10.1126/science.1160778.

[Sch09] Roland Schmidt. *to be announced.* PhD Thesis, Freie Universität Berlin (2009).

[Sea79] M. P. Seah & W. A. Dench. *Quantitative electron spectroscopy of surfaces: A standard data base for electron inelastic mean free paths in solids.* Surface and Interface Analysis **1**, 1, 2 (1979). http://dx.doi.org/10.1002/sia.740010103.

[Smi85] N. V. Smith. *Phase analysis of image states and surface states associated with nearly-free-electron band gaps.* Phys. Rev. B **32**, 6, 3549 (1985). DOI: 10.1103/PhysRevB.32.3549.

[Smi88] N V Smith. *Inverse photoemission.* Reports on Progress in Physics **51**, 9, 1227 (1988). http://stacks.iop.org/0034-4885/51/1227.

[Stä07] J. Stähler. *Freezing Hot Electrons - Electron Transfer and Solvation Dynamics at D_2O and NH_3 - Metal Interfaces.* PhD Thesis, Freie Universität Berlin (2007).

[Ste95] W. Steinmann. *Two-Photon Photoemission Spectroscopy of Electronic States at Metal Surfaces.* physica status solidi (b) **192**, 2, 339 (1995). http://dx.doi.org/10.1002/pssb.2221920210.

[Tan97] Sander J. Tans, Michel H. Devoret, Hongjie Dai, Andreas Thess, Richard E. Smalley, L. J. Geerligs, & Cees Dekker. *Individual single-wall carbon nanotubes as quantum wires.* Nature **386**, 6624, 474 (1997). http://dx.doi.org/10.1038/386474a0.

[Teg05] P. Tegeder, M. Danckwerts, S. Hagen, A. Hotzel, & M. Wolf. *Structural transition in cyclooctatetraene adsorbed on Ru(001) probed by thermal desorption and two-photon photoemission spectroscopy.* Surface Science **585**, 3, 177 (2005). DOI: 10.1016/j.susc.2005.04.027.

[Teg07] P. Tegeder, S. Hagen, F. Leyssner, S. Peters, M.V.and Hecht, T. Klamroth, P. Saalfrank, & M. Wolf. *Electronic structure of the molecular switch*

tetra- tert-butyl-azobenzene adsorbed on Ag(111). Applied Physics A: Materials Science & Processing **88**, 3, 465 (2007). DOI: 10.1007/s00339-007-4047-03.

[Tho06] Tracy L. Thompson & John T. Yates. *Surface Science Studies of the Photoactivation of TiO_2 New Photochemical Processes.* Chemical Reviews **106**, 10, 4428 (2006). DOI: 10.1021/cr050172k.

[Tre02] R. Trebino (Ed.). *Frequency-Resolved Optical Gating: The Measurement of Ultrashort Laser Pulses.* Springer, Berlin (2002).

[Óvá08] László Óvári, Jutta Schwarz, Maike V. Peters, Stefan Hecht, Martin Wolf, & Petra Tegeder. *Reversible isomerization of an azobenzene derivative adsorbed on Au(111): Analysis using vibrational spectroscopy.* International Journal of Mass Spectrometry **277**, 1-3, 223 (2008). DOI: 10.1016/j.ijms.2008.04.024.

[Vaz07a] Tijo Vazhappilly, Stephanie Beyvers, Tillmann Klamroth, Marcello Luppi, & Peter Saalfrank. *Vibrationally enhanced associative photodesorption of molecular hydrogen from Ru(0 0 0 1).* Chemical Physics **338**, 2-3, 299 (2007). DOI: 10.1016/j.chemphys.2007.04.022.

[Vaz07b] H. Vazquez, Y. J. Dappe, J. Ortega, & F. Flores. *Energy level alignment at metal/organic semiconductor interfaces: "Pillow" effect, induced density of interface states, and charge neutrality level.* The Journal of Chemical Physics **126**, 14, 144703 (2007). DOI: 10.1063/1.2717165.

[Vel98] D. Velic, A. Hotzel, M. Wolf, & G. Ertl. *Electronic states of the C_6H_6/Cu(111) system: Energetics, femtosecond dynamics, and adsorption morphology.* The Journal of Chemical Physics **109**, 20, 9155 (1998). DOI: 10.1063/1.477468.

[Váz07] H. Vázquez, F. Flores, & A. Kahn. *Induced Density of States model for weakly-interacting organic semiconductor interfaces.* Organic Electronics **8**, 2-3, 241 (2007). DOI: 10.1016/j.orgel.2006.07.006.

[Wal91] David H. Waldeck. *Photoisomerization dynamics of stilbenes.* Chemical Reviews **91**, 3, 415 (1991). DOI: 10.1021/cr00003a007.

[Wan00] Hanfu Wang, Gregory Dutton, & X.-Y. Zhu. *Electronic Structure at Organic/Metal Interfaces:Naphthalene/Cu(111).* The Journal of Physical Chemistry B **104**, 44, 10332 (2000). DOI: 10.1021/jp002257p.

[Wei71] Karl Weiss, Charles H. Warren, & Gunnar Wettermark. *cis-trans isomerization about the carbon-nitrogen double bond. Structures of the isomers of N-benzylideneaniline.* Journal of the American Chemical Society **93**, 19, 4658 (1971). DOI: 10.1021/ja00748a003.

[Wei02] Martin Weinelt. *Time-resolved two-photon photoemission from metal surfaces.* Journal of Physics: Condensed Matter **14**, 43, R1099 (2002). http://stacks.iop.org/0953-8984/14/R1099.

[Wei06] Sigrid Weigelt, Carsten Busse, Lars Petersen, Eva Rauls, Bjork Hammer, Kurt V. Gothelf, Flemming Besenbacher, & Trolle R. Linderoth. *Chiral switching by spontaneous conformational change in adsorbed organic molecules.* Nat Mater **5**, 2, 112 (2006). http://dx.doi.org/10.1038/nmat1558.

[WGD04] Eric Wei-Guang Diau. *A New Trans-to-Cis Photoisomerization Mechanism of Azobenzene on the S1(n,n*) Surface.* The Journal of Physical Chemistry A **108**, 6, 950 (2004). DOI: 10.1021/jp031149a.

[Wil98] I. Willner & B. Willner. *Layered molecular optoelectronic assemblies.* Journal of Materials Chemistry **8**, 12, 2543 (1998).

[Win76] P Winsemius, F F van Kampen, H P Lengkeek, & C G van Went. *Temperature dependence of the optical properties of Au, Ag and Cu.* Journal of Physics F: Metal Physics **6**, 8, 1583 (1976). http://stacks.iop.org/0305-4608/6/1583.

[Wit05] Gregor Witte, Simon Lukas, Paul S. Bagus, & Christof Woll. *Vacuum level alignment at organic/metal junctions: "Cushion" effect and the interface dipole.* Applied Physics Letters **87**, 26, 263502 (2005). DOI: 10.1063/1.2151253.

[Wol96] M. Wolf, E. Knoesel, & T. Hertel. *Ultrafast dynamics of electrons in image-potential states on clean and Xe-covered Cu(111).* Phys. Rev. B **54**, 8, R5295 (1996). DOI: 10.1103/PhysRevB.54.R5295.

[Wol99] M. Wolf, A. Hotzel, E. Knoesel, & D. Velic. *Direct and indirect excitation mechanisms in two-photon photoemission spectroscopy of Cu(111) and CO/Cu(111).* Phys. Rev. B **59**, 8, 5926 (1999). DOI: 10.1103/PhysRevB.59.5926.

[Woo86] D. P. Woodruff, W. A. Royer, & N. V. Smith. *Empty surface states, image states, and band edge on Au(111).* Phys. Rev. B **34**, 2, 764 (1986). DOI: 10.1103/PhysRevB.34.764.

[Xi94] Ming Xi, Michael X. Yang, Sam K. Jo, Brian E. Bent, & Paul Stevens. *Benzene adsorption on Cu(111): Formation of a stable bilayer.* The Journal of Chemical Physics **101**, 10, 9122 (1994). DOI: 10.1063/1.468041.

[Xin97] Q. S. Xin & X. Y. Zhu. *Temperature dependent photodesorption of methyl radical from GaAs: role of the initial state.* Chemical Physics Letters **265**, 1-2, 259 (1997). DOI: 10.1016/S0009-2614(96)01407-8.

[Yam07] H. Yamane, D. Yoshimura, E. Kawabe, R. Sumii, K. Kanai, Y. Ouchi, N. Ueno, & K. Seki. *Electronic structure at highly ordered organic/metal interfaces: Pentacene on Cu(110).* Physical Review B (Condensed Matter and Materials Physics) **76**, 16, 165436 (2007). DOI: 10.1103/PhysRevB.76.165436.

[Yan01] M. C. Yang, T. J. Rockey, D. Pursell, & H. L. Dai. *Layer-by-Layer Structure in Ultrathin Aniline and Pyridine Films on Ag(111).* The Journal of Physical Chemistry B **105**, 48, 11945 (2001). DOI: 10.1021/jp013229p.

[Zan88] Andrew Zangwill. *Physics at Surfaces.* Cambridge University Press (1988).

[Zho91] X. L. Zhou, X. Y. Zhu, & J. M. White. *Photochemistry at adsorbate/metal interfaces.* Surface Science Reports **13**, 3-6, 73 (1991). DOI: 10.1016/0167-5729(91)90009-M.

[Zho02] Q. Zhong, C. Gahl, & M. Wolf. *Two-photon photoemission spectroscopy of pyridine adsorbed on Cu(111).* Surface Science **496**, 1-2, 21 (2002). DOI: DOI: 10.1016/S0039-6028(01)01502-3.

[Zhu94] X Zhu. *Surface Photochemistry.* Annual Review of Physical Chemistry **45**, 1, 113 (1994). DOI: 10.1146/annurev.pc.45.100194.000553.

[Zhu02] X.-Y. Zhu. *Electron transfer at molecule-metal interfaces: A Two-Photon Photoemission Study.* Annual Review of Physical Chemistry **53**, 1, 221 (2002). DOI: 10.1146/annurev.physchem.53.082801.093725.

[Zim95] Frank M. Zimmermann & W. Ho. *State resolved studies of photochemical dynamics at surfaces.* Surface Science Reports **22**, 4-6, 127 (1995). DOI: 10.1016/0167-5729(96)80001-X.

Publications

Publications within this thesis

P. Tegeder, S. Hagen, F. Leyssner, M.V. Peters, S. Hecht, T. Klamroth, P. Saalfrank and M. Wolf. *Electronic structure of the molecular switch tetra-tert-butyl-azobenzene adsorbed on Ag(111).* Applied Physics A:Materials Science & Processing, 88(3):465-472,2007.

S. Hagen, P. Kate, M. Peters, S. Hecht, M. Wolf and P. Tegeder. *Kinetic analysis of the photochemically and thermally induced isomerization of an azobenzene derivative on Au(111) probed by two-photon photoemission.* Applied Physics A: Materials Science & Processing, 93(2):253 - 260, November 2008

S. Hagen, F. Leyssner, D. Nandi, M. Wolf and P. Tegeder. *Reversible switching of tetra-tert-butyl-azobenzene on a Au(111) surface induced by light and thermal activation.* Chemical Physics Letters, 444(1-3):85 - 90, 2007.

S. Hagen, P. Kate, F. Leyssner, D. Nandi, M. Wolf and P. Tegeder. *Excitation mechanism in the photoisomerization of a surface-bound azobenzene derivative: Role of the metallic substrate.* The Journal of Chemical Physics, 129(16):164102, 2008

Publications concerning other topics

P. Tegeder, M. Danckwerts, S. Hagen, A. Hotzel and M.Wolf. *Structural transition in cyclooctatetraene adsorbed on Ru(001) probed by thermal desorption and two-photon photoemission spectroscopy.* Surface Science, 585(3):177 190, 200

In preparation

F. Leyssner, S. Hagen, L. Óvári, M.V. Peters, S. Hecht, Jadranka Dokić, T. Klamroth, P. Saalfrank, M. Wolf, and P. Tegeder. *Adsorption behavior and electronic structure of the molecular switch tetra-*tert*-butyl-stilbene on Au(111)*

S. Hagen, M. Wolf and P. Tegeder. *Pronounced temperature effect on the photoisomerization efficiency of surface-adsorbed tetra-tert-butyl-azobenzene.*

R. Schmidt, S. Hagen, D. Brete, R. Carley, C. Gahl, P. Tegeder and M. Weinelt. *Molecular orientation and charge transfer time in tetra-tert-butyl-azobenzene on Au(111).*

Der Lebenslauf ist in der Online-Version aus Gründen des Datenschutzes nicht enthalten.

Acknowledgments

Große Aufgaben, so wie diese Doktorarbeit, kann man nur schwerlich allein meistern. Darum möchte ich die folgenden Zeilen nutzen, um mich bei den Menschen, die mir in den letzten Jahren hilfreich zur Seite standen, zu bedanken.

Zuerst möchte ich Professor Dr. Martin Wolf danken, dass ich unter seiner Obhut nicht nur mein Diplom, sondern auch meine Dissertation anfertigen durfte. Die Arbeit in seiner Gruppe war nicht nur aufgrund der hervorragenden experimentellen Möglichkeiten, seines nie enden wollenden Reichtums an Ansätzen zur Problemlösung und des exzellenten Networkings eine große Bereicherung. Nein auch Aufgrund des persönlich familiären Verhältnisses und des, trotz vieler Verpflichtungen, steten Interesses für die Arbeiten der Gruppe habe ich mich hier stets sehr wohl gefühlt.

I also would like to thank Professor Dr. Jose Ignacio "Nacho" Pascual for his interest in my work and to adopt the responsibility of being the second referee.

Einen Großteil meiner persönlichen Motivation habe ich aus dem mehr als angenehmen Umgang mit meinen mir liebgewonnenen Kollegen gezogen. Hier möchte ich insbesondere Frau Dr. Petra Tegeder hervorheben und mich für die aufopferungsvolle Betreuung bedanken, die sie mir hat zuteil werden lassen. Ihre konstruktiv fordernde aber auch umsorgende Persönlichkeit hat mich ein ums andere mal von kleineren und größeren Irrwegen wieder in Richtung Ziel vorangetrieben. Ich entschuldige mich hiermit offiziel für alle grauen Haare, die ich verursacht habe. Nochmals vielen, vielen Dank.

Ein weitere wichtiger Stützpfeiler meiner Tätigkeit war und ist (soon to be Dr.) Felix Leyßner. Ob im Labor, zwischen den Bienenstöcken, auf der Mauer auf der Lauer, zu zweit im Hotel oder bei der inoffiziellen Finanzierung meines Urlaubs....Felix es war schön mit dir und ich bin dir sehr zu Dank verpflichtet.

Ein großes Dankeschön geht auch an die gesamte 2PPE-Labcrew die mir den Arbeitsalltag nicht nur auf professioneller, sondern auch auf persönlicher Ebene mehr als nur erträglich gemacht hat. Auch hier möchte ich mich für den ganzen Unfug den ich verzapft habe, insbesondere die akustische Distribution von mehr oder minder qualitativ hochwertigem Liedgut, entschuldigen (Mathieu if you read this there is a song playing in your head right now...). Vielen Dank Micha, Mathieu, Daniel....hmmmm....Daniel, Patrick, Laurenz, Erwan, Julia und once again Felix.

Aber auch außerhalb unseres "kleinen" Larbors habe ich eine Menge hilfreicher Unterstützung erfahren. Ob Dietgard Mallwitz bei Verwaltungsfragen, Dr. Peter West in technischen Belangen, Marcel Krenz und Dr. Panagiotis "Panos" A. Loukakos beim Bezwingen optischer Unklarheiten oder die vielen weiteren Kollegen beim Borgen, Tauschen, Diskutieren und Spaß haben, ihr alle habt meine Arbeit hier sehr erleichtert darum gebührt auch euch mein Dank.

An dieser Stelle möche ich mich auch bei den wissenschaftlich-technischen Einrichtungen des Fachbereichs bedanken die ich regelmäßig in Anspruch nehmen durfte. Ganz besonders sei hier das freundlich, hilfsbereite Team des Tieftemperatur Labors erwähnt, ohne die ein Schalten (siehe Kapitel 4....) nicht möglich gewesen wäre.

Ein weiterer Dank geht an unsere beiden Synchrotron-Kooperationen, die mir so manche schlaflose Nacht bereitet haben. Dies sind zum einen das BESSY Team vom MBI Berlin: Professor Dr. Martin Weinelt, Dr. Cornelius Gahl, Dr. Robert Carley, Daniel Brete und zu guter letzt Roland Schmidt dem ich hiermit noch einmal ganz besonders danke und viel Erfolg für seine Arbeit wünsche (ich bitte um eine Kopie...). Zum anderen hätten wir das ESRF Team vom Forschungszentrum Jülich: Professor Dr. Stefan Tautz, Dr. Sergey Subach and Giuseppe "I don't need sleep" Mercurio.

Ich bedanke mich ebenso bei all den Arbeitsgruppen die im Rahmen des SfB 658 an der Bereitstellung von experimentellem sowie theoretischen Rüstzeug beteiligt gewesen sind. Hier auch noch einmal vielen Dank an die Gruppe von Professor Dr. Peter Saalfrank, and in particular Jadranka Dokic, für das Zurverfügungstellen der Molekülorbitale.

Meine lieben Eltern, diese Arbeit ist auch ein großes Stück für euch. Vielen Dank für eure immerwährende Unterstützung, besonders in den wenigen schweren Zeiten die es zu meistern galt.

Mein letzter Dank geht an meine lieben Freunde und Bekannten, die es mir außerhalb der Arbeit ermöglichten meinen Horizont mit makroskopischen Dingen zu erweitern.